Università degli Studi di Genova

Doctorate Course in Sciences and Technologies of Chemistry and Materials

Curriculum: Materials Science and Technology

XXXVIII Cycle

Electrospun polysaccharidic nanofibers with bacteria and nanoparticles for cleaning and disinfection of Cultural Heritage

Candidate

SIMONE PETTINEO

Supervisors

Prof. Silvia Vicini and Prof. Maila Castellano

Borsa di dottorato cofinanziata con risorse dell'Unione europea-*NextGeneration EU* Piano Nazionale di Ripresa e Resilienza Missione 4, componente 1 "*Potenziamento dell'offerta dei servizi di istruzione: dagli asili nido all'Università*

Abstract

The present Thesis focuses on the fabrication of biopolymer-based nanofibrous mats via electrospinning technique primarily for, but not limited to, the development of advanced tools for Cultural Heritage conservation. Specifically, this project arose to overcome the limitations of traditional cleaning and disinfection methods, which often lack control or involve hazardous materials. To tackle this task, this Thesis proposes the use of electrospun polysaccharides (like Agar, Agarose, and Gellan) and biodegradable, biocompatible synthetic polymers (like PEO, PVA, and PCL), along with innovative approaches like photo-crosslinking to enhance properties such as water resistance.

In the first Chapters, after a general discussion concerning traditional and innovative cleaning, biocleaning, and disinfection procedures in Cultural Heritage restoration, this Thesis concentrates on briefly presenting the electrospinning technique, the properties of metal nanoparticles, the selected biopolymers and synthetic polymers, and the experimental methodologies and characterization approaches used to achieve the investigated purpose.

Then, polysaccharides (Agar, Agarose) and synthetic polymers (PVA, PEO) are employed for the fabrication of nanofibrous mats as cleaning tools. Their physical-chemical properties, and especially their swelling and deswelling capabilities for the controlled release of organic solvents, are fully characterized. As a matter of fact, the developed systems effectively display significant capacity as supports for cleaning and sustainable conservation procedures.

In the second part, the green synthesis of gold and silver nanoparticles mediated by Agar and Agarose is investigated, leading to the development of electrospun Agar-based nanocomposite mats for artwork disinfection. In parallel, the potential of electrospinning for sustainable biocleaning is assessed through the development of electrospun PCL mats designed as bacterial supports, characterizing their metabolic activity and bacterial adhesion.

These results are an important first step in making straightforward the application of electrospinning for conservation science, granting the possibility to easily prepare nanofibrous meshes with potential uses in various application fields, with particular relevance in the sustainable cleaning, biocleaning, and disinfection of Cultural Heritage

Acknowledgments

I would like to express my deepest and sincere gratitude to my supervisors, Prof. Silvia Vicini and Prof. Maila Castellano, for providing me with invaluable guidance throughout this PhD project. Their dynamism, vision, sincerity, and motivation have deeply inspired me. It was a great privilege and honor to work and study under their direction, and I am extremely grateful for what they have offered me.

I would also like to acknowledge the several collaborators I had during these years:

• Prof. Marina Alloisio of the Department of Chemistry and Industrial Chemistry of the University of Genova for the precious assistance provided during the whole Thesis project.

• Prof. Sonia Scarfì and Prof. Marina Pozzolini of the Department of Earth, Environment and Life Sciences of the University of Genova for the help with experimental biological procedures related to this Thesis project.

• Prof. Alina Sionkowska and Dr. Muhammad Tahir of the Department of Chemistry of Biomaterials and Cosmetics of Nicolaus Copernicus University in Toruń for providing part of the mat's characterization during my period in Poland.

• Dr. Paola Stagnaro and Dr. Roberto Utzeri of the National Council of Research (CNR) SCITEC of Genoa for the great support on the experimentation related to the photo-crosslinking process.

• Prof. Giovanna Simonetti, Prof. Alessio Valletta, and Dr. Chiara Genova of the Department of Environmental Biology of the University of Roma La Sapienza for the great support and help with antimicrobial tests of mats.

• Dr. Paola Parodi, Dr. Angelita Mairani, Dr. Stefano Vassallo, and Dr. Valentina Tonini of the *Soprintendenza Archeologia Belle Arti e Paesaggio per la città metropolitana di Genova e la provincia di La Spezia* for the opportunity to work in our laboratory with a masterpieces of Ligurian School.

• Prof. Ulderico Santamaria, Dr. Fabio Morresi, Dr. Stefania Bani, Dr. Francesca Romana Cibin, Dr. Fabio Luciano Castro, and Dr. Andrea Pernella of Cabinet of Scientific Research in the Vatican Museums (Vatican City) for guiding me during the beautiful experience at the Vatican Museums.

Completing this work would not have been possible without the support of several colleagues and students: Francesco Mancioppi, Erica Risso, Susanna Gatti, and Alessia Callegari.

A huge thank you goes to Eleonora and Ada, precious colleagues and friends who supported me with their invaluable advice and their precious presence, especially during the most challenging moments during these years of my doctorate. Thanks also go to the men and women of the GreenLab laboratory under the direction of Professor Orietta Monticelli, especially Giacomo, Martina, Alberto, Alessandro, and Leonardo. The moments of jokes and friendship, along with those of scientific discussion, have enriched me in unexpected ways. A huge thank you also goes to all the people I met throughout my doctorate: students, colleagues, and friends I met during my experiences at the Vatican Museums, at the CNR, and at the University of Torun, as well as at the various conferences I attended.

Last but not least, I am extremely grateful to my parents, my sisters, and my entire family for their love, caring, and sacrifices for educating and preparing me for my future, and especially to all my closest friends who have given me their support, put up with my odd hours, and provided me with lifts and help.

List of Abbreviations

η	Apparent viscosity
γ	Deformation amplitude
ν	Frequency
σ	Mechanical stress
λ	Relaxation time
τ	Shear stress
$\eta\infty$	Infinite – shear viscosity
$\eta 0$	Zero – shear viscosity
εb	Elongation at break
σb	Tensile strength
ηinh	Inherent viscosity
ηr	Relative viscosity
ηred	Reduced viscosity
ηs	Solvent viscosity
ηsp	Specific viscosity
τy	Yield stress
$\bar{M}v$	Viscosity average molecular weight
$\bar{M}$	Average molecular weight
MWD	Molecular weight distribution
$\dot{\gamma}$	Shear rate
$[\eta]$	Intrinsic viscosity
Ac	Acetone
AFM	Atomic force microscopy
AS	Amplitude sweep test
BPO	Benzoyl peroxide
BS	Bacillus subtilis
CC	Concentric cylinder geometry

CP	Cone – plate geometry
CR	Congo red
DG	Double – gap geometry
DSC	Differential scanning calorimetry
E	Young modulus
E’	Extensional storage modulus
E”	Extensional loss modulus
ECM	Extracellular matrix
EDX	Energy dispersive X – ray
ES	Electrospinning
FESEM	Field – emission scanning electron microscopy
FS	Frequency sweep test
FTIR	Fourier – transform infrared spectroscopy
G’	Shear storage modulus
G”	Shear loss modulus
GAA	Glacial acetic acid
LB	Luria-Bertani growth medium
LVER	Linear viscoelastic region
MB	Methylene blue
NPs	Nanoparticles
PBS	Phosphate buffer solution
PCL	Poly(caprolactone)
PEO	Poly(ethylene oxide)
PP	Plate – plate geometry
PS	Pseudomonas stutzeri
PVA	Poly(vinyl alcohol)
RSM	Root mean squared roughness
SEM	Scanning electron microscopy
TEM	Transmission electron microscopy
Tg	Glass transition temperature

TGA	Thermogravimetric analysis
Tm	Melting temperature
TMPTMA	Trimethylolpropane Trimethacrylate
TS	Temperature sweep test
WCA	Water contact angle

Summary

The present PhD thesis primarily deals with the exploitation of the electrospinning technique as an innovative approach for the fabrication of nanofibrous mats with potential uses as advanced tools for Cultural Heritage conservation. This project was specifically designed to overcome the inherent limitations of conventional cleaning, disinfection, and bio-cleaning methods. As discussed in Chapters 1 and 2, these interventions are critical yet delicate: cleaning involves the selective removal of unwanted surface deposits (like grime or aged varnishes) without damaging the original substrate; disinfection aims to arrest biodeterioration by neutralizing harmful microorganisms (like fungi or bacteria); and biocleaning utilizes living bacterial strains or their enzymes to precisely digest specific unwanted substances. However, traditional procedures for these tasks often lack control, are invasive, or involve hazardous materials. Furthermore, common gel-based systems, while an improvement, often leave unwanted residues on the delicate artwork surfaces, complicating the conservation process. To this end, advanced materials like nanofibrous mats play a crucial role in providing controlled application of cleaning agents, sustainable disinfection, and targeted biocleaning.

As broadly discussed in Chapter 3, electrospinning is a fabrication approach widely employed to produce scaffolds that can be made of different nanofibers with random orientations and in various shapes. For decades, these non-woven scaffolds have been widely utilized in established fields like biomedical engineering, pharmaceuticals, filtration, and textiles. However, their application in Cultural Heritage conservation is completely new, having only been introduced in the last three years. As a matter of fact, the great porosity and the large surface area—properties well-established in other sectors—make nanofibers efficient for the controlled release of solvents or the application of biocides in conservation, at the same time allowing easy removal and preventing the unwanted spread of chemicals.

Specifically, it is noteworthy that electrospun nanofibrous tools can be obtained from natural polymers, synthetic polymers, and mixed polymers. Natural polymers, particularly polysaccharides, offer a wide range of advantages with respect to synthetic ones, including non-toxicity and high water/solvent retention. In this sense, the use of polysaccharide materials, such as those discussed in Chapter 4 (e.g., Agar, Agarose and Gellan), was targeted. These specific biopolymers were selected because they are already well-known and utilized materials in Cultural Heritage conservation, primarily as traditional gels. However, their application as electrospun nanofibers for conservation represents a highly innovative approach, with very few publications found in the literature on the electrospinning of Agar, Agarose, or Gellan for any purpose.

However, despite the above-mentioned advantages, the proficient electrospinning of polysaccharides is not yet completely understood, and it usually implies the use of synthetic co-spinning agents (like PEO or PVA) that can affect the overall response of the obtained nanofibers. Additionally, because of their high solubility in aqueous environments, polysaccharide-based products might be subjected to a crosslinking reaction, which is a critical aspect in ensuring their stability, as explored for PEO-based mats in Chapter 12.

With these premises, the first target of the present Thesis work was to optimize the electrospinning process of polysaccharide-based formulations, aiming to establish a simple protocol for fabricating

nanofibrous mats as cleaning tools. As such, as discussed in Chapters 7 and 8, various polysaccharides (Agar, Agarose) and synthetic polymers (PEO, PVA) were employed for the purpose. Rheology was exploited as a fundamental tool to understand the main parameters affecting the electrospinning phenomenon and the related nanofiber morphology. Noticeably, once prepared, the obtained nanofibers were characterized for their swelling and deswelling capabilities (par. 6.7, 7.5, 8.5), demonstrating their suitability as supports for the controlled release of organic solvents, with a practical application on a XVI-century wood artwork also explored (Ch 8).

Subsequently, to obtain advanced tools for artwork disinfection, metal nanoparticles (par. 2.3) were employed. While literature demonstrates the antimicrobial activity of nanoparticles, their direct application and transport onto an artwork is problematic. This Thesis explored the idea of creating nanocomposite mats to make the application and veiculation of these metal nanoparticles easier and safer. As described in Chapter 9, gold (Au) and silver (Ag) nanoparticles were synthesized ad-hoc via a green, polysaccharide-mediated approach. These were then electrospun with Agar to create nanocomposite mats (Ch 10), which were characterized for their effective antimicrobial activity.

In parallel, an advanced tool for sustainable biocleaning (par. 1.4) was developed. While literature confirms biocleaning is a highly advantageous and gentle method, its practical application suffers from high costs and complex logistics; for each application, a fresh bacterial suspension and a carrier medium must be prepared. To solve this, Chapter 11 explores the development of electrospun PCL mats as bacterial carriers. The idea is to create an easy-to-use, less expensive tool that allows bacteria to remain viable over time, enabling these membranes to be prepared and stored for several months before use. The mats were assessed for their ability to promote bacterial adhesion and maintain viability.

Beyond single-layer systems, the other target of this Thesis work consisted in the development and optimization of an advanced multilayer system. While Agar mats are effective, they can lack mechanical robustness. To overcome this, poly(caprolactone) (PCL) was selected to increase the mechanical properties of the final tool. As examined in paragraph 7., an Agar layer was directly electrospun on a PCL layer, hence obtaining a robust bilayer structure suitable for conservation tasks.

This Thesis work demonstrated a simple and novel methodology for the development of stable biopolymer-based nanofibrous mats capable of effectively acting as controlled cleaning tools, disinfection systems, and supports for sustainable biocleaning.

However, the preparation of such products for widespread use by conservators requires optimization. As such, the likewise future path of the present Thesis project aims to develop practical systems through the following steps: i) Optimization of high-production-rate electrospinning procedures; ii) Use of various cleaning agents, enzymes, and bacteria and evaluation of their release and activity kinetics; iii) In situ experimentation on a wider range of real artworks and substrates; iv) Development of actual prototypes for use by conservators.

Table of Contents

THEORETICAL PART

Chapter 1.
Cleaning Procedures in Cultural Heritage Restoration

1.1 Introduction

The conservation and restoration of cultural property is a discipline predicated on the ethical stewardship of irreplaceable resources[1,2]. Within the spectrum of conservation activities, which range from preventive care to major interventive treatments, the cleaning of artifacts constitutes one of the most critical, complex, and contentious procedures[3–5]. It is an intervention that fundamentally alters the object, and because it is an inherently subtractive and irreversible process, it is an operation inherently associated with the risk of inducing irreversible deterioration[4]. The removal of any material from an artifact's surface, be it accumulated atmospheric deposits, a chromatically altered varnish, or a previous restoration layer, is a decision that permanently modifies its physical and historical composition. This reality places cleaning at the center of a profound ethical paradox. While a core tenet of modern conservation is the principle of reversibility—the ideal that any additive intervention should be removable without damaging the original object—cleaning is, by its very nature, irreversible[6]. This fundamental conflict elevates the decision to clean from a purely technical consideration to one of significant ethical gravitas, demanding a rigorous framework of guiding principles to navigate its complexities[7].

The modern practice of conservation cleaning is governed by a strict set of ethical guidelines designed to safeguard the authenticity and integrity of the cultural asset[8]. These principles form the bedrock upon which all subsequent technical decisions are made:

i) *Minimal Intervention*: This principle dictates that conservators should perform only the minimum necessary actions to stabilize the object and ensure its long-term preservation. It is a direct departure from earlier restoration philosophies, such as the "scrape" methodology advocated by architects like Viollet-le-Duc in the 19th century, which sought to restore a structure to an idealized, often historically inaccurate, state of stylistic unity. Instead, minimal intervention prioritizes the retention of the object's constituent information and historical layers, avoiding unnecessary physical stress[9].

ii) *Compatibility:* All materials and products introduced during a cleaning procedure must be physically and chemically compatible with the original constituent materials of the artwork. The careful selection of cleaning agents is paramount to prevent damage, such as the etching of carbonate-based stone by acidic solutions or the swelling of paint binders by inappropriate solvents[10].

iii) *Respect for the Original (Authenticity and Integrity):* These principal mandates that no intervention should falsify, invent, or obscure the original work as conceived by the artist. It requires a profound respect for the object's history, including the subtle changes it has undergone over time. This includes the concept of "patina," the superficial layer that forms

over time, which can be considered an integral part of the object's historical narrative and aesthetic character. Cleaning must therefore negotiate a delicate balance between removing detrimental accretions and preserving these historically significant layers.

iv) *Reversibility:* This principle requires that materials and techniques used should be removable without causing damage to the original artifact. This is achieved through the careful selection of compatible and reversible materials. While cleaning itself is irreversible, any materials added during the broader restoration process should adhere to this standard[10].

v) *Recognition:* The intervention must be distinguishable from the original material without disrupting the overall aesthetic legibility and longevity of the work. For volumetric or chromatic reintegrations, the chosen techniques must restore the work's aesthetic coherence while ensuring that the restored areas are identifiable upon close inspection[8,10,11].

The Purpose and Importance of Cleaning

The justification for undertaking such a high-risk, irreversible procedure lies in its multifaceted role as a remedial conservation act, a means of restoring aesthetic and intellectual access to the artwork, and a necessary step for disinfection. From a conservation perspective, cleaning is often essential for the physical stabilization of an object[12]. Accumulated surface layers are not inert; they can be chemically and physically damaging. Atmospheric pollutants can be acidic, hygroscopic particulate matter can attract moisture, and biological growths can actively degrade the substrate. The removal of these harmful compounds, including the elimination or inhibition of microbial colonization (disinfection), is a necessary step to arrest or retard ongoing deterioration processes[12]. This is because microorganisms can cause not only aesthetic alterations but also severe physical and chemical degradation of the materials[13].

Beyond stabilization, cleaning aims to restore the legibility of the artwork, allowing it to be properly appreciated, understood, and utilized. A heavily discolored varnish or a thick layer of grime can obscure the artist's composition, color palette, and fine details, effectively rendering the work incomprehensible[12]. In this sense, cleaning is an act of revelation, intended to re-establish the aesthetic value and meaning of the piece. However, the concept of legibility is not an objective, absolute standard. Rather, it is a culturally and historically contingent ideal. The "scrape" versus "anti-scrape" debate of the 19th century illustrates two diametrically opposed views on what constitutes a legible historic building[2]. As the critic Antonio Paolucci has argued, the restorer inevitably reveals "exactly that which is sought in a given moment in history"[1]. This implies that every major cleaning campaign is an interpretation, reflecting the aesthetic tastes and scholarly priorities of its era. The goal is not to return the object to a pristine "new" state, but to a point where its intended message can be perceived without the interference of disfiguring and damaging accretions. This inherent subjectivity underscores the absolute necessity of thorough documentation, which records not only the materials and methods used but also the philosophical rationale behind the intervention for the benefit of future generations who may hold different values[1,2].

To navigate this complexity, the modern paradigm demands a rigorous scientific approach[14]. An intervention must begin with a comprehensive examination and analysis of the artwork to understand its material composition, its state of conservation, the nature of the layers to be removed, and any previous restoration work. This diagnostic phase, which employs techniques ranging from

microscopy to various forms of spectroscopy, is crucial for selecting a cleaning system that is both effective and compatible with the unique needs of the object.

Evolution of Cleaning Methodologies

The history of cleaning cultural heritage mirrors the evolution of the conservation field itself, marking a clear trajectory from craft-based, often empirical practices to a scientifically grounded and ethically informed discipline[14]. Historically, cleaning methods were rudimentary and frequently deleterious, employing materials ranging from plant matter to caustic chemical agents like ammonia and spoiled wine to remove grime and varnish[15]. The Industrial Revolution introduced powerful new chemical agents like bleach and synthetic detergents, but their application was often indiscriminate and lacked a scientific understanding of their long-term effects on delicate art materials[15].

The 20th century witnessed the professionalization of conservation and a growing recognition of the need for more controlled and less invasive methods[7]. This period saw the development and refinement of the traditional mechanical and chemical techniques that form the basis of the modern toolkit. However, this evolution has been marked by a recurring pattern of technological adoption followed by the subsequent identification of damage. Aggressive methods like sandblasting and high-pressure washing were initially lauded for their efficiency before their capacity for irreversible surface erosion was fully understood. Similarly, the widespread use of certain powerful organic solvents led to unforeseen long-term consequences for the stability of paint binders.

This history of unintended consequences has fostered a deep-seated caution within the field and has been a primary driver for innovation. The contemporary "green conservation" paradigm has emerged from this context, seeking to develop and implement cleaning protocols that are safer for the artwork, the conservator, and the environment. This approach champions the use of less toxic "green solvents," microemulsions, and entirely new categories of cleaning systems. Innovative technologies such as precisely controlled lasers, gel delivery systems, and highly selective biocleaning methods using microorganisms or enzymes now constitute the cutting edge of conservation science, offering promising alternatives to the excessive use of harmful and invasive traditional products[16]. These advancements represent a fundamental shift in philosophy: from the application of non-selective, methods to the precise and selective targeting of unwanted layers with minimally invasive tools.

1.2 Traditional methods

Traditional cleaning methods, encompassing a wide range of mechanical and chemical techniques, constitute the foundational methodologies available to the conservator-restorer (Table 1)[17,18]. While some of these methods have been used for centuries, their modern application is guided by a scientific understanding of their mechanisms and a strict adherence to the principle of minimal intervention. They are often employed as initial interventive options, particularly for the removal of superficial and loosely bound soiling matter, or in situations where more advanced systems are unnecessary or inappropriate.

Mechanical Cleaning

Mechanical cleaning involves the physical dislodgement and removal of extraneous material from a substrate[17]. The choice of method is dictated by the nature of the substrate, the type of soiling, and

the fragility of the object. These techniques can be broadly categorized by their level of aggressiveness.

For the most delicate surfaces, the initial step is often the removal of loose dust and particulate matter. This is crucial because such particles can be abrasive and can become irreversibly embedded in the substrate if aqueous or solvent-based treatments are applied first. Gentle methods include[17,18]:

- *Air Puffers and Brushes*: Soft-bristled brushes (e.g., goat hair) and air bulbs are used to gently dislodge and move dust from a surface. This technique must be used with extreme care, as even light brushing can abrade a fragile surface or catch on areas of raised paint (impasto), and some paintings may have micro-flaking paint that is not immediately visible but can be swept away.
- *Controlled Vacuuming*: For more robust objects like textiles, a vacuum cleaner with a high-efficiency particulate air (HEPA) filter and variable suction control is often used. To prevent the loss of any original fibers or fragments, a piece of fine mesh or screen is always placed over the vacuum nozzle. Micro-attachments can provide more precise control for localized cleaning.
- *Specialized Sponges and Erasers*: For more adherent surface grime, specialized dry-cleaning materials are employed. Vulcanized rubber sponges (chemical sponges) are effective for removing soot from surfaces after fires. For paper artifacts, a variety of erasers are used, typically made of vinyl (polyvinyl chloride), factice (vulcanized vegetable oil), or rubber. These can be used in block form or grated into fine crumbs for a gentler, more controlled application. However, their use carries risks, including abrasion of the paper surface, compression of paper fibers, and the potential to leave behind chemical residues (e.g., plasticizers, sulfur) that could be detrimental in the long term.

Historically, more aggressive mechanical methods have been used, primarily in architectural restoration[10]. While their application is now highly restricted due to their potential for causing irreversible damage, refined versions of these techniques are still employed under specific, controlled circumstances.

- *Abrasive Blasting*: This technique involves the projection of particulate media at a surface to effectuate the removal of superficial layers via abrasion[19–21]. Traditional sandblasting is exceptionally harsh and can severely pit and erode stone, brick, and metal surfaces. This has led to its general rejection for most heritage applications. However, modern variations offer more control and use gentler media. Soda blasting, which uses sodium bicarbonate, is effective for removing paint and grime while also neutralizing surface acids. Walnut shell blasting provides a gentle, biodegradable option for cleaning without significant abrasion. Dry ice blasting is a non-abrasive method where frozen carbon dioxide pellets sublimate on impact, lifting contaminants without harming delicate surfaces like intricate stonework. Despite these refinements, all abrasive methods carry a risk of altering the original surface texture and must be carefully tested and controlled by skilled professionals.
- *Pressure Washing:* The use of high-pressure water jets is a common industrial cleaning method but is extremely dangerous for historic materials[22]. High pressure can cause cracking, chipping, and delamination, and can force water deep into porous substrates like historic brick,

limestone, or wood, leading to salt migration, freeze-thaw damage, and biological growth. Modern conservation practice has therefore shifted to low-pressure hydrokinetic cleaning, which operates on fundamentally different principles. This technique uses very low pressures, typically between 100 and 400 PSI, which is significantly lower than the thousands of PSI used in commercial power washing[23,24]. It is combined with precise control over water temperature (warm, not hot), the use of wide-angle fan-tip nozzles to distribute the force and maintaining a safe standoff distance from the surface. When properly applied by a trained conservator, gentle washing can be an effective method for removing biological growth and atmospheric soiling from robust architectural materials.

Chemical and Aqueous Cleaning

Chemical cleaning utilizes liquid agents to affect the solubilization, swelling, or dispersion of undesirable surface materials[25,26]. This approach requires a sophisticated understanding of chemistry, as the potential for damaging the original artwork is significant.

Solvent-Based Cleaning

Organic solvents are the primary tools for removing aged and discoloured varnishes, old overpaints, and other polymeric coatings[25,27]. The selection of a solvent is based on the principle of "like dissolves like," often guided by tools like the Teas solubility triangle. The goal is to find a solvent or solvent mixture that will effectively dissolve the target layer without affecting the original paint layer beneath. This selectivity is the greatest challenge. Many 19th-century paintings, for example, contain additives in the oil paint that can cause the surface to swell or wrinkle when exposed to certain solvents. Furthermore, the artist may have incorporated the varnish into the painting process itself, making it physically and chemically indistinguishable from the final paint glazes. The toxicity of most organic solvents is also a major concern, requiring strict health and safety protocols to protect the conservator.

Aqueous Systems

Water is a powerful and versatile solvent, but its use on cultural heritage must be carefully controlled[28,29]. It is often modified with other chemical agents to create tailored cleaning solutions for removing surface grime.

- *pH-Adjusted Solutions*: The acidity or alkalinity of a water-based solution can be adjusted to enhance its cleaning power. Working at a slightly alkaline pH can be effective for removing oily grime, while an acidic pH may be safer for certain sensitive paint layers. However, the risks are substantial: acidic solutions can permanently etch acid-sensitive stones like limestone and marble, and alkaline solutions can damage certain pigments or binders.
- *Chelating Agents:* Chelators, such as citric acid, are molecules that can form strong bonds with metal ions. They are used to remove metallic stains, such as copper or iron corrosion products. The risk lies in their lack of specificity; a chelator that removes a copper stain might also interact with copper-based pigments (e.g., azurite, malachite) in the original paint, causing irreversible color changes.
- *Surfactants[30]:* Surfactants, or detergents, are molecules that have both a water-loving (hydrophilic) and an oil-loving (lipophilic) part. This structure allows them to break up and lift oily, greasy grime from a surface and disperse it into the water, allowing it to be wiped

away. While effective, they can leave residues that are difficult to remove and may negatively interact with the oil-based binders in paintings over the long term.

Poultices

The poultice represents a significant refinement in the application of liquid cleaning agents and is a direct conceptual forerunner to modern gel systems[29]. A poultice is a composite material comprising a liquid cleaning agent (water, a solvent, or an aqueous solution) absorbed within an inert, solid matrix, such as clay (e.g., sepiolite), cellulose powder, or cotton fibers, to form a paste. This paste is then applied to the surface of the object. The poultice serves several critical functions: it localizes the cleaning agent to a specific area, it slows the rate of evaporation, allowing for a longer and more controlled dwell time, and as the liquid evaporates, it wicks the dissolved soil and cleaning agent back out of the substrate and into the poultice material, which is then physically removed. This method offers far greater control than the simple application of a free liquid with a swab or brush, representing an important evolutionary step toward the scientifically engineered delivery systems used today.

Table 1- Traditional Cleaning Methods

Method	Mechanism	Typical Applications	Advantages	Critical Disadvantages/Risks
		Gentle Mechanical		
Dry Dusting/Brushing	Physical dislodging of loose particulates.	Initial removal of surface dust from paintings, textiles, paper, objects.	Non-invasive; no chemicals used; simple to perform.	Risk of abrasion on fragile surfaces; can snag on raised paint; may remove micro-flaking paint.
Controlled Vacuuming	Suction removal of particulates.	Cleaning of robust textiles, upholstery, and some objects.	Efficient for removing loose dirt from porous surfaces; controlled suction reduces risk.	Not suitable for friable or flaking surfaces; requires protective screen to prevent loss of original material.
Erasers/Sponges	Frictional and adhesive removal of surface grime.	Reducing surface soil on paper, parchment, and some unvarnished paint surfaces.	Targeted removal of ingrained dirt; more effective than simple dusting.	High risk of abrasion; can alter surface texture; may leave chemical residues (plasticizers, sulfur).

		Aggressive Mechanical		
Low-Pressure Washing	Low-pressure water flow (100-400 PSI) to remove soiling.	Cleaning of architectural stone and masonry.	Effective for removing biological growth and atmospheric pollutants from robust surfaces.	Risk of driving water into porous materials; can cause damage if pressure is too high or substrate is fragile.
Micro-Abrasive Blasting	Projection of fine, gentle media to abrade surface layers.	Architectural cleaning; removal of corrosion or tough coatings.	More controlled than sandblasting; can be effective on hard-to-clean layers.	Inherently abrasive; always causes some degree of surface loss; risk of altering original texture and detail.
		Chemical/Aqueous		
Solvent Swabbing	Dissolution of surface layers with organic solvents.	Varnish removal from paintings; removal of old adhesives and overpaints.	Highly effective for dissolving specific polymers.	Low selectivity (can damage original paint); toxic to conservator; solvent can penetrate and swell underlying layers.
Aqueous Solutions	Use of water, often with pH modifiers, chelators, or surfactants.	Removal of surface dirt and grime from paintings and other surfaces.	Can be tailored to specific types of dirt; often less toxic than organic solvents.	Water can damage sensitive materials; additives (acids, bases, chelators) can be non-selective and damage pigments/substrates.
Poulticing	Application of a cleaning liquid within an absorbent solid matrix.	Deep cleaning of porous materials like stone; localized stain removal.	Localizes cleaning agent; slows evaporation for longer contact time; draws dissolved dirt out of the substrate.	It can be difficult to apply and remove completely; risk of leaving matrix material behind.

1.3 Gels

The development of gel-based cleaning systems represents one of the most significant advances in modern conservation science[31,32]. Gels mitigate a primary limitation of free-liquid cleaning systems: the lack of control over solvent delivery and penetration. By entrapping the liquid phase within a

three-dimensional polymeric matrix, gels provide conservators with unprecedented command over the location, dwell time, and penetration of the active agent, thereby enhancing both the efficacy and safety of the treatment. This transition marks a critical shift in conservation practice, moving from a primary focus on the chemistry of the *solvent* to a more sophisticated manipulation of the material science of the *delivery system*[31]. The conservator's role expands from that of a chemist selecting a reagent to that of a materials scientist designing a tailored vehicle for its application.

1.3.1 Classification

The diverse range of available gel systems necessitates a systematic classification to understand their properties and appropriate applications. Gels can be categorized based on several key criteria, including the nature of their internal network, the type of liquid they contain, and their physical form (Table 2)[33–37].

Classification by Network Structure

The fundamental distinction between gel types lies in the nature of the cross-links that form the polymer network[34,38]:

- *Physical Gels*: These networks are formed by reversible, non-covalent interactions such as hydrogen bonds, ionic interactions, van der Waals forces, or simple polymer chain entanglements. Because these bonds are transient, physical gels can often be dissolved or melted. This category includes many materials derived from natural sources, such as polysaccharides (e.g., Agar, Gellan gum, xanthan gum) and cellulose ethers (e.g., Klucel, carboxymethylcellulose). Physical gels can be further subdivided based on the strength of their internal associations:
    - *Strong Physical Gels*: Formed by robust interactions, such as the double-helix structures in Agar and Gellan gum, which create semi-rigid, often peelable films that can be handled as solid slabs.
    - *Weak Physical Gels*: Formed by weaker chain entanglements, resulting in viscous, paste-like materials such as those made with xanthan gum or cellulose ethers.
- *Chemical Gels*: These networks are formed by permanent, covalent cross-links between polymer chains. This robust structure gives them high internal cohesion and mechanical strength. A significant advantage of chemical gels is that they are generally insoluble and swell in the cleaning liquid, which greatly reduces the risk of leaving polymer residues on the treated surface. Prominent examples in conservation include poly(acrylic acid) (PAcA, often sold as Carbopol), polyvinyl alcohol cross-linked with borax (PVA-B), and poly(2-hydroxyethyl methacrylate) (pHEMA).

Classification by Confined Liquid

Gels are also defined by the type of solvent phase they entrap[35]:

- *Hydrogels*: The vast majority of gels used in conservation are hydrogels, in which the polymer network is expanded by water or an aqueous solution containing active agents like buffers, chelators, or surfactants.
- *Organogels*[39–42]: These are systems where the confined liquid is a non-aqueous organic solvent or solvent mixture. Organogels are specifically designed for the removal of non-polar materials, such as aged varnishes, waxes, or synthetic polymer coatings, from solvent-sensitive surfaces.

Classification by Physical form

The practical application of a gel is largely determined by its physical and rheological properties[43]:

- *Rigid or Peelable Gels*: Materials like Agar, Gellan gum, and certain PVA formulations form stiff, self-supporting slabs. These can be precisely cut to the shape of the area to be treated, applied, and then lifted or peeled off in a single piece after the treatment. Their primary advantage is the minimal risk of leaving residues.
- *Soft or Paste-like Gels*: Thickeners like cellulose ethers and Carbopol form soft, viscous pastes that are typically spread onto the surface with a brush or spatula. While their soft consistency allows them to conform well to highly textured surfaces, they carry a much higher risk of leaving polymer residues embedded in the pores and texture of the artwork, sometimes necessitating the use of a barrier layer (e.g., Japanese paper) or extensive rinsing for clearance.

1.3.2 Properties

The performance of a gel in a conservation treatment is governed by a set of interconnected physicochemical and mechanical properties. The ability to tune these properties by adjusting the gel's formulation is what makes these systems so versatile (Table 2)[44].

Solvent Retention and Release Kinetics

A gel's primary function is to act as a reservoir for the cleaning liquid, controlling its delivery to the substrate[45]. The three-dimensional network drastically reduces the rate of solvent evaporation compared to a free liquid, allowing for longer, more effective working times. It also limits the uncontrolled penetration of the liquid into the porous structure of the artwork via capillary action, preventing issues like the swelling of paint layers or the formation of tidelines on paper. The retentiveness and release rate are highly tunable; for instance, a higher concentration of polymer in the gel network generally leads to a denser structure that releases the solvent more slowly[46]. Conversely, a lower polymer concentration allows for a greater release of the aqueous and organic phase and can lead to more effective cleaning. This allows the conservator to precisely calibrate the amount of moisture or solvent delivered to a sensitive surface[47].

Mechanical Properties

The physical behavior of the gel is critical for both its application and its safe removal. There is a fundamental and inherent trade-off in gel design between handling characteristics and surface conformability. No single gel formulation is ideal for all scenarios, and the choice of system must be carefully matched to the topography of the artwork[48].

- *Rigidity vs. Flexibility:* Rigid gels, such as those made from Agar, are lauded for their ease of handling and clean removal, which minimizes residue[49]. This makes them exceptionally well-suited for treating flat surfaces like paper or panel paintings. However, this same rigidity becomes a significant liability on uneven, textured, or rough surfaces—such as a painting with heavy impasto or a carved stone relief—where the gel cannot achieve the intimate and complete contact necessary for uniform and effective cleaning.
- *Softness and Elasticity:* To address the challenge of textured surfaces, softer and more elastic gels have been developed. Formulations based on konjac glucomannan or specialized twin-chain polyvinyl alcohol (PVA) networks exhibit high flexibility, allowing them to conform perfectly to complex surface topographies[50,51]. This ensures better cleaning efficacy but can come at the cost of being more difficult to handle and potentially having a higher risk of tearing or leaving fragments behind upon removal. This trade-off has been a major driver of research into advanced network architectures that seek to combine mechanical robustness with high flexibility.
- *Internal Cohesion and Tensile Strength:* For a gel to be considered "peelable," it must possess high internal cohesion and sufficient tensile strength to be lifted from a surface without fragmenting. Chemical gels, with their permanent covalent cross-links, typically exhibit superior cohesive strength compared to many physical gels[52].

Adhesion and Residue

The potential for leaving residues is a paramount concern in any gel-based treatment. Fragments of the polymer network or individual polymer chains left on or within the porous structure of an artwork could alter its optical properties, attract dirt, and have unforeseen and potentially detrimental chemical effects over the long term. The development of highly cohesive, non-adhesive, peelable gels—both physical (e.g., Gellan gum) and chemical (e.g., Nanorestore Gels®)—represents a major effort to mitigate this risk, aiming for systems that can be removed completely and cleanly after use[53].

Architecture and three-dimensional polymer network

The macroscopic properties of a hydrogel, its stiffness, water retention, and cleaning efficacy, are a direct consequence of its molecular-level architecture. Understanding this structure-property relationship is key to the rational design of new and improved gel systems for conservation[44,52].

A hydrogel consists of hydrophilic polymer chains that are linked together, either physically or chemically, to form a continuous, three-dimensional network that is swollen with water. This network is the fundamental structural unit of the gel. The identity of the polymer dictates the basic chemistry of the system. In natural hydrogels, this framework may be built from the polysaccharide chains of Agar or Gellan gum, which self-assemble into stable double-helical structures that then aggregate to form the network. In synthetic hydrogels, the network is composed of polymer chains like polyvinyl alcohol (PVA) or poly(acrylic acid) (PAcA), which can be cross-linked via chemical bonds or established through physical associations.[50,54].

Porosity and Mesh Size

The arrangement of these polymer chains in three-dimensional space creates a structure with interconnected interstitial pores or channels that hold the water molecules. The average size of these

pores is referred to as the mesh size. This architectural feature is critically important to the gel's function. The mesh size determines the gel's total water-holding capacity, governs the diffusion rate of water and any dissolved cleaning agents out of the gel and onto the artwork, and controls the ability of the gel to absorb and trap solubilized dirt and degradation products from the surface. A gel with a larger, more interconnected porosity will generally release its contents more quickly and have a greater capacity to absorb unwanted materials[55].

Influence of Molecular Structure on Macroscopic Properties

The ability to design hydrogels with specific properties stems from the ability to control their molecular architecture during formulation[33,34,44,56]:

- *Cross-linking Density:* The number of cross-links per unit volume of the gel is a primary control parameter. Increasing the cross-linking density brings the polymer chains closer together, resulting in a smaller mesh size. This typically leads to a mechanically stiffer and more brittle gel that swells less and releases its entrapped solvent more slowly.
- *Polymer Concentration:* Similarly, increasing the concentration of the polymer used to make the gel results in a denser network with more polymer chains per unit volume. This also reduces the average mesh size, which can increase the gel's rigidity and decrease its rate of water release.[33] For example, an Agar gel at 1% concentration will act as a "free water reservoir," releasing water readily, while a 3% or 5% Agar gel will be much more retentive.
- *Advanced Network Topologies:* The frontier of gel design for conservation involves creating more complex network architectures to achieve unique combinations of properties. Interpenetrating Polymer Networks (IPNs) are formed by intertwining two or more distinct polymer networks that are not covalently bonded to each other. For example, a Xanthan-Konjac-Agar (XKA) mixed gel combines the elastic network of xanthan-konjac with the more brittle network of Agar to create a material with enhanced mechanical properties. Another advanced approach is the formulation of twin-chain networks, which combine polymers of different chain lengths (e.g., a mix of long-chain and short-chain PVA). This has been shown to disrupt the regular packing of the polymer chains, transforming the gel's internal structure from one of elongated channels to a more open, sponge-like pattern of interconnected pores. This modified architecture results in a gel that is simultaneously highly flexible, mechanically robust, and more effective at capturing and retaining dirt, representing a significant step towards creating the ideal cleaning tool. A further refinement involves confining nanostructured fluids (NSFs), such as oil-in-water microemulsions, within a highly retentive hydrogel scaffold. This double confinement allows for the controlled removal of solvent-sensitive materials, as the organic solvent is contained first within nanodroplets and then within the gel network, preventing its uncontrolled spread into the underlying artwork.

Table 2- Classification and Properties of Gels in Conservation

Gel Type	Polymer Base	Network Type	Typical Form	Key Properties	Primary Conservation Applications
Agar / Agarose	Polysaccharide	Strong Physical (Double Helix)	Rigid, Peelable	Brittle; good water retention; requires heating to prepare; poor conformability to rough surfaces.	Cleaning paper and parchment; local humidification; poulticing on flat surfaces.
Gellan Gum	Polysaccharide	Strong Physical (Double Helix)	Rigid, Peelable	Less brittle than Agar; forms clear gels; high internal cohesion; requires cations for gelling.	Controlled cleaning and humidification of paper; adhesive removal.
Xanthan Gum	Polysaccharide	Weak Physical (Entanglement)	Soft, Viscous Paste	High viscosity; shear-thinning (becomes fluid under stress); can be used to create emulsions.	Thickener for aqueous solutions; formulation of solvent emulsions for cleaning paintings.
Cellulose Ethers (e.g., Klucel)	Polysaccharide Derivative	Weak Physical (Entanglement)	Soft, Viscous Paste	Can be dispersed directly in water or some organic solvents; high risk of leaving residues.	Thickener for aqueous solutions and organic solvents (organogels); poulticing.
Poly(acrylic acid) (PAcA / Carbopol)	Synthetic Polymer	Chemical (via neutralization)	Soft, Viscous Paste	Forms clear, viscous gels when neutralized with a base; requires amines for	Basis for Wolbers' solvent gels; removal of aged varnishes from paintings.

				gelling in organic solvents.	
Polyvinyl Alcohol-Borax (PVA-B)	Synthetic Polymer	Chemical (Dynamic Covalent)	Elastic, Peelable	Non-sticky; highly flexible; can incorporate a range of organic co-solvents; good mechanical strength.	Removal of varnishes and coatings from paintings, including modern and sensitive surfaces.
pHEMA / Nanorestore® Gels	Synthetic Polymer	Chemical (Covalent)	Elastic, Peelable	High internal cohesion; very high solvent retention; flexible and tear-resistant; minimal residue.	Controlled cleaning of highly water-sensitive surfaces (easel paintings, paper); delivery of microemulsions.

1.4 Biocleaning

Biocleaning represents a paradigm shift in conservation, transitioning from conventional physical and chemical interventions towards the application of controlled biological processes for the removal of unwanted substances[57]. This "green" biotechnology utilizes the specific metabolic pathways of viable microorganisms or the catalytic precision of their isolated enzymes to target and degrade specific materials on an artwork's surface (Table 3)[58,59]. The approach is characterized by its remarkable selectivity, minimal invasiveness, and environmental sustainability, offering a gentle yet powerful alternative to traditional methods that often carry the risk of collateral damage to the artwork. This methodology can be seen as the ultimate expression of the principle of minimal intervention, as it employs a biological system for targeted substrate degradation that is inherently self-limiting and exquisitely substrate specific. Rather than relying on the conservator's manual action or a broad-spectrum solvent, biocleaning employs a targeted biological process that, in theory, knows precisely what to remove and when to stop[60].

1.4.1 Microorganism-Based Cleaning

This technique involves the direct application of viable, non-pathogenic microorganisms to an altered surface. The selected bacteria or fungi utilize the unwanted deposit, such as sulfate crusts, nitrate efflorescence, or aged organic matter, as a nutrient source, effecting its metabolic conversion into benign byproducts[61–63].

The selection of the appropriate microorganism is the most critical step. Strains are chosen for their specific metabolic capabilities and must be rigorously screened to ensure they are non-pathogenic (Biosafety Level 1) and will not cause any secondary biodeterioration of the original artwork[57]. Commonly employed microorganisms include:

- *Sulfate-reducing bacteria*, such as *Desulfovibrio desulfuricans* and *Desulfovibrio vulgaris*, which are used to remove the black gypsum crusts ($CaSO_4$ $2H_2O$) that form on stone monuments in polluted urban environments.
- *Nitrate-reducing bacteria*, most notably *Pseudomonas stutzeri*, which are highly effective at removing nitrate salt efflorescence from frescoes and mural paintings.
- Other bacteria and yeasts, such as *Bacillus subtilis* and *Saccharomyces cerevisiae*, have also been successfully used to remove various organic and inorganic deposits.

For application, the microbial cells are typically immobilized at a high concentration within a delivery system, such as a poultice made of sepiolite clay or a carbogel, to create a "micro-pack". This immobilization matrix provides the moisture and nutrients essential for the microorganisms' metabolic activity, localizes their action, and facilitates easy application and removal. The micro-pack is applied to the surface and left in place for a period ranging from a few hours to overnight, after which it is removed, and the surface is gently rinsed. For particularly water-sensitive substrates, an innovative "dry biocleaning" technique has been developed, which uses dehydrated powdered yeast cells that are activated by ambient humidity, thereby avoiding the introduction of liquid water.

Several high-profile case studies have demonstrated the efficacy of this approach. A notable example is the successful bio-cleaning of Michelangelo's marble sarcophagi in the Medici Chapels in Florence. The procedure used specific bacterial strains to selectively remove centuries-old deposits composed of gypsum, calcium oxalates, phosphates, and proteins, achieving a gradual and controlled cleaning that was respectful of the delicate marble surface. Similarly, *Pseudomonas stutzeri* has been used to remove darkened layers of animal glue from 14th-century frescoes at the Camposanto Monumentale in Pisa, a problem that had proven intractable with traditional methods.

In this Thesis, two new strains in these applications were tested as biocleaning and potential disinfection agents. Following an analysis of the species and strains, their metabolic characteristics and potential applications in cultural heritage are detailed below.

Bacillus subtilis ATCC 6633[64–68]

The strain ATCC 6633, historically classified as Bacillus subtilis but recently reallocated to the species Bacillus spizizenii (or B. subtilis subsp. spizizenii) based on phylogenomic Average Nucleotide Identity (ANI) analyses, represents a Gram-positive, spore-forming model organism defined by its exceptional capacity for the secretion of bioactive secondary metabolites and hydrolytic enzymes. In the context of cultural heritage, this strain functions as a versatile "metabolic factory" capable of producing a broad spectrum of extracellular hydrolases essential for the removal of complex organic residues. Its robust secretion of thermostable α-amylases (encoded by amyE) allows for the targeted hydrolysis of α-1,4-glycosidic bonds in starch pastes used in historical relining, while its production of serine proteases, particularly subtilisins (encoded by aprE), effectively degrades polymerized animal glues and casein-based fixatives often found in historical restorations. Beyond these primary hydrolytic functions, the strain exhibits carboxymethyl cellulase (CMCase) activity, facilitating the gentle degradation of cellulose-based deposits such as paper pulp residues, and produces lipases capable of hydrolyzing fatty acid esters. This lipolytic trait, combined with the synthesis of the potent biosurfactant surfactin (via the srfAA operon), enables the emulsification and removal of aged oily varnishes, waxes, and hydrophobic grime from artwork surfaces. Furthermore,

the strain exhibits a unique "dry biocleaning" potential due to the synergistic action of surfactin—which lowers interfacial tension to emulsify contaminants—and its antifungal cyclic lipopeptides (fengycins and iturins). These metabolites, alongside the production of chitinases that degrade the cell walls of fungi, disrupt the membranes of common heritage biodeteriogens like Aspergillus niger and Penicillium spp., providing a dual action of cleaning and preventative biological control.

Pseudomonas stutzeri ATCC 17588[69–73]

The strain ATCC 17588, the type of strain for the species widely known as *Pseudomonas stutzeri* (recently proposed for reclassification as *Stutzerimonas stutzeri*), is a Gram-negative, facultative anaerobe distinguished by its respiratory plasticity and complete denitrification pathway. Unlike the fermentative metabolism of *Bacillus*, this organism's primary utility in conservation lies in its dissimilatory nitrate reduction capability, encoded by the *nar*, *nir*, *nor*, and *nos* gene clusters. This genomic completeness ensures the total reduction of nitrate salts (NO_3^-), a primary cause of stone pulverization and efflorescence, into inert dinitrogen gas (N_2), crucially avoiding the release of intermediate greenhouse gases like nitrous oxide (N_2O) often produced by incomplete denitrifiers. While capable of general metabolic versatility, its enzymatic profile differs significantly from the highly proteolytic strains (such as *P. stutzeri* A29) often selected for animal glue removal; the type strain ATCC 17588 is typically characterized as gelatinase negative or weakly proteolytic, meaning its primary selection in heritage conservation is for salt remediation (desalination) rather than protein hydrolysis. However, it does possess a defining amylase positive phenotype, allowing it to hydrolyze starch, which enables the use of starch-based delivery systems (poultices) as a carbon source to fuel the denitrification process. Additionally, its metabolic profile includes esterase and lipase activities for the breakdown of aliphatic contaminants and the synthesis of high-affinity siderophores (desferrioxamines E and D2) under iron-limiting conditions. This siderophore production facilitates a strategy of competitive exclusion against iron-dependent fungal biodeteriogens, starving them of essential micronutrients without the need for toxic chemical biocides. Its classification as Biosafety Level 1 (BSL-1) and lack of diffusible pigments (unlike *P. aeruginosa*) further solidify its status as the reference organism for safe, deep-structural bio-restoration of stone heritage.

1.4.2. Enzymatic Cleaning

Enzymatic cleaning utilizes isolated enzymes, the proteins that act as catalysts for all biological reactions, to break down specific molecules with unparalleled precision[74–77]. Unlike whole organisms, which have a broad range of metabolic activities, a purified enzyme typically catalyzes only one specific chemical reaction on one specific type of molecule (its substrate). This "lock-and-key" specificity makes enzymatic cleaning one of the most selective methods available to conservators. The action of enzymes is highly dependent on environmental conditions, requiring precise control of pH, temperature, and sometimes the presence of co-factors to achieve optimal activity.

The most common class of enzymes used in conservation are the hydrolases, which break down large polymers by catalyzing hydrolysis[78]. The main types include:

- *Proteases* (e.g., trypsin, pepsin): These enzymes cleave the peptide bonds in proteins. They are used to break down and remove protein-based materials such as aged animal glues, gelatin, and casein binders from overpaints or old repairs.

- *Amylases* (e.g., α-amylase): These enzymes target and hydrolyze the glycosidic bonds in polysaccharides. They are primarily used to remove starch-based adhesives and pastes, which were commonly used for lining paintings and mounting works on paper.
- *Lipases:* These enzymes break down lipids (fats and oils) by hydrolyzing ester bonds. They have proven exceptionally useful for highly selective cleaning tasks, such as the removal of aged oil-based overpaints from an underlying original oil-resin glaze or varnish—a separation that is often impossible to achieve with solvents due to their similar solubility parameters.
- *Cellulases:* This class of enzymes breaks the β-1,4-glycosidic bonds in cellulose and is used in applications requiring the degradation of plant-based materials.

The primary advantage of enzymatic cleaning is its high selectivity. However, the method also has its challenges. Enzymes can be expensive, and their activity requires careful optimization of the application conditions. A significant concern has historically been the complete removal of the enzyme from the artwork after treatment, to prevent any unwanted residual activity. However, studies have shown that thorough rinsing with water is generally effective at removing enzyme residues to negligible levels. To further control their action, enzymes are often applied within a gel matrix, which localizes their activity and facilitates their subsequent removal[79].

Despite its proven efficacy, the widespread adoption of biocleaning, particularly with live microorganisms, faces significant barriers that are as much methodological and logistical as they are technical. Traditional conservation is rooted in hands-on craftsmanship, where the restorer maintains direct, real-time control over the cleaning process. Biocleaning requires a methodological paradigm shift: the conservator must prepare the system, apply the micro-pack, and then relinquish direct control, trusting the biological process to proceed over several hours or days. This requires a different skill set, one more aligned with a microbiology laboratory—involving the preparation of cell cultures, understanding metabolic pathways, and managing viable organisms—than with a typical restoration studio. Coupled with legitimate concerns about the safety and complete removal of living organisms from priceless artifacts, these factors create a substantial hurdle for the broader acceptance of this highly promising technology. For all these reasons it’s important to develop new innovative tools capable of making the practice of biocleaning increasingly safe and widely used.

Table 3- Overview of Biocleaning Agents

Agent Type	Specific Agent	Target Substrate	Mechanism of Action	Notable Applications
Microorganism	*Bacillus subtilis*	Organic matter	Metabolic digestion of proteins, carbohydrates and lipids	Remove of aged animal glue
Microorganism	*Pseudomonas stutzeri*	Nitrates (NO_3^-), Animal Glue	Metabolic reduction of nitrates; enzymatic digestion of proteins.	Removal of salt efflorescence and aged animal glue from frescoes and wall paintings.
Microorganism	*Desulfovibrio desulfuricans*	Sulfates (SO_4^{2-}) (Gypsum Crusts)	Metabolic reduction of sulfates to hydrogen sulfide gas.	Removal of black gypsum crusts from outdoor stone monuments.
Microorganism	*Saccharomyces cerevisiae* (Yeast)	Salts, Pollutants, Organic Deposits	General metabolic activity to remove complex deposits.	"Dry biocleaning" of salts and pollutants from travertine stonework in Rome.
Enzyme	Proteases (e.g., Trypsin)	Proteins (Animal Glue, Casein)	Catalytic hydrolysis of peptide bonds.	Removal of old protein-based adhesives from paper; removal of casein overpaints from tempera paintings.
Enzyme	Amylases (e.g., α-amylase)	Starch (Pastes, Glues)	Catalytic hydrolysis of glycosidic bonds in polysaccharides.	Removal of starch-based lining and mounting adhesives from works on paper and canvas.
Enzyme	Lipases	Lipids (Oils, Fats)	Catalytic hydrolysis of ester bonds in triglycerides.	Selective removal of aged oil overpaints from underlying oil-resin varnishes or glazes.

Chapter 2.
Disinfection Procedures in Cultural Heritage Restoration

The microbial colonization of cultural heritage substrates, including by bacteria, fungi, algae, and lichens, is a major cause of deterioration[13,16]. This process, known as biodeterioration, leads to a range of damaging effects, from aesthetic alterations like staining and discoloration to severe physical and chemical degradation of the substrate. Fungal hyphae can penetrate and weaken materials like stone and wood, while metabolic byproducts such as organic acids can etch and dissolve mineral surfaces. Consequently, the disinfection of artifacts, the elimination or inhibition of any biological growth, is a critical component of conservation treatment. The field of disinfection is currently undergoing a profound "green transition," driven by a growing awareness that traditional biocides, while effective, can cause unacceptable long-term damage to heritage they are meant to protect, as well as posing risks to human health and the environment. This has spurred the development of innovative and more sustainable methods[80].

2.1 Traditional methods

For decades, the primary method for controlling microbial growth on cultural heritage has been the application of broad-spectrum synthetic chemical biocides[81]. This category includes a wide range of synthetic compounds, such as quaternary ammonium compounds (e.g., benzalkonium chloride), aldehydes (e.g., glutaraldehyde, formalin), and phenols.

The main advantages of these traditional biocides are their low cost, wide availability, and high efficacy against a broad spectrum of microorganisms. However, their use is now viewed with increasing skepticism due to several disadvantages[82]:

- *Toxicity:* Most traditional biocides are toxic to humans and harmful to the environment, posing significant risks to conservators during application and contributing to pollution.
- *Lack of Selectivity:* Their broad-spectrum action means they are often not selective for the specific biodeteriogens causing the problem and can react with the constituent materials of the artwork itself.
- *Material Damage:* Repeated application of chemical disinfectants can cause long-term damage to the heritage material, including discoloration, chemical alteration of pigments and binders, and changes to the physical structure of the substrate.
- *Development of Resistance:* The extensive use of these biocides can lead to the evolution of resistant microbial strains, rendering future treatments less effective and potentially favoring the growth of more aggressive biodeteriogens.
- *Low Long-Term Effectiveness:* The protective effect of many biocides is short-lived, requiring frequent reapplication, which exacerbates all the aforementioned risks.

Due to these significant drawbacks, there is a strong and growing consensus in the conservation community to limit the use of traditional biocides and seek safer, more sustainable alternatives.

2.2 Innovative methods

In response to the limitations of chemical biocides, researchers have developed and adapted several innovative disinfection technologies that are less invasive and more environmentally friendly.

Gamma Radiation

Gamma irradiation is a physical disinfection method that uses high-energy photons, typically from a Co60 source, to sterilize artifacts[83]. The radiation penetrates deeply into organic materials like wood, paper, textiles, and leather, and works by inducing irreparable damage to the DNA and other critical cellular components of microorganisms, killing insects, fungi, and bacteria at all stages of their life cycle. A key advantage of this method is that it is a non-contact process that leaves no chemical residues.

Gamma radiation has been used successfully in several large-scale emergencies, such as the disinfection of hundreds of thousands of flood-damaged books at Colorado State University and the treatment of water-damaged historical archives in Japan following a typhoon. It has also been applied to individual objects, such as mold-infested leather gloves from the Nikola Tesla Museum. The dose is tailored to the objective: lower doses (around 0.5–2 kGy) are sufficient for insect eradication, while higher doses (typically 5–25 kGy) are required for effective fungicidal and bactericidal action[84].

Despite its effectiveness, gamma irradiation is considered a treatment of last resort for "desperate circumstances". The high energy that kills microorganisms can also induce radiolytic degradation of the substrate material itself. In cellulosic materials like paper and parchment, gamma rays can cause chain scission, breaking down the polymer structure. This leads to a decrease in mechanical strength, embrittlement, and yellowing. The damage is cumulative and dose-dependent, meaning the decision to irradiate an object must carefully balance the certainty of stopping biodeterioration against the risk of accelerating the material's chemical aging[85].

Essential Oils

An emerging "green" alternative to synthetic biocides is the use of essential oils (EOs) extracted from aromatic plants such as thyme, oregano, lavender, and fennel. EOs are complex mixtures of volatile organic compounds, primarily terpenoids and phenolic compounds (e.g., thymol, carvacrol, eucalyptol), that possess potent, broad-spectrum antimicrobial properties[86–88]. Their mechanism of action is multifaceted, involving the disruption of microbial cell membrane integrity, interference with metabolic pathways, and inhibition of key enzymes[89].

For conservation applications, EOs offer significant advantages. They are natural, biodegradable, and have low toxicity to humans compared to synthetic chemicals. A particularly valuable application method for delicate surfaces like mural paintings is the use of a "micro-atmosphere," where the artifact is placed in a sealed chamber and exposed to the volatile components of the EO without any direct liquid contact. Studies have shown that EOs can be as effective, or even more effective, than some commercial synthetic biocides at inhibiting fungal growth. While EOs represent a highly promising and sustainable path for disinfection, the primary challenge is the need for more extensive

research into their potential long-term effects on the chemical and optical properties of the wide variety of materials found in cultural heritage[89].

2.3 Metal nanoparticles

The application of nanotechnology represents a new frontier in the disinfection of cultural heritage. Metal and metal oxide nanoparticles (NPs), i.e. particles nanometric in size, exhibit potent antimicrobial activity at very low concentrations[90,91]. This allows for the creation of effective and long-lasting antimicrobial treatments and protective coatings with minimal addition of new material to the artifact. Among the most studied are silver (AgNPs) and gold (AuNPs) nanoparticles, which possess distinct mechanisms of action and properties[92,93].

2.3.1 Methods of synthesis

The antimicrobial efficacy of noble metal is highly dependent on their size, shape, and synthesis method, which can be broadly classified into chemical/physical and green approaches[31,94].

- *Chemical Methods:* These "bottom-up" approaches are the most established for producing NPs. Chemical reduction is the most common method, involving the reduction of a metal salt precursor in solution using a chemical reducing agent. For AuNPs, the precursor is typically tetrachloroauric acid ($HAuCl_4$), which is reduced by agents like sodium citrate in the well-known Turkevich method to produce spherical nanoparticles. For AgNPs, silver nitrate ($AgNO_3$) is the most common precursor, reduced by agents such as sodium borohydride, glucose, or sodium citrate. Stabilizing agents are crucial to control particle growth and prevent aggregation. While these methods offer good control over the final product, they often require harsh chemicals and can generate toxic byproducts.
- *"Green" Synthesis:* In line with the trend towards sustainability, green synthesis methods are gaining significant attention. These approaches use biological entities, such as plant extracts (e.g., from olive leaves) or microbial cultures, to mediate nanoparticle formation. The complex mixture of biomolecules (e.g., flavonoids, polyphenols, proteins, sugars) in these extracts acts as both the reducing and stabilizing agent, making the process cost-effective and environmentally friendly.

2.3.2 Antimicrobial mechanisms

Silver Nanoparticles (AgNPs)

Silver nanoparticles are renowned for their broad-spectrum biocidal properties, exhibiting potent antibacterial, antifungal, and virucidal activity[90,95,96]. Their efficacy stems from a multi-pronged attack on microbial cells, making it difficult for microorganisms to develop resistance.

- *Antibacterial Action:* The primary antibacterial mechanisms include:
    - *Ion Release:* AgNPs act as a reservoir, slowly releasing cytotoxic silver ions (Ag+). These ions have a high affinity for sulfur-containing proteins, such as enzymes in the cell membrane or cytoplasm, leading to their denaturation and the disruption of vital processes like cellular respiration.

- *Direct Physical Disruption and Oxidative Stress:* AgNPs can adhere to and accumulate on the microbial cell wall and membrane, altering their structure and permeability. This can lead to the leakage of cellular contents. Furthermore, AgNPs catalyze the production of reactive oxygen species (ROS), which induce severe oxidative stress, causing widespread damage to lipids, proteins, and DNA.

- *Antifungal Action:* AgNPs are also effective fungicides against a range of species relevant to cultural heritage, including *Aspergillus*, *Candida*, and *Penicillium*[97,98]. The antifungal mechanisms are similar to the antibacterial ones and involve:
  - Inhibition of mycelial growth and spore germination.
  - Permeability increase of the fungal cell membrane, leading to the leakage of intracellular components.
  - Induction of morphological damage, such as hyphal shrinkage, distortion, and vacuolation, indicating degradation of cellular and organelle structures.

Gold Nanoparticles (AuNPs)

Gold nanoparticles are generally considered biocompatible and less intrinsically toxic than AgNPs, often exhibiting their antimicrobial effects through different pathways or in synergy with other agents[92,99–101].

- *Antibacterial Action:* While AuNPs can exhibit direct antibacterial activity, they are extensively studied as adjuvants that enhance the efficacy of conventional antibiotics. Their proposed mechanisms include:
  - Generating holes in the bacterial cell wall, which increases membrane permeability and facilitates the entry of other antimicrobial agents.
  - Binding to bacterial DNA, which can inhibit DNA transcription and replication.
  - Reacting with sulfhydryl (-SH) groups of proteins on the cell wall, inactivating transport proteins and disrupting metabolic processes.

- *Antifungal Action:* AuNPs have demonstrated direct antifungal activity, particularly against *Candida* species, and can also act synergistically with antifungal drugs. Their efficacy is often size-dependent, with smaller particles (generally less than 10 nm) showing greater biocidal action. Key antifungal mechanisms include:
  - *Disruption of Membrane Function:* AuNPs can alter the fungal membrane structure by blocking essential protein pumps, such as the H+ ATPase pump, which is vital for maintaining cellular homeostasis in *Candida*. They can also restrict the transmembrane efflux of H+ ions, disrupting the cell's electrochemical balance.
  - *Induction of Oxidative Stress:* Similar to other metal NPs, AuNPs can generate ROS, leading to increased levels of lactate dehydrogenase (LDH) and subsequent cellular disruption and death.
  - *Interference with Cellular Machinery:* AuNPs have been shown to interfere with ribosomal activity, thereby reducing protein synthesis and cell viability.

This combined chemical and physical assault from multiple directions presents a formidable challenge to microbial defence systems, suggesting that nanoparticle-based disinfection could offer a more durable and robust long-term solution to the problem of biodeterioration in cultural heritage.

Chapter 3.
Electrospinning Technique: Principles, Methods, and Applications

3.1 Introduction

The fabrication of fibers has been a cornerstone of human technological development for millennia, evolving from the manual spinning of natural materials like wool and cotton to the sophisticated industrial production of synthetic fibers[102]. Conventional manufacturing techniques such as wet, dry, melt, and gel spinning rely on mechanical forces, such as shearing and drawing, to extrude polymer solutions or melts through spinnerets. While effective for producing fibers with diameters in the micrometer range (typically 10−100 μm), these methods are inherently limited by the extent to which a jet can be mechanically stretched before breaking. Consequently, achieving continuous fibers with diameters consistently in the sub-micrometer or nanometer scale remained a significant challenge. It is in this context that electrospinning emerged as a transformative technology, leveraging electrostatic forces rather than mechanical ones to produce ultrathin, continuous fibers, thereby opening a new frontier in materials science and nanotechnology[103–105].

The fundamental physical principles underpinning electrospinning were observed centuries before the technique was fully realized[106,107]. In 1600, William Gilbert first documented the deformation of a water droplet into a conical shape under the influence of an electric field, a phenomenon now central to the process. This was followed by observations of electrohydrodynamic atomization by Stephen Gray and the first known electrospraying experiments by Abbé Nollet in 1747, who demonstrated that an electrostatically charged vessel could aerosolize water. The theoretical groundwork was further solidified in 1882 by Lord Rayleigh, who mathematically described the stability limits of charged droplets, introducing the concept that liquid jets could be ejected from a surface when a critical charge was exceeded. These early explorations of electrohydrodynamics laid the conceptual foundation for electrospinning, which can be considered a variant of electrospraying where the viscoelasticity of the fluid is sufficient to maintain a continuous jet rather than allowing it to break into droplets[106,108].

The transition from scientific curiosity to a viable fabrication method began in the early 20th century. In 1900, John Francis Cooley filed the first modern patent for an electrospinning apparatus, followed by a series of patents between 1934 and 1944 by Anton Formhals, who described a setup for producing textile yarns from a cellulose acetate solution[108]. This marked the first attempt to commercialize the technology, envisioning its use in the textile industry. A significant, albeit niche, practical application emerged in the Soviet Union in 1938 with the development of "Petryanov filters." These electrospun nanofiber mats were used in gas masks to capture radioactive aerosol particles, representing the first implementation of the technology for its unique filtration capabilities[108]. Despite these early milestones, the technique remained largely underdeveloped for several decades. A critical breakthrough occurred between 1964 and 1969 when Sir Geoffrey Taylor mathematically modelled the conical shape of a fluid droplet under a strong electric field, now universally known as the "Taylor cone". Taylor's work provided the rigorous scientific framework

needed to understand and control the jet initiation process, transforming electrospinning from an empirical art into a quantitative science[106,108].

The modern era of electrospinning was truly ignited in the early 1990s through the intensive research of groups led by figures such as Darrell Reneker and Gregory Rutledge[106]. Their work demonstrated that a vast array of different polymers, both natural and synthetic, could be successfully electrospun into nanofibers, revitalizing interest in the technique and showcasing its immense versatility. This resurgence was not coincidental; it was enabled by the concurrent maturation of polymer science, which had produced a diverse and well-characterized library of materials with tunable properties. The historical trajectory of electrospinning reveals that while the fundamental physics had been known for centuries, the technology's full potential could only be unlocked when a sufficiently broad palette of spinnable materials became available. The limiting factor was not the process itself, but the materials. This synergy between process and material propelled electrospinning to the forefront of nanotechnology, establishing it as the preeminent method for producing long, continuous fibers with diameters down to the nanometer scale, a capability that continues to drive innovation across countless scientific and industrial fields[109].

3.2 General principles

Electrospinning is an electrohydrodynamic process that utilizes a strong electric field to draw a continuous, ultrafine fiber from a viscoelastic liquid[110,111]. The fundamental setup is remarkably simple, typically consisting of a high-voltage power supply, a syringe pump to deliver the liquid at a controlled rate, a spinneret (often a metallic needle), and a grounded collector. The transformation of a bulk polymer solution or melt into a solid nanofiber occurs through a sequence of distinct physical events, each governed by a balance of electrostatic, viscoelastic, and surface tension forces[111] (*Figure 1*).

The process initiates with the formation of the Taylor cone[112,113]. A droplet of the polymer solution is held at the tip of the spinneret by its surface tension. When a high voltage (typically in the range of several kilovolts) is applied, a potential difference is established between the spinneret and the collector. This electric field induces charge separation within the conductive liquid, causing charges of the same polarity as the spinneret to migrate to the surface of the droplet. The accumulation of these surface charges generates a mutual electrostatic repulsion that acts in opposition to the surface tension, which seeks to maintain a spherical shape to minimize surface free energy. As the applied voltage increases, the electrostatic repulsion intensifies, deforming the droplet into a conical shape. At a critical voltage, the repulsive force becomes strong enough to overcome the surface tension, resulting in the formation of a stable, conical structure known as the Taylor cone. The stability and geometry of this cone are crucial for a consistent and uniform electrospinning process[112,113].

From the apex of the Taylor cone, a charged jet of the polymer solution is ejected. This jet is accelerated toward the collector by the electric field and initially travels in a relatively straight path for a distance of several centimeters. This region is known as the near-field region. During this linear trajectory, the jet undergoes significant stretching and elongation, causing its diameter to decrease progressively. The viscoelastic properties of the fluid, stemming from the entanglement of polymer chains, are critical at this stage. They provide the necessary molecular cohesion to suppress the classical Rayleigh instability, which would otherwise cause the jet to break up into droplets, and maintain the jet as a continuous filament[110].

The most dramatic reduction in fiber diameter occurs due to the onset of a non-axisymmetric whipping instability. As the jet travels away from the spinneret, small, almost imperceptible bends in its path are rapidly amplified by the immense electrostatic repulsive forces acting along its length. This causes the jet to enter a chaotic, high-frequency whipping and spiraling motion in the far-field region[110]. This whipping instability is the defining characteristic of the electrospinning process and the primary mechanism for achieving nanoscale dimensions. The violent whipping motion elongates the jet by several orders of magnitude (up to 10,000 times) within a fraction of a second, stretching it into an extremely thin filament before it has time to solidify. This self-amplifying stretching, driven by electrostatic forces distributed along the entire jet, is fundamentally different from the localized pulling of mechanical drawing and allows for a degree of thinning that is unattainable by conventional means[103,105].

The final stage of the process is the solidification of the jet and deposition of the fiber[114]. As the jet is being rapidly elongated and whipped through the air, the solvent evaporates (in solution electrospinning) or the melt cools and solidifies (in melt electrospinning). The rate of solidification is critical; a slower rate allows for a longer elongation period, resulting in thinner fibers. Once solidified, the instabilities cease, and the continuous fiber, which may still carry some residual electrical charge, is deposited onto the grounded collector. The chaotic nature of the whipping motion typically results in the formation of a non-woven mat of randomly oriented nanofibers. The unique and highly advantageous properties of these mats, specifically, their extremely high surface-area-to-volume ratio and high degree of interconnected porosity, are not merely engineered features but are the direct and inevitable physical consequences of this process. The whipping instability is the cause of the nanoscale fiber diameter, which in turn maximizes the surface area. The random deposition of this rapidly moving fiber is the cause of the porous, non-woven architecture. This intrinsic link between the fundamental physics of the process and the resulting material morphology is what makes electrospinning such a powerful and versatile technique for fabricating advanced materials.

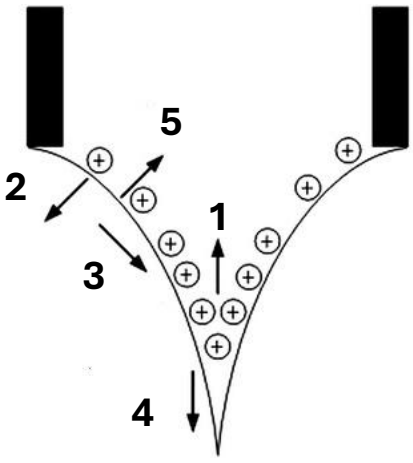

Figure 1- Diagram representing the forces involved in the formation of Taylor's cone: (1) Viscous force (2), Normal electrical stress (3), Tangential electrical stress (4), Weight force (5) Surface tension

3.3 Methods and setup in Electrospinning

The versatility of the electrospinning technique is reflected in the wide array of experimental setups and methodologies that have been developed to control fiber morphology, increase production rates, and fabricate complex, multi-component structures[115–117]. These setups can be broadly categorized by the design of their spinneret, which dictates how the polymer jet is initiated, and the configuration of their collector, which determines the final architecture of the deposited nanofiber mat. The evolution of these systems highlights a fundamental engineering trade-off between achieving fine control over the fiber structure and scaling the process for industrial production.

A primary distinction in electrospinning technology is between needle-based and needleless (or free surface) systems[118,119]. The classic laboratory setup, and the most widely used for research and development, is the single-needle configuration. It employs a syringe and a metallic needle to generate a single, well-defined Taylor cone and polymer jet. This method offers the highest degree of control over the electrospinning process, allowing for precise manipulation of parameters to produce highly uniform fibers. However, its productivity is extremely low, typically less than 1 g/h, making it unsuitable for large-scale manufacturing. A direct approach to improve throughput is the use of multi-needle arrays, where numerous needles are arranged in configurations (e.g., linear, circular) and fed from a common reservoir. While this parallelization does increase the production rate, it introduces new challenges, such as interference between the electric fields of adjacent jets, which can lead to jet repulsion and a decrease in fiber uniformity[118].

To overcome the inherent limitations of needle-based systems, needleless or free surface electrospinning was developed for high-throughput, industrial-scale production[119]. These methods eliminate the need for individual needles and instead generate a multitude of jets from a free liquid surface. Common configurations include rotating drums, wires, or cones that are partially submerged in a polymer solution reservoir, or stationary, sharp-edged spinnerets. As the spinneret rotates or is charged, multiple Taylor cones and jets form along its surface, dramatically increasing the production rate. While this approach successfully addresses the issues of low throughput and needle clogging, it comes at the cost of reduced control. The jets are formed less uniformly, and the resulting fibers often have a broader diameter distribution compared to those from single-needle systems. Furthermore, free surface methods are generally limited to solutions with low volatility to prevent premature solvent evaporation from the large, exposed surface area[120]. The choice between needle-based and needleless systems is therefore a strategic one: needle-based methods are ideal for applications requiring high precision and uniformity, such as biomedical scaffolds, while needleless methods are suited for bulk materials like filtration media where high production volume is the primary concern.

Beyond scaling production, spinneret design has been advanced to create fibers with complex, multi-component morphologies[121,122]. The most significant of these is coaxial electrospinning, which utilizes a spinneret composed of two concentric needles. This setup allows two different, typically immiscible, polymer solutions to be spun simultaneously, with the inner fluid forming the core and the outer fluid forming the sheath of the resulting fiber. This technique is invaluable for creating core-shell nanofibers, which can be used to encapsulate and protect sensitive materials (like drugs or growth factors) in the core, or to combine the properties of two different polymers in a single fiber. By selecting a core material that can be selectively removed after spinning (e.g., via solvent dissolution or calcination), this method can also be used to fabricate hollow nanofibers. The principle

can be extended to multi-axial systems with three or more concentric needles to create even more complex, multi-layered fiber architectures, showcasing a focus on maximal control over the internal structure of a single fiber.

Finally, the design of the collector plays a critical role in determining the macroscopic structure and alignment of the final nanofiber mat[121–123]. The standard configuration is a stationary, flat plate collector, which results in a randomly oriented, non-woven mat due to the chaotic whipping motion of the fiber jet. However, for applications requiring anisotropic mechanical or biological properties, such as tissue scaffolds that need to guide cell growth in a specific direction, aligned fibers are necessary. Fiber alignment can be achieved by using a dynamic collector, most commonly a rotating drum or mandrel. When the tangential speed of the rotating collector is sufficiently high, it imparts a mechanical drawing force on the incoming fibers, pulling them taut and aligning them in the direction of rotation before they are fully deposited. Alternatively, patterned collectors, which use a gap between two conductive electrodes or an array of patterned electrodes on an insulating substrate, can be used[115]. The electric field lines concentrate across the gap, guiding the charged fibers to deposit in an aligned fashion between the electrodes. These various collector configurations demonstrate that by manipulating the electric field or mechanical forces at the point of deposition, it is possible to engineer the architecture of the nanofiber assembly from a random web into a highly ordered structure.

3.4 Materials for Electrospinning

A defining characteristic of the electrospinning technique is its remarkable material versatility[109]. A vast array of substances, including natural and synthetic polymers, polymer blends, composites containing nanoparticles, and ceramic precursors, can be successfully processed into nanofibers. This flexibility allows for the fabrication of materials with a wide spectrum of properties tailored to specific applications, from biocompatible scaffolds for tissue engineering to robust ceramic filters for high-temperature environments. The key requirement for a material to be electrospinnable is its ability to form a solution or melt with sufficient viscosity and chain entanglement to maintain a continuous jet under the high electrostatic forces of the process.

Polymers

Polymers are the most common class of materials used in electrospinning, and they can be broadly divided into synthetic and natural categories[124,125].

Synthetic polymers have been extensively studied and are often easier to electrospin due to their well-defined molecular weights and consistent solution properties. A wide range of synthetic polymers has been successfully electrospun, including[126]:

- *Biocompatible and biodegradable polyesters:* Materials such as poly(caprolactone) (PCL), poly(lactic acid) (PLA), poly(lactic-co-glycolic acid) (PLGA), and polyurethanes (PU) are central to biomedical applications. Their ability to degrade into non-toxic byproducts makes them ideal for temporary implants like tissue engineering scaffolds and drug delivery systems.
- *Commodity and engineering polymers:* Polymers like poly(vinyl alcohol) (PVA), polyacrylonitrile (PAN), polystyrene (PS), and poly(vinylidene fluoride) (PVDF) are used in a variety of applications. PVA is often used as a carrier polymer due to its excellent spinnability and water solubility. PAN is a common precursor for producing carbon nanofibers

through a post-spinning carbonization process. PVDF is valued for its piezoelectric properties in sensor and energy harvesting applications.

Natural polymers are gaining increasing interest due to their inherent biocompatibility, biodegradability, and origin from renewable resources, making them particularly suitable for biomedical and "green" applications[127]. However, their electrospinning often presents significant challenges.

- *Polysaccharides:* Materials like alginate and chitosan are highly valued for their bioactivity. As detailed extensively in the reference thesis, these polymers often exhibit complex polyelectrolyte behavior in solution, leading to very high viscosities that can hinder the electrospinning process. Consequently, they are frequently blended with a synthetic "co-spinning agent," such as poly(ethylene oxide) (PEO), which improves the spinnability of the solution by providing the necessary chain entanglement.
- *Proteins:* Structural proteins like collagen, gelatin, and silk fibroin are ideal for creating biomimetic scaffolds that replicate the native extracellular matrix (ECM) of tissues. Their natural cell-recognition motifs promote cell adhesion and growth.

Composites and Functional Materials

The functionality of electrospun nanofibers can be significantly enhanced by incorporating a secondary phase into the polymer matrix, creating composite nanofibers. This approach allows for the combination of the structural properties of the polymer with the functional properties of the additive.

- *Nanocomposites[128–131]:* Pre-synthesized nanoparticles can be dispersed within the polymer solution prior to electrospinning. This is a common method for imparting specific functionalities. For example, zinc oxide (ZnO) or silver (Ag) nanoparticles are incorporated to confer antibacterial properties for wound dressings and filters. Titanium dioxide (TiO_2) nanoparticles are used for their photocatalytic activity in environmental remediation applications. A critical challenge in this approach is achieving and maintaining a stable, homogeneous dispersion of the nanoparticles in the spinning solution. Aggregation of nanoparticles can lead to nozzle clogging and results in composite fibers with non-uniform properties.
- *Ceramic nanofibers[132,133]:* Pure ceramic nanofibers, which are valuable for applications requiring high thermal stability or specific catalytic properties, can be fabricated using a sol-gel approach combined with electrospinning. In this method, a polymer solution (e.g., PVA or PVP) acts as a carrier for a ceramic precursor, such as a metal salt or alkoxide (e.g., tetraethyl orthosilicate for SiO_2 or titanium isopropoxide for TiO_2). The composite solution is electrospun to form precursor-loaded polymer nanofibers. In a subsequent step, the as-spun mat is subjected to a high-temperature calcination process. This thermal treatment burns off the sacrificial polymer template, leaving behind a non-woven mat of pure, and often crystalline, ceramic nanofibers.

The recurring strategy of using a "carrier" or "co-spinning" polymer is a powerful and generalizable platform in electrospinning. Many materials that are highly desirable for their functional properties, such as polysaccharides, ceramic precursors, or even small molecules, do not themselves form

solutions with the requisite viscoelasticity to be electrospun. Their molecular structures do not provide the long-range chain entanglements needed to stabilize the electrospinning jet[128,134]. By blending these functional but unspinnable materials with a polymer that is exceptionally "spinnable" (like PEO or PVA), a composite solution is created that possesses the necessary rheological properties[134]. The carrier polymer provides the mechanical backbone for the jet during the intense stretching of the whipping phase. Crucially, this carrier polymer is often designed to be a temporary processing aid that can be selectively removed after the fiber architecture is formed—either by washing away a water-soluble polymer like PEO or by burning away a polymer like PVA during calcination. This sophisticated materials engineering strategy effectively decouples the *processability* of the solution from the functionality of the final material, vastly expanding the universe of substances that can be fabricated into a nanofibrous form[134].

3.5 Applications of electrospun nanofibers

The unique structural characteristics of electrospun nanofiber mats, namely their high surface-area-to-volume ratio, high porosity with interconnected pores, and tuneable fiber morphology, have made them highly attractive for a vast range of applications. These properties are leveraged in fields as diverse as biomedical engineering, environmental remediation, energy storage, and, more recently, the specialized field of cultural heritage conservation.

Biomedical and Pharmaceutical Applications

Electrospun nanofibers have made their most significant impact in the biomedical and pharmaceutical sectors, primarily due to their structural resemblance to the natural extracellular matrix (ECM) of biological tissues[105,107,134]. This biomimicry makes them ideal platforms for interacting with cells and tissues.

- *Tissue engineering and regeneration:* Electrospun scaffolds provide a 3D architecture that supports cell adhesion, proliferation, and differentiation, guiding the regeneration of tissues such as skin, bone, cartilage, and nerves. The ability to align the fibers can provide topographical cues that direct cell growth, mimicking the organized structure of tissues like tendons and muscles.
- *Wound healing:* As wound dressings, nanofiber mats offer an optimal microenvironment for healing. Their high porosity allows for gas exchange (cell respiration) and exudate absorption, while the small pore size provides a physical barrier against bacterial infiltration. Furthermore, bioactive agents, such as antibiotics, growth factors, or antibacterial nanoparticles like ZnO, can be incorporated directly into the fibers to promote healing and prevent infection.
- *Drug delivery:* The high surface area of nanofibers allows for a high drug loading capacity. Therapeutic agents can be encapsulated within the fibers during the electrospinning process (e.g., via coaxial spinning) or adsorbed onto their surface post-fabrication. The drug release kinetics can be tailored by controlling the polymer composition, fiber diameter, and mat structure, enabling applications ranging from rapid-release systems for acute treatments to sustained-release implants for long-term therapy.

Potential applications of electrospinning in Cultural Heritage Conservation

The application of electrospinning in the conservation of cultural heritage represents a possible innovative and highly specialized frontier. This field is governed by stringent ethical principles, primarily minimal intervention (the treatment should alter the original object as little as possible) and reversibility (a treatment should be removable in the future without damaging the artifact). The unique properties of electrospun mats offer novel solutions that align well with these principles, addressing long-standing challenges in the preservation of fragile and irreplaceable artifacts. This represents a paradigm shift from traditional conservation methods that often rely on the bulk application of liquid consolidants or adhesives to a more controlled, micro-architectural approach. Instead of flooding a fragile structure with a resin, conservators can now apply a prefabricated, engineered scaffold with precisely defined properties, offering an unprecedented level of control over the treatment process.

Electrospun nanofiber mats are uniquely suited for conservation applications due to a combination of properties that are difficult to achieve with conventional materials:

- *High porosity and breathability:* The interconnected pore network of a nanofiber mat allows it to be highly permeable to water vapor. This "breathability" is critical for treating porous artifacts like stone, wood, or paper, as it prevents the trapping of moisture beneath the treatment layer, which can lead to further degradation.
- *Mechanical support with minimal mass and visual impact:* Nanofiber webs can provide significant mechanical reinforcement to fragile substrates like brittle paper or degraded textiles while adding negligible weight and thickness. This preserves the original handle, drape, and flexibility of the artifact. Furthermore, when the fiber diameter is below the wavelength of visible light and the mat is sufficiently thin, it can be almost completely transparent, fulfilling the critical aesthetic requirement that a conservation treatment should not alter the visual appearance of the object.
- *High surface area for efficient interaction:* The vast surface area of nanofibers makes them highly efficient for applications involving surface interactions, such as acting as carriers for cleaning solvents or as platforms for delivering deacidification agents.
- *Material and structural tunability:* The electrospinning process allows for the use of a wide range of polymers, from synthetic to natural, enabling the selection of materials that are chemically compatible with the artifact. The ability to control fiber diameter, alignment, and mat porosity allows for the design of customized treatments for different types of materials and conservation challenges.

Consolidation and Reinforcement of Fragile Artifacts

One of the primary challenges in conservation is the strengthening, or consolidation, of materials that have lost their structural integrity[2]. Electrospun mats offer a new approach to this problem[135].

- *Paper conservation:* Paper artifacts, particularly those made from acidic wood pulp, become brittle over time as the cellulose fibers degrade. Traditional mending often involves adhesives and repair tissues that can be visually obtrusive and may become irreversible over time. Nanofiber mats, particularly those made from nanocellulose or chitosan, offer a highly compatible solution. These biopolymers are chemically similar to the paper itself. When

applied as a thin, transparent web, the nanofibers form a scaffold that physically bridges and supports the broken paper fibers, significantly increasing tensile strength and folding endurance without the need for a bulk adhesive.

- *Textile conservation:* Historic textiles can become extremely fragile due to light exposure, pests, or chemical degradation. Supporting these textiles often requires stitching them to a backing fabric, a process that is labor-intensive and introduces new points of stress. Electrospun non-woven webs made from flexible polymers like poly(vinyl alcohol) (PVA) or polyamides can serve as lightweight, conforming support linings. These webs can be attached using minimal, reversible adhesives or heat-activation, providing overall support that conforms to the textile's natural drape without the stiffness or localized stress of traditional methods.

Protective coatings and environmental barriers

Electrospun mats can function as multifunctional protective coatings that shield artifacts from environmental damage. By selecting hydrophobic polymers such as poly(vinylidene fluoride-co-hexafluoropropylene) (PVDF-HFP), it is possible to create superhydrophobic surfaces on materials like stone or metal. The resulting nanofiber coating acts as a robust barrier against liquid water, preventing water-induced damage, while its high porosity allows the artifact to remain "breathable," permitting the escape of internal water vapor. This combination of water repellency and vapor permeability is extremely difficult to achieve with traditional film-forming coatings, which often trap moisture and can accelerate decay. Furthermore, UV-absorbing molecules or nanoparticles can be incorporated into the fibers to protect light-sensitive artifacts, such as textiles and manuscripts, from photodegradation.

Controlled delivery systems for conservation treatments

The high surface area and porosity of electrospun mats make them excellent vehicles for the controlled delivery of active conservation agents.

- *Localized Cleaning*[136,137]*:* The removal of aged, discolored varnishes or grime from paintings is a delicate process that requires precise control of potent solvents. Electrospun mats made from inert, solvent-resistant polymers like pullulan can be loaded with a specific cleaning solvent or gel. The mat is then applied to the artwork's surface, acting as a poultice that localizes the solvent and minimizes its penetration into the underlying paint layers. The porous structure of the mat then acts as an absorbent, wicking away the dissolved varnish, which is subsequently removed along with the mat in a single, non-mechanical peeling action. This method offers far greater control than the traditional application of solvents with cotton swabs. The functionality can be further enhanced by incorporating photothermal nanoparticles, such as melanin, into the fibers. When irradiated with light, these particles generate localized heat, accelerating the dissolution of highly resistant coatings like modern spray paints used in vandalism.

- *Paper Deacidification:* The primary cause of degradation for much of the paper produced since the mid-19th century is acid-catalyzed hydrolysis of cellulose. Deacidification treatments aim to neutralize these acids and deposit an alkaline buffer (an "alkaline reserve") to protect against future acid formation. Traditional aqueous methods can be damaging to

water-sensitive inks and papers. Electrospinning provides a novel, non-aqueous delivery system. A mat made from a solvent-resistant polymer (e.g., PVDF-HFP) can be loaded with a dispersion of alkaline nanoparticles, such as magnesium oxide (MgO) or calcium hydroxide ($Ca(OH)_2$). The mat is then placed in contact with the paper artifact. The nanoparticles are transferred from the mat to the paper fibers, where they neutralize acids and provide a long-lasting alkaline reserve. This method avoids the use of liquid solvents, offers a highly controlled and uniform application of the deacidifying agent, and can simultaneously provide a degree of physical reinforcement.

Chapter 4.
Biopolymers and Synthetic Polymers

4.1 Introduction

This chapter examining polysaccharides as a representative and abundant class of biopolymers and three exemplary synthetic polymers: poly(vinyl alcohol) (PVA), poly(ethylene oxide) (PEO), and poly(caprolactone) (PCL). By systematically dissecting the structure-property-application relationships of each material, this chapter aims to illuminate the fundamental trade-offs between the innate biological functionality of polysaccharides and the engineered, high-performance characteristics of their synthetic counterparts. This comparative framework will provide a understanding of the material selection criteria that govern the design of next-generation biomaterials. A summary of the key attributes of these polymer types is presented in Table 4[125,126,138,139] to frame the detailed discussion that follows.

Table 4 - Comparative Overview of Polysaccharides and Selected Synthetic Polymers

Attribute	Polysaccharides	Poly(vinyl alcohol) (PVA)	Poly(ethylene oxide) (PEO)	Poly(caprolactone) (PCL)
Origin	Natural, renewable (plants, algae, microbes)	Synthetic (petroleum-based)	Synthetic (petroleum-based)	Synthetic (petroleum-based)
Typical Monomers	Monosaccharides (e.g., glucose, galactose)	Vinyl alcohol (via hydrolysis of vinyl acetate)	Ethylene oxide	ε-caprolactone
Key Linkage Type	Glycosidic bond	Carbon-carbon backbone	Ether bond	Ester bond
Structural Complexity	High (linear, branched, heterogeneous)	Low (linear, atactic)	Low (linear)	Low (linear)
Molecular Weight Distribution (MWD)	Often monodisperse in vivo; polydisperse upon extraction	Polydisperse (PDI > 1)	Polydisperse (PDI > 1)	Polydisperse (PDI > 1)
Inherent Bioactivity	Often high (e.g., immunomodulatory, anti-inflammatory)	Low (biocompatible but largely bio-inert)	Very low (bio-inert, "stealth" properties)	Low (biocompatible but largely bio-inert)
Typical Mechanical Profile	Generally poor, low strength, brittle gels	Flexible, high tensile strength	Waxy solid or viscous liquid; not structural	Tough, flexible, high strength

		(humidity dependent)		
Primary Degradation Mechanism	Enzymatic hydrolysis	Biodegradable (hydrolysis, oxidation)	Generally stable; low MW cleared renally	Bulk hydrolysis of ester bonds (very slow)
Property Tunability	Limited (via chemical modification)	High (via degree of hydrolysis, MW)	High (via MW)	High (via MW, copolymerization)

4.2 Polysaccharides

Polysaccharides represent the most abundant class of carbohydrates found in nature, functioning as essential biopolymers in nearly all forms of life[138,139]. These macromolecules are constructed from long chains of monosaccharide units joined together by glycosidic linkages. Their roles in biological systems are profoundly diverse, ranging from providing structural integrity to plant cell walls (cellulose) and arthropod exoskeletons (chitin) to serving as the primary means of energy storage in plants (starch) and animals (glycogen). In recent decades, the unique properties of polysaccharides, particularly their origin from renewable resources, inherent biocompatibility, and biodegradability, have made them materials of exceptional interest for a wide array of applications, especially within the biomedical and pharmaceutical fields.

The functional diversity of polysaccharides is a direct consequence of their structural variability[140,141]. Unlike synthetic polymers, which are often built from a single repeating unit, polysaccharides can be composed of various ones, linked in different configurations, and arranged in linear or complex branched architectures.

Chemical Structure and Composition

The fundamental building blocks of polysaccharides arise from monosaccharides, or simple sugars. While the most prevalent monomeric unit derive from D-glucose, the chemical palette of nature includes a wide variety of other sugars such as D-fructose, D-galactose, L-galactose, D-mannose, L-arabinose, and D-xylose[142]. Furthermore, this diversity is expanded by the inclusion of monosaccharide derivatives, including amino residues like D-glucosamine and D-galactosamine, and acidic residues as glucuronic and iduronic acids[142].

These monomeric units are polymerized via the formation of glycosidic bonds, which connect the anomeric carbon of one sugar residue to a hydroxyl group on another[141]. The specific stereo- (α or β) and regio-selectivity of these linkages (e.g., 1→4, 1→6) dictate the overall three-dimensional structure of the polymer chain. For instance, the α-1,4-glycosidic bonds in amylose (a component of starch) result in a flexible, helical coil, whereas the β-1,4-glycosidic bonds in cellulose produce rigid, linear chains that pack into strong, insoluble fibers[138]. The introduction of additional linkages, such as the α-1,6 bonds found in amylopectin and glycogen, creates branch points, leading to highly complex, dendritic structures. This capacity for branching is a key structural feature that distinguishes polysaccharides from the exclusively linear chains of proteins and peptides.

Based on their composition, polysaccharides are classified as either homopolysaccharides (also called homoglycans), which are composed of a single type of saccharide residue (e.g., starch, cellulose,

glycogen), or heteropolysaccharides (heteroglycans), which contain two or more different types of saccharide residues. This inherent heterogeneity, encompassing variations in monomer content, chain length, and branching patterns, is a defining characteristic of this polymer class[138,142].

Physical Properties

The vast structural diversity of polysaccharides gives rise to an equally broad spectrum of physical properties, which are harnessed in numerous industrial and biomedical applications.

Solubility and hydrophilicity[138,139,141,142]: The interaction of polysaccharides with water is highly dependent on their specific structure. The abundance of hydroxyl (-OH) groups along the polymer backbone suggests a high degree of hydrophilicity. However, the ability of these groups to form strong, extensive intra- and intermolecular hydrogen bonds can lead to highly ordered, crystalline structures that are completely insoluble in water. Cellulose is the canonical example; its rigid, linear chains pack into microfibrils with such a high degree of hydrogen bonding that water cannot penetrate the crystalline structure, resulting in considerable mechanical strength and insolubility. However, it is worth noting that cellulose is semi-crystalline and also contains amorphous regions, which possess a lower degree of order and are therefore more accessible to water and chemical reagents. In contrast, other polysaccharides with less ordered structures or with branching that disrupts crystalline packing are readily soluble in water. Many polysaccharides are described as being generally insoluble in cold water and non-sweet to the taste.

Viscosity and rheology[138,143]: In solution, polysaccharides are highly effective at modifying the rheological properties of aqueous systems. Even at low concentrations, the long, entangled polymer chains significantly increase the viscosity of the solution. Many polysaccharide solutions exhibit non-Newtonian, shear-thinning (or pseudoplastic) behavior, where the apparent viscosity decreases as the shear rate increases. This property is advantageous in food applications that need to be thick at rest but easy to pour or swallow. The viscosity of a polysaccharide solution is a complex function of multiple variables, including polymer concentration, molecular mass, temperature, pH, and the ionic strength of the solvent. These characteristics make them invaluable as thickening, stabilizing, and suspending agents in the food, cosmetic, and pharmaceutical industries.

Gelation Mechanisms[140]: One of the most important functional properties of many polysaccharides is their ability to form hydrogels i.e. three-dimensional polymer networks that can entrap large amounts of water. Gelation is typically a thermo-reversible process driven by the formation of non-covalent associations between polymer chains. As a hot polysaccharide solution is cooled, the thermal energy of the polymer chains decreases, reducing their random motion. This allows specific segments of the chains to associate through mechanisms such as hydrogen bonding, ionic interactions, or hydrophobic effects, forming junction zones. As more of these junctions form, a continuous, sample-spanning network is created, leading to a transition from a liquid-like sol state to a solid-like gel state. The mechanical properties of these gels are often described by their viscoelastic moduli: the storage modulus (G′) represents the elastic (solid-like) component, while the loss modulus (G″) represents the viscous (liquid-like) component. A true gel is formed when G′ exceeds G″ and becomes largely independent of frequency.

Biological Properties

From a biomedical perspective, the most compelling attributes of polysaccharides are their favorable interactions with biological systems[138–140,142,143].

Biocompatibility and Biodegradability: Derived from natural sources, polysaccharides are generally recognized by the body as non-foreign materials. This results in excellent biocompatibility, low toxicity, and a lack of significant immunogenicity, making them highly suitable for use in medical implants, drug delivery systems, and tissue engineering scaffolds. Furthermore, the glycosidic bonds that form their backbone are susceptible to enzymatic hydrolysis, rendering them biodegradable. This allows for their gradual resorption in the body, which is a critical feature for temporary medical devices and regenerative medicine applications.

Bioactivity: Beyond simply being well-tolerated, many polysaccharides exhibit specific, intrinsic biological activities that can be therapeutically beneficial. A wide range of pharmacological effects have been documented, including immunomodulatory, anti-tumor, antimicrobial, antioxidant, and anticoagulant activities. For example, certain polysaccharides have been shown to exert anti-inflammatory effects by inhibiting the expression and activity of key inflammatory mediators, such as cytokines (e.g., Interleukin-6, Tumor Necrosis Factor-alpha) and nitric oxide. This inherent bioactivity offers a distinct advantage over most synthetic polymers, which are typically bio-inert.

The extensive portfolio of properties offered by polysaccharides positions them as highly versatile biomaterials. However, their natural origin presents a fundamental challenge in high-performance applications. The very structural complexity and heterogeneity that endow them with desirable bio-functionality also introduce significant variability and a lack of precise control over their physicochemical properties. For example, properties can vary significantly based on the source organism (e.g., plant, algae, or microbe) and the specific extraction and purification conditions employed. This can lead to batch-to-batch inconsistencies, which are a major impediment in the development of regulated medical devices where reproducibility and predictability are paramount. Furthermore, natural polymers often exhibit inferior mechanical properties and less predictable degradation kinetics compared to their synthetic counterparts. This creates a central dilemma for the biomaterials engineer: one can select a biopolymer for its excellent biocompatibility and intrinsic bioactivity but must contend with challenges in processability, mechanical robustness, and reproducibility. Conversely, one can choose a synthetic polymer for its precisely tunable and robust mechanical and degradation properties but must often address issues of bio-inertness or the potential for adverse biological responses. This fundamental trade-off is a primary driver for the development of composite materials, which seek to synergistically combine natural and synthetic polymers to create hybrid systems that capture the most desirable attributes of both classes.

4.2.1 Agar

Agar is a gelatinous polysaccharide, or phycocolloid, that stands as one of the most historically significant and functionally unique hydrocolloids. Its discovery is attributed to Minoya Tarozaemon in Japan in 1658, and it has since become an indispensable material in both science and industry[144,145]. Agar is extracted commercially from the cell walls of various species of red algae (class Rhodophyceae), most notably those from the genera *Gelidium* and *Gracilaria*. Its introduction to the Western scientific community by Robert Koch in 1882 as a solidifying agent for bacteriological

culture media was a transformative event, enabling the isolation and pure culture of microorganisms for the first time and laying the foundation for modern microbiology[145,146].

Chemical Composition

Agar is not a chemically homogeneous substance but rather a complex mixture of polysaccharides. Its properties are determined by the interplay of its two principal fractions: Agarose and Agaropectin (*Figure 2*)[144–148]:

- *Agarose:* This is the major component, typically constituting around 85% of Agar. It is a largely neutral, linear polymer responsible for the remarkable gelling properties of Agar. The chemical structure of Agarose is a repeating disaccharide unit known as Agarobiose. This unit consists of alternating (1→3)-linked β-D-galactopyranose and (1→4)-linked 3,6-anhydro-α-L-galactopyranose residues. The 3,6-anhydro bridge constrains the L-galactose ring into a specific conformation that is critical for the formation of the helical structures necessary for gelation.
- *Agaropectin:* This fraction makes up the remaining ~15% of Agar and is a highly heterogeneous, charged, and generally non-gelling polysaccharide. While it shares a similar galactose-based backbone with Agarose, it is extensively modified with various acidic side groups, including sulfate esters, pyruvate, and glucuronic acid. The presence and quantity of these charged groups vary depending on the seaweed source and contribute to the overall properties of the crude Agar extract.

Physical and Thermal Properties

The defining characteristic of Agar is its ability to form strong, thermo-reversible gels in water[144,147,149,150].

- *Solubility:* Agar is insoluble in cold water, but its granular powder swells significantly by absorbing many times its weight in water. It dissolves completely upon heating in boiling water to form a clear, viscous solution.
- *Gelation:* As a hot aqueous solution of Agar is cooled, it undergoes a sol-gel transition, forming a firm gel. The mechanism of gelation is a physical process driven by the formation of hydrogen bonds. Upon cooling, the disordered polymer chains of Agarose begin to associate, forming double-helical structures. These helices then aggregate into larger bundles or fibers, which interlink to create a robust, three-dimensional network that immobilizes the surrounding water molecules. This entire process is physically cross-linked and remarkably reversible upon reheating.
- *Thermal hysteresis:* Agar's most exceptional property is its pronounced thermal hysteresis, which is the largest among all known hydrocolloids. A typical 1.5% w/v Agar solution will set into a gel upon cooling to a temperature range of 34–43°C, but this gel will not melt again until it is heated to a much higher temperature, typically 85–90°C. This wide gap between the gelling and melting temperatures means that an Agar system can exist in either a liquid or a solid state within the broad temperature range of approximately 35–85°C, depending on its immediate thermal history. This property is invaluable, as it allows gels to be set at room

temperature without refrigeration and remain solid and stable even when heated to temperatures that would melt other gelling agents like gelatin.

Applications

The unique combination of gelling power, thermal stability, and biological inertness has established Agar as a vital material across diverse fields[151]:

- *Microbiology and biotechnology:* Its primary and most famous application is as the solidifying agent in microbiological culture media. It provides a firm, clear, non-nutritive surface for the growth and isolation of bacteria, fungi, and other microorganisms. It is also widely used in plant tissue culture to support the growth of sterile plantlets.
- *Food industry:* In the food industry, Agar is used extensively as a gelling agent, thickener, stabilizer, and emulsifier. It is the key ingredient in many traditional Asian desserts and is used globally in the production of jellies, puddings, candies, marmalades, and dairy products. Since it is indigestible by human enzymes, it contributes dietary fiber without adding calories.
- *Other industrial and medical Applications:* Agar finds use in a variety of other applications. It is used to make casting molds for dentistry, archaeology, and forensic science (e.g., fingerprinting). Its potential as a component in biodegradable food packaging films is also being explored as a sustainable alternative to synthetic polymers.
- *Conservation of Cultural Heritage:* Agar finds use in the field of Cultural Heritage as gel in the cleaning of artworks.

4.2.2 Agarose

While Agar is a highly functional bulk material, the demands of modern molecular biology and biotechnology for materials with high purity and predictable performance necessitated the isolation of its principal gelling component, Agarose[151–153]. Agarose is the purified, neutral polysaccharide fraction of Agar, separated from the heterogeneous, charged Agaropectin component. This purification transforms a useful but variable natural extract into analytical tool.

Definition and Separation from Agar

The primary goal of separating Agarose from Agar is to remove the Agaropectin fraction[150–153]. The charged sulfate and carboxyl groups on Agaropectin are problematic for many biochemical applications, most notably electrophoresis. In an electric field, these fixed negative charges on the gel matrix induce a counter-flow of hydrated positive ions in the buffer, a phenomenon known as electroendosmosis (EEO). This fluid flow can interfere with the migration of charged biomolecules like DNA, distorting separation patterns and reducing resolution. The removal of Agaropectin substantially reduces EEO and minimizes non-specific adsorption of biomolecules to the matrix, ensuring that separation occurs primarily based on the intended physical principle, such as molecular sieving.

Several methods have been developed to achieve this separation, all of which exploit the chemical differences between the neutral Agarose and the charged Agaropectin[148]. Common strategies include the selective precipitation of Agaropectin using quaternary ammonium salts, or the precipitation of the less soluble Agarose from solution using agents like polyethylene glycol or solvents such as

ethylene glycol and isopropanol, which reduce the polarity of the medium. These purification processes are complex and are a major contributor to the significantly higher cost of analytical-grade Agarose compared to food-grade Agar[148].

Refined Structure and Properties

- *Structure[154]:* As the purified linear component of Agar, the structure of Agarose is well-defined as a polysaccharide composed of repeating Agarobiose units—a disaccharide of D-galactose and 3,6-anhydro-L-galactose. The abundant hydroxyl groups along its backbone are responsible for its hydrophilicity and its ability to form extensive hydrogen bonds, which are the driving force for gelation.
- *Gelation[149]:* The gelation of Agarose follows a hierarchical mechanism. In a hot aqueous solution, the polymer chains exist as random coils. Upon cooling, chain segments associate to form double helices, which act as the initial cross-linking points. These helices then further aggregate side-by-side to form thick, rope-like fibers or bundles. The entanglement and interconnection of these fiber bundles create a porous three-dimensional network. The average pore size of this network is a critical property, particularly for electrophoresis, and it is inversely proportional to the concentration of Agarose used; higher concentrations create a denser network with smaller pores.
- *Thermal Properties[154]:* Purified Agarose retains the characteristic thermo-reversibility and pronounced thermal hysteresis of Agar. The temperature gap between gelation (e.g., ~35-42°C) and melting (e.g., ~85-95°C) is typically greater than 30°C. This hysteresis is understood to arise from the cooperative nature of the gel network. While individual helices may form at a lower temperature upon cooling, a much higher thermal energy is required to dissociate the large, stable aggregates of these helices during the melting process.

Applications

The high purity, neutral charge, and well-defined porous structure of Agarose gels make them the gold standard for a range of separation techniques in biotechnology[150,151].

- *Gel electrophoresis:* This is the foremost application of Agarose. Agarose gels act as a molecular sieve for the separation of large macromolecules, particularly DNA and RNA, based on their size. When an electric field is applied, the negatively charged nucleic acid fragments migrate through the gel pores toward the positive electrode. Smaller fragments navigate the porous matrix more easily and travel farther than larger fragments in a given amount of time, resulting in effective size-based separation. By varying the gel concentration, the resolving power can be tuned for different size ranges, from approximately 50 base pairs (50 bp) to over 20,000 base pairs (20 kbp) in standard electrophoresis, and up to several megabases (Mbp) using advanced techniques like pulsed-field gel electrophoresis (PFGE)[150,151].
- *Chromatography:* Agarose is widely used as a solid-phase support matrix for various forms of column chromatography. It can be formed into porous beads for use in gel filtration (size-exclusion) chromatography, where it separates molecules based on size. More importantly, its hydroxyl groups can be chemically activated to covalently attach other molecules, making it an ideal matrix for affinity chromatography and ion-exchange chromatography. In affinity

chromatography, a substrate with specific binding affinity for a target protein (e.g., an antibody or enzyme substrate) is immobilized on the Agarose beads, allowing for the highly selective purification of that protein from a complex mixture.

The evolution from Agar to Agarose for high-technology applications serves as a compelling illustration of a fundamental principle in materials science: the necessity of purification to unlock precision and high performance. Agar, as a natural extract, is a functional and valuable "bulk" material, suitable for applications like food gelling and basic microbiology where absolute chemical purity and predictable behavior are not paramount. However, its inherent heterogeneity, particularly the presence of the charged Agaropectin fraction, renders it unsuitable for sophisticated analytical techniques where subtle confounding factors can invalidate results. The development of methods to isolate Agarose represents a critical step of refinement. By removing the "impurities" of Agaropectin, a material is created the properties of which, a neutral charge, a well-defined gelling mechanism, and controllable porosity, are predictable and consistent. This allows for the precise exploitation of the molecular sieving phenomenon, turning a simple gelling agent into a high-fidelity tool for genomic and proteomic research. This progression underscores a recurring theme in the use of biomaterials: nature often provides a promising but crude starting material, and human purification and modification are required to elevate it to a high-value, high-performance product tailored for a specific, demanding application.

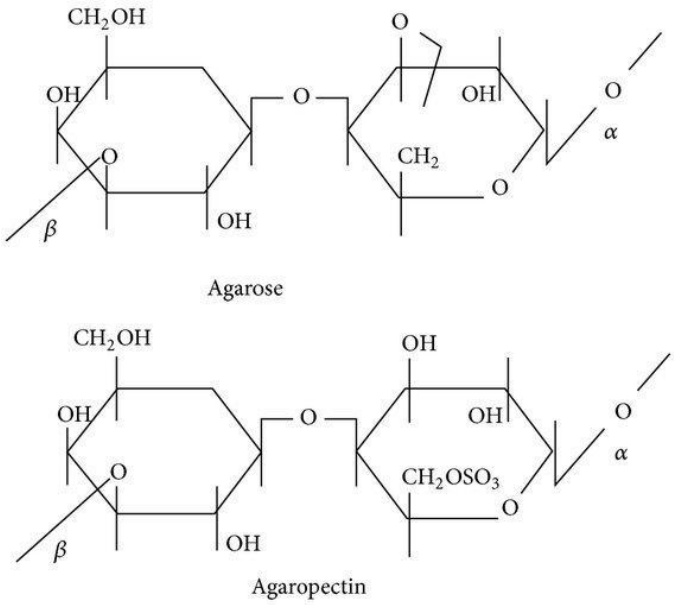

Figure 2-General chemical structure of Agarose and Agaropectin

4.2.3 Gellan gum

Gellan gum is a high-molecular mass microbial exopolysaccharide that has gained significant traction as a high-performance gelling agent in the food, pharmaceutical, biomedical industries and Cultural Heritage conservation. It is classified as a non-toxic, degradable in biological environment, and linear anionic polyanion. It is produced through the aerobic fermentation of the bacterium *Sphingomonas elodea* (formerly Pseudomonas elodea). Its chemical backbone is a tetrasaccharide repeating unit

composed of two β-D-glucose residues, one β-D-glucuronic acid residue, and one α-L-rhamnose residue (*Figure 3*)[56,155–157].

High-Acyl (HA) vs. Low-Acyl (LA) Forms

A critical feature of Gellan gum is that it exists in two primary forms: high-acyl (HA) and low-acyl (LA), which possess dramatically different properties (*Figure 3*)[56]. The native, high-acyl form contains two acyl substituents (glycerate and acetate) on its repeating unit. These groups result in gels that are soft, elastic, and non-brittle. Conversely, low-acyl Gellan gum is produced by removing these acyl groups, typically via alkaline treatment. The absence of these groups results in gels that are firm, non-elastic, and brittle. This fundamental structural difference also impacts their thermal behavior; HA Gellan forms gels at higher temperatures (e.g., 70-80°C), while LA Gellan gels at lower temperatures (e.g., 25-50°C). By blending the two types, a wide variety of textures can be achieved[56,155].

Gelation Mechanism

The gelation of Gellan gum is a sophisticated process driven by both temperature and, critically, the presence of cations. As a hot Gellan gum solution cools, the polymer chains transition from a disordered coil state to a more rigid, ordered double-helical structure[155]. This is followed by an ionotropic gelation mechanism. The Gellan polymer is anionic due to its glucuronic acid carboxyl groups; in the presence of cations (e.g., Na^+, K^+, Ca^{2+}, Mg^{2+}), the electrostatic repulsion between chains is shielded. These cations, particularly divalent ones like Ca^{2+}, form ionic bridges between adjacent double helices, promoting their aggregation into stable junction zones and creating a robust, three-dimensional network[56,155].

The acyl content dictates this mechanism. In LA Gellan, the ion-binding site is exposed, leading to strong, cation-mediated aggregation and brittle gels. The l-glyceryl group in HA Gellan, however, stabilizes the double helix via hydrogen bonds but sterically hinders and abolishes the primary metal ion binding site. This reduces cation-mediated aggregation, resulting in a different network structure that produces softer, more elastic gels[56,155].

Applications in Cultural Heritage Conservation

In recent decades, Gellan gum has been adopted by art conservators as a high-performance tool, particularly for the treatment of works on paper. Alongside Agar and Agarose, it is one of the most commonly used physical gels in modern conservation. Its primary advantage is the ability to deliver moisture, either pure water or aqueous cleaning solutions, in a highly controllable manner. This allows for "wet" treatments that are far less invasive than traditional water baths, which can damage fragile substrates.

Conservators typically use the low-acyl (deacylated) form of Gellan gum, which forms the hard, brittle gels. These gels are remarkably effective at very low concentrations, with 1-2% Gellan forming a rigid structure that is 98-99% water[156–159]. This structure provides high water retention and allows for "better contact" with the artwork's surface compared to Agar, with "no loss of water" during treatment. Unlike other gelling agents, such as xanthan gum, Gellan has been shown to leave less residues on the treated surface.

The applications in paper conservation are diverse. Gellan gum slabs are routinely used to[160]:

- *Clean and Wash*: Reduce general discoloration, remove stains, and wash documents. Studies have shown Gellan hydrogels can improve the mechanical and chemical properties of historical paper.
- *Remove Adhesives*: Assist in lining removal and reactivate adhesive-pretreated tissues.
- *Deliver Active Agents*: The gel acts as a vehicle for complex conservation treatments. It can be loaded with enzymes, such as proteinase K, to create an "eco-friendly and efficient" system for breaking down and removing old animal glues. It is also used for the controlled delivery of deacidification agents and reductive bleaches.
- *Disinfect*: Hybrid Gellan gum hydrogels, such as those incorporating titanium dioxide nanoparticles, have been developed to simultaneously clean and disinfect paper and parchment contaminated with fungi.

The use of Gellan is being extended to many sensitive cultural heritage surfaces. Studies have optimized Gellan and Agar gels for cleaning sensitive acrylic emulsion painted surfaces. Furthermore, its potential is being explored for the consolidation of stone and mortars, and in microemulsion-loaded hydrogels for cleaning wall paintings and coins[161].

A significant innovation is the use of Gellan gum microgels for art preservation. These colloidal-scale particles can better penetrate the porous structure of ancient paper and adapt to irregular surfaces. Research has shown that Gellan microgels can achieve superior cleaning performance for removing degradation byproducts compared to both standard hydrogels and water bath treatments, all within a rapid application time of just a few minutes[155,156,160].

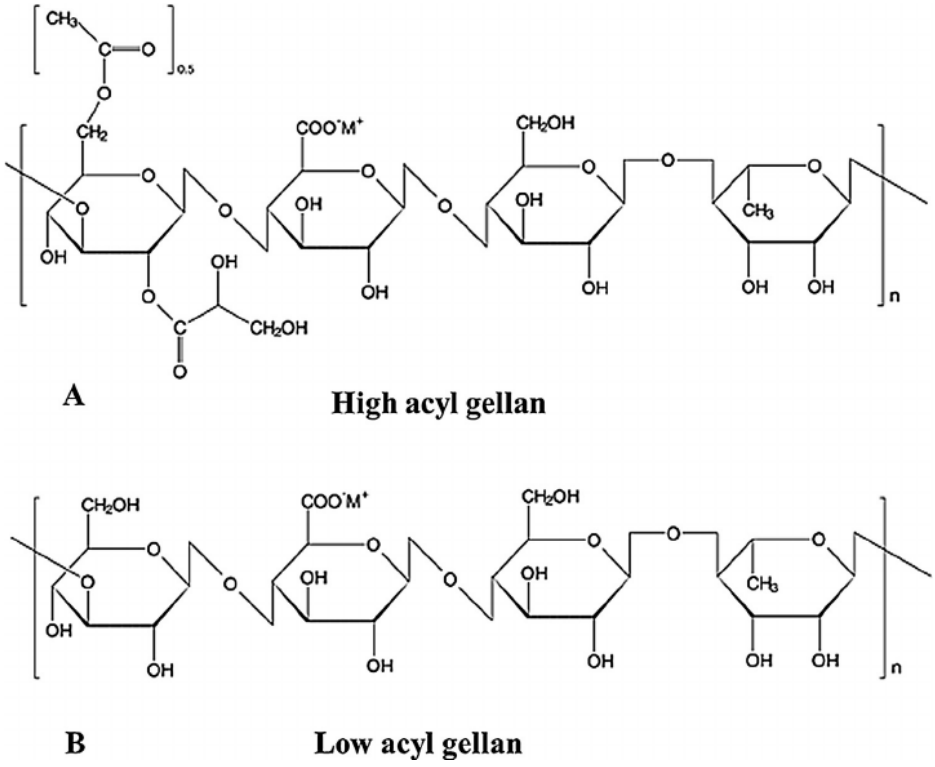

Figure 3- Gellan gum chemical structure

4.3 Synthetic Polymers

In contrast to biopolymers harvested from nature, synthetic polymers are macromolecules designed and created in a laboratory setting[126]. They are the products of polymerization, a process that

chemically links large numbers of small, simple monomers, which are typically derived from petroleum-based feedstocks. The defining feature of this class of materials is the exceptional degree of control that can be exerted over every aspect of their molecular architecture and, by extension, their macroscopic properties. The properties of synthetic polymers are a direct result of their chemical composition and the methods by which they are produced. This ability to tailor polymers for specific functions has made them indispensable materials, underpinning industries from packaging and construction to electronics and medicine[125,126].

The entire field of synthetic polymer science can be understood through a "blueprint to build" paradigm[162]. This approach stands in stark contrast to the "harvest and purify" model that governs the use of biopolymers. The power of synthetic chemistry lies in its ability to design a material from the ground up to meet a specific set of performance criteria. By carefully selecting the monomer chemistry, the polymerization method, and the reaction conditions, a polymer scientist can precisely control the fundamental molecular parameters of the resulting polymer: its average molecular mass, its polydispersity, its chemical functionalities, and its chain architecture (e.g., linear, branched, or cross-linked)[125]. There is a direct and predictable causal relationship between these molecular level "blueprint" specifications and the final macroscopic properties of the material. For example, increasing the average molecular mass generally enhances tensile strength and toughness. Introducing specific comonomers can be used to tune the degradation rate, as seen in the PLGA copolymer system. Even the molecular mass distribution itself can be engineered; for instance, bimodal or trimodal polyethylene grades are deliberately synthesized with distinct populations of high and low molecular weight chains to achieve a synergistic combination of processability (from the short chains) and mechanical toughness (from the long chains[125]). This design-driven process, where properties are engineered rather than simply discovered, is what makes synthetic polymers indispensable for applications that demand high levels of reliability, reproducibility, and performance, such as load-bearing orthopedic implants or long-term drug delivery devices[125].

4.3.1 Poly(vinyl alcohol)

Poly(vinyl alcohol), commonly abbreviated as PVA, is a water-soluble synthetic polymer with a unique synthesis route and a set of properties that make it highly valuable in a wide range of industrial and biomedical applications. It is a semi-crystalline polymer that is odorless, tasteless, non-toxic, and biocompatible[163,164].

Synthesis and Structure

Uniquely among common vinyl polymers, PVA is not synthesized by the direct polymerization of its corresponding monomer, vinyl alcohol. The vinyl alcohol monomer is thermodynamically unstable and readily tautomerizes to its more stable isomer, acetaldehyde. Therefore, PVA is produced commercially through an indirect, two-step process. First, vinyl acetate is polymerized to form polyvinyl acetate (PVAc). In the second step, the PVAc is hydrolyzed (a process also referred to as alcoholysis) using a base catalyst (e.g., sodium hydroxide) in an alcohol solvent (e.g., methanol). This reaction cleaves the acetate groups from the PVAc backbone, replacing them with hydroxyl (-OH) groups to yield PVA (*Figure 4*)[50,54,163,164].

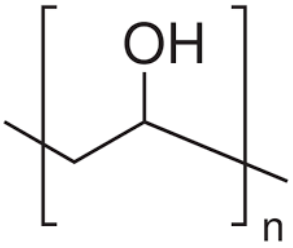

Figure 4- PVA chemical structure

Degree of Hydrolysis and Physicochemical Proprieties

The final properties of a given grade of PVA are determined by two main factors: the degree of polymerization (which dictates the molecular mass) and, most critically, the degree of hydrolysis. The degree of hydrolysis refers to the percentage of acetate groups that have been converted to hydroxyl groups during the synthesis. By controlling this parameter, the properties of PVA can be finely tuned[50,54].

- *Solubility:* The degree of hydrolysis has a deep effect on water solubility. The hydroxyl groups are capable of forming strong intermolecular and intramolecular hydrogen bonds. In fully hydrolyzed grades (>98%), this extensive hydrogen bonding leads to a high degree of crystallinity, making the polymer soluble only in hot water. Conversely, partially hydrolyzed grades (e.g., 87-89%) have residual acetate groups that disrupt the crystalline packing, reducing the strength of the hydrogen bonding network and allowing the polymer to be soluble also in cold water. This tunability of water solubility is a key functional feature of PVA.
- *Mechanical Properties:* Mechanical strength is also strongly dependent on the degree of hydrolysis. The increased hydrogen bonding capacity in more fully hydrolyzed grades leads to significantly higher tensile strength. For example, a 99% hydrolyzed PVA can exhibit a tensile strength in the range of 67-110 MPa, whereas decreasing the hydrolysis to around 89% lowers the tensile strength from 24 to 79 MPa.

PVA is known for its excellent film-forming, emulsifying, and adhesive properties. It is resistant to oils, greases, and most organic solvents[50]. As a hydrophilic polymer, its properties are sensitive to humidity; absorbed water acts as a plasticizer, which decreases the tensile strength but increases the elongation and tear strength of PVA films. PVA is considered biocompatible in particular applications and is relatively degradable in biological environments, especially in aqueous environments, a property attributed to the presence of hydroxyl groups that make it susceptible to hydrolysis and oxidation.

***Hydrogel Formation and Crosslinking*[50,54,164]**

A particularly important property of PVA for biomedical applications is its ability to form hydrogels. Strong, highly elastic, and biocompatible hydrogels can be formed from aqueous PVA solutions through a purely physical crosslinking process involving repeated freeze-thaw cycles. During freezing, the exclusion of PVA chains from the growing ice crystals concentrates the polymer, promoting the formation of small, stable crystalline regions. These crystallites are thermally stable at room temperature and act as physical crosslinks, creating a robust 3D network. The properties of these hydrogels can be controlled by the number of freeze-thaw cycles, PVA concentration, and molecular weight. Additionally, PVA can be chemically cross-linked by reacting its hydroxyl groups with various crosslinking agents (e.g., glutaraldehyde, boric acid) to create more permanent networks with enhanced mechanical stability and reduced water solubility.

***Applications*[54]**

The versatile properties of PVA have led to its use in a multitude of applications:

- *Industrial Applications:* It is widely used as an adhesive, a sizing agent in the textile industry to strengthen yarn for weaving, a coating for paper to improve printability and water resistance, and as a protective colloid in emulsion polymerization. Its water solubility and biodegradability are leveraged in applications like single-use packaging for detergents and agrochemicals.
- *Biomedical Applications:* Due to its excellent biocompatibility, non-toxicity, and low protein adhesion, PVA is extensively used and studied in the medical field. It is a component in contact lenses, eye drops, and wound dressings. PVA hydrogels are particularly promising as biomaterials for soft tissue replacement, such as artificial cartilage, due to their high-water content and rubbery mechanical properties that can mimic natural tissues. It is also used to realize drug delivery systems (DDS) and scaffolds for tissue engineering, often blended with other polymers to modulate properties like hydrophilicity and cell adhesion.

4.3.2 Poly(ethylene oxide)

Poly(ethylene oxide) (PEO) is a synthetic polyether that holds a position of unique importance in the field of biomaterials and pharmaceuticals. It is a linear, non-ionic, and highly hydrophilic polymer with outstanding combination of properties, including water solubility, biocompatibility for particular applications, and a remarkable ability to evade recognition by the immune system[124,162,165].

Synthesis and Nomenclature

PEO is synthesized via the ring-opening polymerization of its cyclic ether monomer, ethylene oxide. The polymerization can proceed through various mechanisms, including anionic, cationic, and coordination pathways. A common convention in the scientific literature distinguishes between the polymer based on its molecular mass: low molecular mass species, typically below 20,000 g/mol, are referred to as poly(ethylene glycol) (PEG), while high molecular mass polymers are called poly(ethylene oxide) (PEO) (*Figure 5*)[124,162,165].

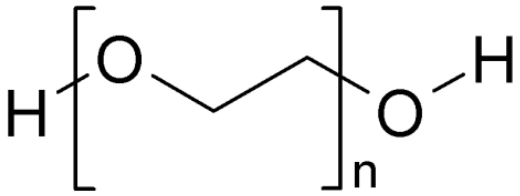

Figure 5- PEO chemical structure

Physicochemical Properties[124,162]

The defining characteristic of PEO/PEG is its high solubility in water across a wide range of concentrations, a property that is unusual for a polymer with a straightforward hydrocarbon-ether backbone. This hydrophilicity is attributed to the ability of the oxygen atoms in the ether linkages to form hydrogen bonds with water molecules. The flexible C-O-C bonds in the backbone allow the polymer chain to adopt conformations in water that maximize these specific interactions. PEO is a semi-crystalline polymer, with a melting point of approximately 65°C for high molecular mass grades. Crucially for biomedical applications, PEO is renowned for its non-toxicity, and extremely low immunogenicity and antigenicity. When present on a surface, the highly hydrated and mobile PEO chains create a steric barrier that effectively prevents the adsorption of proteins and the adhesion of cells.

Applications[165]

The unique properties of PEO/PEG have made it a cornerstone material in the pharmaceutical and biomedical industries.

- *Pharmaceutical Excipients:* PEO is widely used as an excipient in oral drug formulations. It functions as a matrix-former in controlled-release tablets, where the drug is dispersed within a PEO matrix. Upon ingestion, the PEO swells to form a gel layer that controls the rate of drug diffusion out of the tablet. It is also used in osmotic pump tablet systems and as a binder, lubricant, and solubilizing agent.
- *Drug Delivery Systems:* PEG is a fundamental component of many advanced drug delivery systems. It is commonly used as the hydrophilic "corona" block in amphiphilic block copolymers (e.g., PEG-PLA, PEG-PCL), which self-assemble in water to form nanoparticle structures like micelles and polymersomes. These nanocarriers can encapsulate hydrophobic drugs in their core while the PEG shell provides stability and stealth properties.
- *Tissue Engineering and Bioprinting:* The non-toxic and protein-repellent nature of PEO makes it a useful material in tissue engineering. It can be cross-linked to form hydrogels that provide a biocompatible environment for cell encapsulation. It is also frequently incorporated into bio-inks for 3D bioprinting to improve their rheological properties and ensure the viability of printed cells.

4.3.3 Poly(caprolactone)

Poly(ε-caprolactone) (PCL) is a synthetic aliphatic polyester that has become one of the most important and widely investigated biodegradable polymers for biomedical applications. It is distinguished by its combination of biocompatibility for particular applications, mechanical toughness, and, most notably, its slow degradation rate[166–168].

Synthesis and Structure

PCL is a semi-crystalline polymer which can be synthesized by the polycondensation of 6-hydroxycaproic acid or, more commonly, by the ring-opening polymerization (ROP) of the cyclic monomer, ε-caprolactone. Last polymerization is typically catalyzed by metal-based compounds, with stannous octoate ($Sn(Oct)_2$) being one of the most widely used catalysts due to its approval by the U.S. Food and Drug Administration (FDA) for certain applications. The ROP method allows for good control over the final molecular mass and results in polymers with a relatively narrow molecular mass distribution (*Figure 6*)[166].

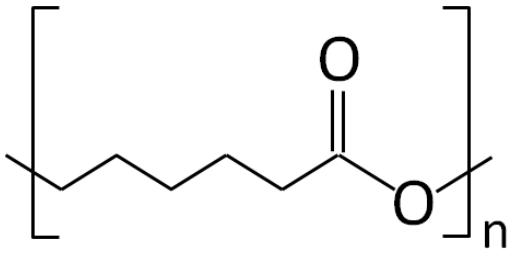

Figure 6- PCL chemical structure

Physicochemical and Mechanical Properties

The properties of PCL make it particularly well-suited for applications requiring long-term structural integrity in a biological environment[169].

- *Solubility and hydrophobicity:* PCL is a hydrophobic polymer. It is insoluble in water and alcohols but is soluble in a range of nonpolar organic solvents such as chloroform, dichloromethane, benzene, and toluene. This hydrophobicity is a key property, but it can also be a limitation in biomedical applications, as it can lead to poor wettability and limited cell adhesion and infiltration into PCL-based scaffolds.
- *Thermal properties:* PCL is characterized by a very low glass transition temperature (Tg) of approximately -60°C and a relatively low melting point (Tm) in the range of 59–64°C. The Tg value far below physiological temperature (37°C) means that the amorphous regions of the polymer are in a flexible, rubbery state under in vivo conditions. This contributes significantly to the material's high toughness and elasticity.
- *Mechanical profile:* PCL possesses robust mechanical properties, including high tensile strength and elasticity, which can be tailored by controlling its molecular weight and crystallinity. Its rheological and viscoelastic characteristics make it readily processable into various forms, such as fibers, films, and 3D porous scaffolds, using techniques like electrospinning, solvent casting, and additive manufacturing.

Degradation Profile[170]

The most defining feature of PCL is its very slow degradation kinetics. Degradation in the body occurs primarily through the non-enzymatic, bulk hydrolysis of the ester bonds in its backbone. Because PCL has a more hydrophobic character and a lower density of ester groups along its chain compared to other aliphatic polyesters like PLA and PGA, its rate of water penetration and subsequent hydrolysis is significantly slower. The complete in vivo resorption of a PCL implant can take two to three years or even longer, depending on its molecular weight, crystallinity, and geometry. This slow degradation profile is ideal for applications that require a stable mechanical support for an extended period, allowing sufficient time for slow-healing tissues, such as bone, to regenerate before the scaffold loses its structural integrity.

Applications[171]

PCL is an FDA-approved biomaterial that has been extensively utilized in a wide array of medical devices and tissue engineering strategies due to its biocompatibility and proven safety profile.

- *Tissue Engineering:* PCL is a dominant material for fabricating scaffolds for the regeneration of hard tissues like bone and cartilage, where its mechanical strength and slow degradation are critical advantages. It provides a durable framework that can withstand physiological loads while the new tissue forms.
- *Controlled Drug Delivery:* Its slow degradation and high permeability to many small-molecule drugs make PCL an excellent candidate for long-term, controlled drug delivery systems. It is used to create implantable devices, microspheres, and nanofibers that can release therapeutic agents in a sustained manner over periods of months to years, which is beneficial for applications like long-acting contraception or chronic disease management.
- *Modification and Blending:* To address the limitation of its hydrophobicity and lack of cell recognition sites, PCL is frequently modified. This is often achieved by blending or copolymerizing it with other polymers. For example, blending PCL with a hydrophilic polymer like PVA can improve the wettability and cell attachment properties of a scaffold. It can also be combined with natural polymers or bioactive ceramics to create composite materials with enhanced biological functionality.

The three synthetic polymers detailed here, PVA, PEO, and PCL, are not merely an arbitrary selection; they represent a "functional triad" that provides biomaterials scientists with a versatile and complementary toolkit for addressing a broad spectrum of design challenges. Each polymer embodies a distinct functional archetype, particularly with respect to its interaction with water and its long-term stability. PVA can be considered the "tunable hydrophile," a material the primary feature of which is its water solubility and ability to form soft, tissue-mimicking hydrogels, with properties that are directly controlled by its degree of hydrolysis. PEO is the "bio-inert shield," a polymer the extreme hydrophilicity of which and unique chain dynamics are leveraged not for structural purposes, but to create an interfacial layer that renders drugs and nanoparticles "invisible" to the immune system. Finally, PCL is the "durable hydrophobe," a material defined by its mechanical robustness and, most critically, its very slow hydrolytic degradation, making it the material of choice for long-term structural support.

This triad covers a wide spectrum of essential design parameters. In terms of water interaction, they range from the extremely hydrophilic and protein-repellent PEO, to the hydrophilic and gel-forming PVA, to the water-insoluble and hydrophobic PCL[126]. In terms of in vivo stability, they span from the long-lasting PCL (degradation over years) to the more moderately degrading PVA, to the largely stable PEO (which is typically cleared rather than degraded). Mechanically, they offer solutions from the tough, load-bearing PCL to the soft, compliant PVA hydrogels, with PEO serving primarily as a non-structural surface modifier. A researcher can therefore select from or combine members of this triad based on the specific needs of an application. A long-term bone scaffold requires the mechanical strength and slow degradation of PCL. A protein drug that needs to circulate longer in the blood requires PEGylation with PEO. A soft material to replace cartilage requires a PVA hydrogel. If the PCL scaffold proves too hydrophobic for optimal cell growth, it can be blended with PVA to enhance its surface hydrophilicity. This strategic interplay demonstrates that these three polymers form a fundamental and powerful toolkit, allowing for the rational design and fabrication of a vast range of advanced biomaterials.

EXPERIMENTAL PART

Chapter 5.
Materials

Polymers

Agar Art was purchased by CTS s.r.l

Agar Purissimo was purchased by Bresciani S.r.l (Agar BS)

Agar was purchased by Sigma-Aldrich (Agar SIGMA)

Agar food-grade imported from the United Kingdom (Agar FOOD)

Agar Noble was purchased by Difco (Agar NOBLE)

Agarose low gelling temperature (Type XI) was purchased by Sigma-Aldrich

Carboxymethylcellulose (CMC) was purchased by Sigma-Aldrich

Gellan Gum Kelcogel was purchased by CTS s.r.l

Poly(ethylene oxide) with $\bar{M}v$=300 kDa was purchased by Sigma-Aldrich

Polyethylene glycol with $\bar{M}v$ = 8 kDa was purchased by Fluka

Poly(vinyl alcohol) fully hydrolysed was purchased by Sigma Aldrich (estimated $\bar{M}v$ = 100kDa)

Poly(caprolactone) with different molecular weights ($\bar{M}v$ =37 kDa, 50 kDa , 80 kDa) was purchased by CAPA

Monomers and initiator

Benzoyl peroxide was purchased by Sigma-Aldrich

Trimethylolpropane Trimethacrylate (TMPTMA) was purchased by Sigma Aldrich

Solvents

Acetone, toluene, ethanol, xylene, n-hexane, cyclohexane, isododecane, and Methyl Ethyl Ketone (MEK), and methanol were purchased by Sigma-Aldrich

Benzyl alcohol was purchased by CTS s.r.l.

Glacial acetic acid was purchased by VWR Chemicals

Surfactants

Triton^{TM} X-100 laboratory grade was purchased by Sigma-Aldrich

Tween ^{TM} 20 for molecular biology was purchased by ITW Reagents

Bacterial strains

Bacillus subtilis ATCC 6633

Pseudomonas stutzeri ATCC 17588 were purchased by the ATCC organization

Salts

$HAuCl_4$ and $AgNO_3$ were purchased from Alfa Aesar

Calcium chloride dihydrate was purchased by Riedel-de Haen

Sodium chloride was purchased by VWR Chemicals

Dyes

Congo red was purchased by Sigma-Aldrich

Amido Black was purchased by Sigma-Aldrich

Others

Peptone from gelatine, pancreatic digest, was purchased from Fluka Analytical

LIVE-DEAD BacLight Bacterial Viability Kit (LZ012) was purchased by Thermo Fisher Scientific (Invitrogen)

Yeast extract for use in microbiological growth medium was purchased by Sigma-Aldrich

Chitin azure substrate for chitinase activity was purchased by Sigma-Aldrich

Tryptic Soy Broth (TSB) was purchased by VWR Chemicals

Gelatin was purchased by Sigma-Aldrich

Glucose for microbiological assay was purchased by Sigma-Aldrich

Skim Milk powder, sucrose and monosodium glutamate were purchased by Sigma-Aldrich

All chemical reagents are commercially available and were used as supplied without further treatment.

Chapter 6.
Experimental Methodologies and Characterization Techniques

6.1 Electrospinning methodology

In the present Thesis work, electrospinning was carried out using an Electrospinning Professional Machine provided by Doxa Microfluidics and equipped with a flat or a rotating drum collector and comprised of an electrical power supply and a volumetric pump.

6.2 Rheological characterization

Rheological measurements have been carried out on the polymer–based solutions by means of a rotational rheometer MCR 301 (Anton Paar, Austria GmbH) equipped with a Peltier heating system and a solvent trap kit. Plate – plate (PP) and cone – plate (CP) geometries with different diameters (25 or 50 mm) were employed depending on the viscoelastic response of the sample of interest. For PP geometries the gap between the plates was fixed at 0,75 mm.

Steady – State Viscosity Measurements

Typically, steady–state viscosity measurements were conducted by applying an increasing shear-rate ($\dot{\gamma}$) at a fixed temperature to evaluate the sample flow behaviour (in our case, 25°C for synthetic polymer-based solutions, 45°C for Agar and Agarose solutions). The most common performances that were observed for the tested samples are reported in Figure 7[172] and summarized in the followings:

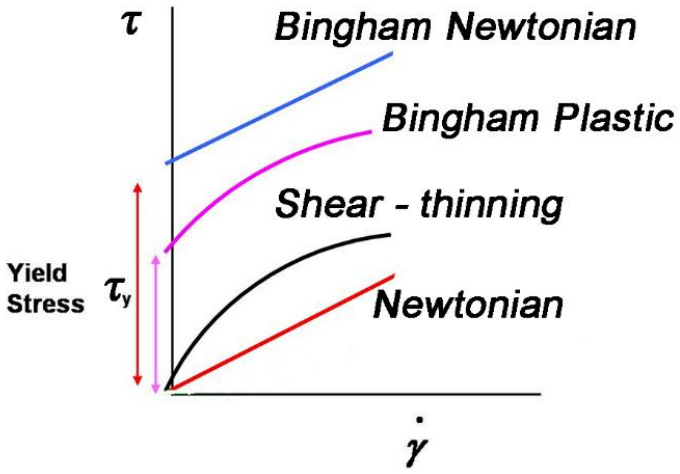

Figure 7- Fluid flow behaviours

i)Newtonian fluids. These fluids are described by Newton' law (Equation 1[172]) and are characterized by a constant viscosity value independent of the applied shear stress:

Equation 1

$$\eta = \frac{\tau}{\dot{\gamma}}$$

where η is the apparent viscosity and τ is the shear stress.

ii)Shear – thinning fluids. These fluids present a viscosity value that depends on the applied shear stress. Most polymer–based formulations involve a constant viscosity region at low shear rate values (i.e., Newtonian plateau) followed by a gradual decrement of the viscosity as the shear rate increases. Such an outcome is mainly related to the polymer chain entanglement. Specifically, at very low shear stress, the macromolecules form a dense and continuous polymer network, creating topological constraints with each other (i.e., physical entanglements). As the applied stress is increased, entanglements are progressively disrupted and the polymer chains tend to assume an oriented configuration, which in turn leads to a decrease in the solution viscosity. In the present Thesis work, shear–thinning fluids have been described with the Carreau–Yasuda model (Equation 2[173]):

Equation 2

$$\eta = \frac{\eta 0 - \eta\infty}{[1 + (\lambda\dot{\gamma})^a]^{\frac{1-n}{a}}}$$

where η0 is the zero–shear viscosity (i.e., fluid viscosity at rest), η∞ is the infinite–shear viscosity (i.e., fluid viscosity once all the polymer chains are aligned), λ is the fluid relaxation time, a is a fluid constitutive parameter, and n is the flow index.

iii) Bingham fluids. These materials behave as elastic solids at low shear stress and as viscous fluids at high shear stress. Specifically, these systems require a minimum stress (i.e., yield stress τy) to flow due to the existence of interactions between the components that form a weak solid structure, preventing the movement of the fluid. In the present Thesis work, Bingham fluids have been described with the Casson model (Equation 3[174]):

Equation 3

$$\sqrt{\tau} = \sqrt{\tau_0} + \sqrt{\eta_c\dot{\gamma}}$$

Where τ is the shear stress, the force per unit area required to make the fluid flow, $\tau_0$is the yield stress, the minimum amount of shear stress that must be applied to the fluid before it starts to flow, η_c is the plastic viscosity and $\dot{\gamma}$ is the shear-rate.

Temperature Sweep Measurements

Temperature sweep tests (TS) were conducted at a fixed deformation amplitude within the LVER (1%) and frequency (1 Hz), varying the temperature with a heating rate of 1 °C/min, in the range between 80°C-20°C.

6.3 Morphological characterization

Scanning electron microscopy (SEM) has been performed on electrospun mats either using a Hitachi TM3000 (Oxford Instruments) benchtop microscope with the specimen chamber was maintained in a vacuum, and the accelerating voltage was 15 kV, or a LEO Electron Microscopy Ltd (1430 VP, 2001) instrument, using backscattered and secondary electrons. Good conductivity of the samples was achieved with a thin layer of gold sputter–coated.

Field–emission scanning electron microscopy (FESEM) has been carried out on electrospun mats by means of a ZEISS SUPRA 40 VP operating in direct or back-scattering configuration. Good conductivity of the samples was achieved with a thin layer of carbon sputter–coated, using a Polaron E5100. In any case, the obtained micrographs have been analysed with the open–source software ImageJ.

Atomic force microscopy (AFM) has been executed on electrospun mats via a Veeco instrument operating in contact mode with a sampling rate of 1024 points/line. The micrographs obtained have been analysed with the software Mountains Software.

Transmission electron microscopy (TEM) has been performed on gold and silver nanoparticle suspensions using a JEOL JEM 2100 Plus (JEOL Ltd) instrument operating at 200 kV. Specimens were prepared by evaporating a sample drop on a 300 mesh carbon-coated copper grid (Lacey).

6.4 Mechanical characterization

Mechanical investigation was performed on electrospun mats via uniaxial tensile test by using a displacement–controlled dynamometer, Instron 5565. Sample testing has been performed on rectangular specimens (10x30x0.1 mm) at room temperature with an elongation rate of 0.2 mm/s. Young modulus (Y), tensile strength (σb), and elongation at break (εb) were derived from the obtained stress–deformation curves.

6.5 Spectroscopic characterization

Fourier–transform infrared spectroscopy (FTIR) has been conducted on polymer films and powders by means of a Bruker Vertex 70 instrument, operating in ATR mode, in the 400 – 4000 cm^{-1} wavenumber range with a resolution of 2 cm^{-1} (128 scan).

X-ray fluorescence spectroscopy (XRF) has been conducted directly on the Agar's powders by a portable energy-dispersive spectrometer ELIO (XG Lab, Milan, Italy; Bruker Optics, Billerica, MA, USA) with a beam collimated to 0,65 mm in diameter. The working conditions were 30 kV and 120 μA without helium flux to avoid sample loss.

An EDX probe SwiftED3000 was combined to the Scanning electron microscopy Hitachi TM3000 for elemental analyses directly on raw Agar particles. Analyses were repeated on five zones for each type of Agar.

UV-VIS spectra of the colloidal suspensions were recorded at room temperature through a Shimadzu UV-1800 spectrophotometer with fused silica cuvettes of different path lengths. To monitor the stability of colloidal solutions over time, UV-Vis spectra were carried out after 1, 3, 7, 14, 28 and 60 days after 30 minutes of stirrer at 50 °C to avoid gelation of the samples.

6.6 pH measurements

To evaluate the pH of the polysaccharide solutions from which the nanoparticles were synthesised (Chapter 9), the XS PH50 VIOLAB bench pH meter was used.

6.7 Stability and Swelling-Deswelling characterizations

The stability of the mats was evaluated with an immersion test in water and in different organic solvents usually used in the cleaning of Cultural Heritage. Pieces of the mats, with a comparable weight and thickness, have been inserted in some ad hoc pre-prepared pockets of Teflon to maintain the shape during the test. Membranes were weighed on an analytical balance before the test and after 5 minutes of immersion with manual stirring in solvents. After washing and before each weighing the mats were placed in the oven for 1 h at 70°C.

Data were expressed in terms of weight loss by Equation 4[175]:

Equation 4

$$\Delta W\ \% = \frac{(W_i - W_f)}{W_i} \cdot 100$$

Where ΔW % is the weight loss after 5 minutes of immersion, W_i is the initial weight of the mats and W_f is the final weight after immersion and dry.

The mat swelling degree ($\Delta SW\%$) was described by Equation 5[175]:

Equation 5

$$\Delta SW\ \% = \frac{(W_{si} - W_i)}{W_i} \cdot 100$$

Where W*si* indicates the weight of the "wet" membrane at different times i-th (i=1, 3, 5, 10 minutes) and W*i* indicates the initial weight of the membrane.

The measurements were performed at room temperature (25 °C). In order to measure W*si*, pieces of mat with an area of 2 cm^2 were put into 50 ml of solvents for 1, 3, 5, and 10 minutes.

To study the swelling reversibility, the swollen samples were taken out from the solvents and placed over a Teflon disc until the excess of solvent was eliminated and then left at room temperature for different times (1, 3, 5, 10, 30, 60 minutes) on a worthless painted canvas as a standard porous surface.

The deswelling was described by Equation 6[175]:

Equation 6

$$\Delta dSW\% = \frac{(Wdsi - W_i)}{W_i} \cdot 100$$

where W*dsi* indicates the weight of the membrane after the i-th time of application on the paint (i=1, 3, 5, 10, 30, 60 minutes) and W*i* indicates the initial weight of the membrane.

6.8 Wettability and Surface Tension Characterization

The wettability of mats was evaluated as water contact angle investigation (WCA) and measured by the deposition of a small drop of glycerol on the sample surfaces using a DSA 10, Krüss (Hamburg, Germany) tensiometer.

The pendant drop method was used to measure the surface tension of the polymer solution with an automatic surface tension detector (*Attension Tetha Light*). Experiments were performed at 25 °C. The volume of a single droplet is 3 μL suspended at the bottom of the syringe. Recording and analyzing time were set every 0.25 s for a total of 10 s for every drop. Each sample was tested 5 times to take an average surface tension value and improve the measurement precision.

6.9 Bacterial metabolic characterization

A study of the metabolic activity of two species of bacteria already used in the field of bio-cleaning of Cultural Heritage was conducted with five protocols selected from the literature based on the ability of bacteria to degrade characteristic chemical compounds[176–181].

- *Lipolytic activity*: lipid hydrolysis due to esterase production was evaluated on solid growth medium consisting of peptone 10 g/L, NaCl 5 g/L, $CaCl_2$ $2H_2O$ 0.1 g/L, Agar 15 g/L, Tween20 10 mL/L solubilized in distilled water. Esterase activity was revealed by a turbid zone around the streaked colonies on the plates.

- *Cellulolytic activity*: was evaluated on a solid growth medium consisting of 0,1 g/L of yeast extract, 0,5 g/L of CMC and 1,5 g/L of Agar solubilized in distilled water. After bacterial incubation, CMC hydrolysis was evidenced by covering with a 1% (w/v) aqueous solution of Congo Red for 15 min and removing the dye with 1M NaCl for 15 min to stabilize the reaction. Any areas of hydrolysis manifested as clarification halos.

- *Proteolytic activity*: test was performed using a solid medium prepared using 3 g/L of TSB, 1,5 g/L of Agar, 0,1 g/L of gelatin, 0,8 ml/L of glucose (0.25% w/v) dissolved in distilled water. After bacterial incubation gelatin hydrolysis was evidenced by covering with a 0,1 % w/v solution of Amido black in methanol-acetic acid-water in the ratio 30/10/60 for 1 hour at 30°C and decolorized with a solution of methanol-acetic acid-water, in the same ratio for 15 minutes. Any areas of hydrolysis manifested as clarification halos.

- *Chitinolytic activity (first method)*: an initial medium was prepared using 0,75 g/L Agar and 0,10 g/L yeast extract dissolved in distilled water. After sterilization, the medium was dispensed into plastic tubes with caps (2 ml per tube) and left to cool under a sterile hood in an upright position.

  A second medium consisting of two solutions was then prepared:

  A - 0.1125 g Agar, 0.015g yeast extract and 10 ml distilled water (2/3 of the total volume).

  B - 0.0300 g of Chitin Azure and 5 ml of distilled water (1/3 of the total volume).

  Media A and B were sterilized and mixed while still warm and poured into the tubes above the already solid base medium layer. Using a pipette, 0.5ml of medium was poured per tube

and left to solidify under sterile conditions. The tubes were incubated and inspected periodically for any diffusion of dye into the base soil layer.

- *Chitinolytic activity (second method)*: bacteria were incubated with 1 g of *Velella velella* dehydrate and 2 ml of PBS; degradation of chitin in *Velella* was checked after 2 days.

Each test medium was autoclaved at 121°C for 20 minutes and 10^8 bacterial cells were incubated for seven days at 30°C for optimal bacterial growth.

6.10 Bacterial adhesivity tests

This chapter details the comprehensive methodology used to evaluate the adhesion of *Bacillus subtilis* and *Pseudomonas stutzeri* onto the surface of Polycaprolactone (PCL) mats. The study employed a standardized protocol incorporating sample sterilization, bacterial culture preparation, an adhesion incubation phase, and subsequent quantification via a fluorescence-based Live/Dead viability assay. The LIVE/DEAD BacLight Bacterial Viability Kits utilize mixtures of the SYTO 9 green-fluorescent nucleic acid stain (dye A) and the red-fluorescent nucleic acid stain, propidium iodide (dye B). These stains differ both in their spectral characteristics and in their ability to penetrate healthy bacterial cells. When used alone, the SYTO 9 stain generally labels all bacteria in a population — those with intact membranes and those with damaged membranes. In contrast, propidium iodide penetrates only bacteria with damaged membranes, causing a reduction in the SYTO 9 stain fluorescence when both dyes are present. Thus, with an appropriate mixture of the SYTO 9 and propidium iodide stains, bacteria with intact cell membranes stain fluorescent green, whereas bacteria with damaged membranes stain fluorescent red. The excitation/emission maxima for these dyes are about 480/500 nm for SYTO 9 stain and 490/635 nm for propidium iodide. The background remains nonfluorescent.

Preparation of Substrate and Bacterial Suspensions

The PCL mats were prepared by cutting them into uniform circular discs with a 3 mm diameter. Sterilization was achieved sequentially: first, immersion in ethanol for 30 minutes, followed by exposure to UV-C irradiation (254 nm) within a laminar flow hood for 15 minutes on each side.

For the bacterial preparation, single colonies of both species were grown in 25 mL Falcon tubes containing Luria-Bertani (LB) medium 24 hours at 37°C with agitation. The resultant suspensions were then washed to remove residual growth medium. This involved centrifugation at 4000 rpm for 10 minutes, removal of the supernatant, and re-suspension of the pellet in 5 mL of sterile physiological solution (0,9 % w/v NaCl). This process was repeated once, and the final pellet was re-suspended in 5 mL of sterile physiological solution.

The concentration was standardized by measuring Optical Density (OD) at 600 nm using a (NAME of Spectrophotometer) and correlating this value to previously determined CFU/mL data. The final working suspensions were diluted to a standardized inoculum of 1 × 10^7 CFU/mL for both bacterial species.

Adhesion Incubation and Washing Procedure

The adhesion experiment was initiated by submerging the thirty sterilized PCL mat discs into two separate Petri dishes containing sterile physiological solutions. The standardized bacterial suspensions (1x × 10^7 CFU/mL) were then added to the respective Petri dishes. Adhesion proceeded during

a 20-hour incubation at 37°C under 100 rpm agitation. The use of physiological solution prevented bacterial proliferation during the test, ensuring the measurement focused on the initial adhesion event.

To isolate firmly adhered bacteria, a rigorous washing step followed the incubation period. The PCL discs were transferred to fresh Petri dishes containing sterile physiological solutions and subjected to manual agitation for 15 minutes. This washing procedure was repeated a second time by transferring the discs to a new batch of physiological solution and agitating for another 15 minutes, thereby removing non-specifically bound or planktonic cells.

Preparation of Controls and Reagents

For robust quantification, Live/Dead controls were prepared alongside a standard curve. The Live Control was prepared by mixing 1 mL of the standardized bacterial suspension in 20 mL of sterile physiological solution, while the Dead Control involved mixing 1 mL of the bacterial suspension in 20 mL of isopropanol. Both controls were incubated for 1 hour at 37°C, and their OD600 was measured. Additionally, serial dilutions were prepared to obtain reference concentrations ranging from 1x 10^7 CFU/mL to 1x 10^4 CFU/mL.

The staining solution was prepared by combining 30 µL of Dye A and 30 µL of Dye B in 10 mL of sterilized distilled water.

Spectrofluorimetric Analysis

The washed PCL discs (nine samples for each species with 100 µL of physiological solution), blank samples mat (in triplicate and with 100 µL of physiological solution), blank solution (100 µL of physiological solution, in triplicate), reference concentrations, and live/dead ratio solutions (each well with 100 µL of medium) were transferred into two 96-well plates as suggested by the protocol.100 µL of the prepared dye solution was added to each well. The plate was then incubated in the dark for 15 minutes to facilitate the staining process. The fluorescence intensity was subsequently measured using a spectrofluorometer at the specific excitation and emission wavelengths corresponding to the Live (Dye A) and Dead (Dye B) stains, allowing for the differential quantification of viable and non-viable bacteria adhered to the PCL surface.

6.11 Mat-bacteria coupled conservation methods and biodegradability tests

Conservation methods

To evaluate the viability of adhesive bacteria on mats over time, after the immobilization process (see the previous paragraph), four different conservation methods were applied. All the procedures were conducted under a biological laminar flow cabinet to ensure sterility.

I) *Dry conservation*
Ten samples of mat-bacteria coupled were conserved in an Eppendorf tube without any solvent or solution at 4°C.

II) *Physiological solution conservation*
Ten samples of mat-bacteria coupled were conserved in an Eppendorf tube with physiological solution as conservation medium at 4°C.

III) Phosphate buffer solution (PBS) conservation

Ten samples of mat-bacteria coupled were conserved in an Eppendorf tube with phosphate buffer solution as conservation medium at 4°C.

IV) Freeze-drying conservation

The freeze-drying standard method was ad hoc modified for our application[182–186]. To ensure the sterility of all phases of the process, Spin-X centrifuge tubes were used: the filter inside the tubes can guarantee the passage of air without microorganism contamination.

To prepare the bacteria on the mat for the freeze-drying process, five samples of mat-bacteria were incubated in a cryoprotectant solution composed of skim milk (20% w/v), sucrose (20% w/v), and monosodium glutamate (2% w/v), as suggested in the literature. To ensure the sterility of the suspension, skim milk powder was irradiated with a UV lamp for 30 minutes, and sucrose and monosodium glutamate pre-prepared solutions were sterilized by a syringe filter. After 30 minutes of immersion, the mat's samples were put in the Spin-X centrifuge tubes under a laminar flow cabinet and put at -80°C for two hours. Finally, samples were put in a freeze-dryer LIO-5P for 24 hours. After the lyophilization process, samples were conserved in Spin-X tubes at 4°C.

After two months of conservation, to evaluate the viability of bacteria and the number and percentage of live bacteria on the mats, the LIVE/DEAD kit was used (see previous paragraph). Furthermore, a growth test in LB broth was carried out (one sample for each bacterial species in 25 ml of growth medium, in triplicate).

Biodegradability evaluation

To evaluate the biodegradability of PCL mats, samples of mat (circular disc) were conserved in 20 mL of bacterial suspension of *Bacillus subtilis* and *Pseudomonas stutzeri* (10^8 cfu/ml) in LB broth.

The state of conservation of the mats was checked weekly for a total observation period of 30 days.

6.12 Crosslinking with acrylic monomer

Crosslinking tests of PEO mats in presence of TMPTMA were conducted with two different methods:

i) Photo-crosslinking with *Helios-Italquartz* UV-lamp (range 240-320 nm) on the prepared mats: UV rays were irradiated on both sides for 10 and 20 minutes respectively at distance of 25 cm from the samples to the lamp.
ii) Thermal crosslinking with oven at 40 °C for four days.

In particular, four different solutions were prepared with different PEO/TMPTMA ratios: 4:1, 3:2, 2:1 and 1:1 w/w of PEO/TMPTMA and with BPO as polymerization initiator (2% v/v on monomer concentration).

To check the stability of fibers after crosslinking, a water immersion test of 5 minutes was carried out. After immersion, to prevent the fibers from collapsing due to water evaporation, a freeze-drying process was carried out using a lyophilizer (24 hours in vacuum after a previous freezing process in a refrigerator at -20 °C for one hour).

Chapter 7.
Agar-based electrospun mats as a cleaning support for controlled release of organic solvents

7.1 Introduction

This section presents the experimental results for the development of electrospun Agar mats designed for cleaning applications, particularly within the field of Cultural Heritage. The methodology involved preparing aqueous solutions of Agar blended with various co-spinning agents: poly(vinyl alcohol) (PVA) fully hydrolysed and poly(ethylene oxide) (PEO) of two distinct molecular weights.

These polymer blends were formulated in five specific ratios (0/100, 30/70, 50/50, 70/30, and 100/0). Prior to electrospinning, the solutions underwent thorough characterization. Rheological and spectroscopic analyses were conducted to evaluate critical parameters such as viscosity and to investigate the molecular interactions between the polysaccharide and the co-spinning agents.

For the fabrication of nanostructured mats via electrospinning, PEO with a higher molecular weight was specifically selected, taking advantage of its favourable rheological properties and surface tension. The resulting electrospun mats were systematically characterized using field-emission scanning electron microscopy (FE-SEM) to assess morphology and through mechanical testing to determine their physical robustness.

Based on these characterizations, the Agar/PEO 50/50 mat was selected for further functional evaluation. This involved testing its stability, as well as its swelling and deswelling capabilities, in various solvents relevant to Cultural Heritage conservation (as detailed in Table 5).[25,27,187,188]

Finally, to enhance the mechanical properties of the polysaccharide layer, a multilayer composite mat comprising Agar/PEO and polycaprolactone (PCL) was fabricated and characterized.

Table 5- Organic solvents used in Cultural Heritage cleaning and tested

Solvents	Primary use in CH cleaning
Water	Aqueous cleaning, mixtures for aged varnishes
Ethanol	Aged varnish removal, wood/paper antifungal treatment
Acetone	Aged varnish/adhesive removal (ceramics), controlled cleaning (organogels)
MEK	Paint softening, varnish removal, and architectural marble cleaning
Benzyl Alcohol	Solvent for waxes/shellac, oil swelling, varnish removal (gels)
Isododecane	Potential for non-polar cleaning
Toluene	Dissolving acrylate, aged dammar mixtures
Xylene	Aged dammar mixtures, controlled cleaning (organogels)
Cyclohexane	Solvent for resins/waxes, component in paper coatings
n-Hexane	Adhesives

7.2 Agar-based mats

Samples preparation

The PEO and PVA solutions were obtained by adding powders in glass flasks (10 ml of volume) with deionized water at concentrations of 3 and 10 % w/v by stirring for 1 hour at 70 °C; the Agar solution, at concentration of 3 % w/v, was carried out by adding powder in water, stirring and heating until boiling point (100 °C).

Blend solutions Agar/PEO and Agar/PVA, 70/30, 50/50, 30/70 ratio, containing 3% w/v of total polymers, were prepared by adding a correct amount of Agar powder and deionized water to the co-spinning agent 3 % w/v solution. The samples were placed on a magnetic heating plate and stirred until to boiling point to allow the complete dissolution of polymers. The total concentration of polymers and the ratios in the blend's solutions were selected to reduce the Agar gelling ability but maintain an adequate viscosity.

Triton X-100 was added at polysaccharide blends in a concentration of 1% wt in comparison with the total polymers concentration, maintaining the final solution under stirring for 30 min. To conduct the spectroscopic characterization, solutions of PEO, PVA, Agar, and their mixtures were placed in Petri dishes, obtaining film and gel (when Agar is present), respectively. Subsequently, the samples were cooled at room temperature for at least 1 hour and dried in an oven at 40 °C overnight to obtain films.

Rheological characterizations

To detect the gelation point, a temperature sweep test was carried out. Typical gelation profiles for Agar solution are shown in *Figure 8*. Initially, at high temperature, the Agar solution showed G'' (loss modulus)>G'(storage modulus) with values around 100 and 2 Pa, respectively. Both modules gradually increase as the temperature decreases. At around 40°C, G'=G'', indicating that the gelation point was achieved.
The gelling temperature of Agar may be influenced by the co-spinning agent, however, for the blends could not be determined due to the presence of PEO and PVA transition temperatures (Tg and Tm) within the investigated range[189,190].

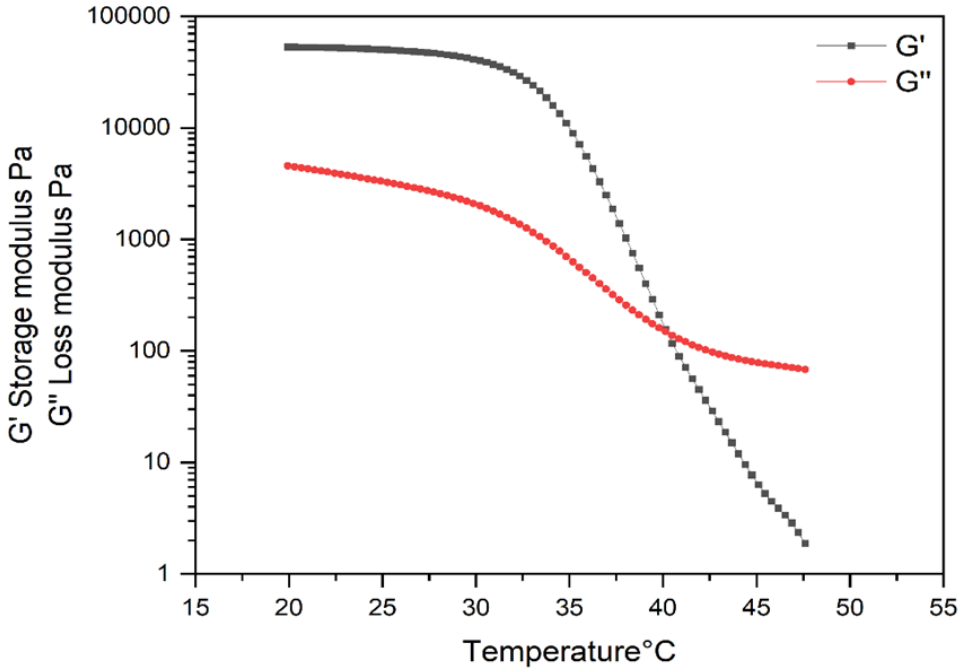

Figure 8- Temperature sweep test of Agar. Gelling temperature appears as the crosspoint of G' and G'' around 40°C

The rheological evaluation at 45°C of Agar and its blends with PEO 300k, PEO 8k, and PVA reveals distinct flow behaviours depending on the polymer composition (*Figure 9*). The Agar-rich systems (pure Agar and blends with high Agar content) exhibit a marked viscoplastic behavior, characterized by the presence of a yield stress (τ_0).

In the flow curves (τ vs $\dot{\gamma}$), this is evidenced by a non-zero intercept on the stress axis and an upward concavity in the double-logarithmic plot, confirming that a critical stress threshold is required to start the flow. This behavior corresponds to the viscosity curves showing a slope approaching -1 at low shear rates, indicative of an infinite viscosity at rest due to the formation of a physical gel network. The application of stress exceeding τ_0 fractures these cohesive forces, resulting in a dramatic viscosity

drop; experimental data for these systems were successfully described using the Casson model, which accounts for both the yield stress and the subsequent shear-thinning flow.

In contrast, the PEO 300k flow curve extrapolates to the origin, consistent with a liquid lacking a yield point. It displays a typical polymer solution behavior: a Newtonian plateau at low shear rates (zero-shear viscosity), followed by a shear-thinning region caused by the alignment of polymer chains along the flow direction. Finally, PEO 8k and PVA solutions are characterized by a purely Newtonian behavior with significantly lower viscosity values, attributed to their lower molecular weight, which prevents significant chain entanglement.

It is well known that in the electrospinning process, needle size, flow rate, and flow velocity are the main parameters affecting the viscosity of the solution and, consequently, the size and morphology of the fibres obtained. Therefore, it was necessary to understand the actual viscosity of the solution during the process.

In fact, when the solution entered the syringe needle, the high viscosity decreased significantly due to the increasing shear rate.

For this reason, the shear force that the solution undergoes can be approximated calculated by Equation 7[191,192]:

Equation 7

$$\dot{\gamma} = \frac{4Q}{\pi R^3}$$

where $\dot{\gamma}$ is the shear rate at the needle wall, Q is the volumetric flow rate, and R is the radius of the needle.

Considering that the shear rate to which the solutions are subjected, in our experimental setup, was around 32 s^{-1} (flow rate and inner needle diameter were fixed at 0,7 ml/h and 0,4 mm, respectively), the real viscosity of the solutions during the process was below 0,5 Pa s for all pure and blend solutions (Table 6).

In particular, for the PEO 8k solution and its blends with Agar, the viscosity is very low, above $0{,}1s^{-1}$ suggests that this co-spinning agent is not adequate for this process, as the average viscosity in the literature suggests for this type of application.

On the other hand, the viscosity of PEO 300k and PVA blends suggests that it is probably possible to electrospun these solutions.

Table 6- calculated shear rate, viscosity and τ_0 for Agar/PEO 8k, Agar/PEO 300k and Agar/PVA blends; electrospinning of pure solutions of PEO 8K, PEO 300k and PVA (3 % w/v) failed

Sample 3 wt%	η @32 s^{-1} (Pa s)	τ_0 (Pa)
Agar/PEO 70/30	0,46	6,99
Agar/PEO 50/50	0,14	0,46
Agar/PEO 30/70	0,07	0,13
PEO 300K	0,06	-

Sample 3 wt%	η @32 s^{-1} (Pa s)	τ_0 (Pa)
Agar/PEO 70/30	0,081	0,12
Agar/PEO 50/50	0,016	0,04
Agar/PEO 30/70	0,010	0,00
PEO8K	0,009	-

Sample 3 wt%	η @32 s^{-1} (Pa s)	τ_0 (Pa)
Agar/PVA 70/30	0,31	5,75
Agar/PVA 50/50	0,09	0,95
Agar/PVA 30/70	0,04	0,20
PVA	0,01	-

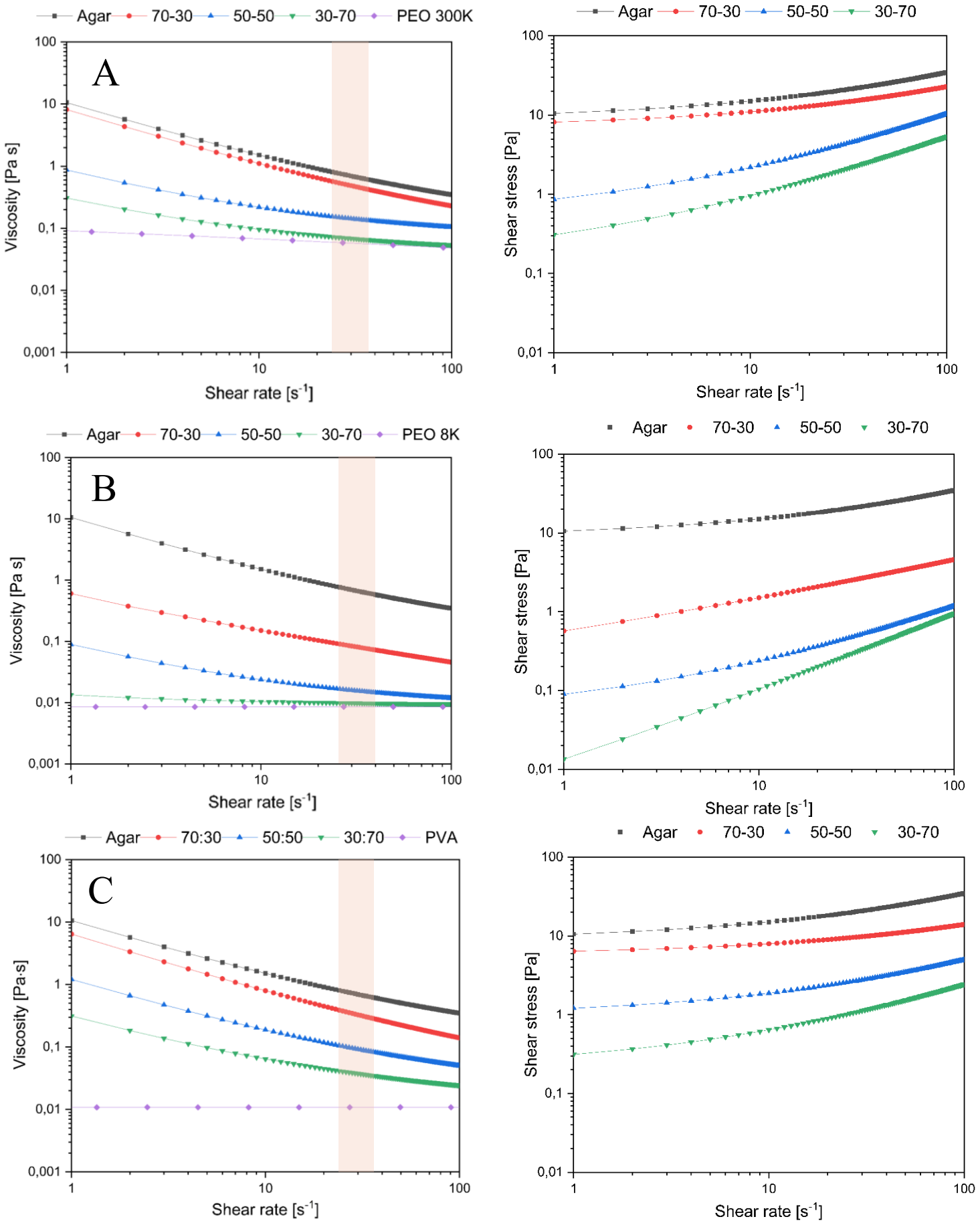

Figure 9- Viscosity and flow curves of PEO 300k (A), PEO 8k (B), PVA (C), and blends (3% w/v). Orange rectangles show the common shear rate range during the electrospinning process (25-35 s^{-1})

Surface tension characterization

To further elucidate the factors governing the electrospinnability of the polymer blends, the role of surface tension was investigated. Direct measurement of the surface tension of the Agar/PEO blend solutions was not feasible due to instrumental limitations. The pendant drop tensiometer used for the analysis lacks a temperature-controlled chamber, and the Agar component would undergo gelation at the temperature of the measurement, preventing the formation of a stable droplet for analysis.

Consequently, the study focused on characterizing the surface tension of 3% w/v aqueous solutions of the PEO and PVA component. The results revealed a clear influence of molecular weight and chemical composition on this property. The PEO 8k solution exhibited a surface tension of 59.9 mN/m, whereas the PEO 300k solution showed a slightly but significantly lower value of 56.8 mN/m. This trend is consistent with the established literature on PEO solutions, confirming that an increase in polymer molecular weight correlates with a decrease in the solution's surface tension. PVA, on the other hand, presents a surface tension of 48,8 mN/m.

These results provide a clear illustration that solution viscosity, while critical, is not the unique determinant of electrospinnability[104]. The importance of surface tension became evident when comparing the electrospinning outcomes of two blends formulated to have very similar solution viscosities: Agar/PEO 300k 30/70 and Agar/PEO 8k 70/30. The former could be successfully electrospun into fibers, while the latter failed, resulting only in electrospraying. Since the critical viscous forces resisting jet breakup were comparable in both solutions, the success of the PEO 300k blend can be attributed, at least in part, to its inherently lower surface tension. This lower surface tension presented less resistance to the elongational forces of the electric field, tipping the balance in favor of stable fiber formation. Similarly, considering it’s possible for Agar/PVA blends, whereas the viscosity evaluation suggests that the solutions could be electrospinnable, but for lower PVA surface tension, the electrospinning process was not possible (electrospraying process and film formation).

Furthermore, the study revealed a synergistic effect of the Agar component, highlighting that electrospinning success is multifactorial. A pure 3% (w/v) solution of PEO 300k could not be successfully electrospun, whereas the Agar/PEO 300k 30/70 blend, with a similar viscosity, readily formed fibers. This suggests that Agar' role extends beyond simply modifying viscosity. As a natural polyelectrolyte, Agar introduces charge carriers into the solution, which significantly increases its electrical conductivity. This enhanced conductivity improves the charge-carrying capacity of the polymer jet, making it more responsive to the applied electric field and promoting stable jet elongation. It may also further modify the surface tension of the blend. These findings collectively demonstrate that successful electrospinning relies on a complex interplay of multiple solution parameters, where sufficient viscosity must be balanced with optimized surface tension and electrical conductivity.

Fourier-transform infrared spectroscopy (FT-IR)

FT-IR spectra of pure Agar, PEO (8k and 300k), and PVA show the characteristic absorption bands of the materials[144–146], with no difference between the powders and the dried films (*Figure 10-11*).

Agar shows a strong and broad band in the range 3400–3300 cm^{-1} assigned to the stretching vibration of OH groups. At lower wavenumber (region 2900–2800 cm^{-1}) the weak IR absorptions are assigned to CH stretching modes. The peaks observed in the region between 1430 and 1200 cm^{-1} can be assigned to sulphates and C-O-H bending vibrations of hydroxyl groups. The most prominent band in IR spectra of Agar powders at 1068 cm^{-1} and 1040 cm^{-1}, respectively, can be assigned to the C-O stretching of 3,6-anhydro-l-galactose, with the contribution of the C-C-O out-of-phase stretching of primary and secondary alcohols of saccharide rings. Peaks at approximately 930 and 890 cm^{-1} are assigned to 3,6-anhydro-l-galactose and galactose units, respectively. FTIR spectra also show several other weak features that can be assigned to sulphate side-groups on d-galactose: indeed, the weak signal at 870 cm−1 is assigned to the C-O-SO_3 vibration of the sulphate group in position C6 of d-galactose. The region of the spectra between 770 and 740 cm^{-1} presents other characteristic bands of Agar assigned to the skeletal bending of pyranose rings.

PEO (8k and 300k) spectra show characteristic absorption bands have been identified as follows: C–O, C–C stretching, CH_2 rocking at 840 cm^{-1}, CH_2 rocking, CH_2 twisting at 960 cm^{-1}, C–O, C–C stretching, CH_2 rocking at 1058 cm^{-1}, C–O, C–C stretching at 1095 cm^{-1}, C–O stretching, CH_2 rocking at 1145 cm^{-1}, CH_2 twisting at 1241 and 1278 cm^{-1}, CH_2 wagging at 1341 cm^{-1} and CH_2 scissoring at 1466 cm^{-1}. There is no difference in FTIR spectra due to their different molecular weights, only the PEO 300k spectrum is reported.

Blend solutions with different ratios of Agar and PEO show a shift of wavenumbers (OH stretching and bending, CH stretching and CO stretching), highlighting a good interaction between the two polymers. In particular, the peaks related to carbon-oxygen bonds in the range 1100-1000 cm^{-1} are shifted. In addition, the peak shape also appears to be more slanted and intense, reaching a maximum in the 50/50 mixture. This effect can be traced to the phenomenon of molecular association. The oxygen atom present in the PEO chain acts as a proton acceptor toward the proton-donor hydroxyl hydrogens of the Agar. The established intermolecular interaction (hydrogen bridge) changes the bond strength constant by altering the absorption frequency of IR radiation. As said, his change is observed through the shift and increase in intensity of the relative peak.

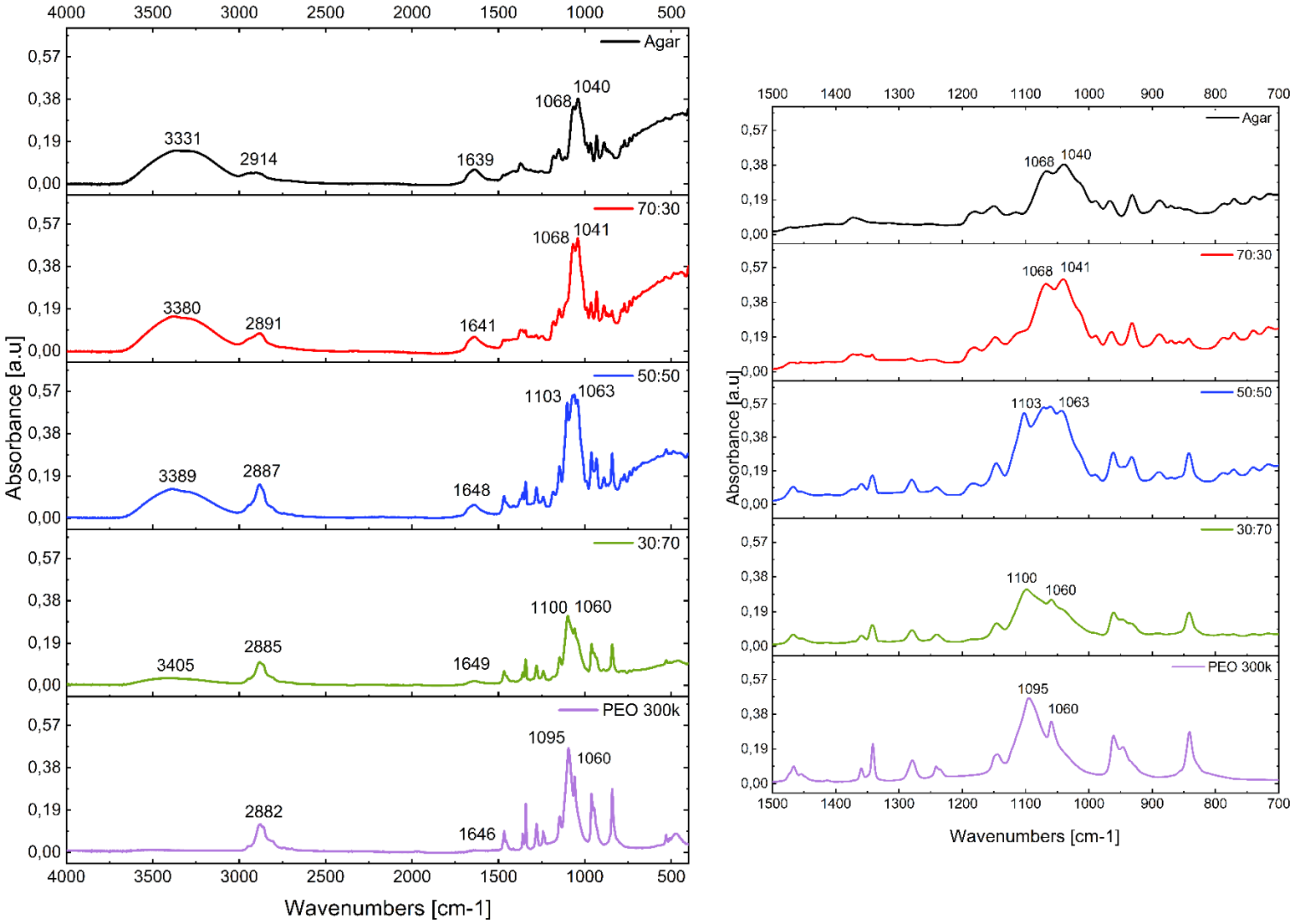

Figure 10- FT-IR curves of Agar, PEO 300k and blends. Magnification of the spectra in the 1500-700 cm^{-1} spectral region (on the right).

Regarding the mixtures between Agar and PVA, the spectra are shown in *Figure11*. For the spectrum and peaks related to Agar, the considerations previously made regarding *Figure 10* remain valid. Considering the PVA spectrum, a broad signal is noted at 3268 cm^{-1}, indicative of the O–H bond stretching that characterizes the repeating unit of this polymer (unlike PEO). At 2923 cm^{-1}, the signal related to the C–H bond stretching in the polymer's carbon chain is observed. Finally, at 1084 cm^{-1}, there is a signal likely resulting from the merging of two unresolved peaks: the peaks related to the C–O and C–O–C bond stretching, which are also present in the Agar spectrum and are more easily visible in the mixtures of the two polymers. In this case as well, by analyzing the spectra of the mixtures between the two polymers, and particularly the pair of peaks around 1050 cm^{-1} (*Figure 11*), a progressive increase in signal intensity can be noted, up to the maximum reached for the 50/50 mixture. However, in this case, a significant shift in the peak's wavenumber is not observed. This result nonetheless indicates a certain degree of compatibility between the two polymers, as confirmed

in other studies that led to the creation of electrospun membranes made precisely from these two polymers.

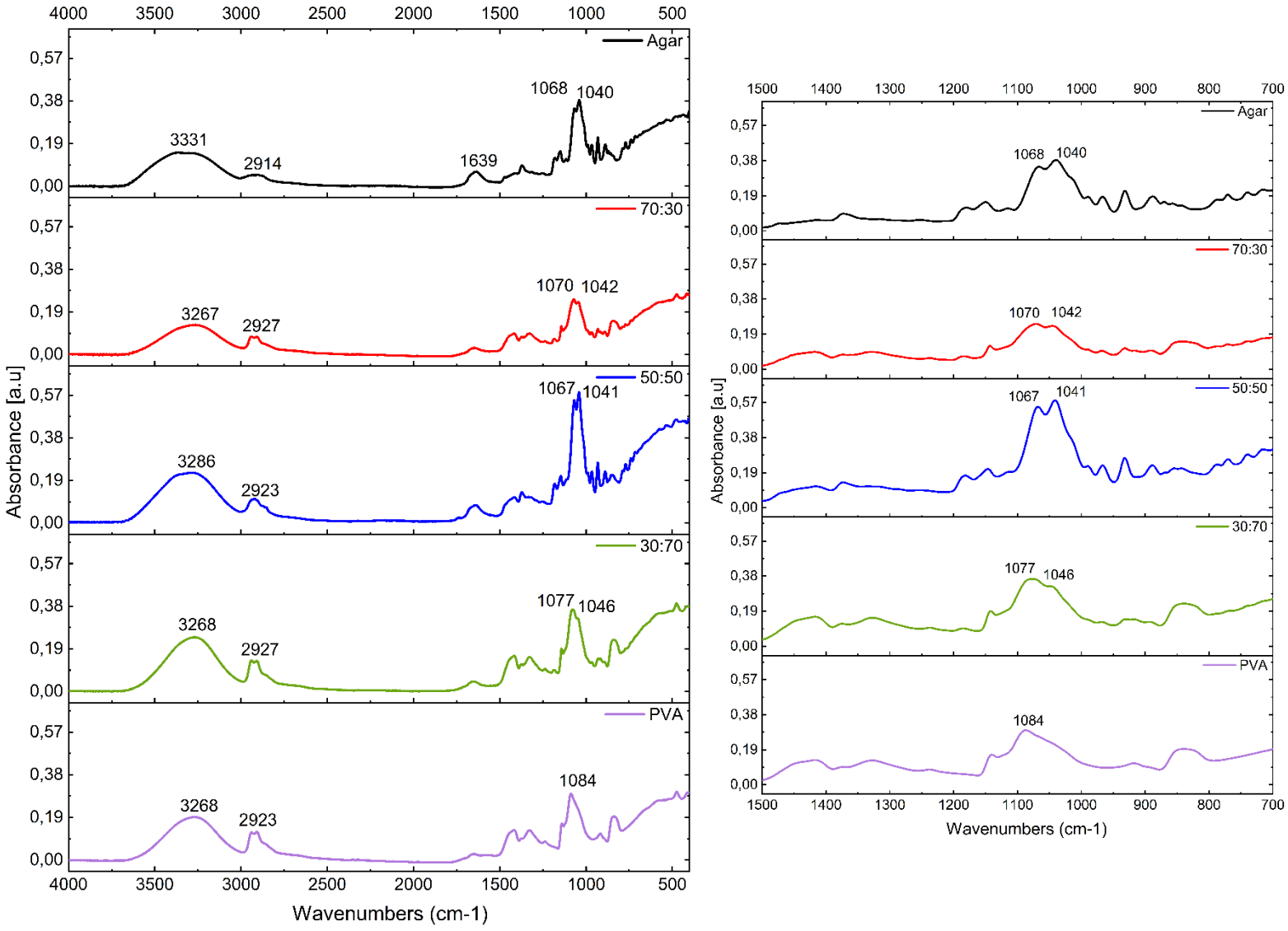

Figure 11- FT-IR curves of Agar, PVA and blends. Magnification of the spectra in the 1500-700 cm-1 spectral region (on the right).

Electrospinning process

Electrospinning machine was used to electrospun the prepared solutions using a flat collector. In order to avoid the gelation of Agar the chamber temperature was fixed at 45 °C. Typically, 3 mL of blend solutions were electrospun using a voltage between 22 to 25 kV, a spinneret−collector distance of 15 cm, a flow rate of 0.7 mL/h and an inner needle diameter of 0,4 mm. As references, electrospun mats of PEO 300k was obtained (solutions 10%w/v) with a spinneret−collector distance of 20 cm, a flow rate fixed to 1 mL/h, and an applied voltage of 17 kV (room temperature).

As reported above, preliminary rheological analyses of solutions and blends suggest an inadequate viscosity of PEO 8k, PEO 300k and PVA pure solutions at 3% w/v for the electrospinning process. To overcome the surface tension, a high polymer concentration (10wt%), and hence, high viscosity, is required. Furthermore, Agar/PVA blends, due to too low surface tension and non-optimal solution conductivity, were not electrospun. Only the blends of Agar/PEO 300k, in 70/30, 50/50, and 30/70 ratios, and a solution of PEO 300k 10% w/v were electrospun.

In addition, the 3% w/v pure Agar solution was tested with different parameters (injector-collector distance, flow rate, voltage) but as mentioned, it was not possible to obtain an electrospun membrane due to its gelation inside the needle, which prevents the impossibility of a stable Taylor cone during the process. Indeed, the process is more difficult when the concentration of Agar inside the solution increases, particularly for Agar/PEO 300k 70/30 ratio, for which the viscosity increases and the gelling temperature increase. Thus, the electrospinning of the solutions was carried out with particular attention to the temperature within the set-up to avoid the Agar gelation inside the needle from causing it to clog, thus preventing the production of mats.

7.3 Mats characterization

In *Figure 12* the FE-SEM micrographs of the membranes obtained with three Agar/PEO 300k and one PEO 300K solutions were reported with a nanofiber diameter distribution. Independent of the Agar content, a well-defined, uniform, and highly porous structure was obtained for all the electrospun membranes. In particular, randomly oriented nanofibers are clearly observable in the reported images and present a quite narrow diameter distribution, although an increase in the presence of beads (number and size) is clearly observable as the amount of Agar in the solution increases.

However, evident differences can be seen between the samples, with a significant linear decrease in fibre diameter with increase of Agar concentration, as shown in *Figure 13.*

This is probably ascribable to the content of Agar in the starting solutions, which under process conditions starts to form microgels, which increase the formation and size of microbeads, reducing the concentration of polymer available to form fibres, with consequence of the formation of membrane defects[189].

The mechanical behaviour of a material is fundamental to obtaining the appropriate performance for the selected purpose. First of all, from a macroscopical analysis mats appeared with a good flexibility and good resistant to manipulation. Therefore, uniaxial tensile tests have been carried out to evaluate the Young modulus (E), the tensile strength (σb), and the elongation at break (ϵb).

As shown in *Figure 14* the presence of Agar affects the mechanical properties of mats with a particularly the Young Modulus.

On increasing of Agar content, the mats show better mechanical properties in terms of Young Modulus that increase until to the 50/50 membrane; also, elongation at break increases thanks to the addiction of Agar component, while tensile strength being constant (increases slightly but within the experimental error). Unfortunately, in confirmation of the morphological analysis, the properties of the 70/30 Agar/PEO mat could not be studied due to the presence of some defects, particularly holes.

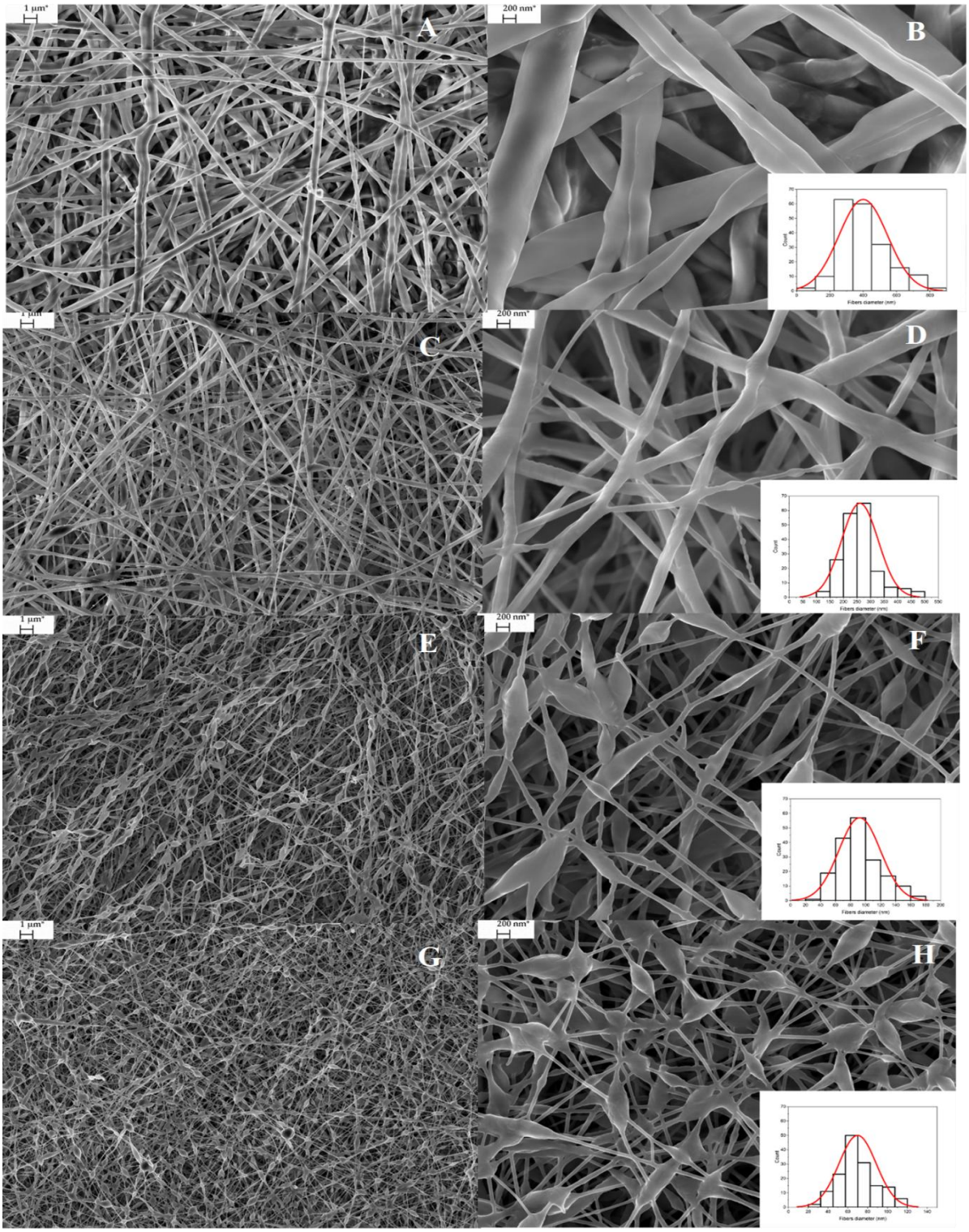

Figure 12 – FE-SEM images at two different magnifications of electrospun nanofiber mats of PEO 300K (A-B), Agar/PEO 300K 30/70 (C-D), Agar/PEO 300K 50/50 (E-F), and Agar/PEO 300K 70/30 (G-H)

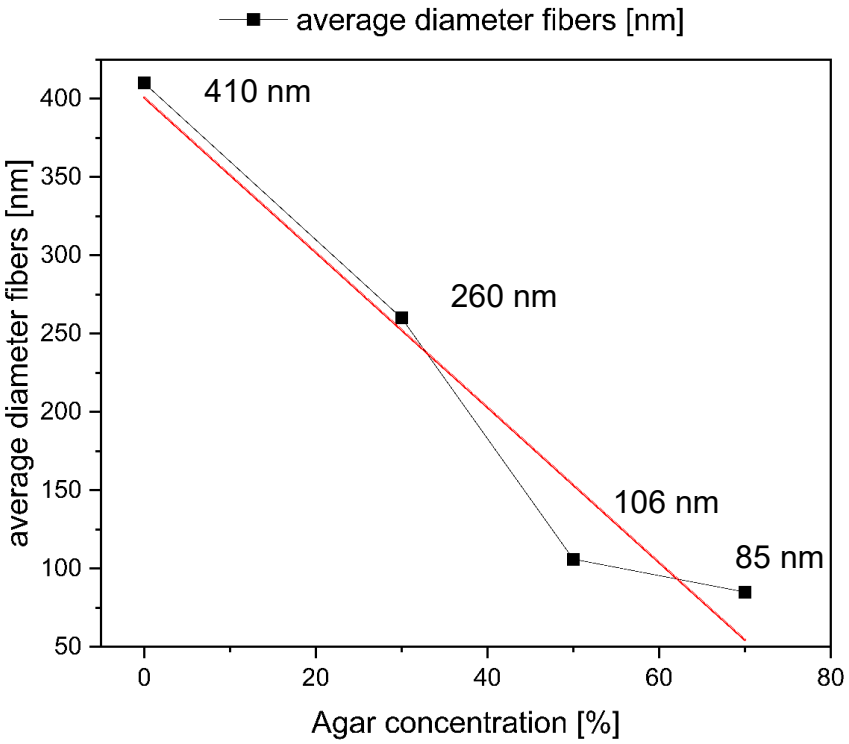

Figure 13 -Trend of fiber diameters with Agar concentration

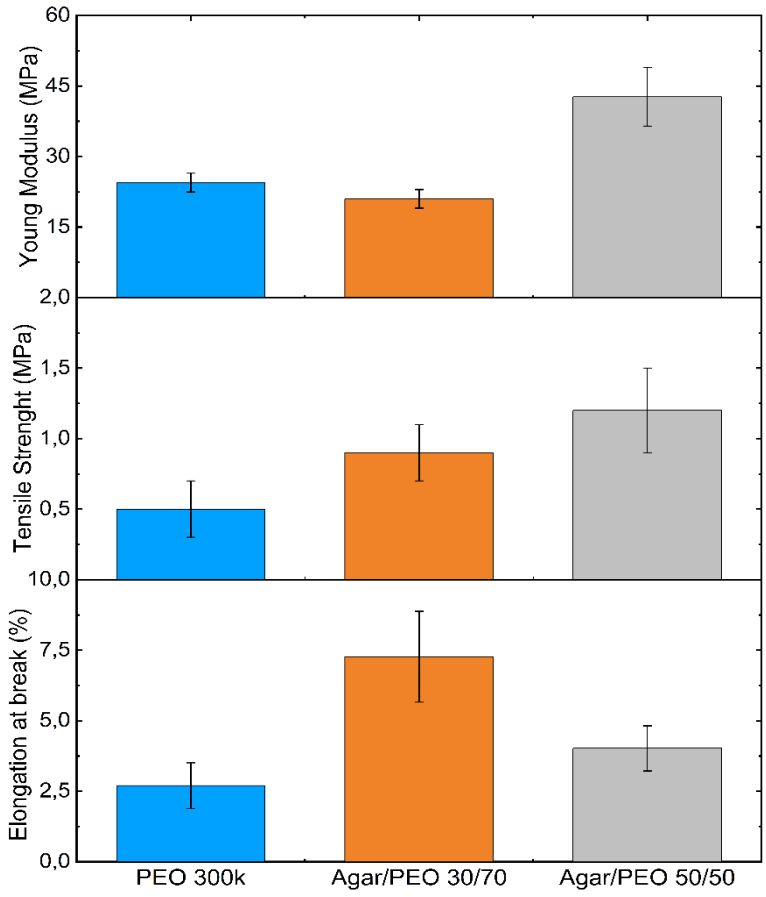

Figure 14 - Tensile test results on the mats of PEO 300k and Agar blends; the mat 70/30 ratio was not studied for the presence of holes and defects.

7.4 Swelling and deswelling

Mats' stability in solvents

The stability of the electrospun Agar/PEO 50/50 mat was evaluated by immersing standardized mat samples in a series of solvents with varying polarity and volatility. This analysis aimed to assess the compatibility of the mat with common cleaning solvents used in cultural heritage applications, and to determine the degree of morphological or structural changes induced by solvent exposure.

Solvents were selected based on their representative polarity and their relevance in cleaning formulations for artwork restoration. The polarity was arranged in decreasing order, and the volatility of each solvent was reported in terms of vapor pressure at 25 °C (Table 7). The mat's physical integrity, swelling behavior, and morphological consistency were monitored over a fixed exposure time (5 min) via weight loss percentage (Table 8) and SEM images (*Figure 15*).

Table 7- Solvent physical properties

Solvent	Dielectric Constant (εr)	Vapor Pressure (mmHg)	Boiling Point (°C)
Water	78.3	23.8	100,0
Ethanol	24.3	58.7	78.5
Acetone	20.7	230,0	57,0
MEK	18.5	89,0	79.6
Benzyl Alcohol	13.1	0.05	203,0
Isododecane	4.6	0.30	208,0
Toluene	2.4	28.5	110.6
Xylene	2.3	6.7	138,0
Cyclohexane	2.02	96.5	80.7
n-Hexane	1.9	120.0	69,0

The quantitative analysis revealed a strong correlation between solvent polarity and the stability of the mat. The highest weight loss, approximately 80%, was recorded after immersion in deionized water. A significant, though lesser, degree of dissolution was observed in polar protic solvents, with a weight loss of 27% in ethanol and 18% in benzyl alcohol. Conversely, the mat demonstrated exceptional stability in all tested non-polar and low-polarity organic solvents. Immersion in toluene, acetone, methyl ethyl ketone (MEK), n-hexane, cyclohexane, isododecane, and xylene resulted in a negligible weight loss of 0%, indicating the complete insolubility of the polymer blend in these media.

Table 8- Weight loss of Agar/PEO 300k 50/50 after solvent immersion

Solvents	ΔW (%)
Water	80
Ethanol	27
Benzyl alcohol	18
Toluene	0
Acetone	0
MEK	0
n-Hexane	0
Cyclohexane	0
Isododecane	0
Xylene	0

These results were substantiated by the morphological characterization via SEM (*Figure 15*). In the presence of water, the highly polar nature of the solvent induced the complete dissolution of the hydrophilic polymer components, leading to the collapse of the fibrous network into a continuous, film-like structure with residual microporosity. Exposure to ethanol resulted in a similar, albeit less pronounced, collapse of the fibers; however, the resulting surface appeared rougher, and a greater degree of porosity was retained compared to the water-treated sample. In benzyl alcohol, a solvent with lower polarity and volatility than ethanol, the mat showed a partial structural preservation. While partial fiber coalescence was evident, the overall porous, fibrous architecture remained largely intact. In stark contrast, the morphology of the mat was entirely unaffected by the non-polar and low-polarity organic solvents. SEM micrographs confirmed that the distinct, well-defined fibrous structure was perfectly preserved after immersion in toluene, acetone, and the other non-solvents, showing no signs of swelling, fusion, or collapse.

This behavior is directly attributable to the chemical affinity between the solvents and the hydrophilic Agar/PEO polymer blend. The high polarity of water facilitates the dissolution of both polymers, causing significant material loss and structural collapse. The intermediate polarity of ethanol and benzyl alcohol[25] allows for partial solvation and swelling of the fibers, whereas the non-polar character of the other tested organic solvents prevents any significant interaction, thus ensuring the physical and structural integrity of the mat.

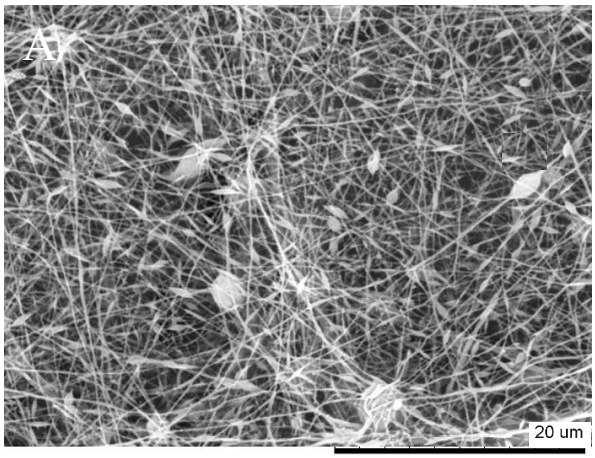
A
20 um

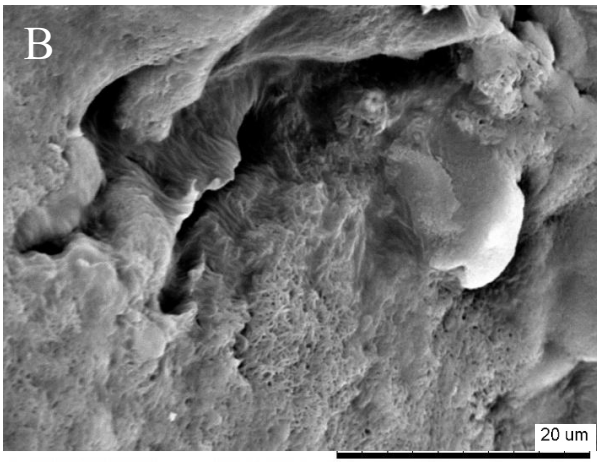
B
20 um

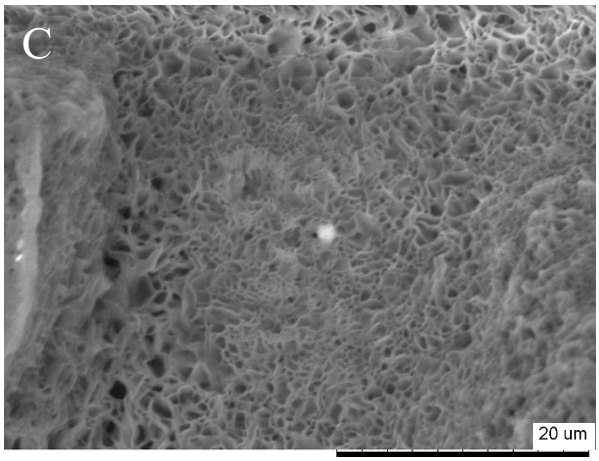
C
20 um

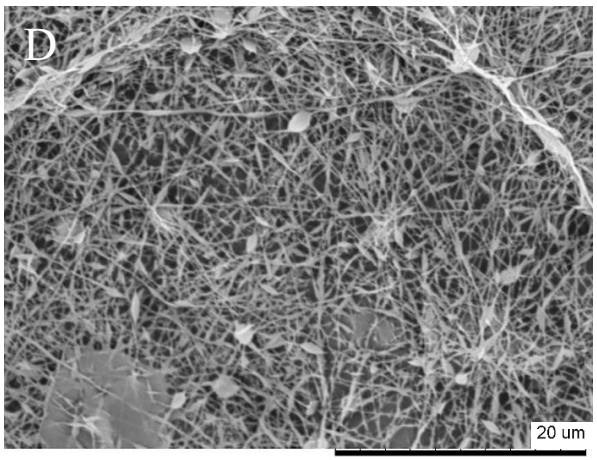
D
20 um

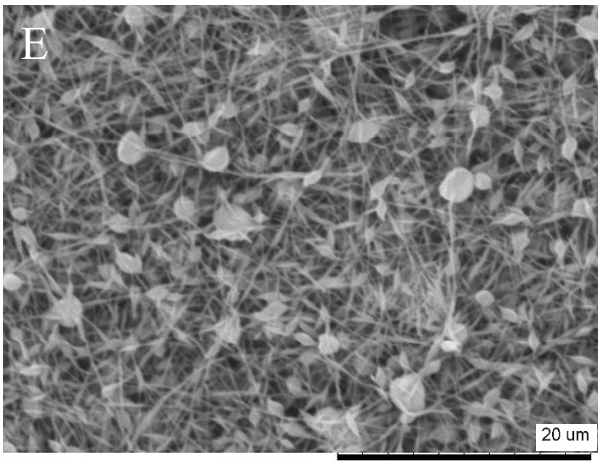
E
20 um

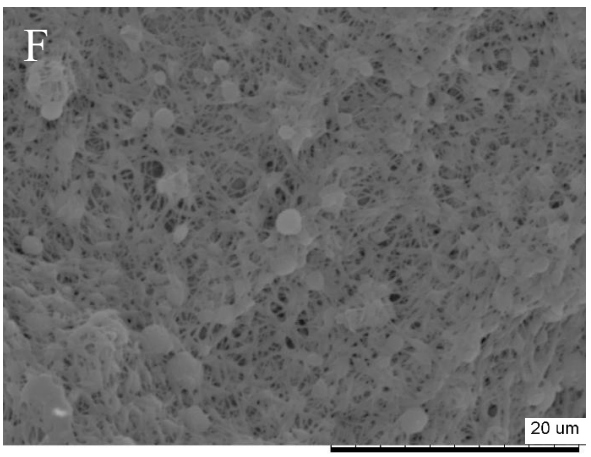
F
20 um

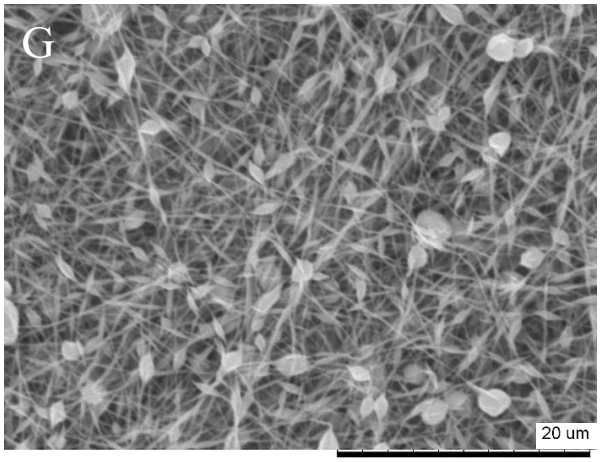
G
20 um

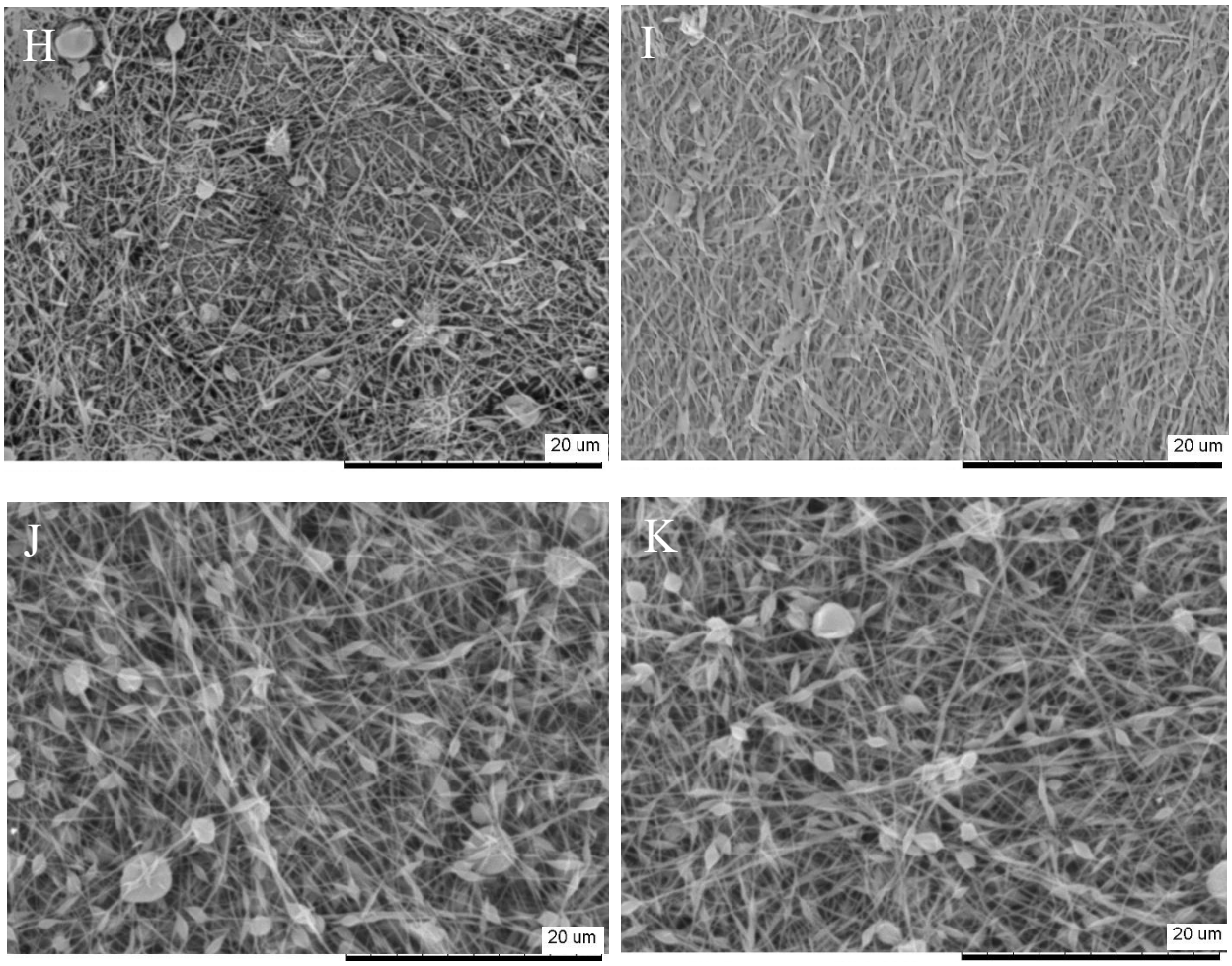

Figure 15- SEM images of Agar/PEO 300k 50/50 mat before (A) and after immersion in water (B), ethanol (C), acetone (D), methyl ethyl ketone (E), benzyl alcohol (F), isododecane (G), toluene (H), xylene (I), n-hexane (J) and cyclohexane (K).

Finally, the observed partial or complete dissolution of the Agar/PEO matrix in polar and polar protic solvents (such as water, ethanol, and benzyl alcohol) requires specific methodological considerations for practical conservation, as the release of solubilized polymer chains onto the artwork's surface could leave unwanted residues. To mitigate this risk and comply with the principles of minimal intervention and reversibility, two complementary operational strategies can be adopted. First, a pre-conditioning protocol can be implemented: by subjecting the mat to a preliminary immersion and rinsing phase in the target solvent, the highly soluble PEO fraction acts as a sacrificial co-spinning agent and is leached out, leaving a stable polysaccharide matrix to be loaded and applied. Secondly, consistent with standard conservation practices for gel and poultice applications, a final clearance step is highly recommended after the mat's removal. This involves gently swabbing the treated area with an appropriate clearance solvent to effectively lift and remove any residual traces of PEO or solubilized matter from the artwork's porosity, ensuring a completely residue-free surface.

Mats' Swelling and Deswelling

Following the stability assessment, the swelling behavior of the Agar/PEO mat was investigated. While the mat proved to be structurally stable in a wide range of organic solvents, the experimental conditions required a careful selection based on solvent volatility. Solvents such as n-hexane and cyclohexane were found to be too volatile for an accurate, time-resolved measurement. Although

acetone and MEK also possess high vapor pressures, their polar nature results in stronger intermolecular interactions (dipole-dipole) with the PEO component of the mat. This affinity leads to a greater retention of the solvent within the fibrous network, making a reliable swelling measurement feasible. In contrast, the non-polar alkanes exhibit only weak London dispersion forces with the mat, leading to extremely rapid evaporation from the high-surface-area structure that precluded accurate weight determination. The quantitative swelling study was therefore focused on the remaining stable solvents: toluene, acetone, MEK, isododecane, and xylene. The study aimed to quantify the solvent uptake capacity and kinetics for these solvents, which are critical parameters for the mat's application as a cleaning tool.

The results, presented in *Figure 16*, demonstrate that the mat possesses a high and rapid absorption capacity for all tested solvents. A general trend of rapid initial swelling within the first 3 to 5 minutes was observed, after which the absorption rate decelerated as the mat approached its equilibrium swelling capacity. This behavior is characteristic of a highly porous, capillary-driven system, where the void spaces within the fibrous network are quickly filled with the solvent. Significant differences in the maximum swelling capacity were recorded depending on the solvent. Acetone and MEK exhibited the highest affinity for the mat, reaching maximum swelling values of approximately 380% and 350%, respectively. For both ketones, equilibrium was largely achieved within 5 minutes. Xylene and isododecane showed intermediate absorption, with the swelling plateauing around 275% and 240%, respectively. Toluene displayed the lowest uptake among the tested solvents, with a maximum swelling ratio of approximately 125%, reaching a stable value after only 3 minutes of immersion. This differential swelling behavior, despite the mat's insolubility in these liquids, is directly correlated with solvent polarity. The superior performance of acetone and MEK can be attributed to their higher polarity and dielectric constants compared to the other tested solvents[25,187]. The polar carbonyl group (C=O) present in these ketones allows for stronger dipole-dipole interactions with the polar ether linkages (-C-O-C-) of the PEO chains within the polymer matrix. These favorable interactions facilitate greater penetration of the solvent into the amorphous regions of the fiber network, leading to a higher degree of swelling. In contrast, the non-polar nature of toluene, xylene, and isododecane results in weaker, London dispersion force-based interactions, limiting their ability to permeate the polymer structure and resulting in lower overall absorption. The ability of the mat to quickly absorb and retain a significant volume of these organic solvents—up to 3.8 times its own weight in the case of acetone—confirms its potential as a highly effective and controllable reservoir for the delivery of cleaning agents in conservation treatments.

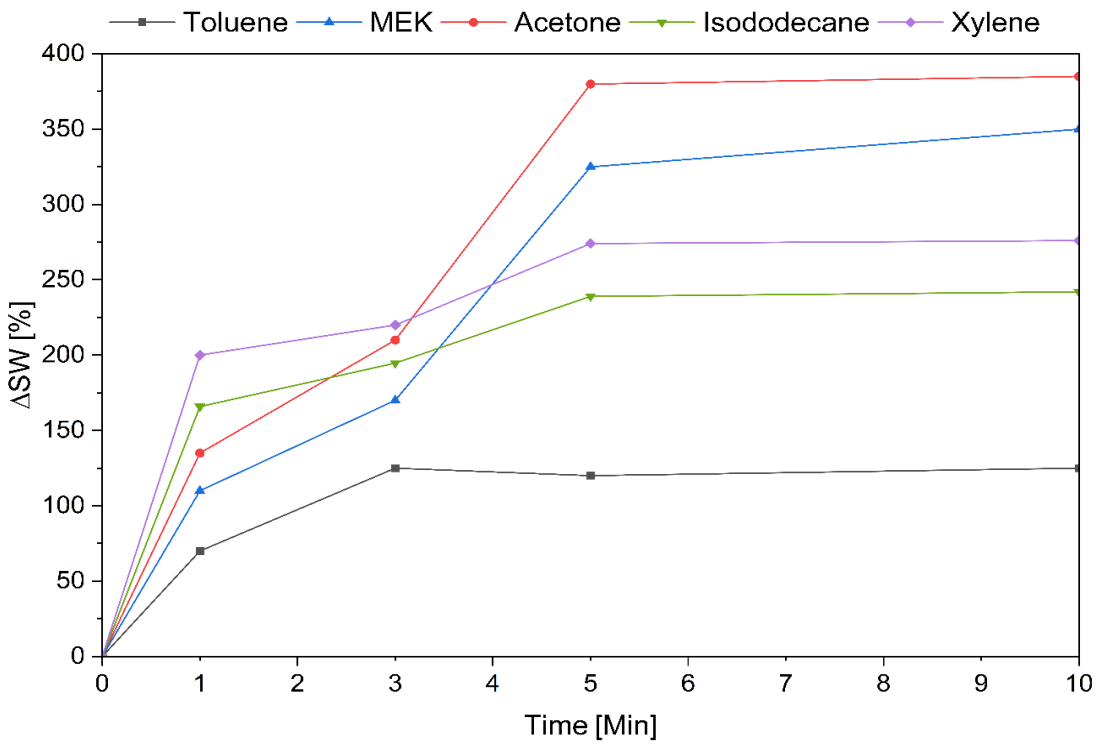

Figure 16- Swelling (ΔSW%) during time for Agar/PEO 300k 50/50 mat after immersion in toluene, MEK, acetone, isododecane, and xylene

Deswelling properties of the Agar/PEO mat were evaluated to assess its performance as a solvent delivery system for cleaning applications. The experiment was designed to measure the rate and extent of solvent release from a saturated mat when placed in contact with a standard porous substrate (a piece of canvas). Preliminary tests revealed that the more volatile solvents—acetone, MEK, and toluene—evaporated almost completely from the mat's surface within 30 seconds of application, making a reliable measurement of solvent transfer to the substrate unfeasible. Consequently, the quantitative deswelling study focused on the less volatile solvents, xylene and isododecane, which are also frequently used in conservation[25]. The results of the solvent release over 60 minutes are presented in *Figure 17*. The deswelling curve (ΔdSW%) represents the percentage of solvent remaining in the mat over time. For both solvents, a biphasic release pattern was observed. An initial, rapid desorption occurs within the first 5-10 minutes of contact with the canvas. During this phase, the mat containing xylene released approximately 35% of its absorbed solvent, while the isododecane-loaded mat released about 36%. This initial, fast release is attributed to the capillary-driven transfer of the solvent from the mat's porous network into the canvas substrate upon contact. Following this initial phase, the rate of solvent release decelerates significantly, entering a prolonged period of slow, controlled desorption. After 60 minutes, the mats still retained a substantial amount of solvent: approximately 175% ΔdSW for xylene and 150% for isododecane. This demonstrates that while the mat effectively delivers a portion of its solvent load to the substrate, it also functions as a controlled reservoir, retaining a significant volume. This behavior is highly desirable for cleaning cultural heritage, as it ensures that the target surface is wetted sufficiently to perform the cleaning action without being flooded with excess solvent, which could cause damage or uncontrolled spreading.

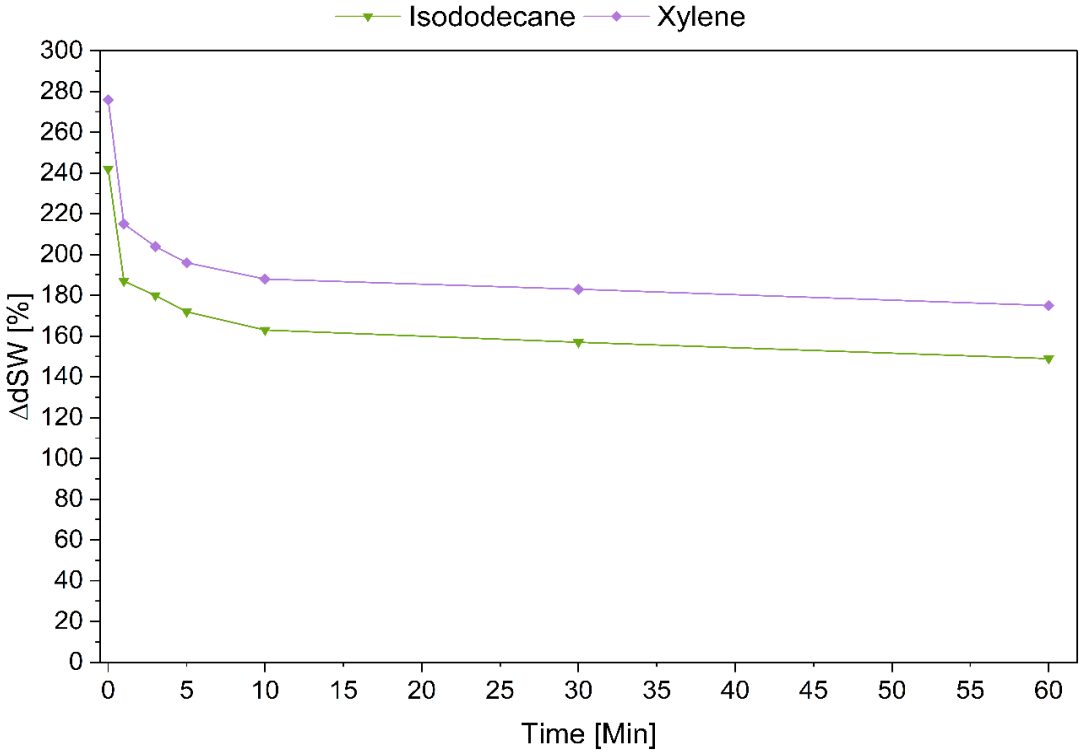

Figure 17- Deswelling (ΔdSW%) during time for Agar/PEO 300k 50/50 mat after immersion in isododecane and xylene

7.5 Agar-poly(caprolactone) Multilayer mats

To improve the mechanical properties of the Agar/PEO 300k 50/50 membrane, which proved to be the best in terms of its morphological properties, it was decided to combine it with a poly(caprolactone) membrane, a synthetic polymer with excellent mechanical properties[166], particularly in terms of elongation at break. The aim was to improve the handling of these membranes in Cultural Heritage cleaning applications, a fundamental aspect when it comes to restoration products. In addition, this multilayer design was conceived to provide essential structural support during wet applications. While the hydrophobic PCL layer cannot prevent the chemical dissolution or gelation of the underlying hydrophilic Agar/PEO layer when in direct contact with aqueous environments, it is hypothesized to act as a robust mechanical backbone. This ensures that even if the active polysaccharide layer loses its fibrous architecture, the overall composite tool maintains sufficient macroscopic integrity to be safely and cleanly removed from the delicate artwork surface in a single peeling action, without tearing or leaving fragmented residues Finally, the effects of the injector-collector distance and the total polymer concentration in the Agar/PEO mixture in the electrospinning process were studied.

Solutions preparation

Blend solutions of Agar/PEO 50/50 containing 2, 2,5 and 3% w/v of total polymers were prepared by adding a correct amount of Agar powder and deionized water to the co-spinning agent 3% w/v solution. The samples were placed on a magnetic heating plate and stirred until to boiling point to allow the complete dissolution of polymers.

Solutions (30% w/v) of three samples of PCL with different molecular masses (Mv= 37, 50, 80 kDa) in a mixture of glacial acetic acid and acetone (3:1 v/v) were prepared. The samples were placed on a magnetic heating plate and stirred at 40°C, allowing the complete dissolution of polymers.

Rheological characterization

To check the PCL zero-viscosity values and the influence of different polymers' molecular weights, rheological analyses at 25 °C with cone-plate geometry were carried out. The resulting flow curves are presented in *Figure 18.*

As expected[193,194], the molecular weight of PCL has a strong influence on viscosity (Table 9). The PCL 6800 (80 kDa) solution exhibited the highest viscosity, with a zero-shear viscosity (η_0) of approximately 25 Pa·s. This solution shows the typical shear-thinning behaviour of a polymer solution, as can be described by models such as the Carreau-Yasuda equation.

The PCL 6500 (50 kDa) solution registered a η_0 value of approximately 5 Pa·s and remained mostly Newtonian, with only slight shear-thinning appearing at very high shear rates. In contrats, PCL 6400 (37 kDa) solution presented typical Newtonian behaviour with the lowest viscosity approximately of 1.2 Pa·s.

From our previous works and from the literature[195,196], the best-performing zero-shear viscosity for the electrospinning process for PCL is in the range of 1-2 Pa·s. For this reason, the PCL sample with 37 kDa (CAPA 6400) mass was selected for further study.

Table 9- Zero viscosity of PCL solutions with three different molecular weights

	CAPA 6800 (80 kDa)	**CAPA 6500 (50 kDa)**	**CAPA 6400 (37 kDa)**
η_0 [Pa s]	25,38	5,46	1,25

The stability of PCL 6400 in a binary solvent system of acetic acid and acetone (3:1) was assessed via time-dependent rheological monitoring[195]. Given the polyester nature of PCL, the acidic environment provides a catalytic source of protons, facilitating random chain scission via hydrolysis (and potentially acidolysis)[166]. This degradation manifests macroscopically as a reduction in solution viscosity, governed by the disruption of polymer entanglements and the reduction of the viscosity-average molecular weight according to the Mark-Houwink relationship[197].

The rheological data for this stability test is shown in *Figure 19.* The curves of PCL (CAPA 6400) at different times show a clear viscosity decrease. The initial viscosity at t=0 h was measured at ~1.2 Pa·s. The solution exhibited a 25% viscosity decrease up to 6 hours of aging. After this point, the degradation rate slowed significantly, with the solution settling at a constant η value of 0.94 Pa·s. This final value, observed at 24 and 30 hours, was taken as a reference vaue for the degraded solution (Table 10). For this reason, the PCL solution was electrospun after 24 hours.

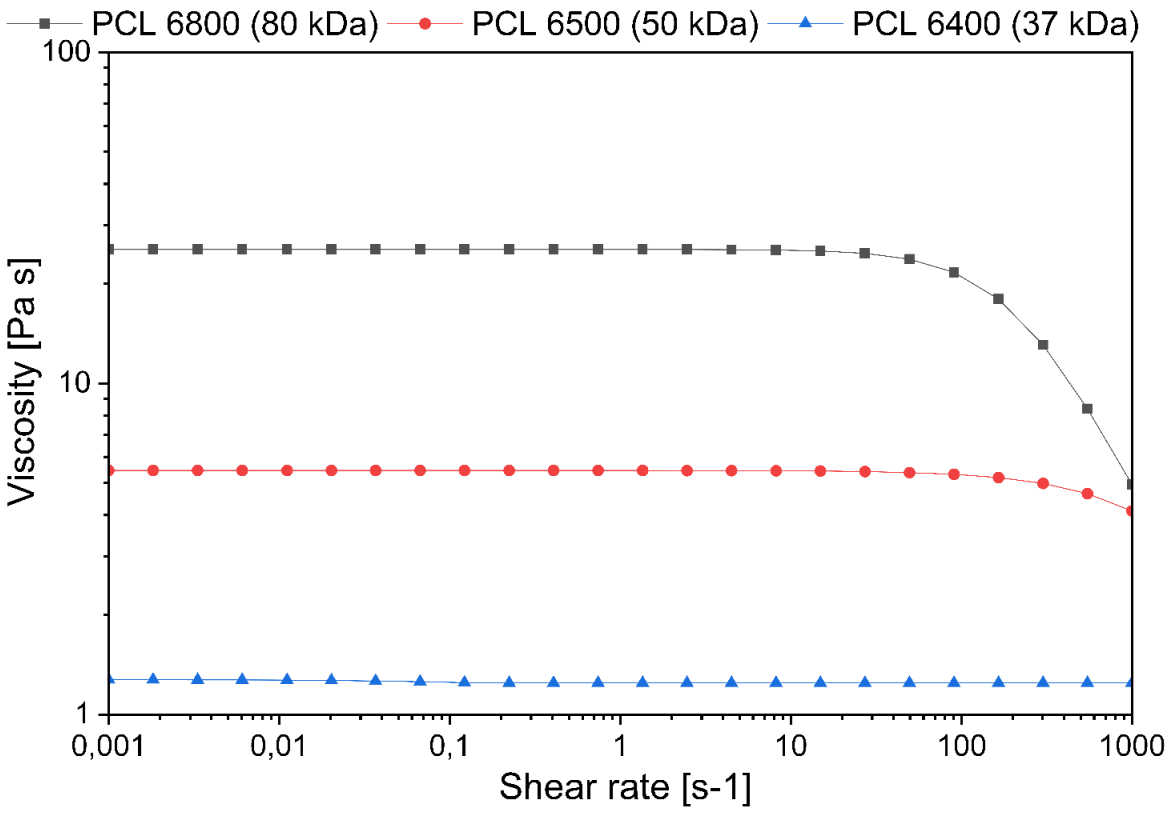

Figure 18- Flow curves of PCL solutions with three different molecular weights of polymer

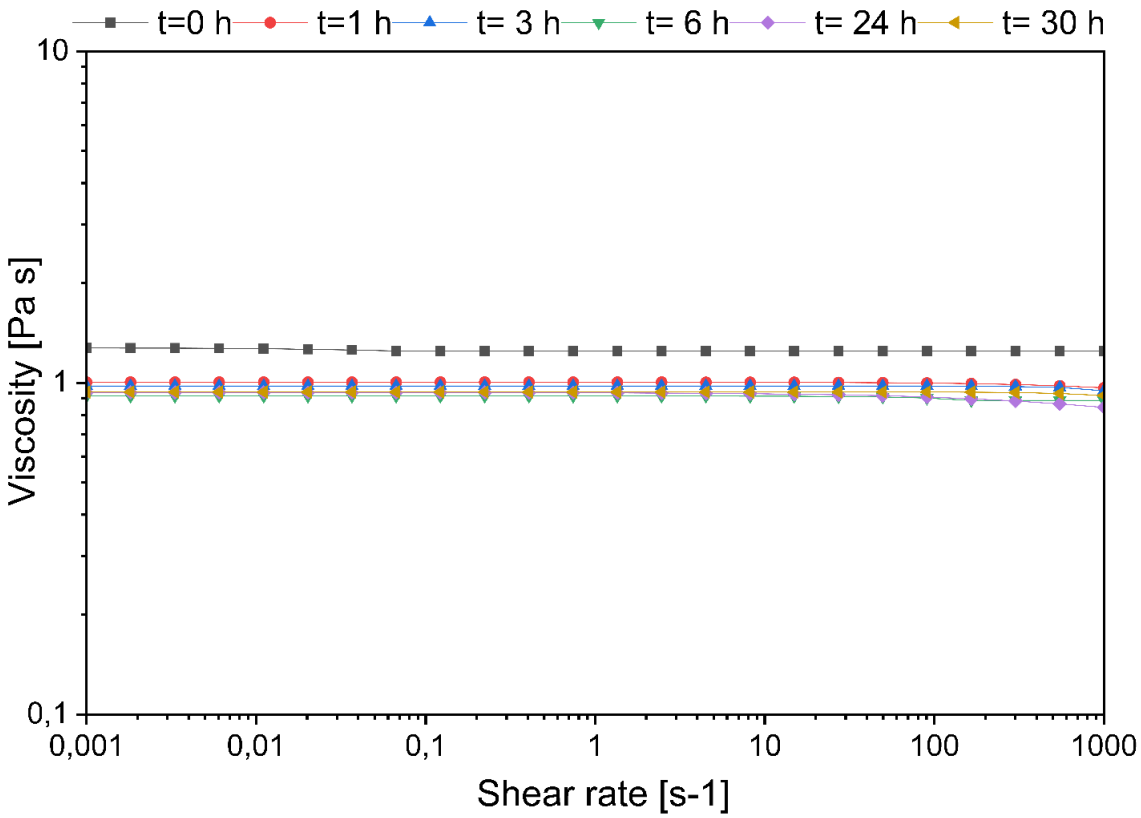

Figure 19- Flow curves of PCL solution (CAPA 6400, Mv= 37 kDa) after different times of agitation

Table 10- Zero-viscosity of PCL 37 kDa solution at different time of aging

Time [hours]	η_0 [Pa s]
0	1,25
1	1,01
3	0,98
6	0,94
24	0,94
30	0,94

In a separate analysis, Agar/PEO 300k rheological curves (at 2, 2.5 and 3 % w/v) were evaluated (*Figure 20*). These solutions show a typical yield stress behavior (viscoplastic), which is indicative of an initial gelation at the measurement temperature of 45 °C[198]. Based on previous results (Chapter 7), the viscosity in the typical shear rate range of electrospinning (25-35 s^{-1}) is suitable for the 2,5% and 3% Agar/PEO solutions, but not for the 2% w/v solution, which has too low viscosity in comparison with other electrospun solutions (Table 11- see previous paragraphs).

Table 11- calculated shear rate and viscosity for Agar/PEO 50/50 at three different total polymer concentrations (flow rates of 0,7 ml/h and inner diameter of 0,4 mm)

Sample (50/50 w/w)	η @32 s^{-1} (Pa s)
Agar/PEO 3 %w/v	0,14
Agar/PEO 2,5 % w/v	0,06
Agar/PEO 2% w/v	0,03

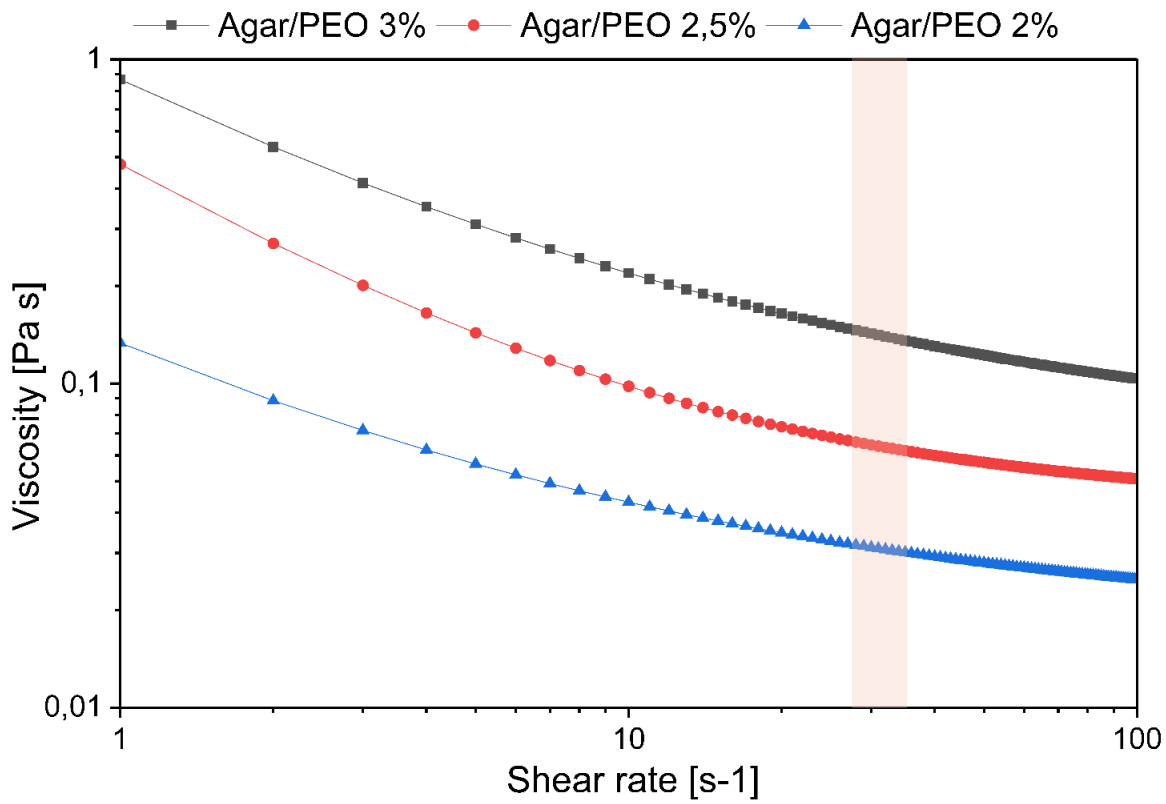

Figure 20- Flow curves of Agar/PEO 50/50 solutions with different total polymer concentrations. Orange rectangles show the common shear rate range during the electrospinning process (25-35 s^{-1})

Electrospinning process

The double-layered mat was prepared in two steps:

i) *First step.* The optimal 24-hour-aged PCL solution, as evaluated with rheological solution, was electrospun on a cylinder rotating at 100 rpm to try to obtain oriented nanofibers. The operative conditions used are summarized in Table 12.

ii) *Second step*. Agar/PEO 300K solutions were electrospun at 45 °C to avoid Agar's gelation directly on the previously prepared PCL membrane at the experimental conditions, once again indicated in Table 9. Two different distances from the injector to the collector were studied.

The needle inner diameter was fixed to 0,4 mm.

Table 12- Electrospinning process parameters

Solutions	Distance (cm)	Voltage (kV)	Flow rate (mL/h)	Temperature (°C)
PCL	**25**	**18**	**1,5**	**25**
Agar/PEO 2,5 % w/v	**15/20**	**23**	**0,7**	**45**
Agar/PEO 3% w/v	**15/20**	**23**	**0,7**	**45**

Mat's characterization

Scanning Electron Microscopy (SEM) characterization was carried out on both surfaces of the resulting mats to evaluate the distinct microstructures of the constituent layers (*Figure 22*) The PCL layer was found to be composed of partially oriented fibers with an average diameter of 420 nm. While the overall fibrous network was established, the images also revealed the presence of some drops or bead-like defects interspersed within the mesh. This phenomenon is most likely attributed to the low solvent evaporation rate of the acetic acid/acetone system[103,104]. If the solvent does not fully evaporate during the flight from the injector to the collector, the polymer reaches the target in a semi-wet state, causing the formation of flattened drops rather than uniform cylindrical fibers[104]. On the upper surface, the Agar/PEO layer shows morphological features that vary significantly with the concentration of the starting solution and the distance between injector and collector, consistent with literature suggestions[103–105,115] (*Figure 21*). Two key trends were observed regarding the solution parameters:

i) First, with the decrement of viscosity (effected by reducing the concentration from 3% to 2.5% w/v), the fiber diameter decreased from 106 nm to 90 nm (at a constant 15 cm distance). However, this reduction in diameter was accompanied by an increase in the number of beads, likely due to insufficient chain entanglement to stabilize the jet.
ii) Second, with the increase in the injector-collector distance (from 15 to 20 cm) the number of beads increased further, suggesting jet instability over longer flight paths.

For these reasons, the most homogeneous structure, characterized by quite regular fibers with an average diameter of 106 nm and the presence of only a few beads, was obtained from the 3% w/v solution (*Figure 21*). Consequently, these parameters were selected for the fabrication of the final composite.

Additionally, the hydrostability of the composite was assessed (*Figure 22*). After just five minutes of immersion in water, the Agar/PEO layer lost its fibrous morphology, and a polymeric film appears. While the underlying hydrophobic PCL mesh cannot shield the hydrophilic polysaccharide layer from morphological collapse and gelation, it successfully acts as a macroscopic physical scaffold. The PCL backing prevents the complete disgregation of the system, ensuring that the resulting gel-like film remains anchored to a solid, handleable support rather than dispersing into the aqueous medium

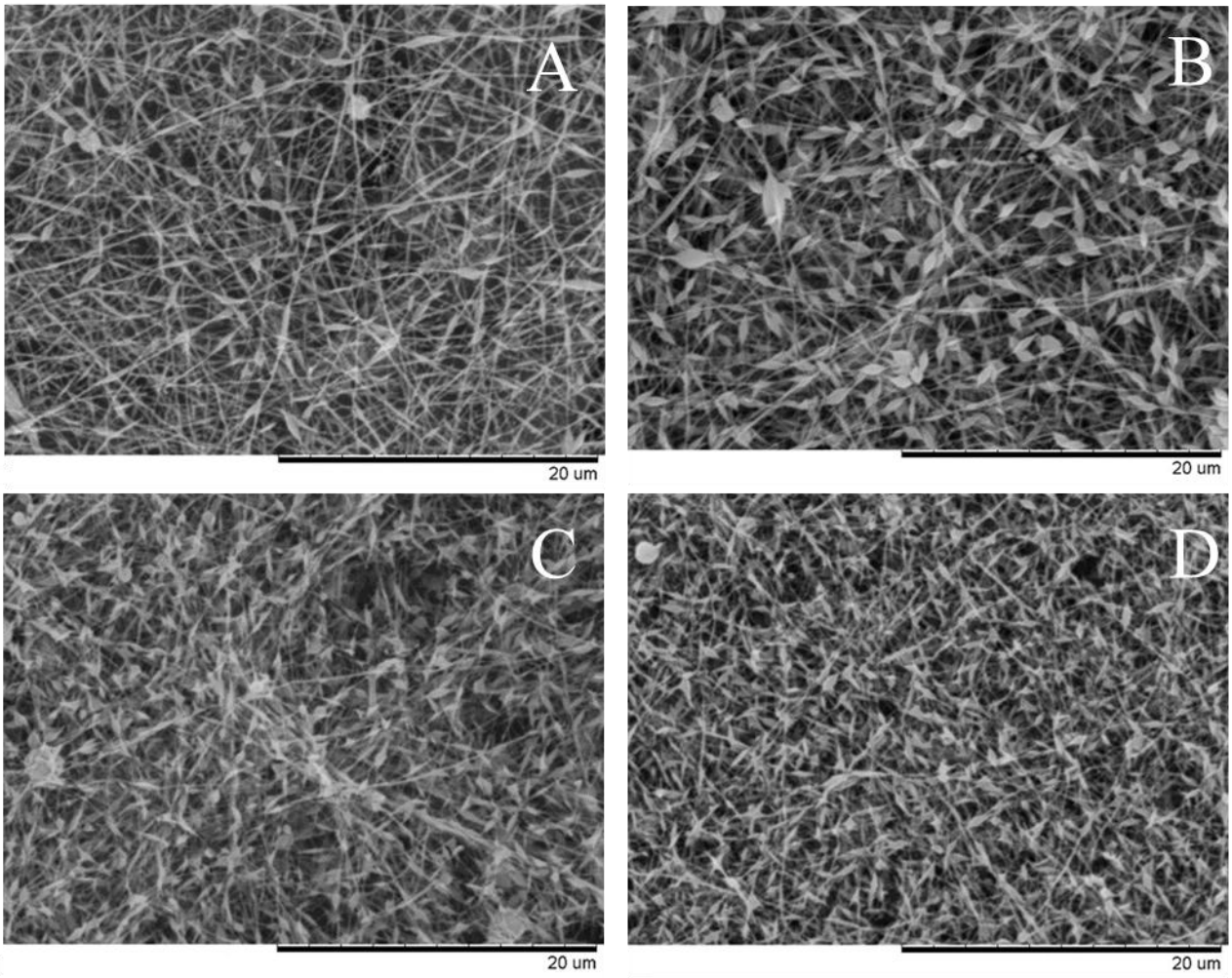

Figure 21- SEM images of (A) Agar/PEO 50/50 3% (15 cm), (B) Agar/PEO 50/50 3% (20 cm), (C) Agar/PEO 50/50 2,5% (15 cm), (D) Agar/PEO 50/50 2,5% (20 cm)

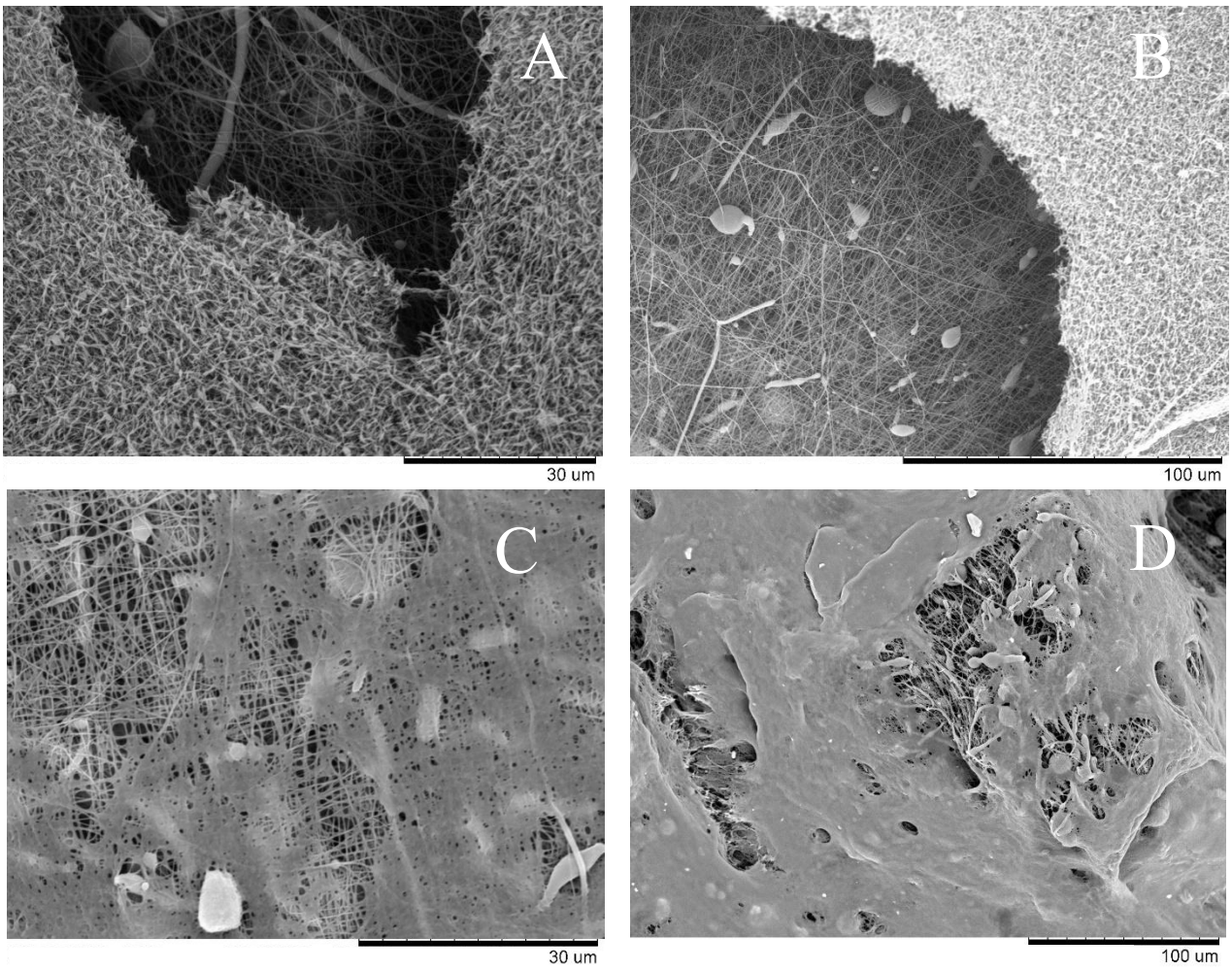

Figure 22- SEM images of PCL-Agar/PEO 50/50 3% (15 cm) mat before (A-B) and (C-D) after 5 minutes immersion in water

The mechanical properties of the electrospun scaffolds were evaluated through tensile tests to determine Young's modulus, tensile strength, and elongation at break. The results, comparing the pure Agar/PEO mat, PCL mats (tested in two orientations), and the multilayer composite (along fibers), are summarized in *Figure 23.*

The Agar-PEO 50/50 mat demonstrated the highest stiffness among all samples, with a Young's Modulus of approximately 46 MPa. However, this high stiffness was accompanied by brittle behavior, as evidenced by a very low elongation at break (< 5%). In terms of strength, the Agar/PEO mat reached a tensile strength of ~1.4 MPa, though with significant variability as indicated by the large standard deviation.

In contrast, the PCL mats exhibited typical ductile behavior characteristic of thermoplastic elastomers[166]. The testing direction played a crucial role in the mechanical response, highlighting the structural anisotropy of the fibrous mesh. When tested "along fibers" (parallel to the collection direction), the PCL mat showed higher mechanical performance compared to the "perpendicular fibers" direction. Specifically, the tensile strength along the fibers was approximately 1.2 MPa, nearly

double the value observed in the perpendicular direction (~0.7 MPa). Similarly, the elongation at break was slightly higher along the fibers (~42%) compared to the perpendicular orientation (~37%), suggesting that fiber alignment contributes effectively to load distribution.

The multilayer PCL-Agar/PEO composite displayed mechanical properties that were predominantly governed by the PCL component. Despite containing the stiff Agar/PEO layer, the multilayer scaffold exhibited a low Young's Modulus (~2 MPa) and low tensile strength (~0.5 MPa), values comparable to or slightly lower than the pure PCL mats. However, the composite retained significant ductility, showing an elongation at break of approximately 38%. This suggests that under tensile load, the brittle Agar/PEO layer likely fractures at low strains, leaving the ductile PCL layers to bear the load and undergo deformation until failure. Consequently, the multilayer system combines the biological potential of the hydrogel component with the flexibility and extensibility of the PCL mesh.

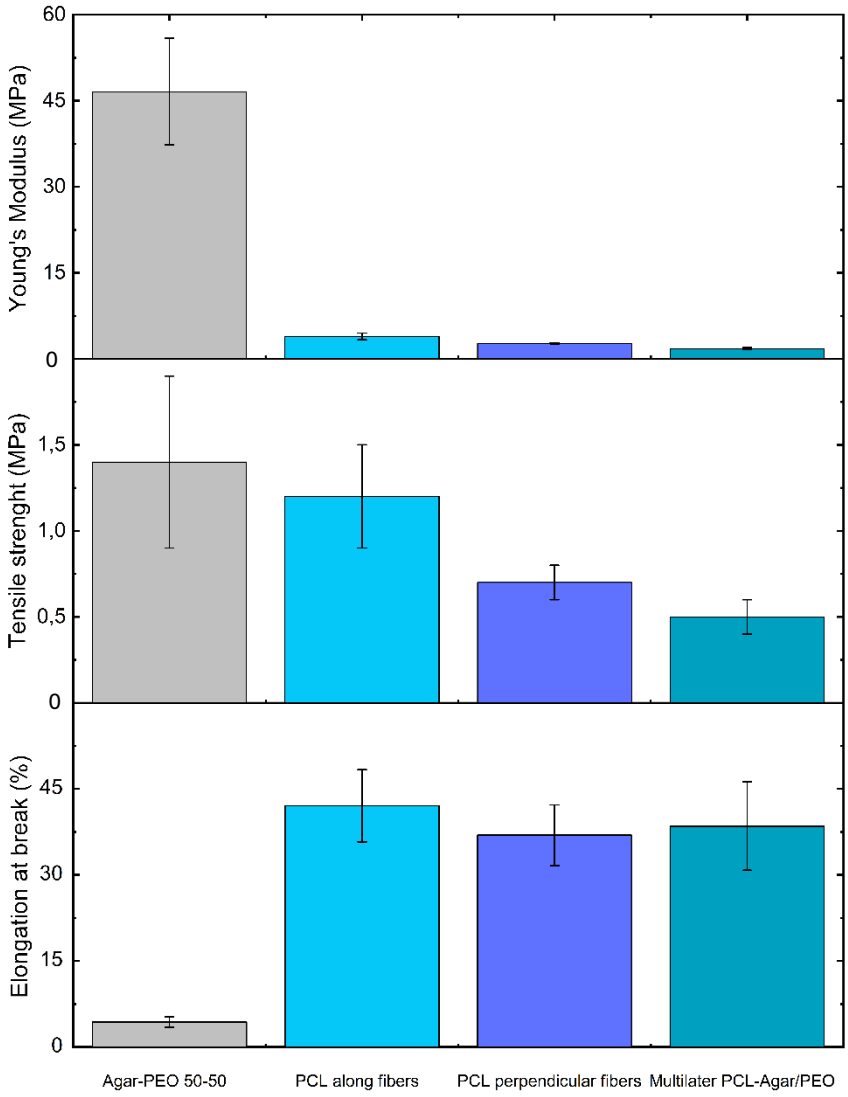

Figure 23- Tensile test results on the mats of Agar/PEO, PCL, and multilayer mats

Conclusions

This study demonstrates the successful fabrication of electrospun nonwoven mats from a blend of Agar and high molecular weight Polyethylene oxide (PEO 300k) using water as a solvent. The use of an aqueous system represents a green and safe processing route, avoiding the need for aggressive or toxic organic solvents.

Preliminary investigations revealed that the choice of PEO molecular weight was critical; blends using low molecular weight PEO (8k) failed to produce fibers due to insufficient solution viscosity and chain entanglement, resulting in electrospraying. In contrast, the high viscosity imparted by PEO 300k was essential for stabilizing the polymer jet and enabling the formation of continuous fibers.

However, the research also conclusively shows that successful electrospinning is a multifactorial process where an adequate viscosity is a necessary but not sufficient condition. FT-IR analysis confirmed the good miscibility between the two polymers at a molecular level, evidenced by a characteristic shift in wavelength. The role of Agar as a polyelectrolyte was identified as a key contributing factor, increasing the solution's electrical conductivity and enabling the fabrication of fibers from polymer concentrations that would otherwise be unspinnable. FE-SEM investigation of the final mats confirmed that the optimized 50/50 Agar/PEO blend yielded smooth, partial bead-free fibers with a uniform morphology. It was observed that increasing the Agar content led to a desirable decrease in fiber diameter but also an increase in bead defects, establishing the 50/50 ratio as the optimal balance.

The functional properties of the optimized mat were systematically evaluated for its intended application in the cleaning of Cultural Heritage. The mat demonstrated exceptional stability in a wide range of non-polar and low-polarity organic solvents, while being readily soluble in water, offering a dual functionality. Swelling tests confirmed the mat's ability to rapidly absorb and retain large quantities of organic solvents, with the uptake capacity being directly correlated to solvent polarity. Mechanical testing revealed that the presence of Agar significantly enhanced the material's performance, increasing both the Young's modulus and the elongation at break. Crucially, deswelling studies on a model canvas substrate showed a desirable biphasic release mechanism: a rapid initial solvent transfer followed by a slow, controlled release, which is ideal for preventing damage to sensitive surfaces.

To further enhance the mechanical versatility of the system, a multilayer strategy was adopted, coupling the Agar/PEO mat with a Polycaprolactone (PCL) substrate produced using a low-toxicity acetic acid/acetone solvent system. Mechanical characterization of this composite highlighted the complementary roles of the layers: while the Agar/PEO layer provided high stiffness (Young's modulus ~46 MPa), it was inherently brittle. The addition of the PCL layer, which exhibited ductile behavior and fiber alignment dependence, imparted necessary flexibility to the system However, morphological analysis of the multilayer construct in aqueous environments clarified the distinct roles of the two layers. Although the hydrophobic PCL layer formed a robust supporting mesh of 420 nm fibers, it inherently cannot preserve the nanoscale fibrous morphology of the hydrophilic Agar/PEO layer upon water immersion, resulting in the coalescence of the polysaccharide nanofibers into a film within five minutes. Nevertheless, the PCL layer successfully fulfils its primary objective: providing a flexible and resistant mechanical backbone that allows the composite to be handled and removed safely as a single piece, even when the active polysaccharide layer transitions into a gel state

Chapter 8.
Polysaccharide-based and polymer-based electrospun mats as a cleaning tool for XVI-century wood artwork

8.1 Introduction

The cleaning of painted surfaces, particularly those with complex stratigraphic layers, remains one of the most challenging and irreversible operations in art conservation[24]. The objective is to selectively remove superimposed materials, such as aged varnishes, grime, or later repaints, without damaging the original paint layers. This challenge is exemplified by the subject of this study: an oil tempera painting on a poplar wood support, attributed to the Ligurian School of the late 16th century. The artwork, prepared with a traditional chalk and glue ground, presents a significant conservation problem: a very thick and tenacious repainting executed with oil-based colors, likely dating to the second half of the 19th century. Based on preliminary assessments and in consultation with restorers, benzyl alcohol was identified as a potentially effective solvent for tackling this problematic oil layer. However, the high potency and low volatility of benzyl alcohol necessitate a highly controlled application method to prevent uncontrolled diffusion, swelling, or leaching of original components.

This chapter explores the potential of electrospun mats to serve as advanced, controllable vehicles for solvent-based cleaning, transitioning from material fabrication to direct practical application. The core idea is to test this novel tool to address the complex cleaning requirements of the Ligurian artwork. Electrospun mats offer a unique combination of properties, including high porosity, vast surface area-to-volume ratio, and physical conformability, that make them ideal candidates for holding and delivering precise dosages of solvents to a target surface.

Building upon the foundational work in the previous chapter, which detailed the successful fabrication and characterization of electrospun mats from Poly(ethylene oxide) (PEO), Polycaprolactone (PCL), and an Agar/PEO blend, this section expands our materials. Here, we introduce the development of mats based on Poly(vinyl alcohol) (PVA) and a novel composite of Agarose/PEO. The use of polysaccharides like Agar and Agarose is of particular interest for conservation due to their hydrophilic nature and biocompatibility, but their strong tendency to gel poses a significant challenge for continuous processes like electrospinning[144].

To circumvent this, we employed a low-gelling-point (LGP) Agarose. This modified biopolymer is typically produced via hydroxyethylation, a chemical functionalization that introduces hydroxyethyl groups onto the polysaccharide backbone[150]. This modification effectively disrupts the extensive intermolecular and intramolecular hydrogen bonding that facilitates the helical aggregation responsible for gelation. Consequently, the gelling temperature is significantly lowered[150]. This material characteristic was critical to our process, enabling a stable and continuous electrospinning workflow at a moderately elevated temperature of 45 °C, thereby preventing premature gelation within the spinning apparatus while still being gentle on the polymer blend.

The work presented in this chapter is twofold. First, we conduct a preliminary laboratory investigation to systematically study the behavior of all five types of electrospun mats (PEO, PVA, PCL, Agar/PEO, and Agarose/PEO) when loaded with benzyl alcohol. This phase was designed to understand their solvent uptake capacity, retention, and release characteristics. Second, we transition from the laboratory bench to the case study. The most promising mat systems are applied directly to the surface of the 16th-century painting. This practical phase includes a series of swelling and deswelling tests on the artwork, adapting our laboratory methodology to a real-world scenario. These adaptations involved critical adjustments to the solvent application time and the physical thickness of the mat samples to optimize the selective removal of the 19th-century repaint while ensuring the safety of the original underlying stratigraphy.

8.2 Agarose-based mats

Solutions preparation

To study the gelation temperature of Agarose and its rheological behaviour in water, solutions at concentrations of 3, 5, 7, 10 % w/v were prepared by adding powder in water, stirring and heating until boiling point (100 °C).

Blend solutions Agarose/PEO 300k 70/30, containing 3, 5, 7, and 10 % w/v of total polymers, were prepared by adding a correct amount of Agarose powder and deionized water to the PEO 300k 3 % w/v solution. The samples were placed on a magnetic heating plate and stirred until to boiling point to allow the complete dissolution of polymers. The total concentration of polymers and the ratio in the blend's solutions were selected to find the best solution for the electrospinning process, based on the result of the previous experimentation (Chapter 7).

Triton X-100 was added to polysaccharide blends in a concentration of 1% wt in comparison with the total polymer concentration, maintaining the final solution under stirring for 30 min.

Rheological characterization

The rheological characterization started with a gelling temperature evaluation to elucidate the structural differences between the two polysaccharide matrices. *Figure 24* compares the temperature-dependent evolution of the storage (G') and loss (G") moduli for Agar and Agarose water solutions (3% w/v). A distinct disparity in the sol-gel transition is observed: while Agar exhibits a sharp gelling point at approximately 40 °C, the Agarose selected for this study undergoes gelation at a significantly lower temperature of 35,7 °C. This lower transition temperature confirms the "low gelling" nature of the Agarose, indicating that its polymer chains form a less rigid network at physiological or room temperatures compared to the naturally more aggregated Agar matrix.

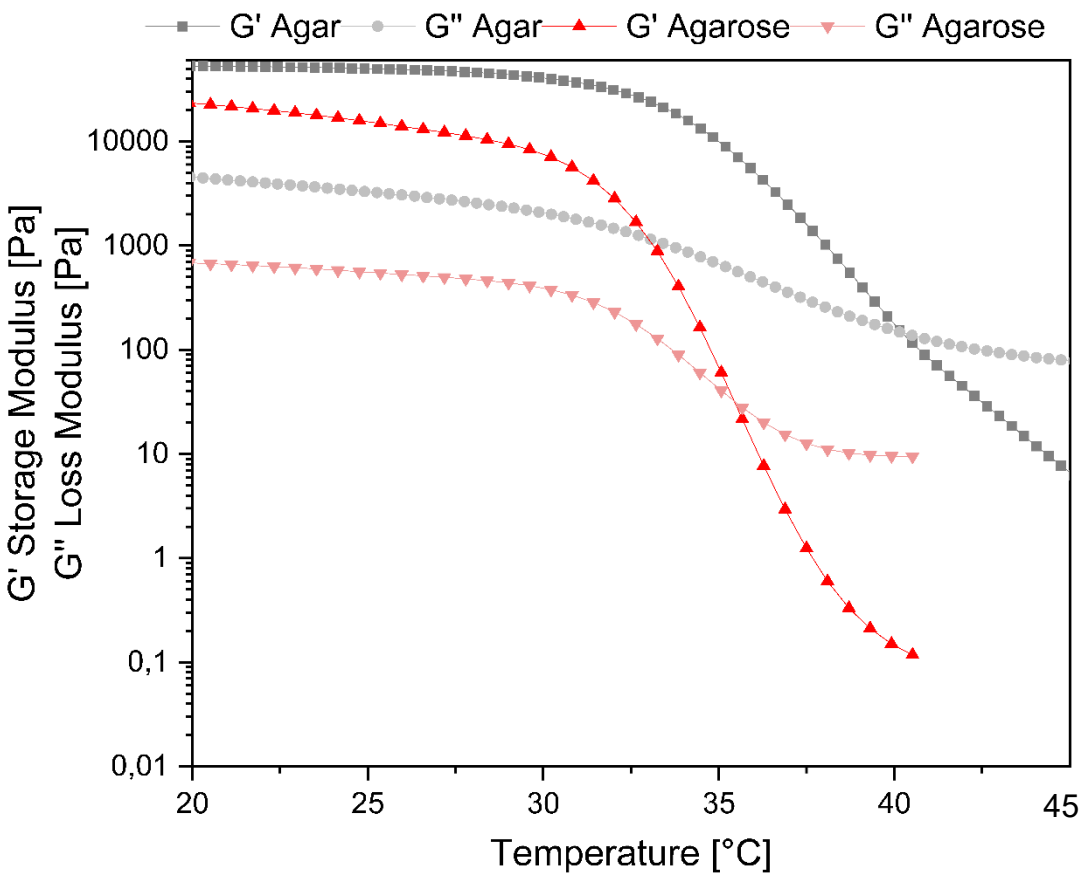

Figure 24- Temperature sweep test of Agar and Agarose. Gelling temperatures appear as the crosspoint of G' and G''

Following the gelling temperature evaluation, the flow behavior of the Agarose-based solutions was investigated to assess their processability. *Figure 25* illustrates the viscosity profiles of pristine Agarose. These solutions exhibit a non-Newtonian response where viscosity increases with concentration; notably, a yield stress behavior is detected at low concentration, attributed to the incipient gelation of the Agarose chains at the measurement temperature. In any case, the effect of "low gelling" nature of Agarose is notable in comparison with the Agar 3% w/v rheological curve (see Chapter 7): yield stress behaviour is present but with a drastic decrement in τ_0 value.

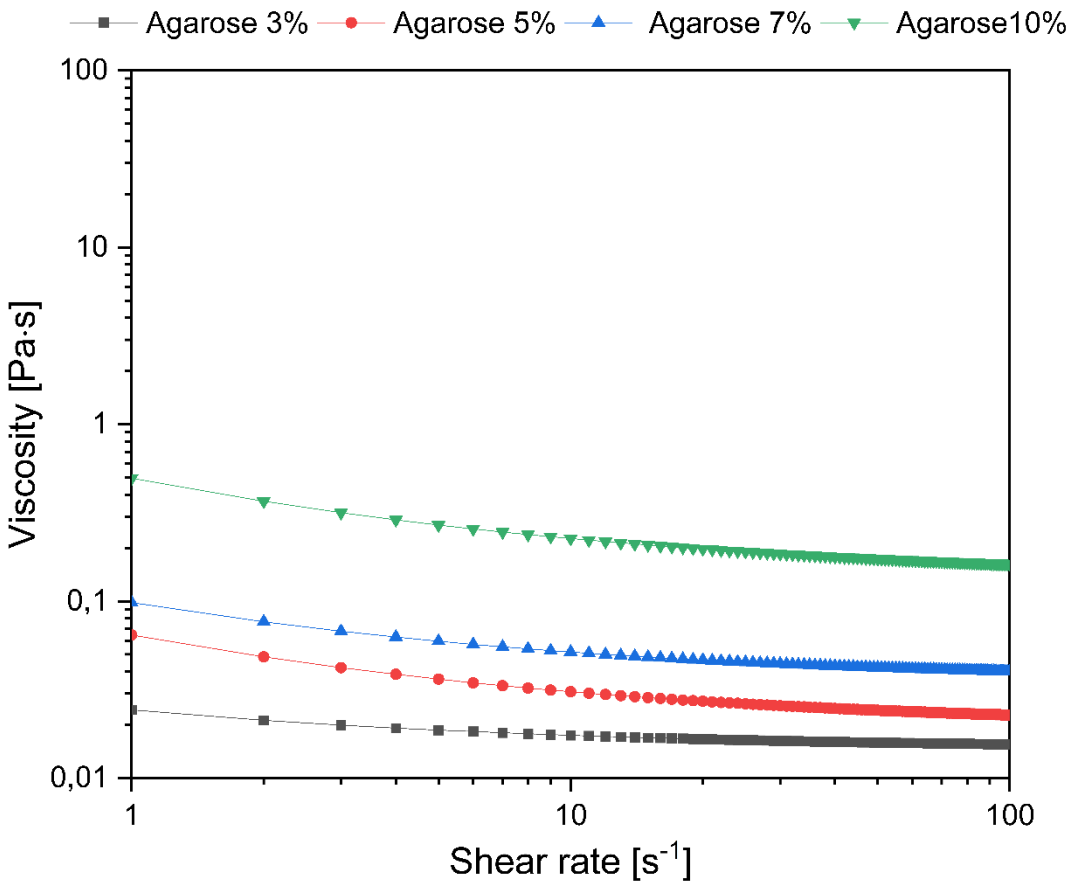

Figure 25- Flow curves of Agarose low gelling temperature at different concentrations

The introduction of PEO significantly modifies this profile (*Figure 26*). The Agarose/PEO blends show a rheological transition strictly governed by concentration. At lower concentrations (3 and 5%), the blend displays a constant viscosity (Newtonian behavior), suggesting the polymer chains are in a dilute regime with minimal overlap. However, as the concentration increases to 7% and 10%, the system exhibits a distinct non-Newtonian profile characterized by yield stress behavior. This response implies that at these higher concentrations, the PEO and Agarose chains form a structured network with finite structural strength, requiring a specific threshold of stress to initiate flow[199].

This structural transition is quantitatively summarized by plotting the apparent viscosity against total polymer concentration (*Figure 27* and Table 13). Measured at the critical process shear rate 66 s^{-1} (calculated with the equation 7 on the previous Chapter with fixed flow rate of 1,5 ml/h and an inner diameter of 0,4 mm), the relationship is non-linear, following a rapid, concave-up increase. This behavior is consistent with the power-law scaling of polymer solutions, where viscosity (η) is related to concentration (c) by Equation 8:

Equation 8

$$\eta \propto c^{x}$$

The steep rise observed between 5% and 10% signifies the transition from the semi-dilute unentangled state to the entangled regime. In this entangled regime, the exponent (x) increases drastically, reflecting the topological constraint imposed by the overlapping chains. This entanglement is crucial for process stability: solutions falling within this high-viscosity regime (≥7%) were confirmed to possess the necessary structural integrity at 66 s^{-1} to ensure stable fiber formation, while lower concentrations led to electrospraying.

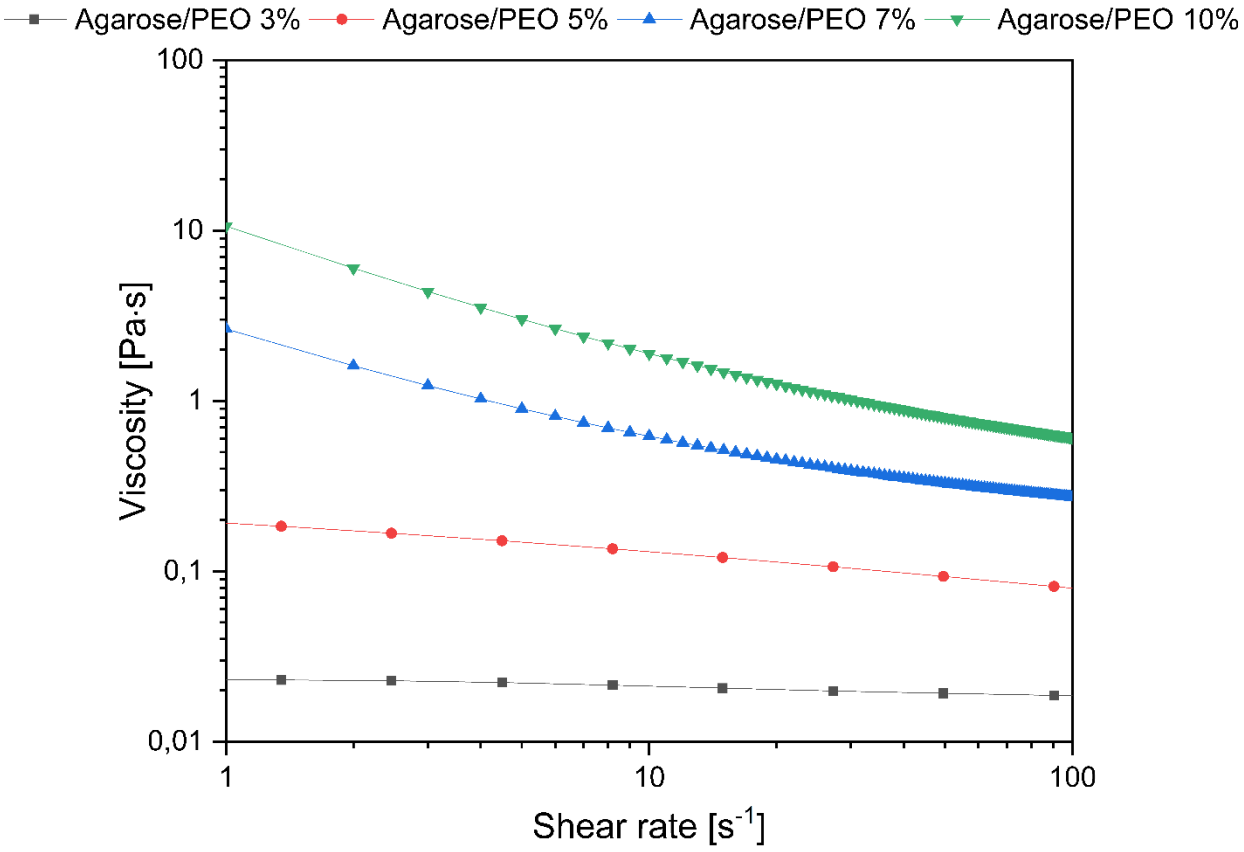

Figure 26- Flow curves of Agarose/PEO 300k 70/30 at different total polymer concentrations

Table 13- calculated shear rate (1,5 ml/ of flow rate and 0,4 ml/h) and viscosity for Agarose/PEO 70/30 at three different total polymer concentrations

Sample (70/30 w/w)	**η @66 s^{-1} (Pa s)**
Agarose/PEO 3% w/v	0,02
Agarose/PEO 5% w/v	0,09
Agarose/PEO 7% w/v	0,30
Agarose/PEO 10% w/v	0,71

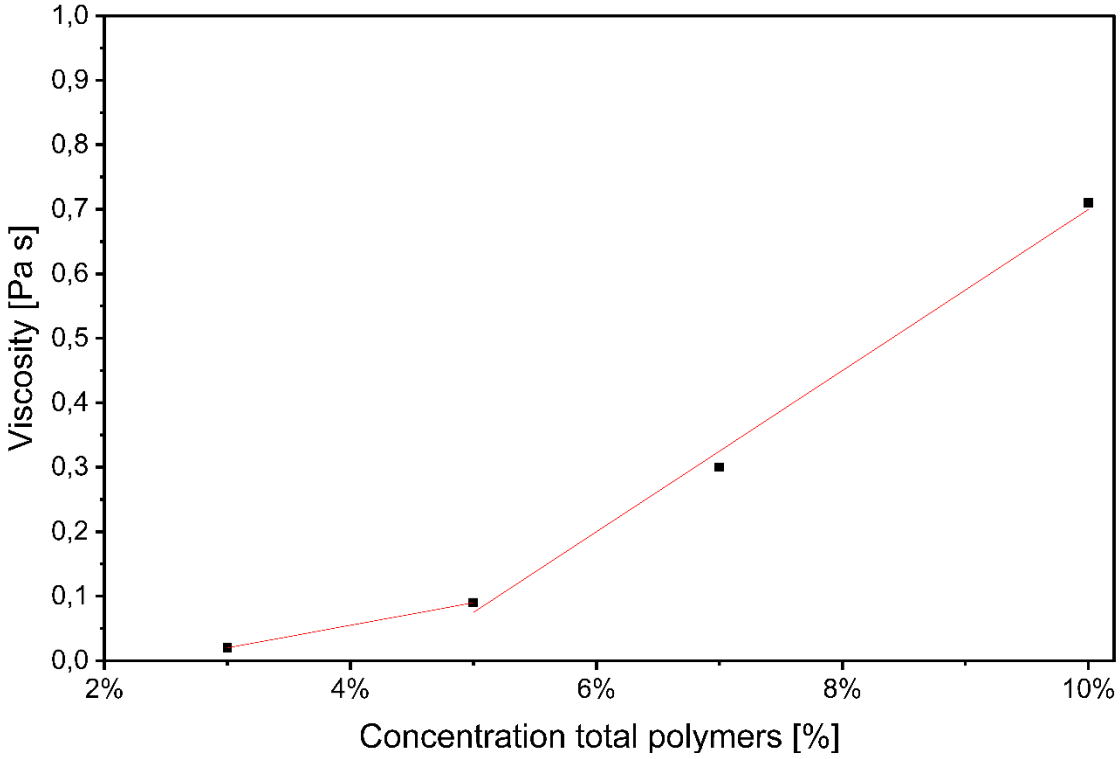

Figure 27- Viscosity at 66 s^{-1} of Agarose blends vs concentration of total polymer

Furthermore, to further highlight the structural differences observed in gelling temperature evaluation, the influence of PEO was compared between the two polysaccharides. A critical evaluation reveals that PEO plays an opposing rheological role depending on the matrix. In the Agarose system, PEO acts effectively as a thickening agent. Since the nascent Agarose network is weak (due to the low gelling temperature), the addition of high molecular weight PEO facilitates chain entanglement. This is evident when comparing pure Agarose (low viscosity) to the Agarose/PEO blends, where viscosity increases with polymer concentration. Conversely, in the Agar system, the presence of PEO leads to a reduction in viscosity. As observed in the Agar blend flow curves, the viscosity decreases as the PEO content increases (Pure Agar > 70/30 > 50/50). In this scenario, the pure Agar naturally forms a rigid, highly interconnected network. The introduction of flexible PEO chains likely interferes with the Agar-Agar self-association, effectively disrupting the rigid gel domains. This difference is starkly visible when comparing the blends at 3 and 5% of concentration:

- The Agarose/PEO blends behave as a low viscosity pseudoplastic fluid (0,02 Pa s) as the PEO is structuring a fluid matrix.
- The Agar/PEO blends exhibit a viscosity nearly two orders of magnitude higher with shear-thinning behavior, as the Agar matrix remains dominant despite the disrupting effect of PEO.

Electrospinning process

As explained in the theoretical chapters, polysaccharide solutions are very difficult to electrospun due to their electrolyte nature. For this reason, only the blend solutions were processed at 45°C with parameters summarised in Table 14. To study the effects of polymer concentration and viscosity on the process, the best parameters found were fixed for all blends.

Table 14- Electrospinning optimal parameters Agarose/PEO 300k

Solutions	Distance (cm)	Voltage (kV)	Flow rate (mL/h)	Temperature (°C)
Agarose/PEO 70/30 (all concentrations)	15	20	1,5	45

8.3 Poly(ethylene oxide) and Poly(vinyl alcohol) mats

Solutions preparation

The PEO ($\bar{M}v$=300 kDa) and PVA (approximal $\bar{M}v$=100 kDa) solutions were obtained by adding powders in glass flasks (10 ml of volume) with deionized water at concentrations of 10 % w/v by stirring for 1 hour at 70 °C.

Rheological characterization

For homogeneous electrospinning, the production of uniform, continuous nanofibers are generally associated with a stable cone-jet mode; the rheological characteristics of the polymer solutions are critical to ensuring consistent processing and fiber quality.

Both solutions exhibit viscosities well above the critical entanglement concentration, which is a prerequisite for forming continuous fibers rather than droplets (*Figure 28*). The PEO 300k solution displays a much higher zero-shear viscosity (8,6 Pa s) compared to the PVA solution (1,9 Pa s). This difference is a key factor in dictating the stability of the Taylor cone and the resulting jet (Table 15). The higher viscosity of PEO suggests a stronger internal network of polymer chains, which enhances the solution's ability to resist the breakup forces (Rayleigh instability) as the jet is stretched by the electric field, thus promoting a more stable and potentially easier-to-control homogeneous mode.

The observed shear-thinning in both solutions at higher shear rates is highly beneficial for the fluid delivery system (syringe pump/spinneret). This behavior allows for a smooth and consistent flow rate through the narrow nozzle under high pumping shear, which is essential for maintaining the homogeneity of the process and preventing fluctuations in the mass flow that could destabilize the cone-jet.

The overall magnitude of viscosity directly influences the final fiber diameter. Solutions with higher apparent viscosity (like PEO) tend to resist stretching more, generally yielding thicker fibers compared to lower-viscosity solutions (like PVA) under otherwise identical operating conditions. Therefore, to produce a homogeneous mat of similarly sized fibers, the PEO solution would likely require higher electric field strength or slower flow rates than the PVA solution to achieve comparable thinning and diameter uniformity.

Ultimately, the higher viscosity of the PEO solution suggests a wider processing window for achieving a stable, homogeneous cone-jet, although it will also likely result in larger-diameter fibers unless the process parameters are aggressively tuned.

Table 15- Zero-viscosity of PEO and PVA water solutions

Viscosity	PEO 10% w/v	PVA 10% w/v
η_0 [Pa s]	13,1	1,9

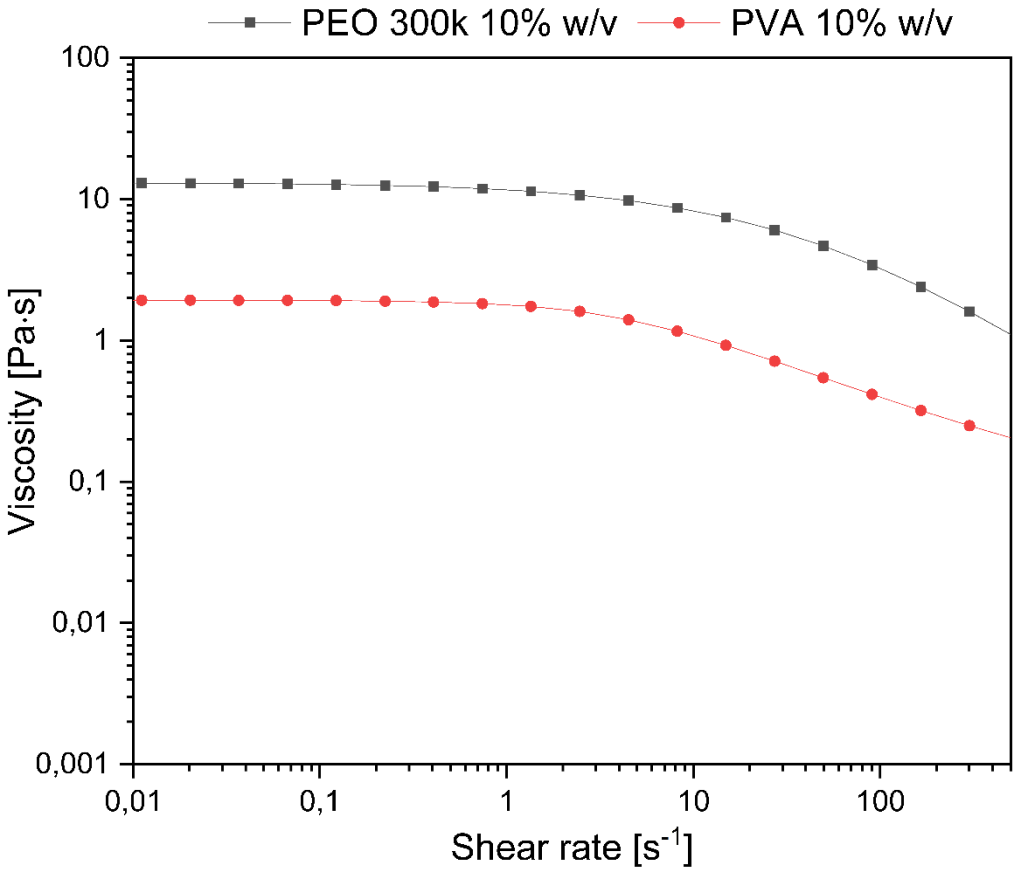

Figure 28- Flow curves of PEO and PVA 10% w/v water solutions

Electrospinning process

Polymer solutions were electrospun at 25 °C with the parameters summarized in Table 16. Parameters were selected after different tests to stabilize the Taylor Cone.

Table 16- Electrospinning optimal parameters

Solutions	Distance (cm)	Voltage (kV)	Flow rate (mL/h)
PEO	20	17	1,0
PVA	20	17	0,7

8.4 Mats characterization

Agarose mats

The Scanning Electron Microscopy (SEM) images (*Figure 29*) reveal a distinct morphological transition in Agarose/PEO electrospun mats driven by changes in polymer concentration and solution viscosity. At a low concentration of 3% w/v, the microstructure is characterized almost exclusively by the presence of beads without significant fiber formation, a defect caused by the solution's viscosity being too low to stabilize the electrospinning jet. As the concentration increases to 5% w/v, the viscosity rises sufficiently to allow the emergence of nanofibers, characterized by a diameter of approximately 160 nm, though some beading may persist. Further increasing the concentration eliminates these defects and results in thicker, more continuous fibers; specifically, the average fiber diameter grows to 210 nm at 7% w/v and reaches 320 nm at 10% w/v. This trend confirms that higher concentrations and viscosities are essential not only for suppressing bead formation but also for directly controlling the diameter of the resulting nanofibers (*Figure 30*). Furthermore, the homogeneous fibers that we obtained with Agarose/PEO 70/30 7% and 10% w/v of total polymers in comparison with Agar/PEO mats confirm the impact of gelling temperature on the performance of the electrospinning instrument, in fact, no bead-fibers are present in Agarose-based mats.

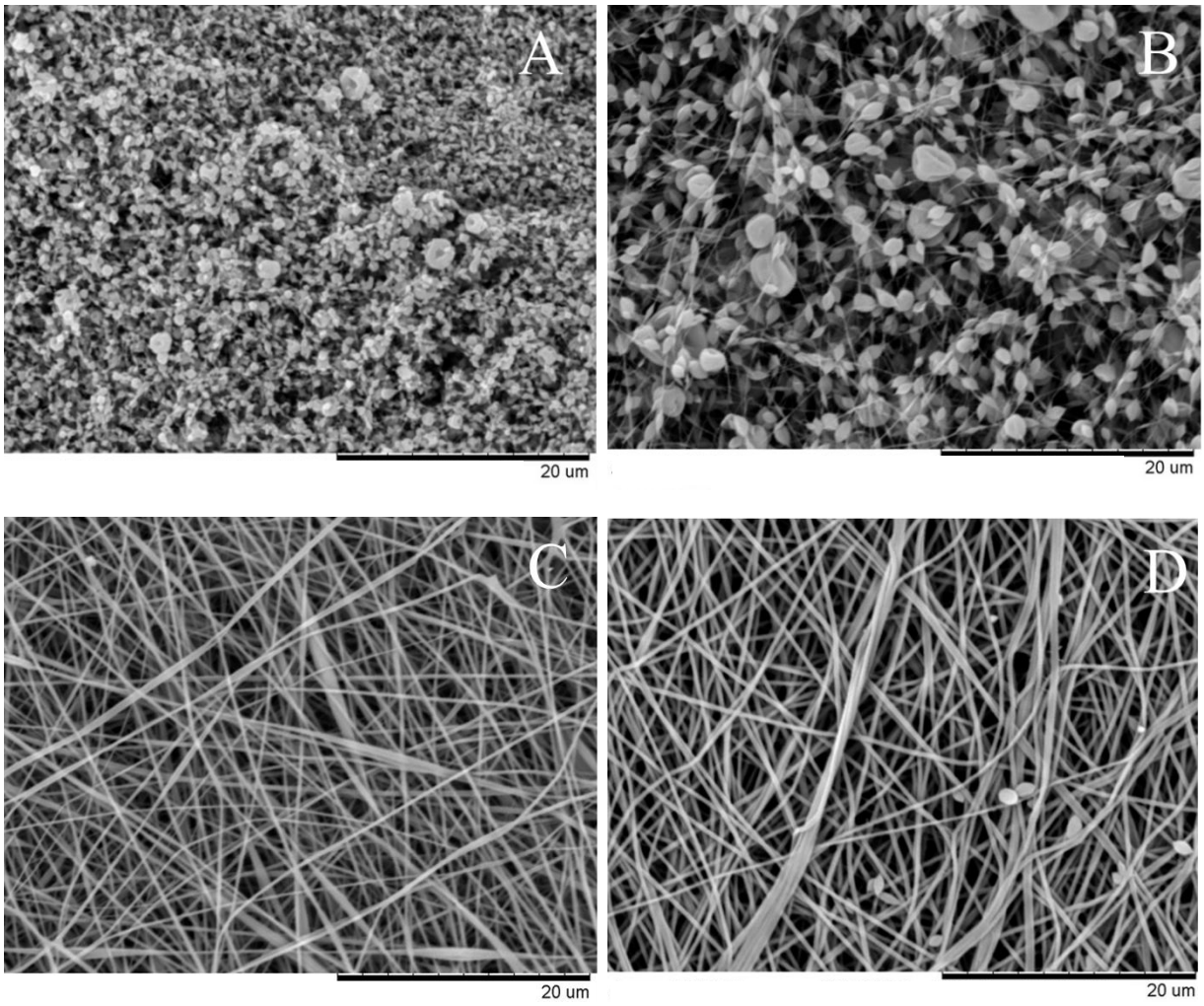

Figure 29- SEM images of Agarose/PEO 70/30 3% w/v (A), 5% w/v (B), 7% w/v (C), 10% w/v (D)

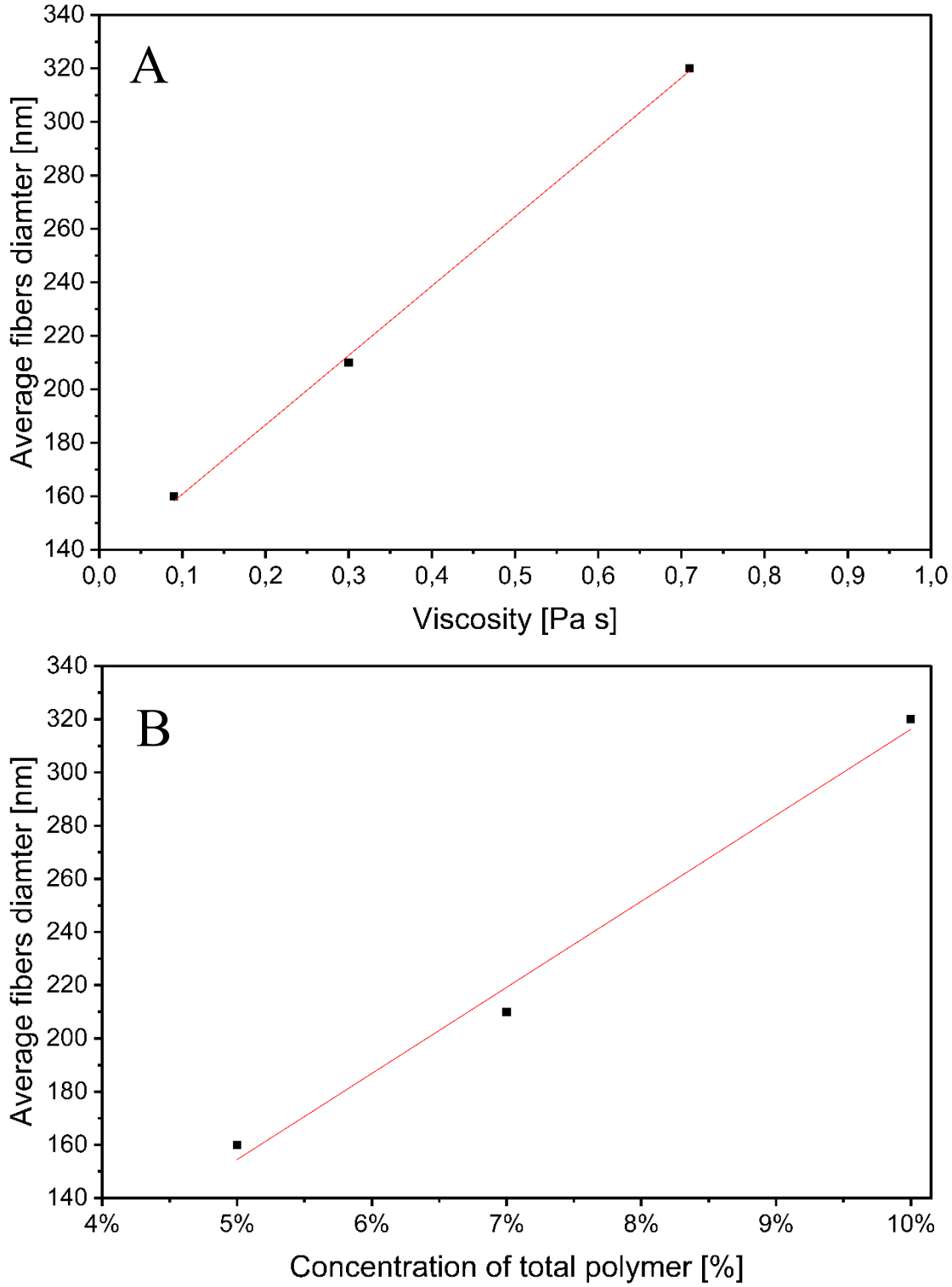

Figure 30- Average fiber diameter as a function of (A) viscosity at 66 s-1, (B) concentration

To evaluate the structural integrity and mechanical competence of the fabricated scaffolds, tensile testing was performed on the best optimized Agarose/PEO mats (7% and 10% w/v). These results were compared against a baseline sample composed of Agar/PEO (50/50, 3% w/v). It is important to clarify that a direct comparison at equal concentrations was not feasible due to the distinct rheological limits of the two polysaccharides. Specifically, while Agarose solutions required concentrations

above 5% w/v to achieve sufficient viscosity for fiber formation, Agar formulations exceeding 3% w/v exhibited premature gelation, which hindered the electrospinning process. Therefore, the comparison was established between the optimized, spinnable formulations for each specific system. The analysis focuses on isolating the contributions of morphological defects (beads) and fiber geometry to the resulting mechanical properties, specifically Young's Modulus (stiffness), tensile strength, and elongation at break. The results are summarized in *Figure 31.*

The Young's Modulus measurements reveal a fundamental disparity between the baseline and the optimized scaffolds, driven primarily by the microstructural architecture of the mats. The Agar/PEO baseline exhibited a negligible stiffness of < 50 MPa. This poor mechanical response is attributed to the high prevalence of bead defects observed in the 3% w/v sample.

In a beaded morphology, the polymer matrix is discontinuous; the beads act as stress concentrators rather than load-bearing elements. Consequently, the applied load cannot be effectively transferred across the mat, resulting in a structure that behaves more like a loose aggregate of particles than a cohesive fibrous network. Furthermore, the thinner, discontinuous proto-fibers connecting these beads possess a significantly smaller diameter, which limits the orientation of polymer chains and reduces the overall crystallinity usually associated with drawing during electrospinning.

In distinct contrast, the Agarose/PEO samples (7% and 10% w/v) exhibited a dramatic stiffness increase to approximately 240 MPa. This enhancement is caused by the transition to a continuous nanofibrous network. The formation of uniform, defect-free fibers allows for efficient stress distribution along the axis of the aligned polymer chains. While the chemical purity of Agarose (lacking the interference of Agaropectin) contributes to the formation of a rigid double-helix matrix, the dominant factor in this nearly five-fold increase in stiffness is the elimination of structural defects and the establishment of a robust, interconnected fiber mesh.

The tensile strength results further corroborate the impact of fiber diameter and continuity. The Agar baseline displayed negligible strength (~1.5 MPa), confirming that structural discontinuities (beads) lead to premature brittle failure under tension.

Conversely, the 10% w/v Agarose sample achieved the highest tensile strength (~11 MPa), noticeably outperforming the 7% sample (~7.5 MPa). This progressive increase suggests a direct correlation between fiber diameter and load-bearing capacity. The thicker fibers (320 nm) produced at 10% w/v provide a larger cross-sectional area per fiber, enabling the mat to withstand higher tensile forces before yielding, whereas the thinner fibers (210 nm) at 7% w/v rupture at lower stress levels.

The elongation at break values highlights the "toughness" of the optimized network. The Agar baseline fractured at a low strain of approximately 4%, consistent with the brittle nature of a defect-ridden structure where cracks propagate rapidly between beads.

The 10% w/v Agarose sample demonstrated superior ductility (~10%), nearly double that of the 7% sample. This indicates that a denser network of thicker fibers allows for significant reorientation and "drawing" of the fibers during stretching. The 10% formulation appears to provide the optimal balance of entanglement and individual fiber strength, allowing the scaffold to absorb significant energy via plastic deformation prior to catastrophic failure.

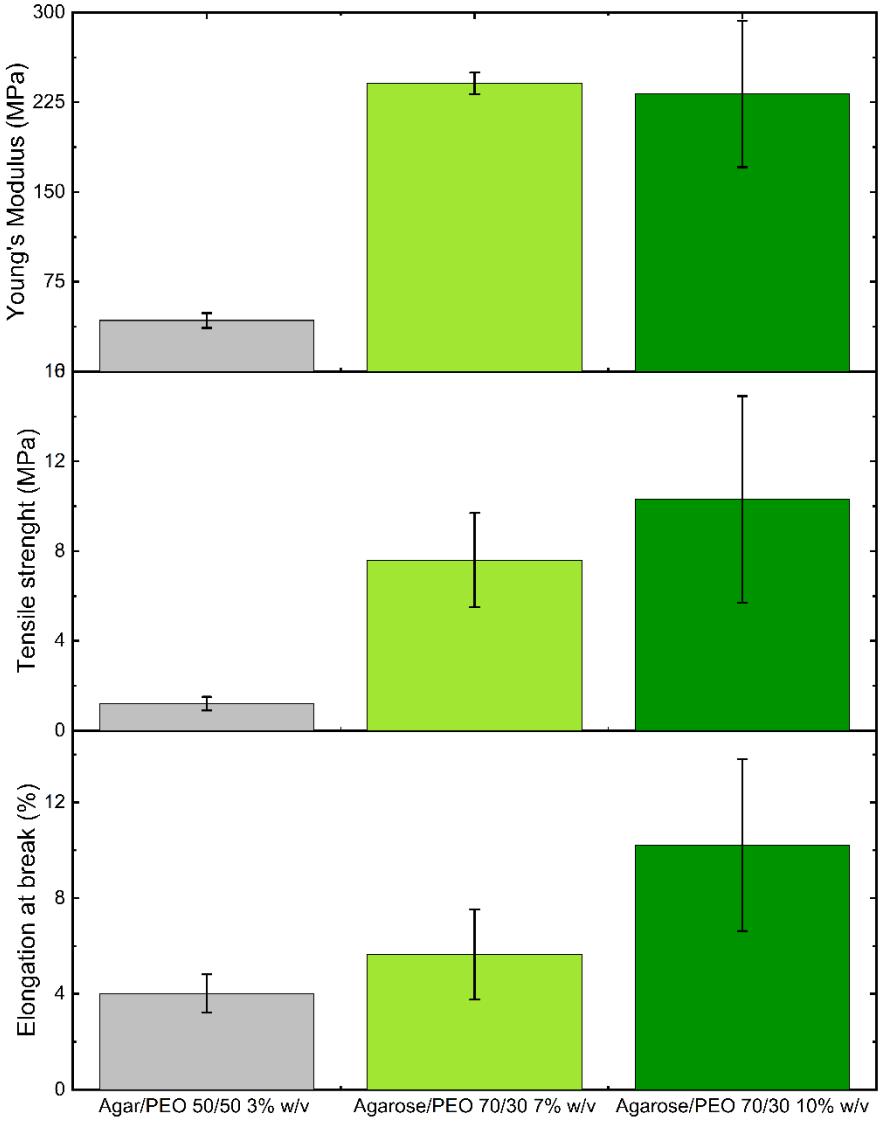

Figure 31- Tensile test results on the mats of Agarose/PEO 7% w/v and 10% w/v. Results of Agar/PEO 50/50 3% w/v mat was added as a comparison.

PEO and PVA mats

The morphological analysis, conducted via Scanning Electron Microscopy (SEM), revealed distinct structural differences between the electrospun mats (*Figure 32*). The PVA fibers exhibited a smooth, uniform, and bead-free morphology with an average fine diameter of 200 nm. In contrast, the PEO mats were composed of coarser fibers with a significantly larger average diameter of 410 nm. These morphological characteristics played a critical role in the macroscopic mechanical behavior of the scaffolds.

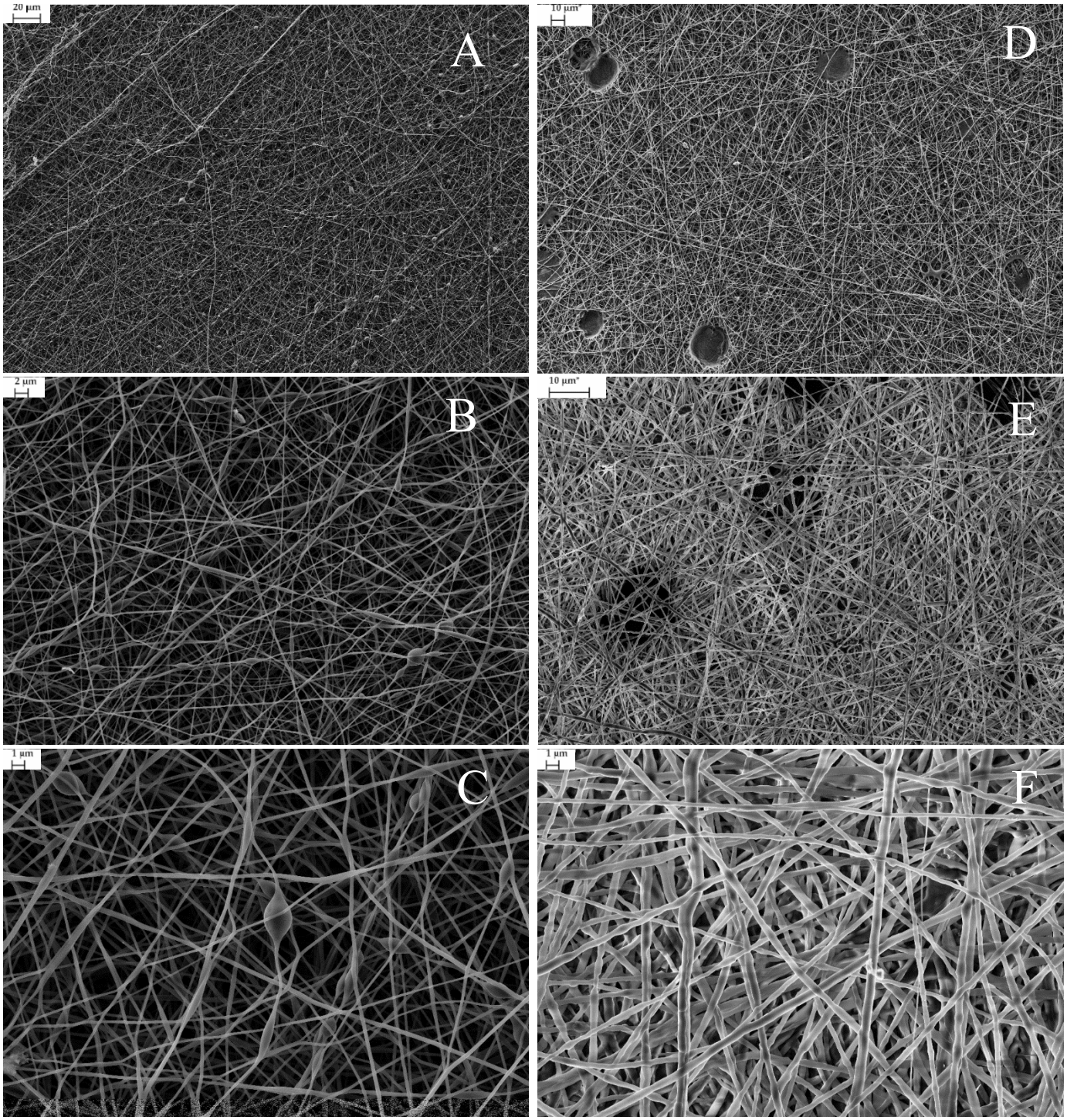

Figure 32- FE-SEM images of PVA 10% w/v mat (A-B-C) and PEO 300k 10% w/v (D-E-F)

Mechanical testing demonstrated that the PVA mats possessed superior mechanical integrity compared to the PEO mats across all evaluated parameters. As shown in the tensile data (*Figure 33*), the PVA mats achieved a Young's modulus of approximately 75 MPa, which is a threefold increase over the PEO mats (~25 MPa), indicating a much higher stiffness. The disparity was most evident in

the ultimate tensile strength, where the PVA mats reached 7.1 MPa, vastly outperforming the PEO mats, which exhibited a negligible strength of roughly 0.5 MPa.

Furthermore, the post-yield behavior highlighted a fundamental difference in ductility. The PEO mats displayed brittle failure characteristics with an elongation at break of less than 3%. Conversely, the PVA mats exhibited a ductile response with an elongation at break of approximately 19%, suggesting a tougher material capable of absorbing more energy before failure. This dramatic enhancement in mechanical performance for the PVA mats can be attributed to two primary factors: firstly, the abundant hydroxyl groups in the PVA side chains facilitate strong intermolecular hydrogen bonding, providing high cohesive energy density compared to the weaker intermolecular forces in PEO. Secondly, the significantly smaller fiber diameter of the PVA (200 nm vs. 410 nm) results in a higher specific surface area and denser fiber packing, which enhances the mat's ability to distribute load effectively through the network.

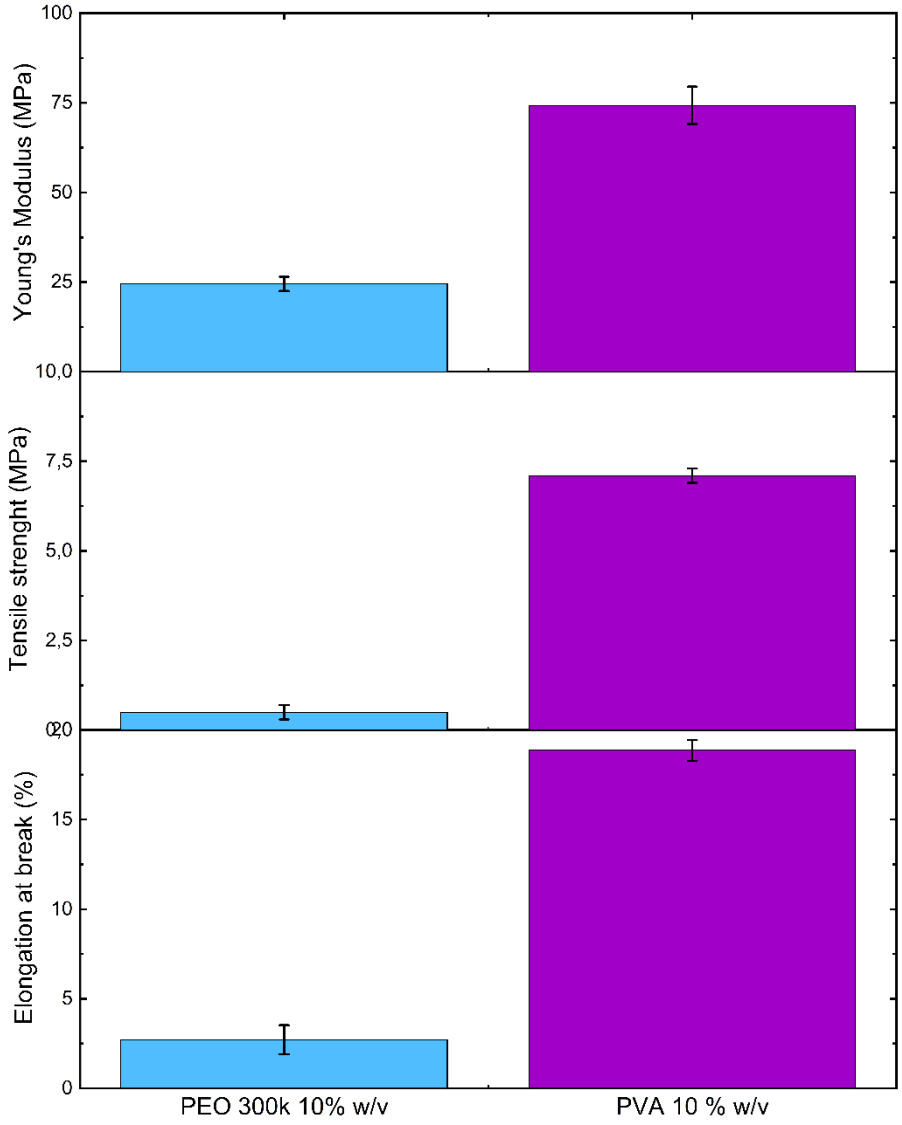

Figure 33- Tensile test on PVA and PEO 10% w/v mats

8.5 Application to a real case

Electrospun mats, specifically Agarose/PEO 70/30 (7 % w/v), PEO (10 % w/v), PVA (10 % w/v), and PCL (30 % w/v), were initially evaluated as supports for benzyl alcohol cleaning agents. Among the Agarose-based options, the Agarose/PEO (7 % w/v) mat was selected for further testing due to its superior morphology and optimal fiber diameter.

Before applying the mats directly to the artwork, laboratory preliminary tests were conducted to establish a protocol for the procedure on two reference surfaces (pieces of canvas and painted glass (*Figure 34*). For these characterization tests, mat samples were cut to a standard area of 5 cm^2 with a thickness of 50 µm. The stability of the mats in the solvent, swelling, and deswelling evaluation of benzyl alcohol was studied. After that, the procedure was tested directly on the artwork to study the behavior of the best membranes on the surface of the paint and their cleaning ability.

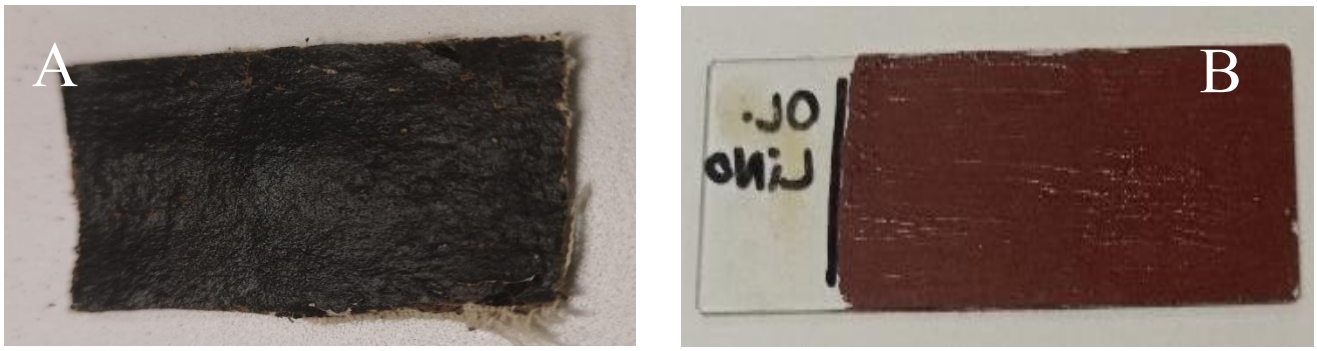

Figure 34- Reference surfaces for deswelling test: (A) pieces of tempera on canvas and (B) painted glass composed of linseed oil and iron oxide-based pigment.

Stability tests performed in benzyl alcohol indicated complete solubilization of PEO and PCL membranes within 5 minutes of immersion, consistent with their known solubility profile in this solvent. The Agarose/PEO 70/30 (7 % w/v) membrane exhibited partial weight loss (8.5 %), likely attributable to the solubilization of the PEO fraction; however, SEM analysis revealed that the fibrous morphology remained well-preserved (*Figure 35, A-B*). However, it is important to note that this leaching of PEO primarily occurs during the solvent loading step (5 minutes), before the application on the artwork surface. Furthermore, should any minor PEO residues be transferred, the high-water solubility of this polymer ensures their complete removal during the standard aqueous clearance step typically performed after solvent cleaning.

The PVA 10 % w/v membrane demonstrated no weight loss, with SEM confirming the stability of the fibrous structure post-immersion (*Figure 35, C-D*). Consequently, Agarose/PEO (70/30, 7 % w/v) and PVA (10 % w/v) membranes were selected for subsequent experiments.

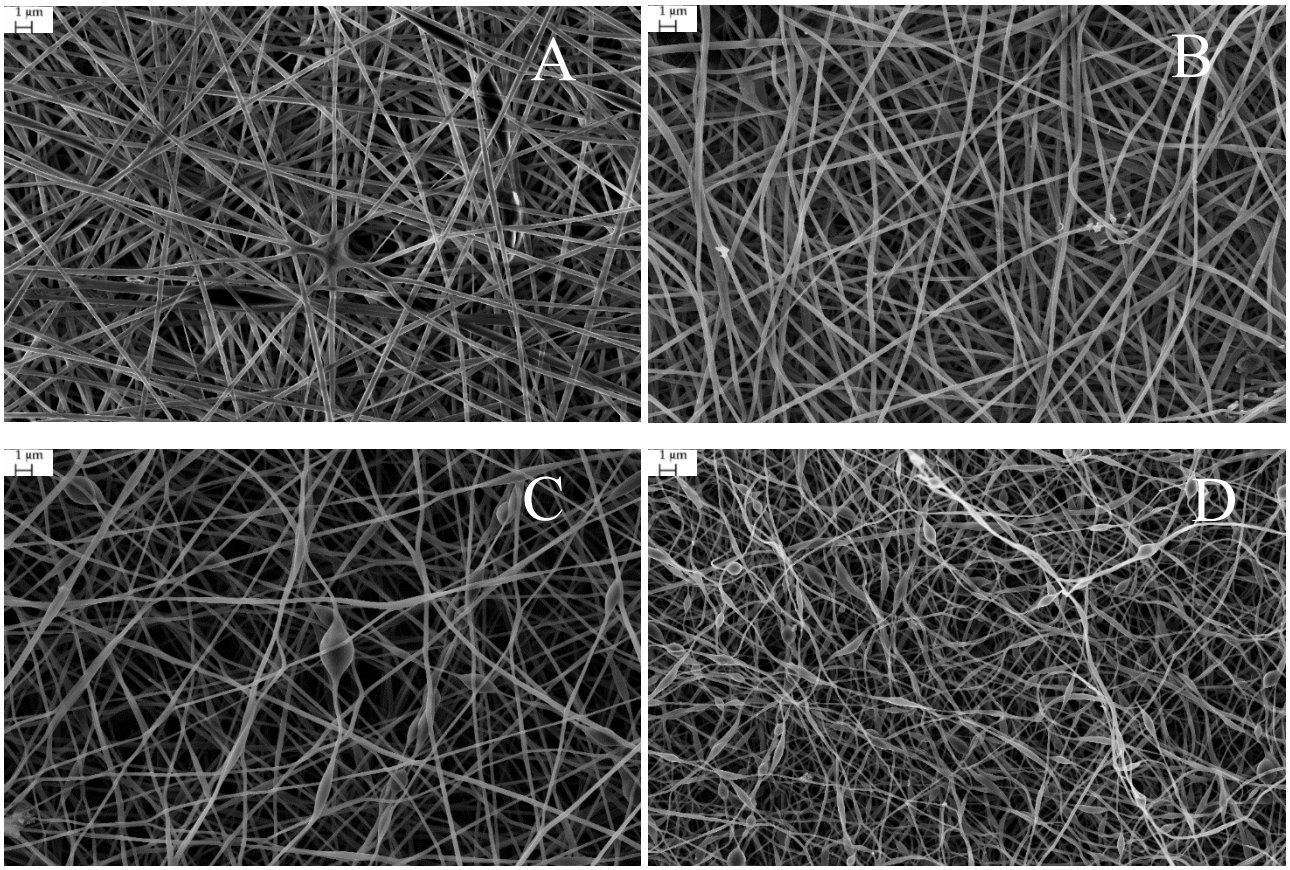

Figure 35- FE-SEM images of Agarose/PEO (A-B) and PVA (C-D) mats before (on the left) and after immersion (on the right) in benzyl alcohol

Absorption studies indicate that maximum solvent uptake occurs within 5 minutes of immersion, at which point the swelling curve reaches a plateau. The Agarose/PEO membrane demonstrated a superior absorption capacity, taking up approximately 14 times its initial weight. In comparison, the PVA membrane absorbed approximately seven times its weight (*Figure 36*). This disparity is likely due to differences in membrane porosity and the greater affinity of Agarose for benzyl alcohol compared to PVA. Based on these kinetics, a 5-minute absorption time, the minimum required for mat saturation, was established for the subsequent release (deswelling) tests.

Deswelling profiles on canvas reveal that, following an immediate solvent loss during the first minute of application, the release becomes controlled and gradual. After 60 minutes, the membrane remained saturated (>70 % solvent retention), suggesting the feasibility of prolonged applications exceeding one hour (*Figure 37*).

Results on glass slides showed a similar retention trend but with a different initial release profile. Unlike the canvas, the release on glass was gradual from the first minute. This variation is attributed to the substrate porosity; the canvas is significantly more porous than the glass, promoting an initial rapid transfer via capillary action. Both membranes maintained effectively high solvent levels (>70 %) after one hour (*Figure 38*).

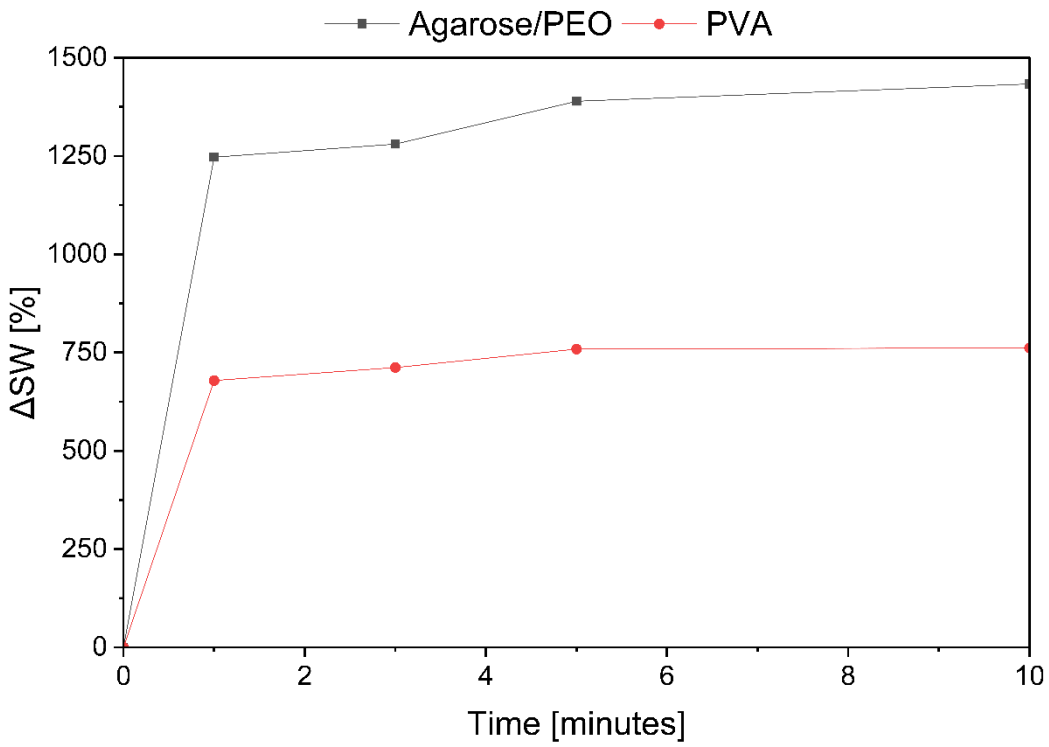

Figure 36- Swelling (ΔSW%) during time for Agarose /PEO and PVA mats after immersion in benzyl alcohol.

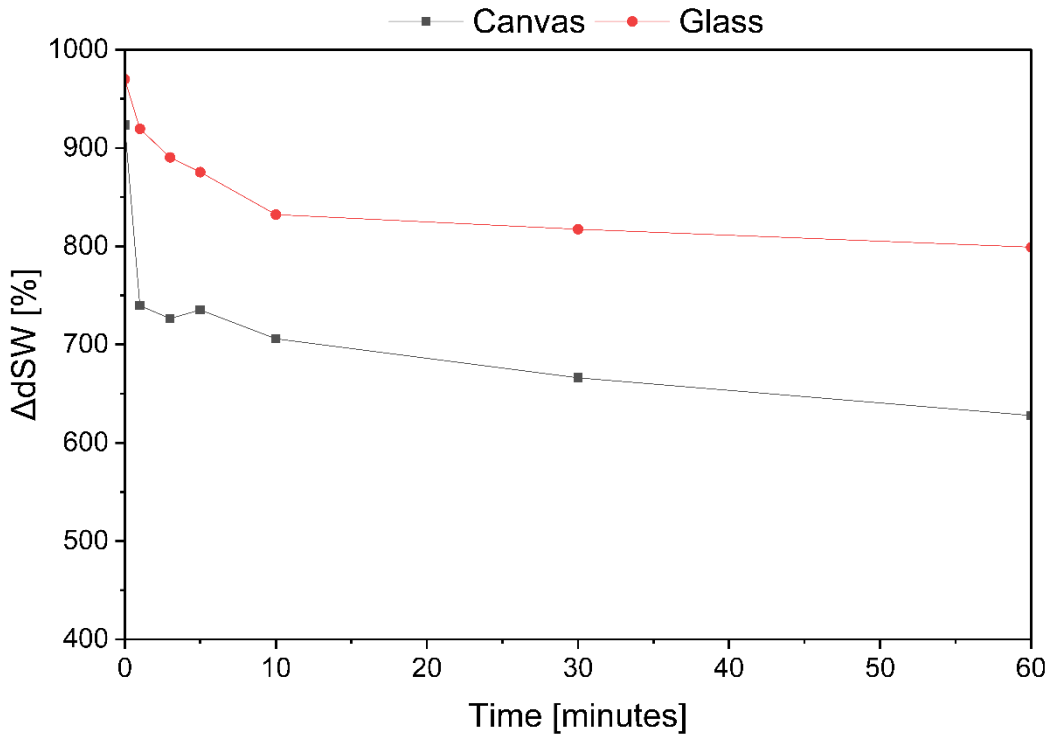

Figure 37- Deswelling (ΔdSW%) during time for Agarose/PEO mat after immersion in benzyl alcohol and application on canvas and painted glass.

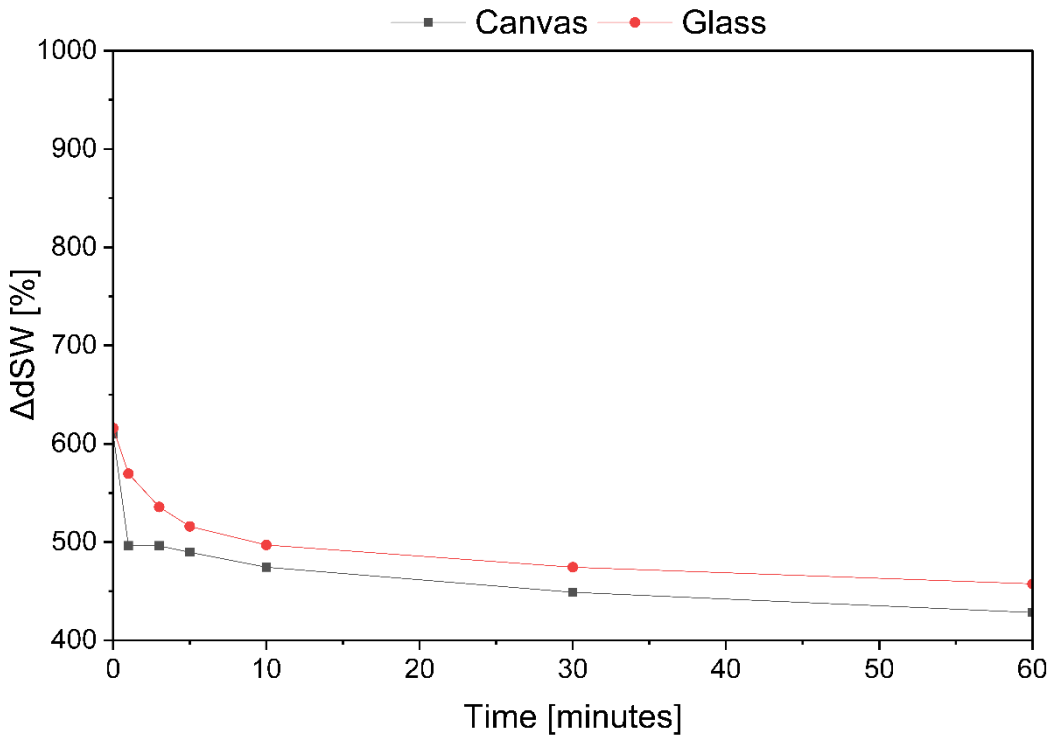

Figure 38- Deswelling (ΔdSW%) during time for PVA mat after immersion in benzyl alcohol and application on canvas and painted glass.

Macroscopic examination of 60 minutes post-treatment highlighted significant physical differences dictated by the substrate. Mats retrieved from the canvas exhibited significant chromatic alteration towards a yellow-brown spectrum and retained a negative plastic impression of the textile weave, providing evidence of high conformability (*Figure 39*). In contrast, the matrices applied to the glass reference retained their original planar geometry, lacking the topographical deformation observed in the textile trials. Furthermore, the chromatic shift on the glass-applied mats was markedly less pronounced, presenting a uniform, fainter discoloration consistent with the lower contaminant load and smoother surface profile of the glass substrate (*Figure 40*).

Field Emission Scanning Electron Microscopy (FE-SEM) elucidated the mat-substrate interfacial mechanics, revealing a distinct differentiation in morphological adaptation induced by the two substrates. Micrographs of mats retrieved from the canvas model displayed pronounced morphological deformation, where the nanofibrous layers were observed to be deeply compressed and molded to the specific warp and weft geometry of the textile, exhibiting a complex, three-dimensional topography (*Figure 41*). In contrast, mats recovered from the glass slides retained a predominantly planar and smooth surface profile, reflecting the rigid nature of the substrate (*Figure 42*). Regarding the capture mechanism, FESEM revealed a marked divergence between the polymer matrices. Agarose/PEO mats, despite containing trapped particles, maintained a open porous network (*Figure 41-42*). Conversely, PVA mats displayed a "clogging" effect, where entrapped particulate matter filled the interstitial voids and coated the fibers, resulting in a dense, quasi-composite structure (*Figure 41-42*). This microstructural evidence substantiates the gravimetric data (mats were weighed after cleaning process of one hour and after complete evaporation of the solvent.): PVA demonstrated a superior removal capacity with a mass increment of 205 %, compared to 110 % for the Agarose/PEO system.

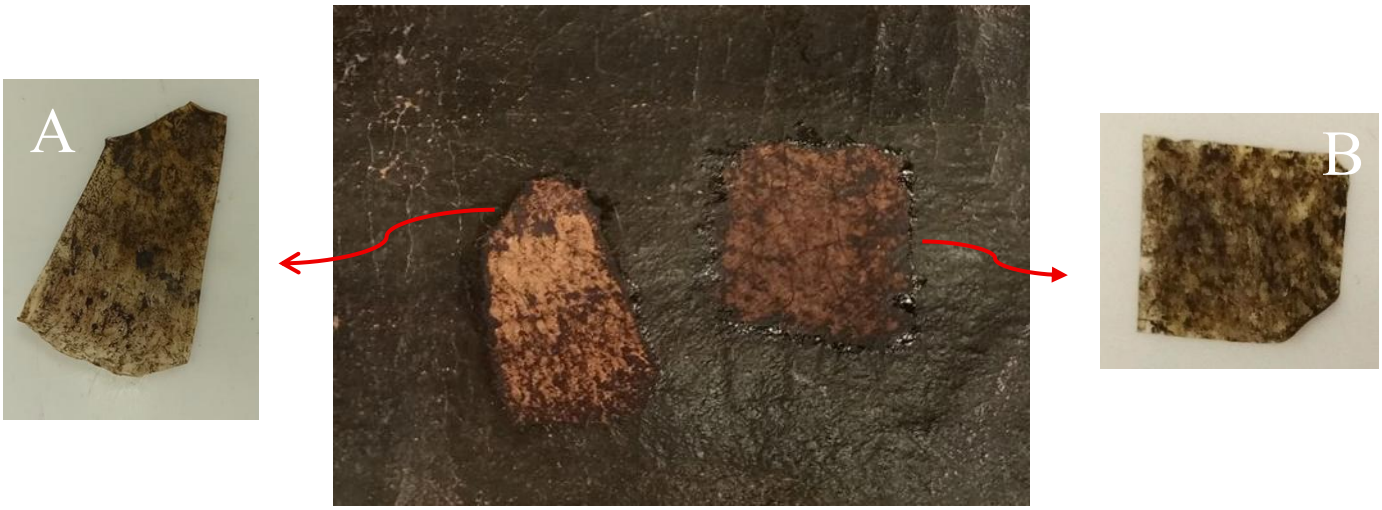

Figure 39- Agarose/PEO (A) and PVA (B) mats after 60 minutes of application on canvas; in the center, the canvas after mats application.

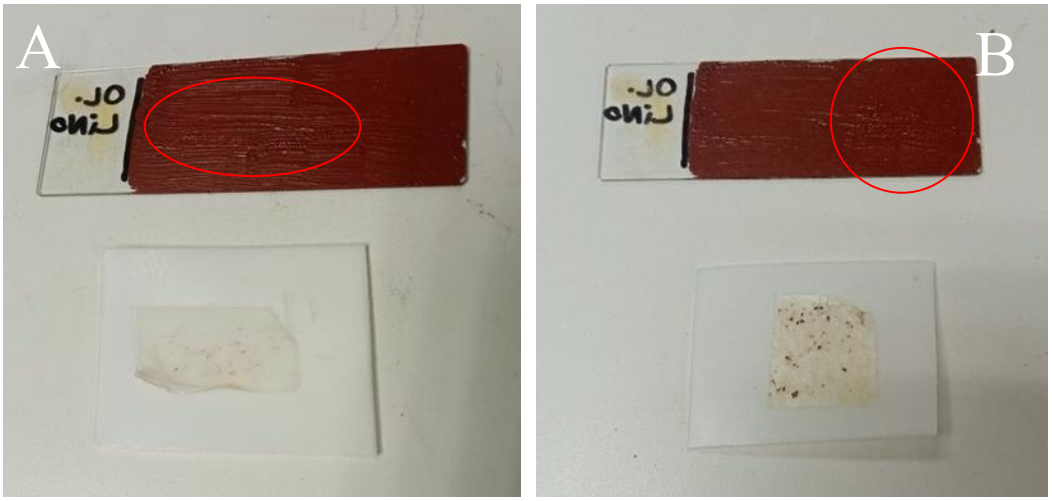

Figure 40- Agarose/PEO (A) and PVA (B) mats after 60 minutes of application on painted glass; in the red circle, the application areas are visible.

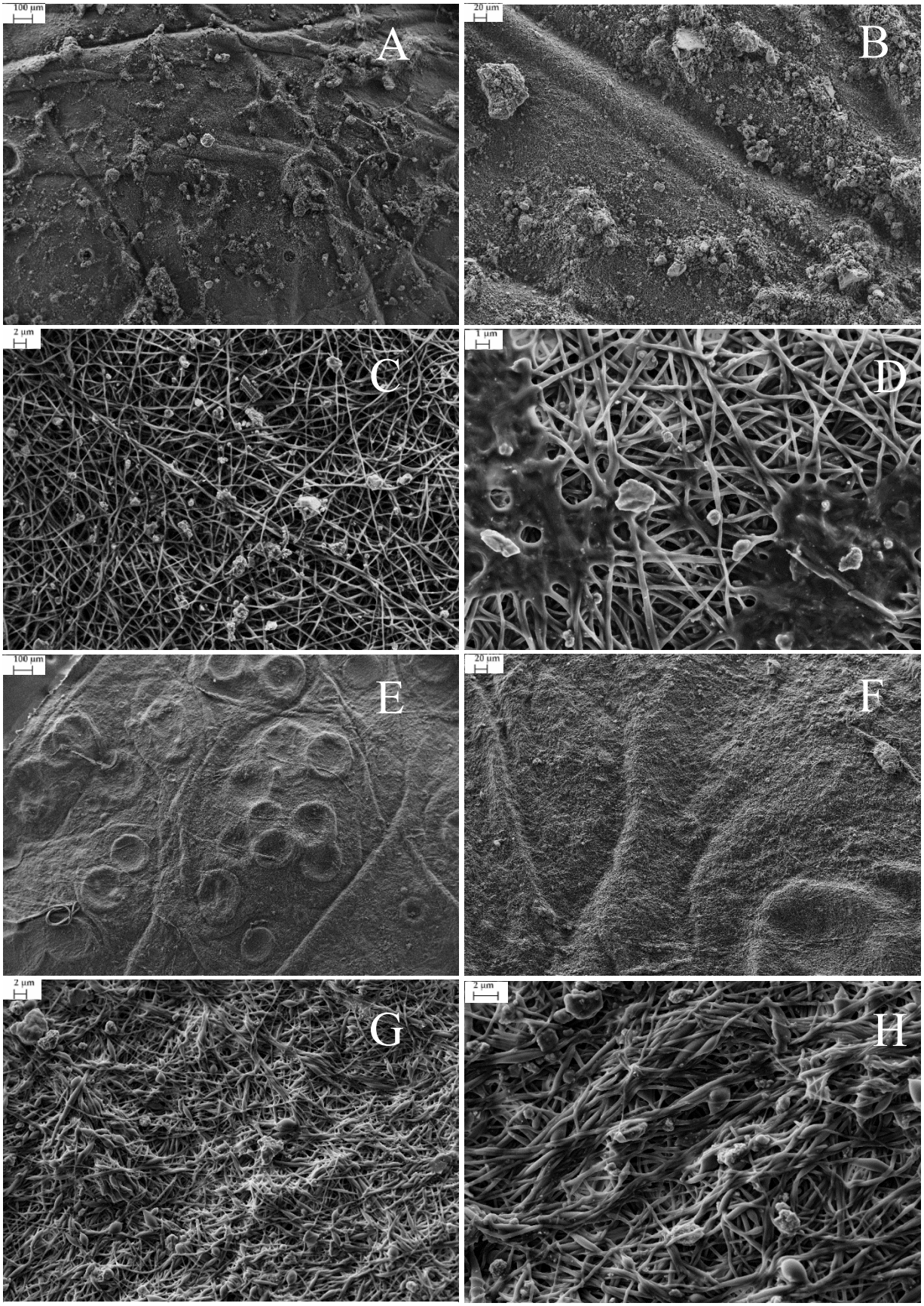

Figure 41- Agarose/PEO (A-B-C-D) and PVA (E-F-G-H) mats after 60 minutes of application on canvas

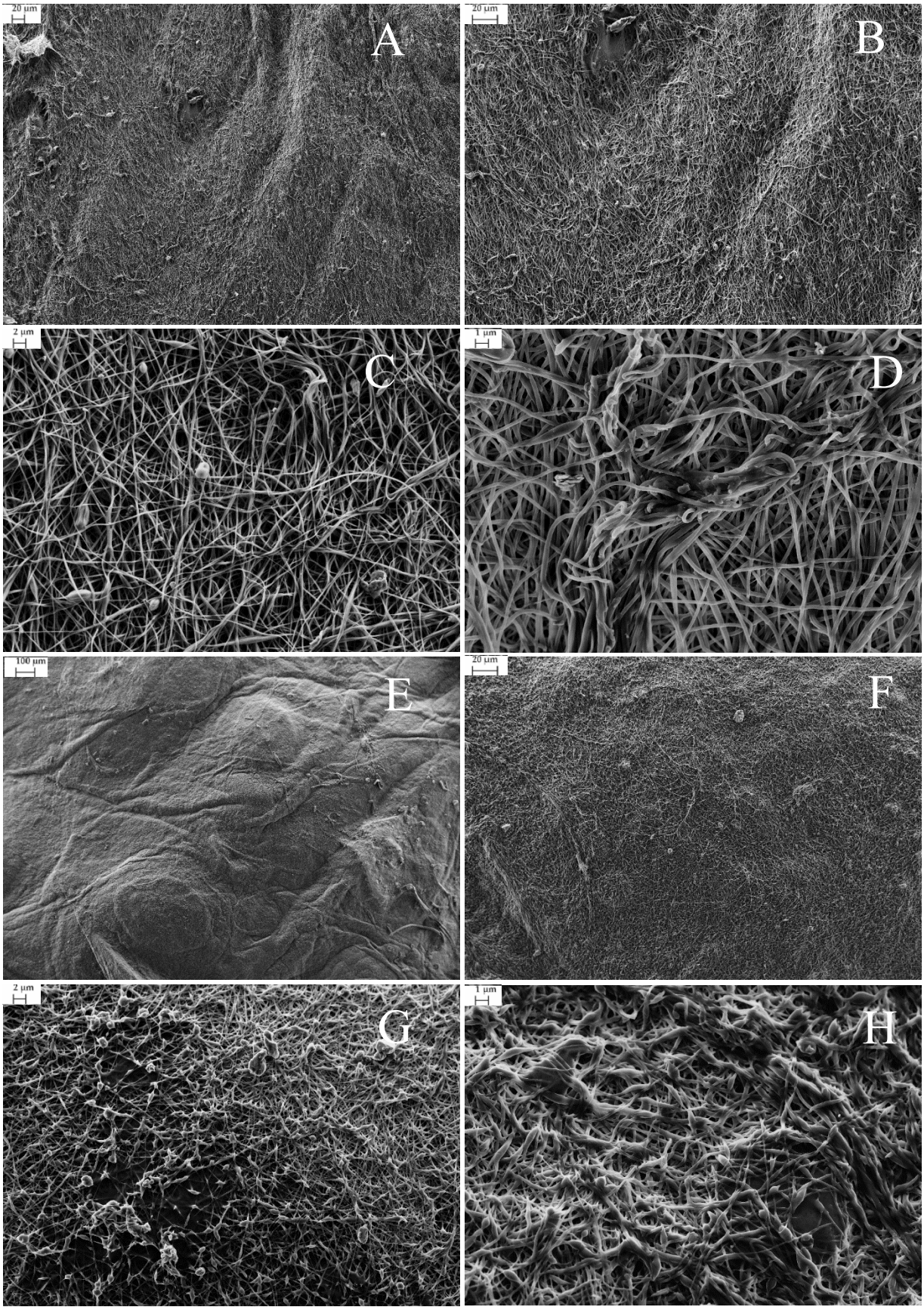

Figure 42- Agarose/PEO (A-B-C-D) and PVA (E-F-G-H) mats after 60 minutes of application on painted glass

Following validation, the procedure was tested directly on the wood artwork to evaluate the behavior of the membranes on the paint surface, in particular in the repainting and varnish areas (*Figure 43*). For this application, the protocol was optimized to ensure the safety of the artwork: the mat thickness was reduced to 30 μm, and the deswelling times were modified to reduce the duration of the initial application step (0.5, 2, 4, 15, 30, 60 minutes).

Figure 43- Repainting (A) and aged varnish (B) areas

The *in situ* application fully confirmed the trends observed in the preliminary phase, demonstrating a controlled solvent release with no lateral diffusion. Visual monitoring during the procedure revealed that the Agarose/PEO mat established a superior interfacial contact with the artwork surface compared to PVA, attributed to the high solvent affinity and flexibility of the Agarose network (*Figure 46*). The solvent release kinetics were notably influenced by the specific stratigraphy of the treatment area, with a higher release rate recorded on the yellowed varnish compared to the denser repainted areas (*Figure 44-45*). Crucially, the cleaning mechanism was visually confirmed directly on the artwork surface, revealing that the degree of removal for both the repainting and varnish layers is a function of the application time and the thickness of paint layer (*Figure 47-48*). Extended contact facilitated the gradual solubilization of the non-original repainting layer, resulting in evident discoloration, while the varnish area demonstrated the progressive removal of yellowed oxidation products. Macroscopic inspection of the mats post-treatment further validated their high cleaning potential, as both polymer systems exhibited visible darkening due to captured soil (*Figure 49*). Quantitatively, gravimetric analysis performed after 60 minutes of application reaffirmed the superior efficiency of the PVA mat in contaminant sequestration, registering a weight increment of 25 % due to entrapped exudates, in contrast to the 10 % increase measured for the Agarose/PEO mat for both artworks' areas.

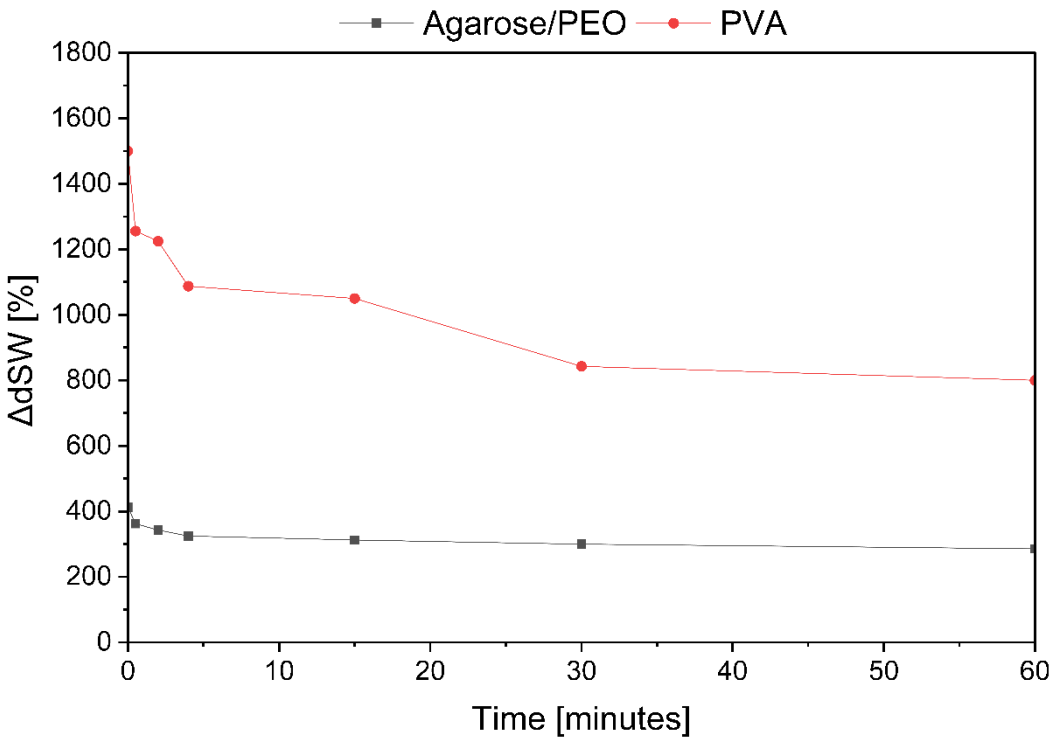

Figure 44- Deswelling (ΔdSW%) during time for PVA and Agarose/PEO mats after immersion in benzyl alcohol and application on repainting area.

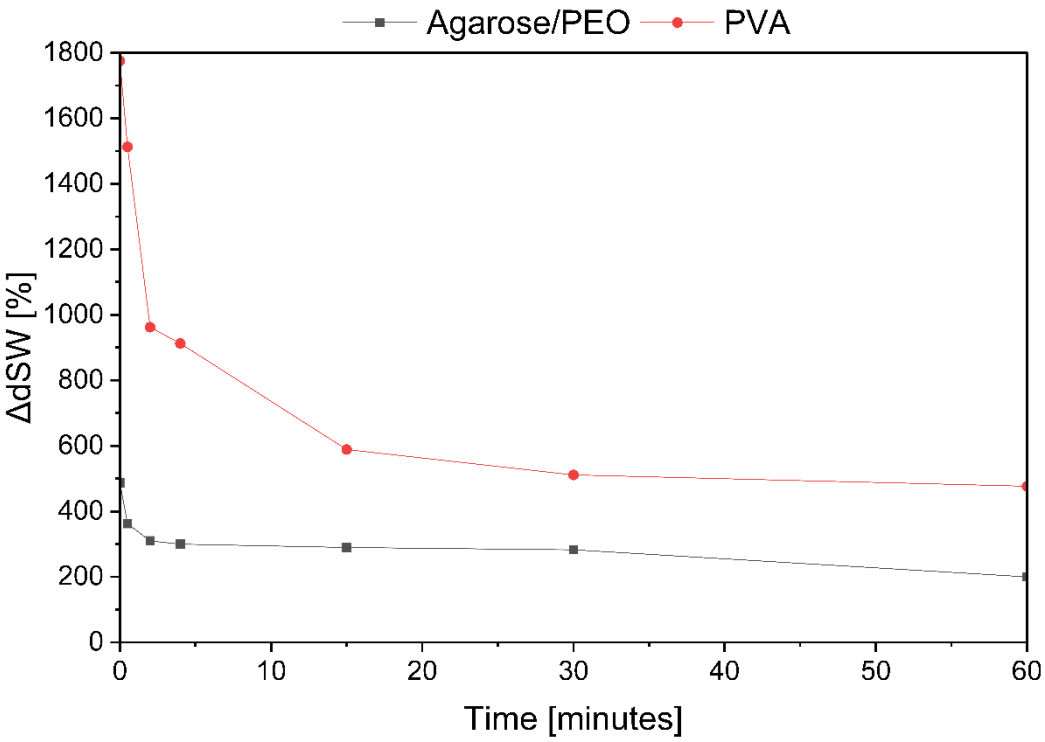

Figure 45- Deswelling (ΔdSW%) during time for PVA and Agarose/PEO mats after immersion in benzyl alcohol and application on aged varnish area.

Figure 46- Repainting (A) and aged varnish (B) areas with application of Agarose/PEO (left) and PVA (right) mats.

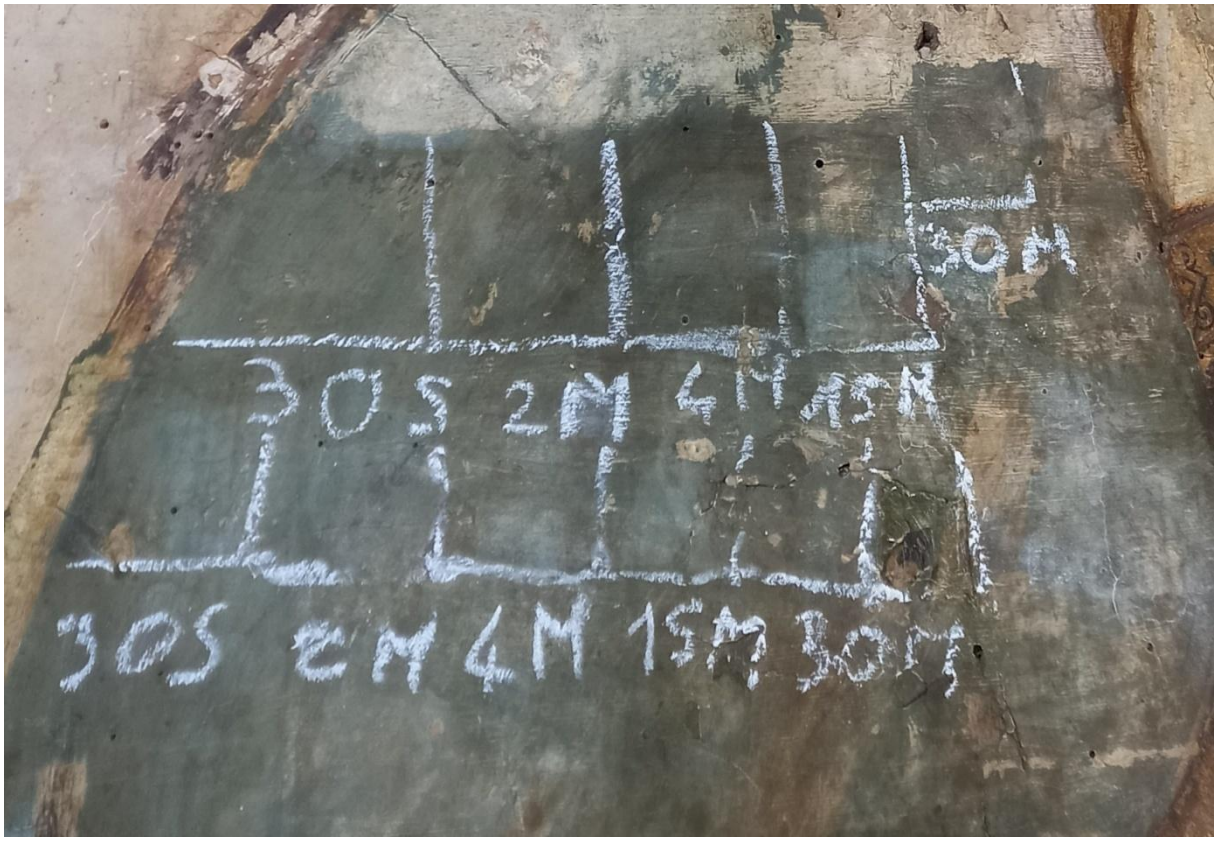

Figure 47- Repainting area after application of Agarose/PEO (above line) and PVA (below line) mats for different times.

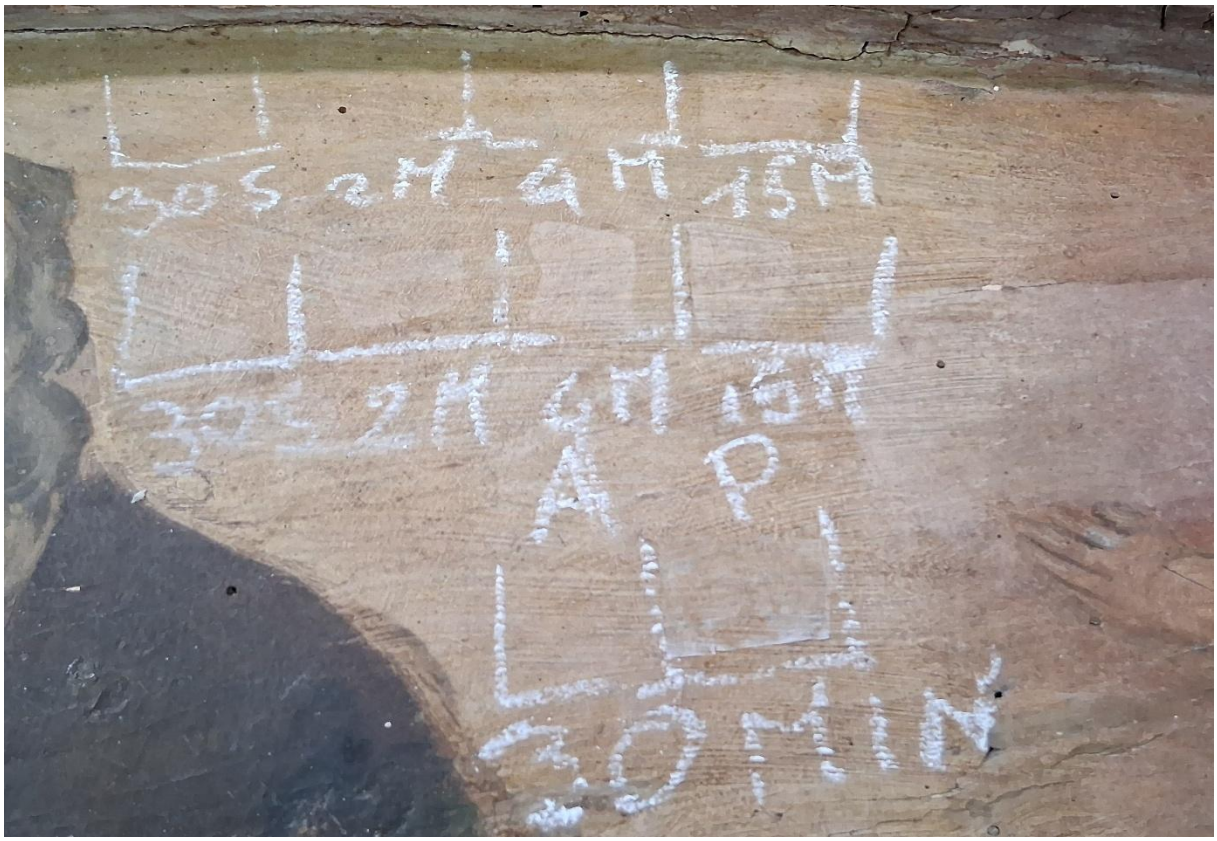

Figure 48- Aged varnish area after application of Agarose/PEO (above line) and PVA (below line) mats for different times.

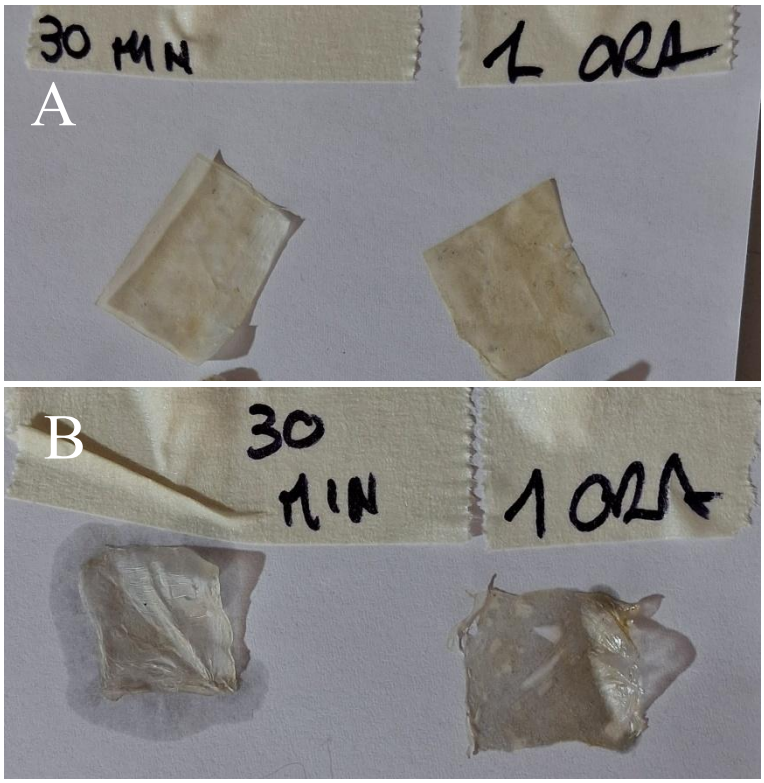

Figure 49-PVA (A) and Agarose/PEO (B) mats after 30 minutes (left samples) and 60 minutes (right samples) of application in varnish area.

Conclusions

This study successfully demonstrated the potential of electrospun nanofibrous mats as advanced, controlled delivery systems for organic solvents in the conservation of cultural heritage. The experimental workflow, ranging from the optimization of electrospinning parameters to *in situ* application on polychrome wood artwork, provided critical insights into the relationship between polymer morphology, solvent kinetics, and cleaning efficacy.

In the initial fabrication phase, uniform nanofibrous mats were successfully produced using PEO, PVA, and Agarose/PEO blends. While pure PEO and PCL membranes proved unsuitable due to rapid dissolution in benzyl alcohol, the PVA (10 % w/v) and Agarose/PEO (70/30, 7 % w/v) systems demonstrated the necessary chemical resistance. Specifically, the Agarose/PEO blend maintained its structural integrity despite a minor mass loss associated with the PEO fraction, while PVA remained chemically inert, preserving its fiber morphology entirely.

Characterization of solvent interactions revealed distinct behaviors dictated by the polymer matrix. Swelling assays indicated that the hydrophilic Agarose/PEO network possesses a significantly higher loading capacity (approx. 1400 %) compared to PVA (700 %). However, deswelling tests on reference substrates (canvas and glass) proved that both systems function effectively as retentive reservoirs, releasing benzyl alcohol through a controlled mechanism that mitigates the risk of uncontrolled solvent diffusion. The release kinetics were found to be substrate-dependent: a biphasic release driven by capillary forces was observed on porous canvas, whereas a gradual, steady-state release characterized the application on non-porous glass.

Morphological analysis provided definitive evidence of the cleaning mechanism. The electrospun mats exhibited exceptional mechanical conformability, plastically deforming to mirror the topography of the substrate (e.g., the canvas weave) to maximize interfacial contact. FESEM also elucidated the superior cleaning capacity of the PVA mats, which displayed a "clogging" effect characterized by the dense entrapment of particulate matter within the fiber voids. This was quantitatively corroborated by gravimetric analysis, where PVA mats recorded a weight increment of 205 % after cleaning, significantly outperforming the 110 % increment of the Agarose/PEO mats.

Finally, the translation of the protocol to historical wood artwork validated the laboratory findings. Optimized to a thickness of 30 μm the mats enabled the selective and gradual removal of both yellowed varnish and non-original repainting layers without lateral spreading. While the Agarose/PEO mat offered superior surface adhesion due to its solvent affinity, the PVA mat confirmed its dominance in extraction efficiency, sequestering a greater mass of degradation byproducts (25 % vs. 10 % weight increase) after 60 minutes of contact.

Crucially, the success of this transposition to a real case study is defined not merely by quantitative efficiency, but by strict stratigraphic selectivity. A major operational advantage of these electrospun mats is the ability to finely modulate the depth of solvent penetration by simply varying the application time. The biphasic and gradual solvent release kinetics, combined with specifically tuned contact times (ranging from 0.5 to 60 minutes), prevented the uncontrolled diffusion of benzyl alcohol into the original 16th-century layers. Visual and macroscopic assessments confirmed that the cleaning action was strictly confined to the superficial boundary of the 19th-century oil-based overpaints and

the targeted oxidized varnishes, fully safeguarding the original tempera and its underlying chalk and glue ground

In summary, this work establishes that while Agarose/PEO mats offer advantages in wettability and contact, PVA electrospun mats represent the most efficient system for the controlled delivery of benzyl alcohol, offering a high-performance balance between solvent retention, mechanical adaptability, and contaminant capture capacity for delicate cleaning operations.

Chapter 9.
Green synthesis of gold and silver nanoparticles mediated by Agar and Agarose: A comparative study.

9.1 Introduction

The synthesis of noble metal nanoparticles, particularly gold (AuNPs) and silver (AgNPs) nanoparticles, has garnered significant attention in contemporary materials science due to their exceptional physicochemical characteristics. These nanostructures exhibit unique optical, electronic, and catalytic properties that render them indispensable in advanced applications ranging from biomedical imaging and drug delivery to biosensing and environmental remediation.

Beyond these established fields, as discussed in Chapter 2, these nanoparticles are emerging as highly promising tools in the conservation of Cultural Heritage. The biodeterioration caused by fungal and bacterial colonization poses a severe threat to historical artifacts. Since traditional chemical biocides exhibit high toxicity and potential for long-term material damage, the potent, broad-spectrum antimicrobial properties of AuNPs and AgNPs offer an effective and sustainable alternative for artwork disinfection. However, the traditional chemical protocols employed to generate these nanoparticles often necessitate the use of toxic reducing agents and stabilizers[91,96,98,200]. The reliance on such hazardous substances raises substantial concerns regarding environmental safety and biocompatibility, thereby necessitating a paradigm shift toward "green" chemistry. Consequently, the development of sustainable synthesis strategies using biological resources has become a critical avenue of research, aiming to mitigate environmental impact while maintaining high efficiency.

In this context, the utilization of biopolymers as dual-functional reducing and stabilizing agents has emerged as a promising methodology[91,96,98,99,201]. Among the various biopolymers available, Agar and Agarose, polysaccharides derived from red algae species such as *Gelidium* and *Gracilaria*—offer distinct advantages due to their non-toxic nature, acceptable biocompatibility degree, and inherent ability to form hydrogels. The extraction of these materials involves a series of purification steps, starting with the alkali treatment of algal biomass to remove lipids and proteins, followed by hot water extraction to isolate Agar, which consists of a heterogeneous mixture of the neutral gelling fraction agarose and the sulfated non-gelling fraction agaropectin**.** Agarose, a purified fraction obtained through further chromatographic separation, consists primarily of repeating units of D-galactose and 3,6-anhydro-L-galactose. This structural specificity makes Agarose ideal for applications requiring high purity, while the broader composition of Agar offers a cost-effective alternative for diverse industrial uses (Chapter 4).

The potential of Agar and Agarose in nanotechnology stems from their rich chemical composition. These polysaccharides possess an abundance of hydroxyl groups and other functional moieties that can effectively act as reducing agents, converting metal ions into their corresponding elemental atoms without the need for external chemical reductants. Furthermore, the polymer chains serve a crucial

role as capping agents. The gel-forming properties of the matrix create a steric barrier that stabilizes the nascent nanoparticles, preventing agglomeration and allowing for the modulation of particle size, morphology, and distribution. This dual functionality simplifies the synthesis process, making it a one-pot, eco-friendly reaction[202–204].

Building upon these principles, this study explores the green synthesis of gold and silver nanoparticles using Agar and Agarose solutions. The primary objective is to investigate the influence of the chemical composition of various commercial Agar and Agarose powders (see Chapter 5) on the morphological and stability characteristics of the synthesized nanoparticles. Comprehensive characterization is conducted using XRF, SEM-EDX, FT-IR, UV-Vis spectroscopy, transmission electron microscopy (TEM), and rheological analyses. Crucially, to interpret the complex interplay between synthesis variables and nanoparticle quality, a chemometric approach was employed. Specifically, Principal Component Analysis (PCA) was utilized to identify which physicochemical parameters are most critical for obtaining nanoparticles with homogenous shape, uniform size, and optimal stability. By combining experimental characterization with statistical modeling, this work aims to provide a robust framework for reproducible biopolymer-based synthesis, contributing to the advancement of sustainable nanomaterial development.

9.2 Synthesis of nanoparticles

Five different Agar powders (Agar CTS, Agar BS, Agar FOOD, Agar SIGMA, and Agar NOBLE) and Agarose powders, as a reference term, were selected for this experimentation (see Chapter 5).

For the synthesis of gold nanoparticles, 10 mL of an aqueous solutions of Agar and Agarose (1% w/v) were prepared and stirred on a magnetic plate at 100°C until the polymer was completely dissolved. At the boiling point, 15 µL of an aqueous $HAuCl_4$ solution (0.025 mol/L) was added and stirred for 60 minutes. The synthesis of the nanoparticles was confirmed by the color change of the mixture from yellow to red/purple. The colloidal solutions were allowed to stand for 1 hour and then placed in a refrigerator to prevent polymer degradation.

The synthesis of the silver nanoparticles was carried out using the same procedure settled for the gold ones: 120 µL of an aqueous $AgNO_3$ solution (0.03 mol/L) was added to Agar and Agarose solutions (1% w/v) brought to the boil on a magnetic plate. The solutions were first stirred for 60 minutes at the boiling point, therefore stirred at room temperature overnight, and then placed in the fridge to prevent polymer degradation and silver oxidation. The successful synthesis of the silver nanoparticles was confirmed by the color change of the mixture from soft yellow to darker yellow.

The choice of concentrations for the polysaccharide solutions and metal salts was evaluated based on literature data[202–204]. The final concentration of silver in the solutions was set at 0.36 mmol/L, while that of gold was set at approximately ten times lower (0.037 mmol/l).

9.3 Characterizations

Powders characterization

The chemical characterization of the polysaccharide precursors, comprising various commercial Agar grades (CTS, BS, FOOD, SIGMA, NOBLE) and purified Agarose, was carried out. Spectroscopic analysis via FT-IR (*Figure 50*) shows a high degree of reproducibility for all samples, suggesting that the fundamental polymer backbone is preserved regardless of the refinement level; all spectra exhibit overlapping characteristic bands, most notably the broad hydroxyl stretching at approximately 3400 cm^{-1} and the glycosidic linkage vibrational mode around 1070 cm^{-1}, confirming that all polysaccharides provide the essential functional groups required for metal reduction.

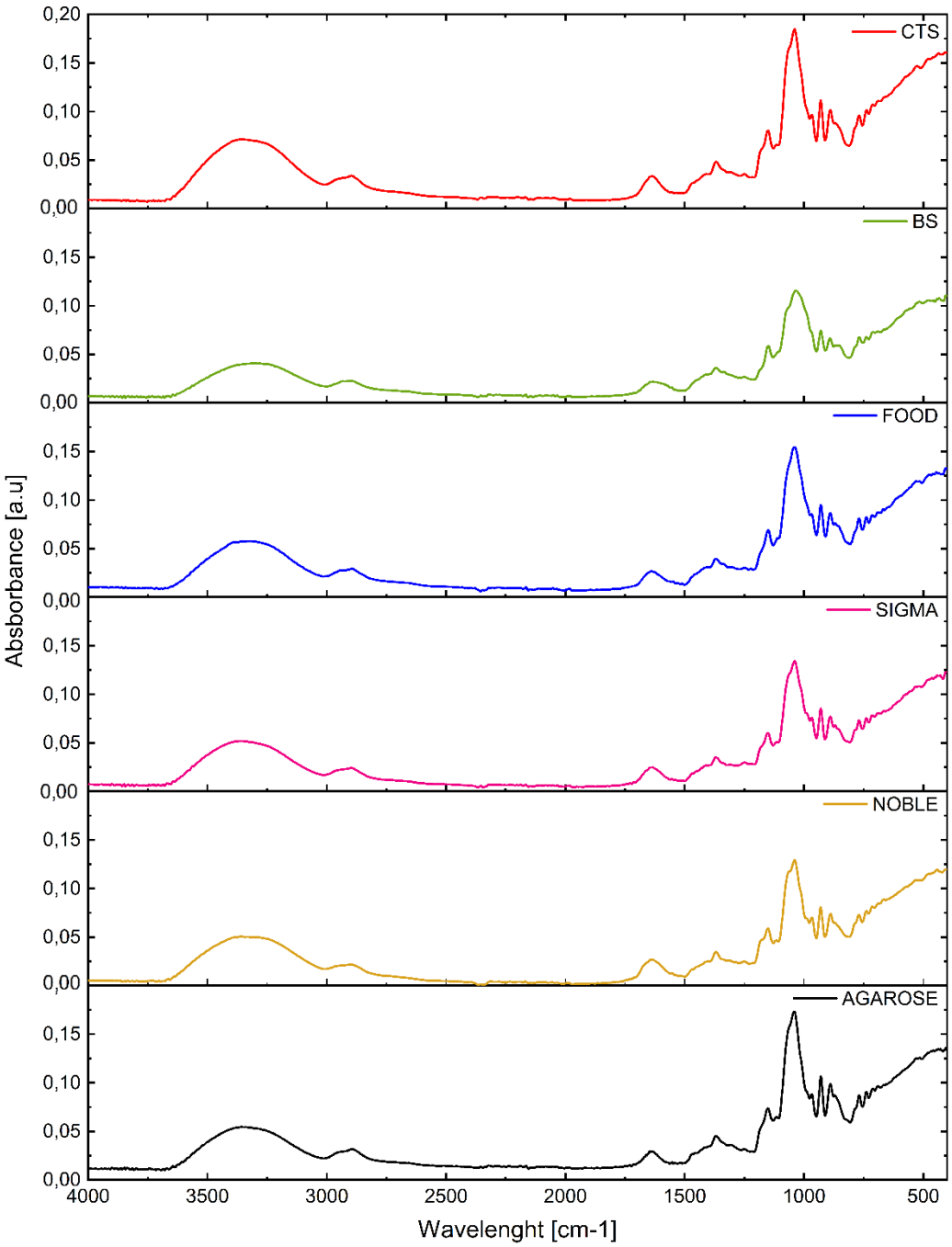

Figure 50- FT-IR spectra of different Agar and Agarose powders

Divergences quantitatively arise from the elemental analyses (Table 17), which expose a vast disparity in ionic burden that the vibrational spectra do not capture. The Agarose reference acts as a chemically inert control with negligible detectable mineral content, whereas the commercial Agars are characterized by specific, dominant inorganic impurities that vary significantly by brand. Methodologically, the comparative use of XRF and SEM-EDS highlights the heterogeneity of these crude powders: the discrepancies between the datasets—such as the Calcium content in CTS (47.9% by XRF vs. 43.7% by EDS) or the Chlorine fraction in FOOD (41.7% vs. 23,0%)—arise because XRF provides a volumetric "bulk" average of the total ionic load, while EDS reflects only the localized surface composition where mineral phases may be clustered[205,206]. Despite these variations, clear elemental fingerprints emerge: BS is uniquely Potassic-rich (52.2% K by XRF), NOBLE is Calcium-rich (59.3%), and SIGMA exhibits the highest degree of sulfation (S/C ratio of 1.6) with a massive relative sulfur abundance (~69%). Most critically for synthesis, the FOOD variant is heavily doped with Chlorine, a known oxidative etchant[207,208].

Table 17- XRF and SEM-EDX analyses of Agar and Agarose powders

	Ca		K		S		Cl		S/C
	XRF	EDX	XRF	EDX	XRF	EDX	XRF	EDX	%
CTS	47,9	43,7	9,4	/	42,7	56,2	/	/	0,4
BS	39,1	36,9	52,2	32,3	8,7	30,8	/	/	0.4
FOOD	30,6	28,9	2,0	4,0	24,5	44,2	41,7	23,0	1,2
SIGMA	30,7	12,4	/	/	69,3	67,9	/	19,8	1,6
NOBLE	59,3	46,9	/	/	40,7	41,4	/	11,7	0,8
AGAROSE	/	/	/	/	/	/	/	/	/

Solutions characterization before synthesis

Complementing the structural and elemental profiling, pH measurements of the 1% w/v precursor solutions reveal an acidity gradient ranging from 4.96 to 6.61, a variance that functions as a direct probe of the ionic environment. As elucidated by the structural model, the sulphate groups in the commercial Agars are covalently bound as esters ($R\text{-}OSO_3^-$), implying that the solution pH is defined not by free sulfuric acid, but by the hydrolysis behavior of the charge-balancing counter-ions. Consequently, the specific ionic dominance directly dictates the acidity profile through distinct chemical mechanisms.

The near-neutral pH observed in the Potassium-rich BS variant (pH 6.22) and the Chlorine-rich FOOD variant (pH 6.12) serves as an indicator of stable, neutral salt speciation. In the specific case of FOOD Agar, the observation that a massive Chloride burden (41.70% in XRF) coincides with a pH above 6.0 provides compelling evidence that the halides are present as fully dissociated, non-hydrolyzable salts (e.g., KCl or NaCl) rather than acidic residues, thereby maintaining a buffered, non-corrosive synthesis environment. Conversely, the Calcium-rich variants exhibit a pronounced

shift toward acidity. Agar CTS (pH 5.53) and Agar NOBLE (pH 4.96) constitute the most acidic fraction of the series, a behavior characteristic of divalent cation chemistry. Calcium ions (Ca^{2+}) act as weak Lewis acids in aqueous media, capable of inducing the hydrolysis of hydration water ($Ca^{2+} + H_2O\ CaOH^+ + H^+$) or displacing protons from residual uronic acid moieties within the matrix, thus actively depressing the bulk pH relative to the monovalent samples[209]. The correlation is quantitative: NOBLE, possessing the highest Calcium load (59.3%), exhibits the lowest pH, whereas CTS, with a lower Calcium content (47.9%), displays a proportionally higher pH.

Finally, the purified Agarose serves as the critical thermodynamic baseline, registering an intermediate pH of 5.66. Lacking both the buffering mineral salts of the crude Agars and the acidifying calcium load, this value reflects the intrinsic, unbuffered pH of the solvated polygalactan chains. Collectively, these data demonstrate that the reactive environment in the aqueous solution of the utilized polysaccharides presents diversities that can influence the NP synthesis reaction.

Spectroscopic characterization and temporal kinetics

The presence, growth, and subsequent colloidal stability of the noble metal nanoparticles were evaluated by monitoring the UV-Vis absorption spectra over time (*Figure 51*). This longitudinal analysis tracked the evolution of three spectral parameters associated to the Surface Plasmon Resonance (SPR) band typical of noble metal nanoparticles[91,96,201,210], namely the absorption maximum (λ_{max}), the bandwidth, and extinction profile from the synthesis (T_0) through a 60-day aging period (T_{60}) (*Figure 52*). Variations in these spectral features provided critical insights into the dimensional stability, aggregation state, and morphological evolution of the nanostructures within the different hydrogel matrices.

The spectral analysis of gold nanoparticles revealed a dependency on the matrix purity, characterized by distinct kinetic regimes that distinguish steric stabilization from aggregation and anisotropic growth.

The UV-Vis spectrum of gold nanoparticles synthesized in Agarose displayed a complex aging behavior (*Figure 51 F* and black symbols and line of *Figure 52A*). At the initial time point (T_0), the spectrum exhibited a sharp, symmetric peak cantered at approximately 535 nm. This spectral signature aligns with the expected value for stable, monodisperse, spherical-like gold colloids under 30 nm of size as confirmed by the literature. Over the 60-day observation period, the position of the maximum absorption remained virtually invariant at 535 nm. However, the spectral profile after sixty days revealed significant morphological changes in the colloidal state. A marked hypochromic effect was observed, as the absorption intensity is reduced by approximately 30%. Moreover, the aged spectrum exhibited a pronounced broadening, manifesting as an elevated extinction tail or "shoulder" extending significantly into the longer wavelength region (600–1000 nm). This widening in the near-infrared region, occurring without a shift in the primary $\lambda_{max,}$ suggests the partial flocculation of the primary particles into loose clusters that adsorb at longer wavelengths, or the emergence of a secondary population of larger particles, although in a minority percentage.

The spectral profile of Agar FOOD was distinct from the onset (*Figure 51 C*). At T_0, the spectral profile shows an asymmetric trend, with a main absorption maximum red-shifted at 552 nm and a shoulder positioned around 650 nm. These features suggest the immediate, contemporary presence of isotropic and anisotropic structures, such as triangular prisms or nanoplates. Over the 60-day aging period, the spectral profile continues to red-shift and broaden, accompanied by a significant decrease

in absorbance intensity. The monotonic increase of λ_{max} (*Figure 52A*, blue symbols and line) could denote a continuous growth of the isotropic nanoparticles and/or of the anisotropic population.

The spectra for the remaining commercial Agar matrices (CTS, BS, SIGMA, NOBLE) show SPR peaks centered in the 530–535 nm range, suggesting a primary population of quasi-spherical particles (*Figure 51 A, B, D, E*). All spectral profiles exhibit limited redshift and loss of asymmetry of the plasmonic band at T_{60}, more pronounced for the BS sample but still less significant than those found in the Agarose sample. The detailed analysis of the λ_{max} trend over time (*Figure 52*, red, green, purple and yellow symbols and lines) reveals that changes in the spectral profile, most likely associated with changes in the morphology of the nanoparticles, begin to appear only after a 14-day ageing period. These results suggest that commercial Agars represent more efficient stabilizing agents for the AuNPs synthesis in that they are able to prolong the colloidal integrity over more extended storage periods.

The spectral features and evolution of silver nanoparticles differed fundamentally from that of gold, displaying kinetic profiles suggestive of continuous scalar growth rather than shape changes. A critical distinction was observed starting from the synthesis of AgNPs. Agar BS and Agar CTS failed to produce any detectable product yield of silver nanoparticles, as evidenced by the complete absence of a characteristic SPR absorption band in the 400 nm spectral region. This suggests that the specific chemical environment determined by of the two Agars—likely the pH or the amount/type of the reducing groups present—was ineffective to reduce silver nitrate under the experimental conditions employed.

Also, for the matrices that supported synthesis (Agarose, FOOD, SIGMA, NOBLE), quite variable results in term of spectral lineshape and evolution were observed. (*Figure 51 C, D, E, F*).

The Agarose matrix yielded AgNPs with a well-defined, single SPR band centered at 418 nm, which does not show significant shifts over two months (*Figure 52 B,* black symbol and line*).* This result suggests that the Agarose matrix is more effective in produce stable AgNPs than AuNPs.

When commercial Agars are used, the spectra show indefined profiles characterized by a shoulder at around 400 nm, probably due to small nanoparticles with dimensions close to the quantum size restriction (below 2 nm) (*Figure 51 C, D, E)*. Nevertheless, the aged spectra reveal the presence of well-structured, symmetrical SPB bands centered between 410 and 420 nm, evidence of the formation of larger nanoparticles. These results suggest that the AgNPs synthesis is a slow chemical reaction that takes time to complete. The upward trends of λ_{max} over time seems to confirm this hypothesis.

GOLD

A

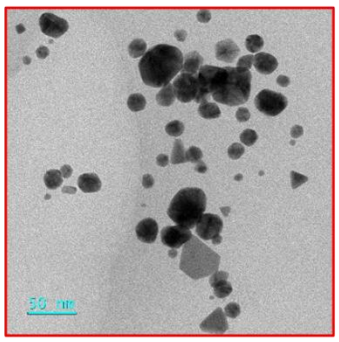
50 nm

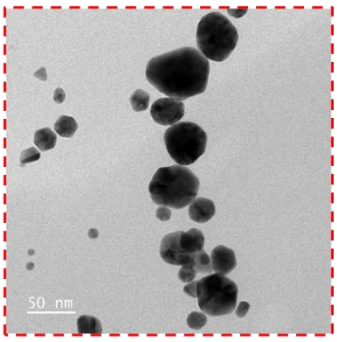
50 nm

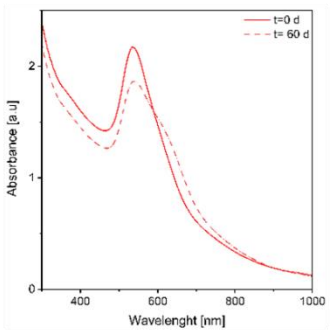
t=0 d
t= 60 d
Absorbance [a.u]
Wavelenght [nm]

B

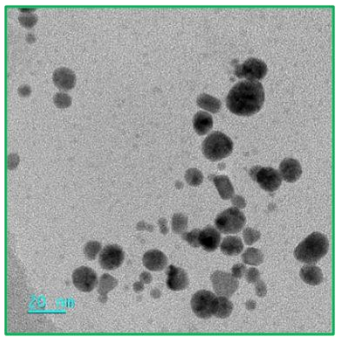
50 nm

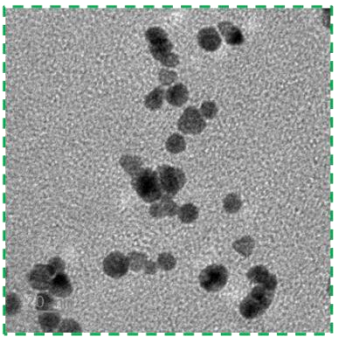

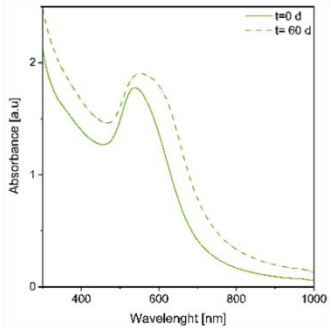
t=0 d
t= 60 d
Absorbance [a.u]
Wavelenght [nm]

C

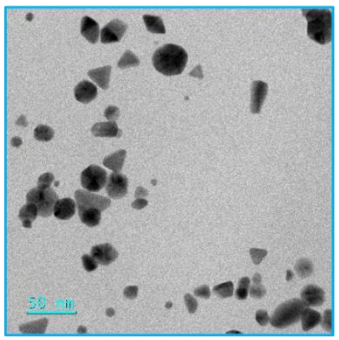
50 nm

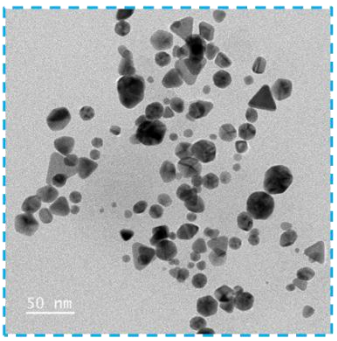
50 nm

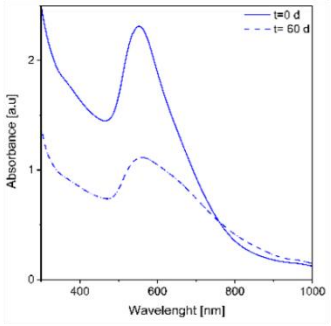
t=0 d
t= 60 d
Absorbance [a.u]
Wavelenght [nm]

D

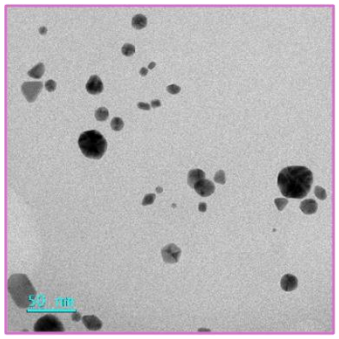
50 nm

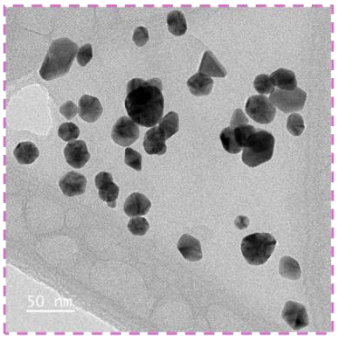
50 nm

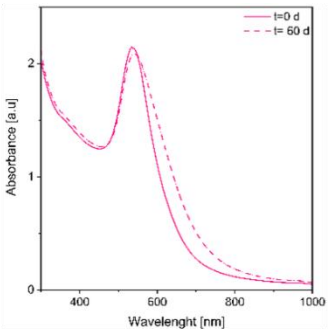
t=0 d
t= 60 d
Absorbance [a.u]
Wavelenght [nm]

E

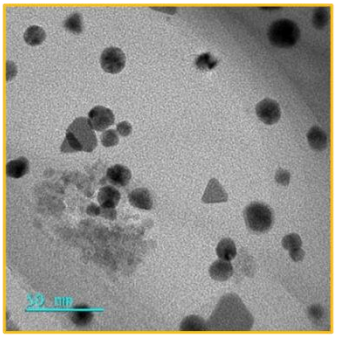
50 nm

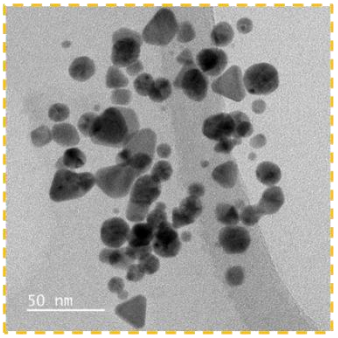
50 nm

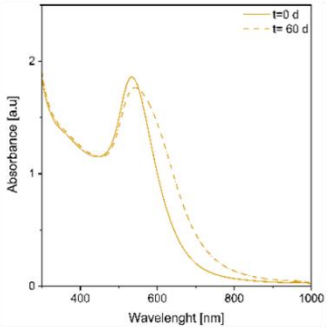
t=0 d
t= 60 d
Absorbance [a.u]
Wavelenght [nm]

F

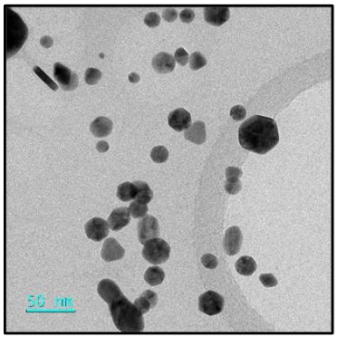
50 nm

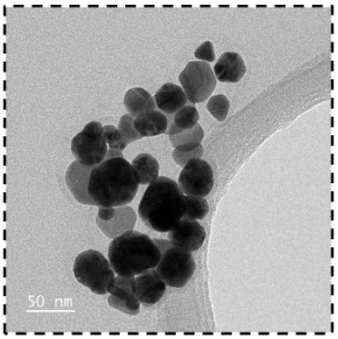
50 nm

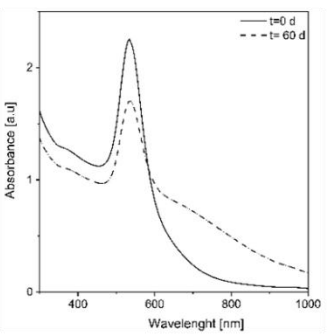
t=0 d
t= 60 d
Absorbance [a.u]
Wavelenght [nm]

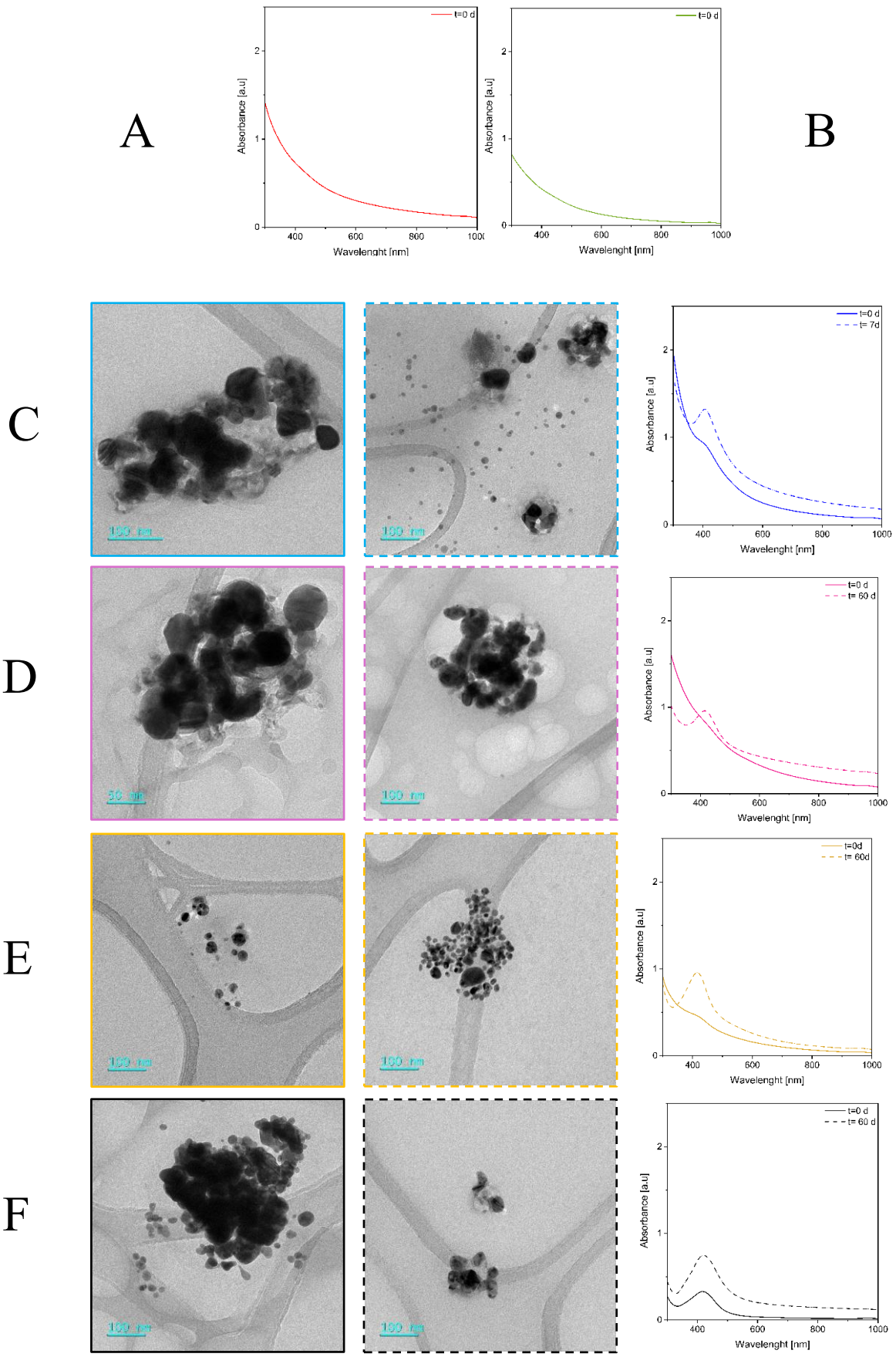

Figure 51- TEM images and UV-Vis spectra of (A) Agar CTS, (B) Agar BS, (C) Agar FOOD, (D) Agar SIGMA, (E) Agar NOBLE, (F) Agarose suspensions with GOLD and SILVER nanoparticles. Fresh and aged samples (after sixty days of conservation) were respectively indicated with a full line and a dotted line. Agar CTS and Agar BS failed in the silver nanoparticles synthesis.

A

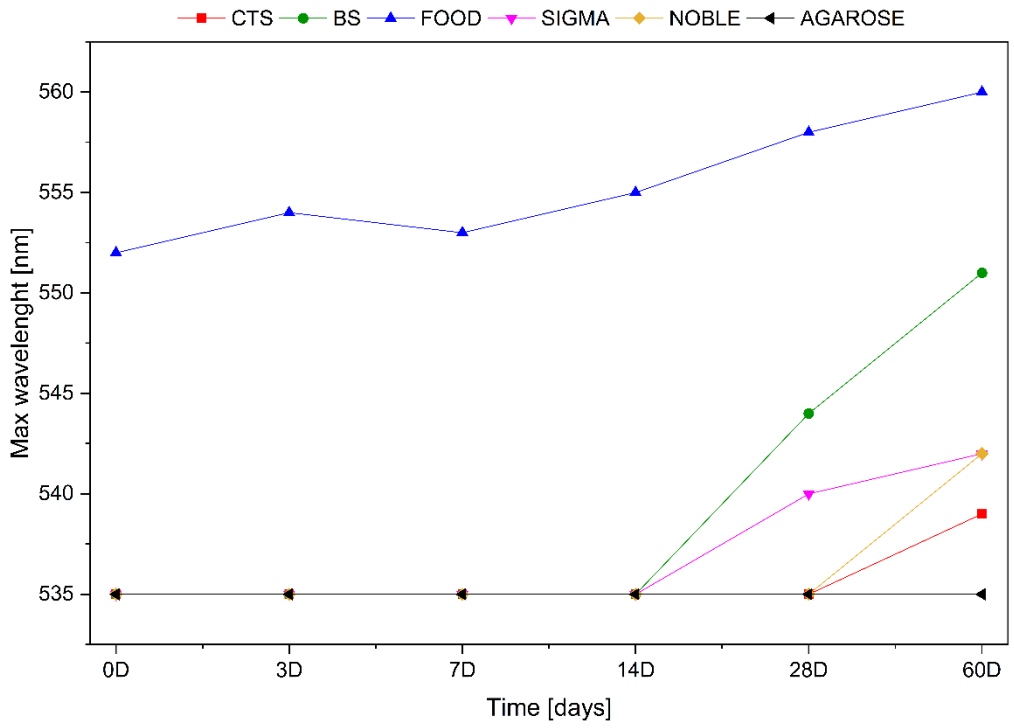

B

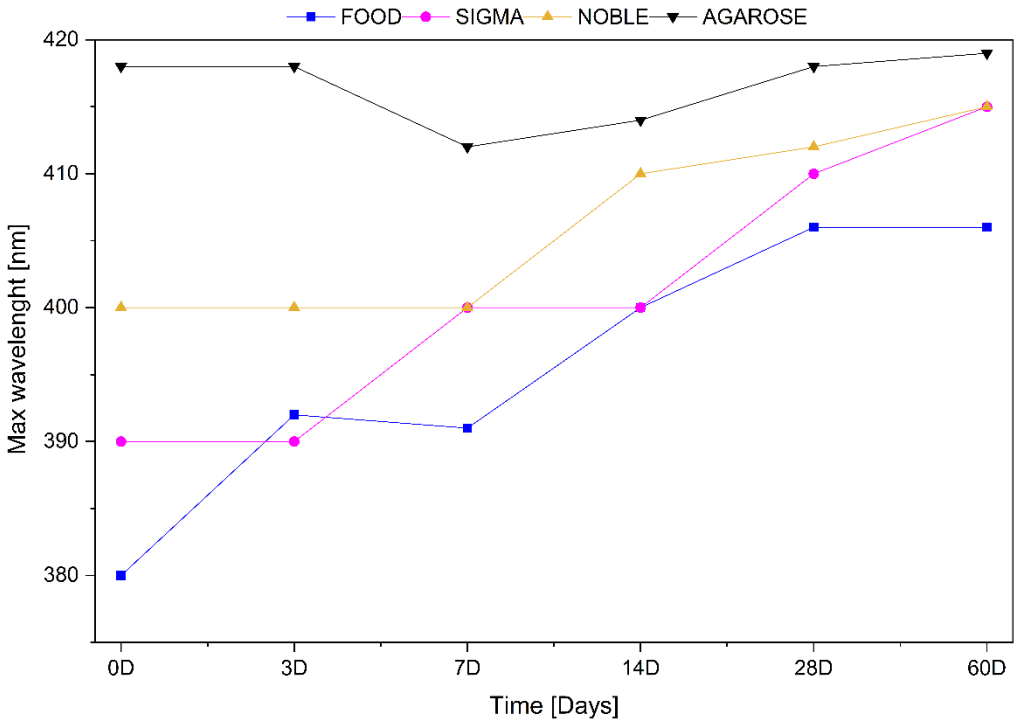

Figure 52- Maximum wavelength peaks for each Agar and Agarose matrix for (A) gold and (B) silver nanoparticles suspensions.

Quantification of gold concentration

Following the evaluation of temporal kinetics, the synthesis yield of AuNPs was quantified by determining the concentration of reduced metallic gold (Au^0) in the colloidal solutions. To this purpose, UV-Vis spectroscopy has been usually applied since it is a low-cost and simple technique in addition to its wide availability. The method commonly used is based on the correlation between the extinction (or absorbance) value at 400 nm and the Au^0 concentration. Indeed, below 500 nm the interband transition region for bulk gold allows obtaining a linear correlation of the increase of extinction value at this wavelength value when increasing the nanoparticle volume, e.g. the Au^0 concentration, independently of the size and morphology of the nanoparticles. Moreover, *Scarabelli et al*.[211,212] demonstrated that 0.5 mmol/L of Au^0 concentration corresponds to an optical density (absorbance with 1-cm pathlength cuvette) of 1.2 at 400 nm.

Applying this calculation method to the experimental absorbance data recorded at 400 nm revealed an inverse relationship between the purity of the Agar matrix and the reaction yield. The Agar FOOD matrix exhibited the highest absorbance (1.640), corresponding to concentration of elemental gold of 0.683 mmol/L. This value was to that found for Agar CTS, which yielded a concentration of 0.668 mmol/L (Abs: 1.602). In contrast, the highly purified matrices demonstrated significantly lower reduction efficiencies. Agar NOBLE yielded a concentration of 0.511 mmol/L (Abs: 1.227), while Agarose produced the lowest yield of 0.503 mmol/L (Abs: 1.208). This data indicates that the impurities present in crude commercial Agars, likely sulfated polysaccharides or residual proteins, act as auxiliary reducing agents, driving the reduction of the auric precursor more efficiently than the chemically inert Agarose backbone.

Morphological analysis and statistical analysis of dimensional evolution

Fig. 51 reports also the TEM images of both fresh (left) and aged (right) AuNPs and AgNPs. The main results deriving from the morphological analysis carried out by *Image J software* on over 50 particles are summarized below.

The purity of the hydrogel matrix exerted a decisive influence on the geometric symmetry of the gold nanoparticles. Agarose and Agar NOBLE favoured isotropic growth, producing spherical populations with non-spherical defects remaining below 1 % and 5 %, respectively. Moreover, the morphology of these nanoparticles is stable over time. In contrast, the reducing environment of the crude Agars promoted anisotropy. Agar FOOD samples contained approximately 20% non-spherical forms, predominantly identified as triangular prisms. The presence of nanotriangles in Agar FOOD provides a possible explanation for its asymmetrical spectral profile, as anisotropic plates exhibit longitudinal plasmon resonances that absorb at longer wavelengths (>550 nm). Agar SIGMA and Agar CTS exhibited shape heterogeneities of 15 % and 9 %, respectively.

Unlike AuNPs, silver nanoparticles maintained a spherical morphology across all matrices (FOOD, SIGMA, NOBLE, AGAROSIO), and their shape persisted for two months. These results suggest that the nature of the metal strongly influences the mode of interaction between the stabilising functional groups of the polysaccharide chain and the surface of the nanoparticles.

Insights on the mechanism underlying the morphological changes observed for spherical-like fractions over time was further elucidated by comparing the particle size distributions of fresh (T_0) versus

aged (T_{60}) samples (*Figures 53, 54).* This statistical evaluation allows for a matrix-by-matrix interpretation of the colloidal systems evolution.

As far as gold nanoparticles are concerned, the analysis of Agar NOBLE proves the occurrence of Ostwald ripening phenomena. The fresh sample was highly monodispersed, characterized by a dominant population in the 0–10 nm range (>80 %). Upon aging, this distribution broadened significantly; the fraction of small particles (<10 nm) decreased, while a new population emerged in the 20–30 nm range. This growth comes at the expense of the smallest particles and is consistent with the delayed spectral red-shift observed after 28 days. The Agar CTS matrix initially produced a population centered at 10 nm with a secondary fraction centered at 20 nm. During the aging period, the distribution broadened and shifted towards larger diameters, with the 10-20 nm range and 30-40 nm particle range populations becoming co-dominant (>25 % each). This diameter increased to larger mean diameters provides the physical basis for the spectral red-shift and suggests that the stabilizing functional groups in CTS inefficient to prevent gradual nanoparticles coalescence or growth over long durations. Similar to the trend in CTS, Agar SIGMA showed a clear dimensional evolution Fresh samples exhibited a distribution mainly distributed in 0–10 nm and 10-20 nm ranges, which coalesced into a dominant mode at 20 nm after aging. This increase in average particle size correlates directly with the observed spectral red-shift to 542 nm. The statistical analysis for Agar BS presents an apparent contradiction to its spectral data. Fresh and aged samples displayed invariant histograms centered on very small particles (0–10 nm). However, the corresponding aged UV-Vis spectrum showed a significant hyperchromic and bathochromic shift (>550 nm) with respect to the fresh one. This discrepancy can be explained by assuming that the spectral changes are likely due to flocculation (the reversible clustering of particles) rather than particle fusion into larger individual spheres. The electron microscopy preparation may have dispersed these loose flocs, revealing only the presence the unchanged primary particles, differently from the solution spectrum, which can captured the collective plasmonic features of the sample. The Agar FOOD samples presented a counterintuitive trend. While the UV-Vis spectrum displayed a continuous red-shift (attributable to nanoparticle growth), the histogram showed a narrower size distribution with an increase of *smaller* particles (0-10 nm range) after aging. In the case of Agarose, the size distribution shifted from fresh particles with predominant 10- 20 nm size to aged particles with predominant diameter in the 20-30 nm range. However, based on the literature data, the global 10-nm increase of nanoparticles size distribution seem to be not enough to justify the appearance of the "shoulder" at around 600 nm in the aged spectrum.

The dimensional evolution of silver nanoparticles further differentiated the matrices behaviour (*Figure 54*). The analysis of Agar SIGMA (AgNPs) confirmed the continuous growth hypothesis derived from the spectra. Fresh samples were dominated by particles in the 0-10 nm range, whereas aged samples shifted clearly into 20-nm range. This growth of the silver nanospheres aligns with the 25-nm spectral red-shift of the corresponding SPB band. Agar NOBLE shifted from a broad 10–30 nm range to a narrower 0-10 nm dominant population. This suggests that for these matrices, the apparent spectral "growth" (red-shift) may be due to the formation of specific clusters that may have precipitated out of solution, leaving only the smaller populations on the TEM analysis grid. The Agarose matrix maintained a broad polydisperse size distribution (20–60 nm) in both fresh and aged conditions, suggesting a role of passive stabilizer for the matrix that arrests significant morphological evolution histograms.

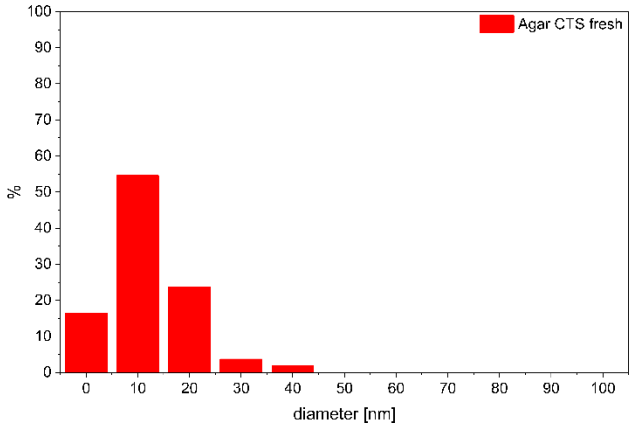
Agar CTS fresh
%
diameter [nm]

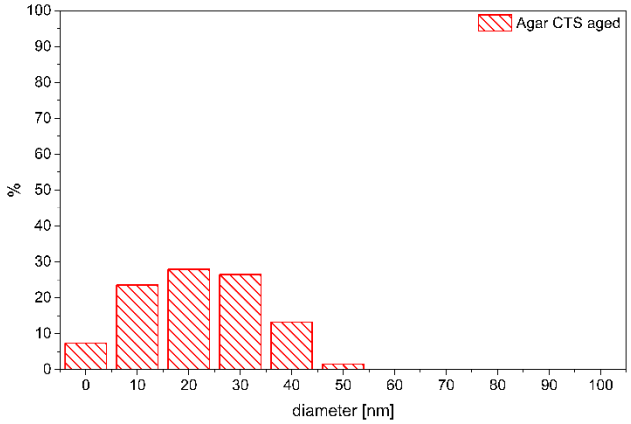
Agar CTS aged
%
diameter [nm]

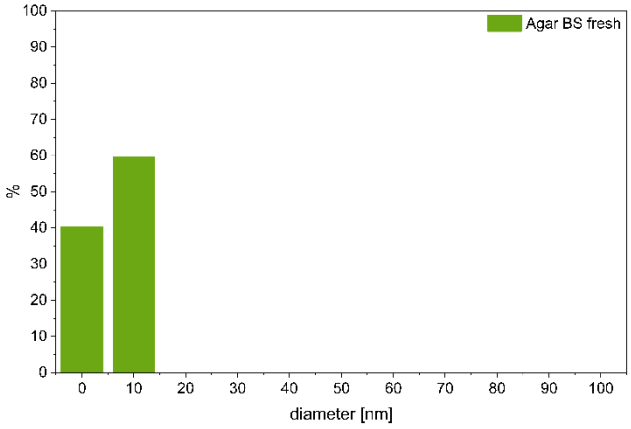
Agar BS fresh
%
diameter [nm]

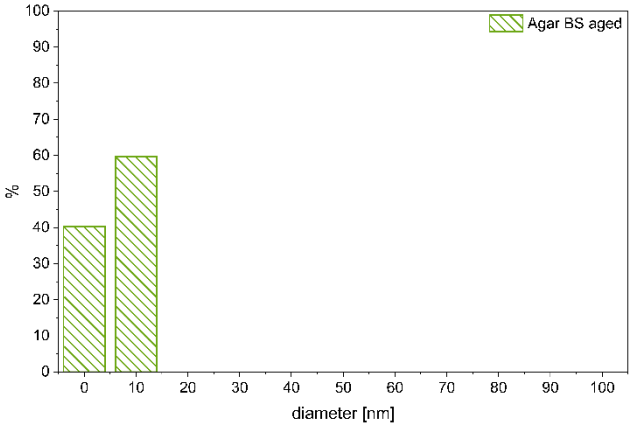
Agar BS aged
%
diameter [nm]

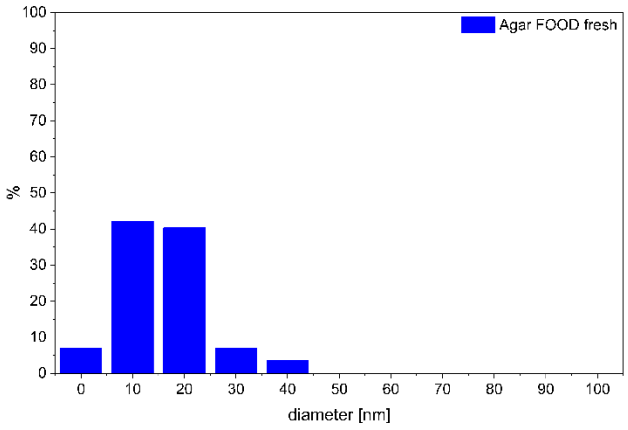
Agar FOOD fresh
%
diameter [nm]

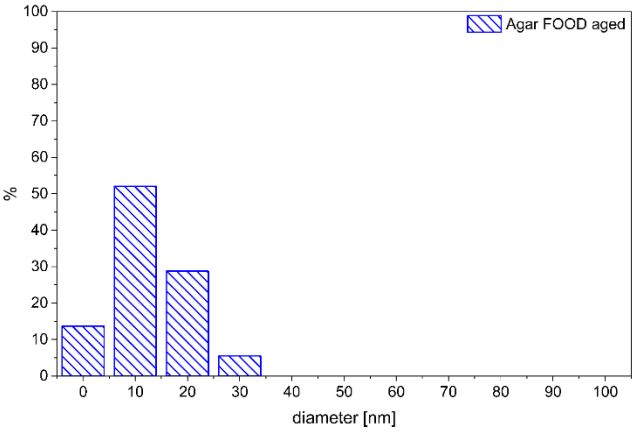
Agar FOOD aged
%
diameter [nm]

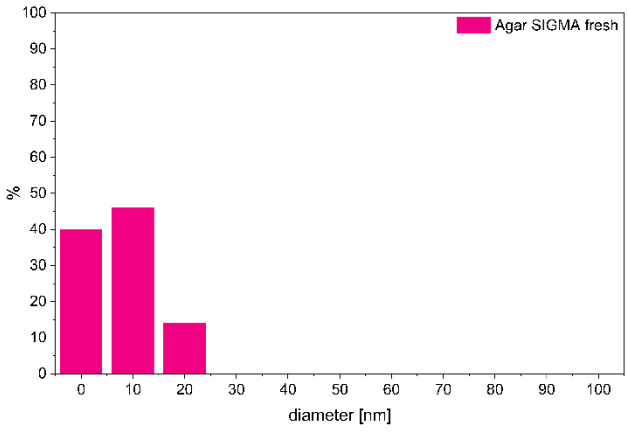
Agar SIGMA fresh
%
diameter [nm]

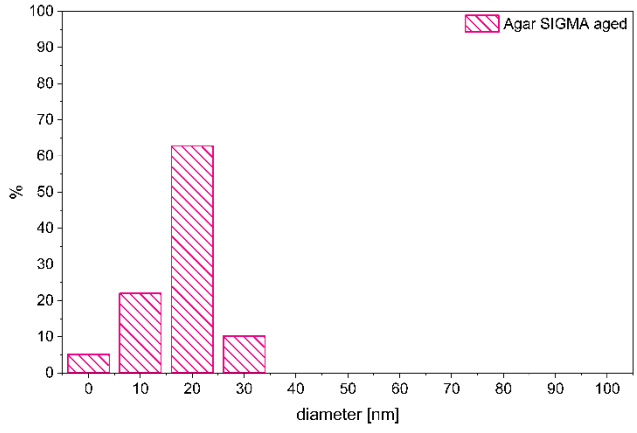
Agar SIGMA aged
%
diameter [nm]

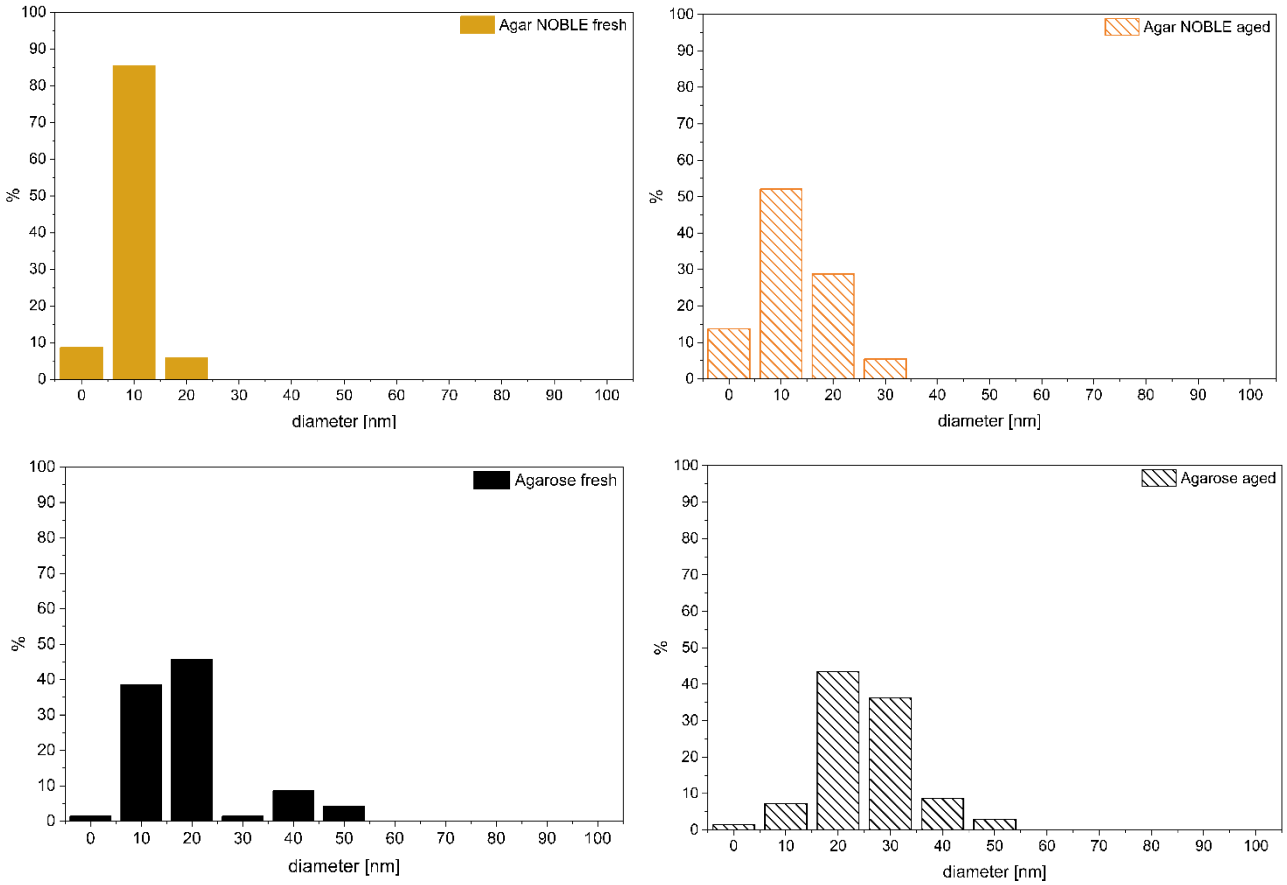

Figure 53- Statistical dimension analysis of gold nanoparticles synthesized with Agar and Agarose solutions In the X-axis ranges of diameters were presented.

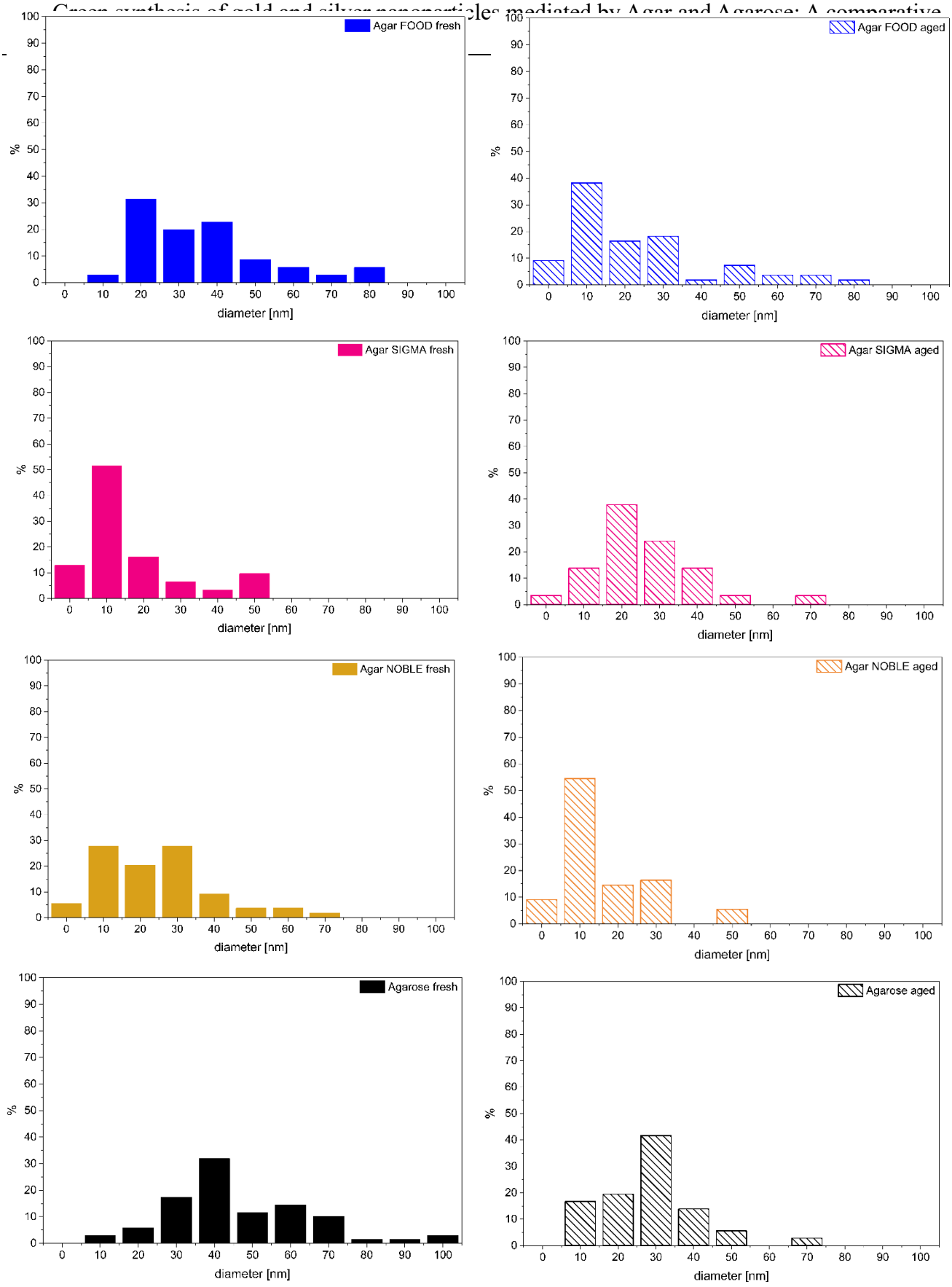

Figure 54- Statistical dimension analysis of silver nanoparticles synthesized with Agar and Agarose solutions. In the X-axis ranges of diameters were presented.

9.4 Chemometric analysis

To elucidate the complex multivariate relationships between the chemical composition of the gelling matrices and the chemical properties of the synthesized nanoparticles, a Principal Component Analysis (PCA) was performed using the CAT (Chemometric Agile Tool) software. PCA is an exploratory statistical technique used to reduce the dimensionality of complex datasets, transforming correlated variables into a smaller set of uncorrelated variables called Principal Components (PCs). This transformation reveals underlying patterns, clusters, and correlations that are not immediately apparent in univariate analysis.

In this study, the dataset was constructed using two distinct categories of variables to correlate matrix inputs with synthesis outputs. The input variables defined the chemical environment and included the elemental concentration of Calcium (Ca), Potassium (K), Chlorine (Cl), and Sulfur (S), the Sulfur-to-Carbon ratio (S/C), and the pH of the precursor solution. The output variables quantified the resulting nanoparticle characteristics: the percentage of nanoparticles with diameters below 20 nm in both fresh and aged states, the number of dimensional intervals (a metric for size heterogeneity), the maximum absorption wavelength (λ_{max}) at T_0 and T_{60}, and, specifically for gold, the concentration of reduced metal and the percentage of non-spherical anisotropic shapes. This chemometric approach was applied separately to the gold and silver nanoparticle datasets to deconstruct the specific chemical drivers governing the synthesis of each metal nanoparticles.

Multivariate analysis of gold nanoparticles (AuNPs) in water suspension

The PCA model for gold nanoparticles captured a significant majority of the dataset's information, with the first two principal components explaining 63.4% of the total variance (38.7% for PC1 and 24.7% for PC2). The resulting Biplot allows for the simultaneous visualization of sample distribution (scores) and variable correlations (loadings), revealing three distinct chemical regimes governing size, shape, and stability (*Figure 55*).

The first principal component (PC1) serves as a proxy for the reactivity axis, distinguishing matrices based on their reducing power and shape-directing capability. The loading vectors for Gold Concentration (*concentr.*.), anisotropy (*other.shapes*.), and Chlorine (*Cl*) are tightly clustered in the bottom-right quadrant and are strongly correlated with Agar FOOD. This grouping provides statistical evidence that the high chloride content in the impure Food Agar is the primary driver for the formation of non-spherical shapes (nanotriangles). Chemically, this supports the mechanism in which chloride ions preferentially adsorb onto specific crystallographic facets (e.g., {111}), promoting kinetic growth into anisotropic shapes rather than thermodynamically stable spheres. Furthermore, the correlation with concentration confirms that the impurities associated with high-chloride matrices (likely organic residues) act as powerful auxiliary reducing agents, significantly increasing the reaction yield compared to the purified controls.

The second principal component (PC2) separates systems based on their nucleation density and particle size. Agar BS is isolated in the top-right quadrant, showing a strong positive correlation with Potassium (*K*) and the percentage of small nanoparticles (*NP..fresh/aged*). This indicates that a potassium-rich ionic environment favors a burst-nucleation mechanism that produces a high density of very small seeds (<20 nm). Crucially, the vector for aged small particles points in the same direction,

suggesting that these potassium-stabilized seeds are remarkably resistant to Ostwald ripening, maintaining their small individual dimensions even if they undergo reversible flocculation.

On the negative side of PC1, the Agarose and Agar CTS matrices are spatially separated from the vectors driving anisotropy and rapid growth. Instead, Agarose is associated with the number of dimensional intervals (*No. DI.*) vector. This confirms that in the absence of strong directing agents (like Cl^-) or capping ions (like K^+), the neutral Agarose network exerts a purely steric influence. This results in a passive stabilization regime that, while preventing catastrophic aggregation, allows for a specific thermodynamic evolution toward heterogeneity and/or size increase. In particular, the largest broadening of the size distribution distinguishes it from the other capped matrices.

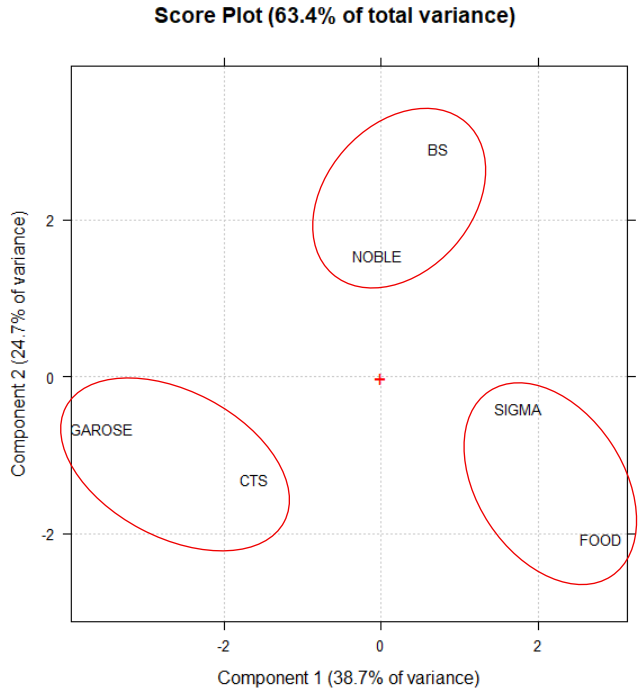

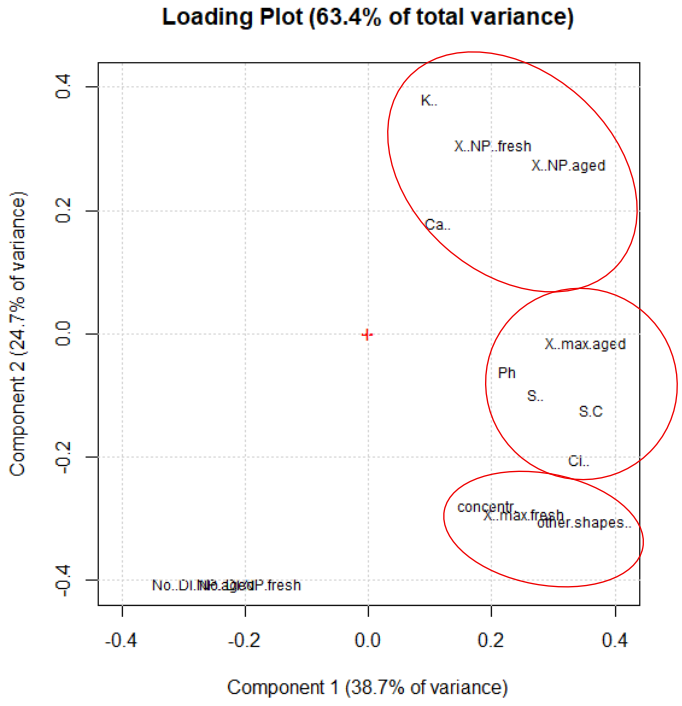

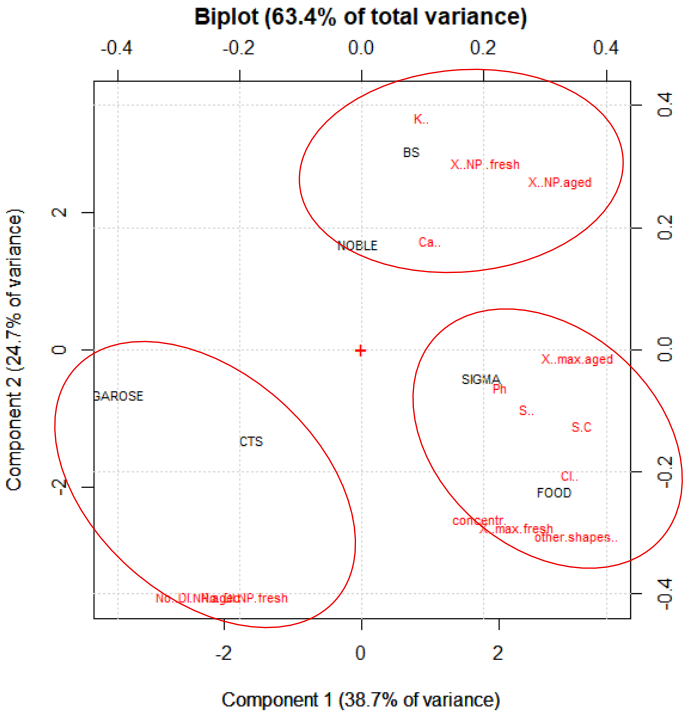

Figure 55- Loading plot, Score plot and Biplot of PCA for gold nanoparticles synthesis

Multivariate analysis of silver nanoparticles (AgNPs) suspensions

The PCA for silver nanoparticles provided an even more distinct separation of the samples, with the first two components explaining 79.2% of the total variance (*Figure 56*).

The first component (PC1) isolates the non-productive matrices. Agar BS and Agar CTS are located on the far right of the score plot, heavily loaded by the variables Potassium (*K*) and Calcium (*Ca*). The isolation of these samples on the positive extreme of PC1 suggests that these cations at given concentration ratios create a chemical environment that inhibits the reduction of silver nitrate. Unlike gold, which reduced successfully in these matrices, silver reduction appears highly sensitive to ionic strength or specific cation competition, possibly due to the formation of insoluble silver-halide or silver-protein complexes that sequester the Ag^{+} ions before reduction can occur.

The second component (PC2) vertically differentiates the productive matrices based on particle size stabilization. Agar SIGMA is positioned in the top-left quadrant, strongly correlated with Sulfur (*S*), Chlorine (*Cl*), and the percentage of small nanoparticles (*NP. fresh*). This strong correlation implies that sulfur-containing functional groups (likely sulfates in Agaropectin) act as effective capping agents for silver. These groups bind to the surface of the nascent silver nuclei, arresting their growth early in the synthesis and resulting in a population dominated by small (<20 nm) particles in the fresh state.

In contrast to the sulfur-stabilized Sigma matrix, Agarose is located at the very bottom of the plot (negative PC2), strongly associated with the Number of dimensional intervals (*No. DI*) and the lambda max position vectors. This geometric arrangement confirms that the high-purity Agarose environment, lacking the sulfur-capping capability found in Sigma, produces silver nanoparticles with a larger hydrodynamic radius (red-shifted λ_{max}) and a broader, more polydisperse size distribution.

The vectors for λ_{max} (both fresh and aged) point away from the small particle quadrant, reinforcing the finding that high purity in the matrix correlates with larger particle sizes due to the absence of chemical growth inhibitors.

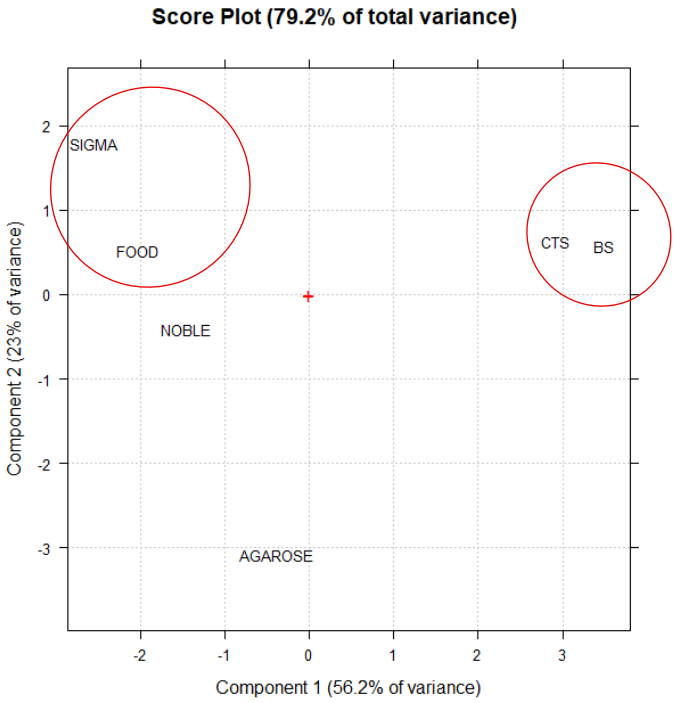

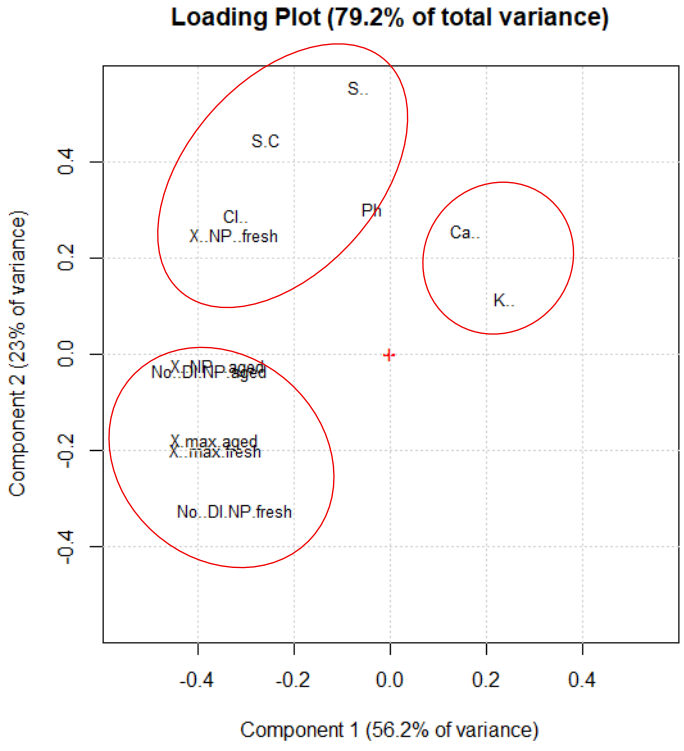

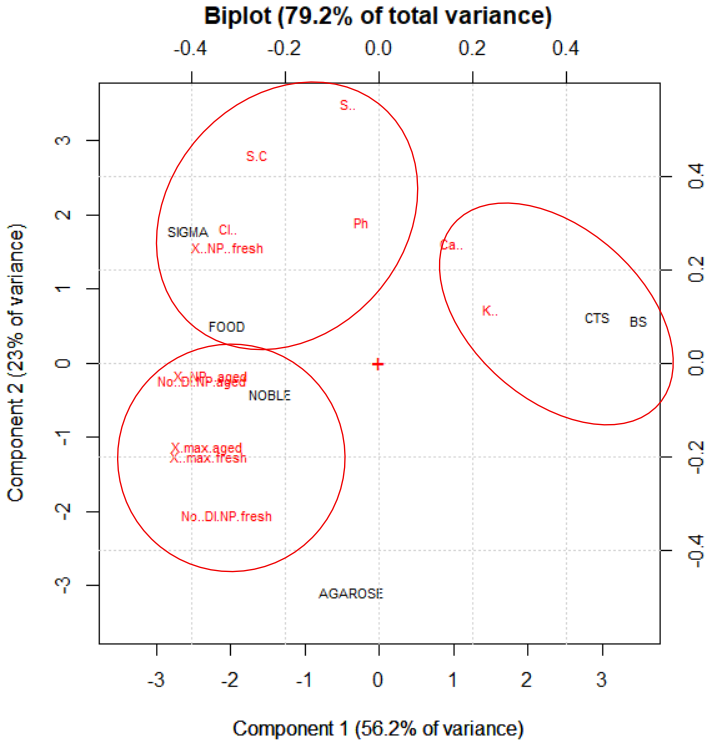

Figure 56- Loading plot, Score plot, and Biplot of PCA for silver nanoparticles synthesis

Correlation between sulfur and reducing ability

A central hypothesis of this study was that sulfur-containing impurities, such as sulphated polysaccharides (Agaropectin), drive the reduction efficiency of the metallic precursors. The chemometric analysis enables direct validation of this hypothesis by examining the vector correlations in the PCA biplots.

In the PCA model for gold nanoparticles, the vector representing Sulfur (*S*) exhibits a strong positive correlation with the vector for gold concentration (*concentr.*). Both vectors are oriented towards the bottom-right quadrant of the biplot, characterized by high positive loadings on PC1. This alignment statistically confirms that sulfur content is a significant predictor of reducing power for gold. Matrices with higher sulfur levels, such as Agar FOOD and Agar SIGMA, consistently yielded higher concentrations of elemental gold.

For silver nanoparticles, the relationship is more complex. While the Sulfur (*S*) vector is strongly associated with Agar SIGMA, a productive matrix located in the top-left quadrant (positive PC2), it is orthogonal to the non-productive Agar BS and Agar CTS, which are located on the far right (positive PC1). This implies that while sulfur is not the sole determinant of reducing power, as Agar FOOD also reduced silver but lies somewhat away from the strong S vector, its presence is crucial for successful nanoparticle stabilization. The failure of BS and CTS suggests that without the specific stabilizing or catalytic environment provided by Sulfur, the reduction of silver is kinetically or thermodynamically inhibited. Thus, for silver, Sulfur is correlated less with raw power and more with the enabling capacity to support stable nucleation.

Chemometric interpretation by matrix

Integrating the spectral, morphological, and statistical data, the chemometric analysis provides a distinct profile for each Agar matrix, clarifying its specific role in nanoparticle synthesis.

Agar FOOD functions as an aggressive reducing agent. Defined by its high impurity load, specifically Chlorine (Cl) and Sulfur (S), it drives the reactivity axis in the gold PCA, exhibiting the highest reduction yield. In particular, the presence of chloride ions in high concentration increases the reduction speed, making the nanoparticle formation process less controlled. Consequently, the shape heterogeneity of AuNPs increases, as evidenced by the appearance of nanotriangles. For silver, it similarly functions as a favorable reducing environment but lacks the specific capping efficiency to arrest growth, leading to continuous Ostwald ripening overtime.

Agar CTS acts as a selective reducer. For gold, it supports high yields comparable to Food Agar but offers limited long-term stability, eventually succumbing to aggregation. However, for silver, the specific cationic ratio (high Ca/K) combined with insufficient sulfur-based stabilization creates an inhibitory environment, leading to a complete failure to synthesize nanoparticles.

Agar BS serves as a nucleation specialist for gold but an inhibitor for silver. Its high Potassium (*K*) content correlates with the retention of the smallest gold particles (<10 nm). The ionic strength provided by potassium likely creates a dense electrical double layer that favors burst nucleation but inhibits subsequent crystal growth, trapping the gold in a seed state. Conversely, for silver, this same ionic environment acts as a quenching factor, preventing reduction entirely.

Agar SIGMA functions as a sulfur-mediated stabilizer. It occupies a middle ground for gold, containing sufficient sulfur to drive moderate yield and showing signs of Ostwald ripening. For silver, however, it is the ideal matrix; the strong correlation with Sulfur (*S*) identifies it as the source of capping agents that stabilize small silver nuclei (10 nm). This stabilization is effective but temporary, allowing for controlled growth (ripening to 20 nm) over 60 days.

Agar NOBLE represents the purified baseline. Lacking the chemical fuel (S/Cl) of the crude Agars, it yields lower concentrations of gold but promotes predominantly spherical particles due to the absence of shape-directing agents. The PCA places it near the center-left, indicating a balance between steric stabilization and low reactivity. For silver, it permits gradual, controlled evolution of particle size, preventing the chaotic growth seen in cruder matrices.

Agarose defines a regime of imperfect steric stabilization. Located at the negative extreme of PC1 in the Gold PCA, it is inversely correlated with concentration and anisotropy. Its unique chemometric signature is its association with the Number of Dimensional Intervals (*No. DI*). This association reflects the second family anomaly observed in the experimental data: while Agarose prevents the chaotic aggregation seen in commercial Agars (Food/CTS), its lack of specific chemical capping agents (like S or K) renders it permeable to slow thermodynamic relaxation. This results in the evolution of a distinct secondary population of particles (spectral shoulder) over time.

Conclusions

The comprehensive investigation into the synthesis of noble metal nanoparticles using commercial Agar and purified Agarose matrices has provided a multifaceted understanding of how the complex chemical environment of polysaccharide hydrogels governs the nucleation, growth, and stabilization of noble metal colloids. By integrating elemental analysis, vibrational spectroscopy, optical characterization, morphological statistics, and chemometric modeling, this study establishes a deterministic link between the chemical composition of the gelling matrix and the physicochemical properties of the resulting nanostructures.

The elemental analysis, which informed the multivariate models, revealed that the impurity content of commercial Agars is not merely passive residue but the active engine of the synthesis. The presence of high chloride concentrations, particularly in Agar FOOD, was identified as the critical factor inducing anisotropy. The strong statistical correlation between Chlorine content and the formation of nanotriangles, which constituted approximately 20% of the population, supports a mechanism where oxidative etching or preferential adsorption of chloride ions on specific crystallographic facets directs the kinetic growth of non-spherical gold structures. The Sulfur content, attributed to sulphated Agaropectin, played a dichotomous role. For gold nanoparticles, it acted as a marker for high reducing power, correlating with increased reaction yields via the oxidation of associated impurities. Conversely, for silver nanoparticles, it functioned as an essential electro-steric stabilizer. The failure of low-sulfur or ionic-imbalanced matrices, such as Agar BS and Agar CTS, to produce silver nanoparticles contrasts with the success of Agar SIGMA, where sulfur capped the nuclei at small diameters of approximately 10 nm. Furthermore, the ionic background proved decisive for nucleation kinetics; high potassium levels in Agar BS favored a burst-nucleation regime for gold, trapping particles in a seed state below 10 nm, while acting as an inhibitory factor for silver reduction.

The UV-Vis monitoring over 60 days elucidated three distinct stability regimes. Silver nanoparticles in commercial Agars exhibited a continuous ripening profile, characterized by a continuous monotonic red-shift, such as the 26 nm shift observed in Agar FOOD. This indicates a dynamic surface interaction where the matrix could not permanently arrest Ostwald ripening. In contrast, commercial Agars provided a metastable environment for gold, characterized by a step-change instability profile. This regime featured an induction period of 14 to 28 days followed by a rapid transition to larger aggregates or flocculation, as evidenced by the red-shifts in Agar BS and Agar SIGMA. The purified Agarose matrix defined a passive steric stabilization regime, maintaining the primary Surface Plasmon Resonance peak position at 535 nm for gold and 418 nm for silver with remarkable constancy. However, the emergence of a spectral shoulder in the aged gold samples revealed that this stabilization prevents chaotic aggregation but permits the slow, diffusion-controlled evolution of the nanoparticle shape overtime.

The morphological analysis highlighted a fundamental trade-off between synthesis yield and product homogeneity. Crude matrices like Agar FOOD acted as aggressive chemical reactors, achieving the highest metallic concentrations of 0.683 mmol/L for gold but at the cost of morphological heterogeneity, producing polydisperse populations with both isotropic and anisotropic geometry. Conversely, high-purity Agarose yielded lowest metallic concentrations of 0.503 mmol/L due to the absence of auxiliary reducing groups. However, it excelled at producing spherical-like nanoparticles with high size homogeneity. The statistical anomaly of Agarose, where a bimodal distribution emerged over

time without shifting the main SPB peak, confirms its role as a viscous trap that retards but does not chemically cap the nanoparticle surface.

The chemometric analysis unified these observations into a coherent predictive model. The Principal Component Analysis successfully deconstructed the variance into clear chemical drivers, demonstrating that chlorine drives anisotropy, sulfur facilitates silver stabilization and gold yield, and potassium dictates nucleation density. In conclusion, the study demonstrates that green synthesis in polysaccharide gels is not a generic process but a chemically tunable one. For applications requiring high catalytic activity or infrared absorption, such as photothermal therapy, the impurity-rich Agar FOOD is the optimal choice to generate anisotropic forms. Conversely, for applications demanding spherical uniformity, purified Agarose is superior, provided that the evolution of the secondary particle family is mitigated by appropriate storage or cross-linking strategies. The commercial Agars, such as SIGMA and NOBLE, serve as intermediate substrates, offering a balance of yield and stability defined by their specific sulfated polysaccharide content.

Chapter 10.
Electrospun Agar-based Nanocomposite Mats for Artworks Disinfection

10.1 Introduction

Following the successful green synthesis and stabilization of gold (Au) and silver (Ag) nanoparticles reported in the previous chapter, the focus of this research now shifts from synthesis to the development of a functional delivery system. While the "Agar Sigma" formulations yielded the most stable and uniform nanoparticle suspensions, utilizing these materials for cultural heritage conservation requires a solid-state application method that allows for controlled handling and removability. Consequently, this chapter details the transformation of these colloidal suspensions into nanofibrous membranes via electrospinning.

Based on the optimization parameters established in earlier experimental phases, the functionalized Agar Sigma suspensions were blended with Poly(ethylene oxide) as a co-spinning agent. A polymer ratio of 50/50 and a total concentration of 3% w/v were selected to ensure stable jet formation and uniform fiber morphology. Crucially, to understand the spinnability of these fluids, the solutions underwent a detailed rheological characterization before processing. This analysis compared Agar Sigma suspensions with the final Agar/PEO blends, both with and without the inclusion of nanoparticles, to isolate and evaluate the specific influence of the co-spinning agent and the metallic nanomaterials on the rheological behavior and viscosity of the system.

Once the electrospinning process was performed, the study focused on the comprehensive characterization of the resulting nanocomposite mats. SEM-EDS and AFM were utilized to verify nanoparticle distribution and fiber morphology, while contact angle measurements were performed to assess surface wettability. Furthermore, mechanical testing was conducted to evaluate changes in tensile strength and elasticity, comparing the functionalized mats against pristine Agar/PEO controls to determine if the nanomaterials acted as reinforcement or structural defects.

Finally, the practical utility of these novel materials will be assessed through biological testing. The functionalized mats will be addressed for their biocidal efficacy against specific biodeteriogens commonly responsible for the severe degradation of cellulosic and lignocellulosic artifacts. Specifically, the assays target Aspergillus niger, a ubiquitous fungus known for degrading paper archives and historical textiles, alongside Coniophora puteana (brown rot) and Trametes versicolor (white rot), which are primary agents in the structural destruction of archaeological and historical wooden artworks. By targeting these specific species, the study aims to frame these functionalized mats as dedicated tools for the disinfection of wood, paper, and canvas supports

10.2 Agar-based nanocomposite mats

Solutions preparation

The electrospinnable solutions were prepared using the functionalized Agar Sigma suspensions synthesized as described in the previous chapter (Agar Sigma@MNPs, 1% w/v). For each formulation, 5 mL of the pre-prepared nanoparticle suspension served as the base volume. To achieve the optimized properties for electrospinning, a calculated amount of aqueous Poly(ethylene oxide) solution ($\bar{M}v$= 300 KDa 3% w/v) and pristine Agar powder were added to the base suspension. Finally, distilled water was added to adjust the final volume to 10 mL.

This procedure ensured a total polymer concentration of 3% w/v with a final ratio of 50/50 (Agar/PEO). The mixtures were stirred until complete homogenization and dissolution of the additional Agar powder were achieved, resulting in two distinct nanocomposite blends ready for processing: Agar/PEO@AuNPs/PEO and Agar@AgNPs/PEO.

Rheological characterization

Before electrospinning, the flow behavior of the precursor suspensions and the final polymeric blends was analyzed to evaluate the influence of nanoparticles and the co-spinning agent on solution viscosity. Understanding the rheological profile is critical, as the viscosity determines the stability of the Taylor cone and the continuity of the resulting fibers.

A preliminary comparative analysis was conducted to validate the processability of the Agar Sigma-based matrix by bridging the findings of the current study with the optimization established in Chapter 7. In the previous phase of this research, the electrospinnability of Agar CTS/PEO blends was successfully demonstrated. To verify the suitability of Agar Sigma for the same processing window, its rheological behavior was compared to the established Agar CTS system (*Figure 57*). The flow curves revealed that the substitution of the Agar type did not induce significant deviations in the yield stress behavior or the overall viscosity profile. Crucially, at the specific shear rate of 32 s^{-1}, which corresponds to the shear stress experienced by the fluid within the spinneret needle under the employed processing parameters, the viscosity of the Agar Sigma/PEO control was found to be analogous to that of the previously optimized Agar CTS/PEO system. This rheological equivalence confirms that the process parameters defined in Chapter 7 are directly transferable to the Agar Sigma formulations.

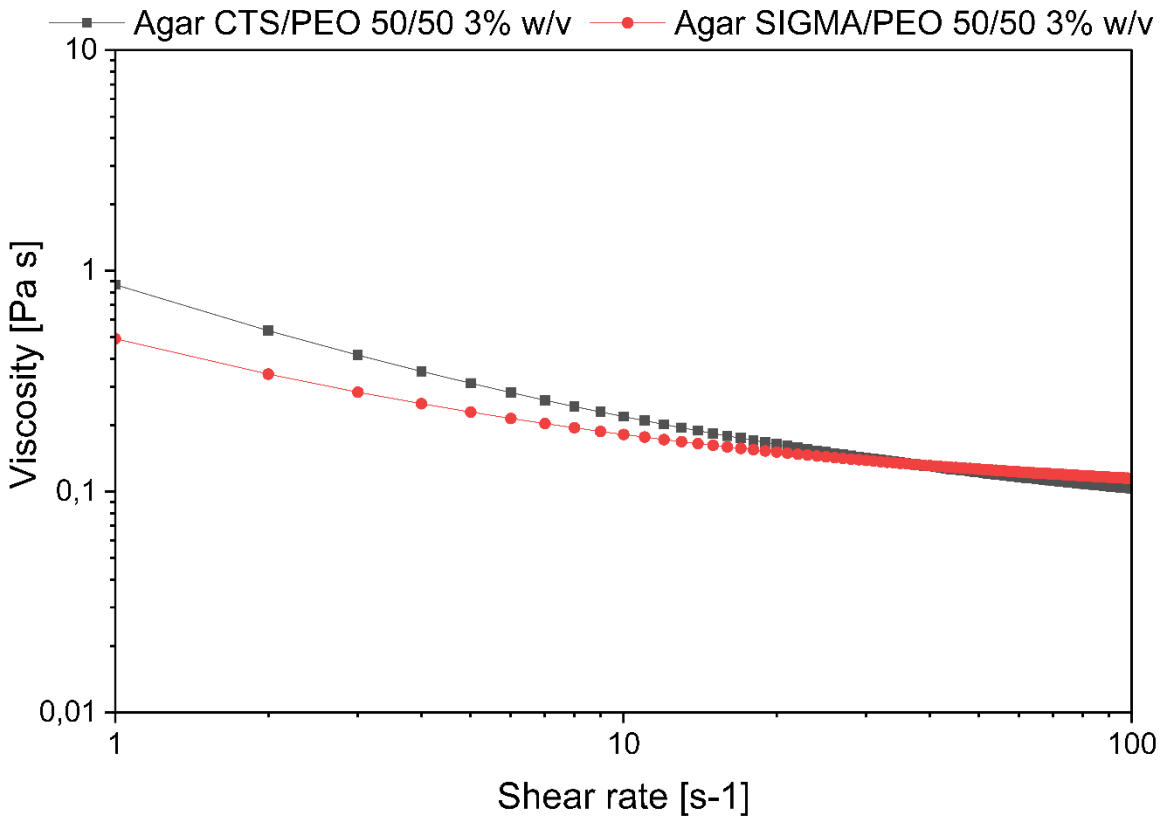

Figure 57- Flow curves of Agar/PEO 300k 50/50 3% w/v solutions with Agar CTS and Agar SIGMA

With this baseline established, the specific influence of the metallic nanofillers immediately after the synthesis (fresh) and after 2 months of conservation (aged) was evaluated. The introduction of metallic nanoparticles induced distinct changes in the fluid dynamics of the pure Agar solutions at 1% w/v (*Figure 58*). The presence of fresh silver nanoparticles resulted in a noticeable increase in viscosity compared to the pure Agar control. This suggests that the AgNPs facilitate the formation of a structured network, likely acting as active fillers that reinforce the gel structure through favourable electrostatic or hydrogen-bonding interactions with the Agarose matrix[213,214].

Conversely, the presence of gold nanoparticles (AuNPs) resulted in a drastic reduction in viscosity, leading to a near-Newtonian behavior (*Figure 58- b*). This divergence can be attributed to the specific surface chemistry of the gold nanoparticles and their interaction with the hydroxyl (-OH) groups of the Agar backbone[215–217]. Agar gelation relies on the ability of polysaccharide chains to form intermolecular hydrogen bonds, leading to the formation of a double helix and subsequent network aggregation. It is hypothesized that the AuNPs interact competitively with the -OH groups, effectively "capping" the hydrogen-bonding sites. This steric hindrance disrupts the self-assembly of the Agar chains, preventing the formation of the double helices necessary for gelation and maintaining the polymer in a disordered, low-viscosity state.

The temporal stability of these effects was also investigated, revealing a direct correlation between the rheological behavior and the optical properties observed in the previous chapter. The silver-based suspensions exhibited a marked time-dependency: while fresh samples were viscous, the aged samples showed a significant reduction in viscosity. This rheological collapse aligns with the kinetic data obtained from UV-Vis spectroscopy, where the characteristic Surface Plasmon Resonance (SPR)

peaks of the silver nanoparticles were observed to grow over a two-month period. This optical evolution indicates a continuous process of particle growth or aggregation (Ostwald ripening).[218,219] As the silver nanoparticles increase in size, their specific surface area-to-volume ratio decreases, reducing the density of available interaction sites for the Agar chains. Consequently, the initial reinforcing network is metastable; as the "cross-linking nodes" grow and become fewer, they lose their ability to effectively bridge the polymer matrix, resulting in the observed loss of viscosity. In contrast, the gold-based suspensions demonstrated high stability, with aged samples maintaining the same low-viscosity profile as the fresh ones, confirming that the disruption of the Agar network is a permanent alteration.

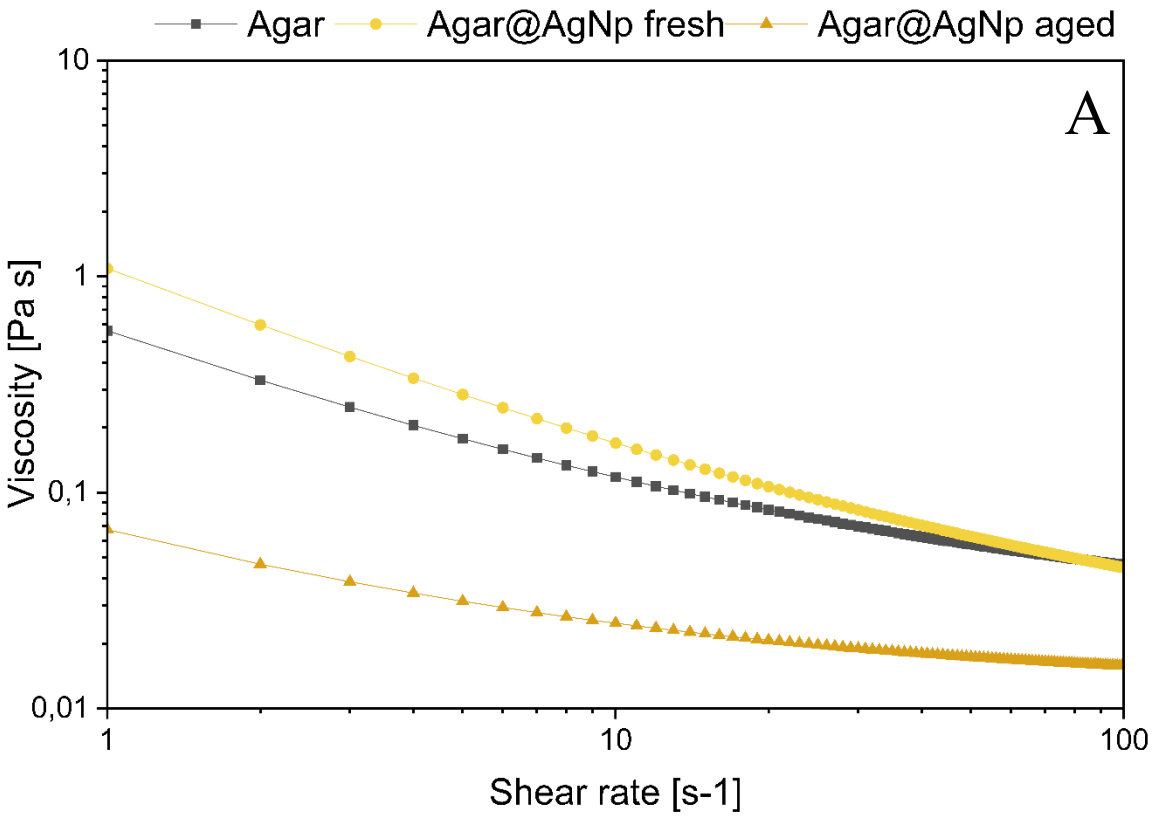

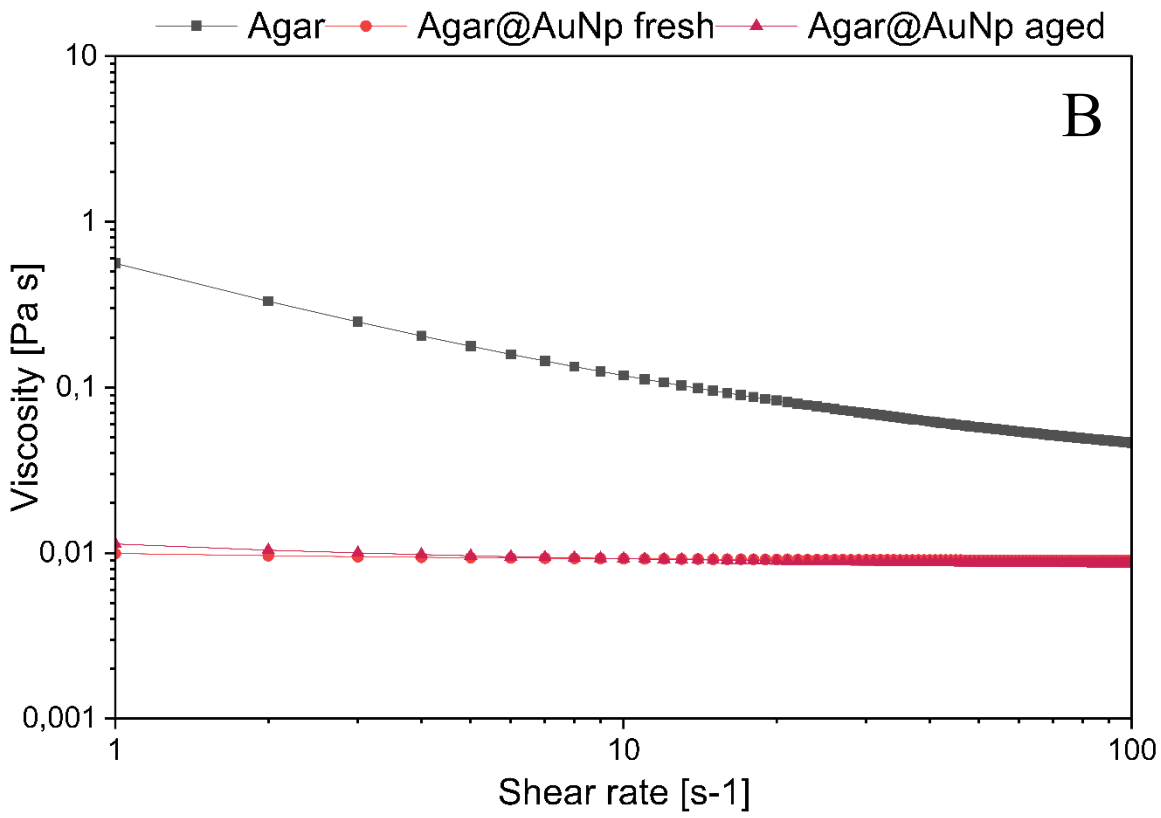

Figure 58- Flow curves of pristine Agar SIGMA 1% w/v solution, (A)Agar SIGMA@AgNPs 1% w/v, and (B)Agar SIGMA@AuNPs 1% w/v suspensions (fresh and aged)

To enable the electrospinning of these suspensions, Poly(ethylene oxide) was added as a co-spinning agent (*Figure 59*). The addition of PEO successfully increased the viscoelasticity of all systems, which exhibited a marked yield stress behavior. Notably, the inclusion of nanoparticles in the PEO blends inverted the trend observed in the pure gold suspensions. In the presence of PEO, the Agar@AuNp/PEO blend displayed the highest viscosity at low shear rates. This recovery suggests that while AuNPs disrupt the self-association of pure Agar, they possess a high affinity for the ether oxygen atoms in the PEO chains. Upon mixing, the AuNPs likely act as physical cross-linking nodes that bridge the high-molecular-weight PEO chains, creating a highly entangled PEO-AuNP network that compensates for the lack of Agar gelation, resulting in the high yield stress behavior observed.

When analysing the final nanocomposite blends at a critical shear rate of 32 s^{-1} (calculated with a flow rate of 0, 7 ml/h and an inner needle diameter of 0,4 mm, as described in Chapter 7), both the gold and silver formulations exhibited viscosity values that were comparable to or higher than those of the validated Agar/PEO control (Table 18). Specifically, the Agar@AuNp/PEO blend displayed the highest viscosity at low shear rates, while the Agar@AgNp/PEO blend maintained a consistently higher viscosity than the pristine control. Since the viscosity values of all nanocomposite blends at 32 s^{-1} satisfy or exceed the threshold established by the spinnable Agar CTS reference, all formulations were deemed suitable for the electrospinning process without the need for further formulation adjustments.

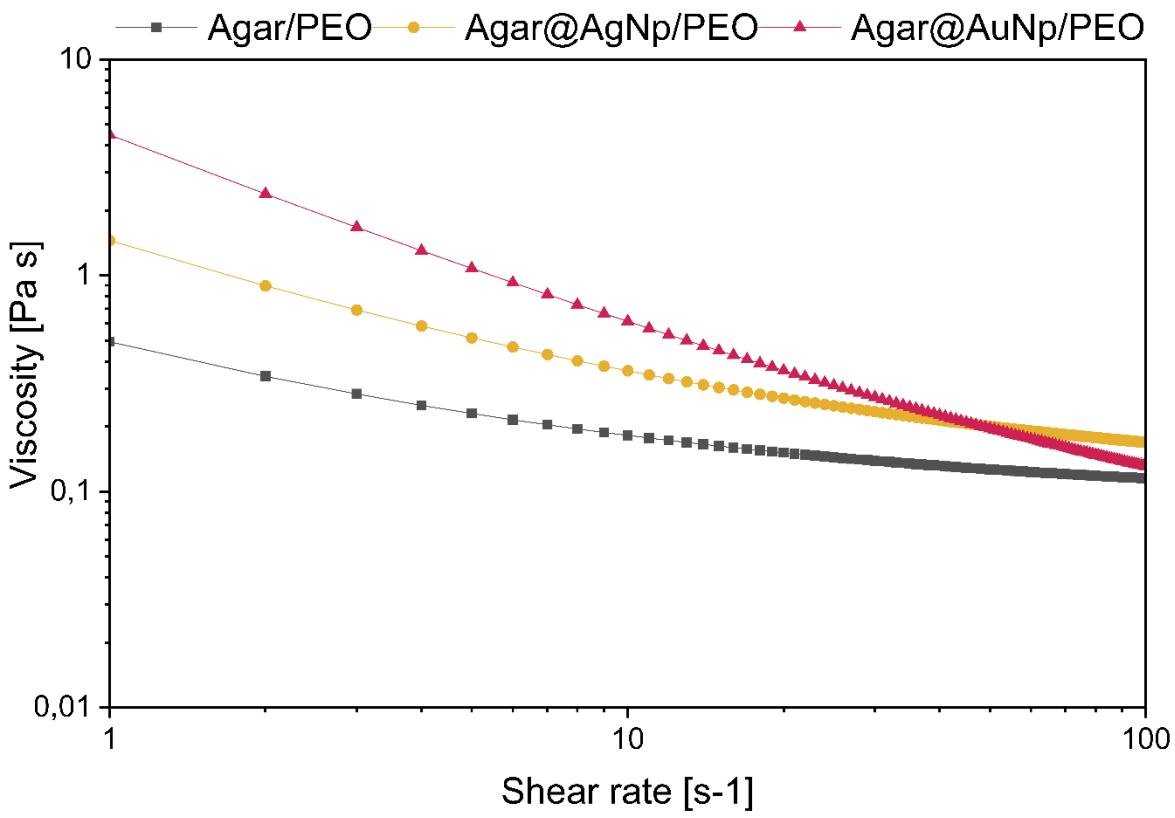

Figure 59- Flow curves of Agar/PEO blend with and without gold and silver NPs

Table 18- calculated shear rate and viscosity for Agar-based solutions and suspensions

Sample (50/50 w/w)	**η @32 s^{-1} (Pa s)**
Agar CTS/PEO 3% w/v	0,14
Agar SIGMA/PEO 3% w/v	0,14
Agar@AgNP/PEO 3% w/v	0,23
Agar@AuNP/PEO 3% w/v	0,26

Electrospinning process

The fabrication of the nanocomposite mats was performed using a professional electrospinning apparatus equipped with a flat collector. Consistent with the optimized processing window established and validated in Chapter 7, the operational parameters were carefully reproduced to ensure the stability of the jet and the uniformity of the fibers. To prevent the premature gelation of the Agar component during processing, the temperature of the electrospinning chamber was strictly maintained at 45 °C. Typically, 3 mL of the blend solutions were electrospun using an applied voltage of 22 kV, a fixed spinneret-to-collector distance of 15 cm, a constant flow rate of 0.7 mL/h, and an inner needle diameter of 0.4 mm.

10.3 Mats characterization

Mats' characterization results were summarized in Table 19.

Table 19- Experimental results for Agar/PEO@MNps

	Agar/PEO	**Agar@AuNP/PEO**	**Agar@AgNP/PEO**
Average fiber diameter [nm]	106±25	100±13	160±24
Root mean square height Sq [nm]	58,5±3,6	55,7±2,4	52,5±3,5
Arithmetical mean height Sa [nm]	42,3±2,1	44,5±1,8	39,2±3,1
Contact angle [°]	38±2	40±2	36±3
Surface Free Energy [mN/m]	53±2	52±2	54±2
Young's Modulus [MPa]	47±8	35±6	273±67
Tensile strenght [MPa]	1,4±0,4	1,7±0,2	9,8±1,9
Elongation at Break [%]	4,4±0,8	8,6±0,8	6,7±1,6

Morphological analysis via FE-SEM confirmed the successful incorporation of nanoparticles. While the primary shape and size of the individual nanoparticles remained stable—indicating they withstood the electrospinning process without degradation—they were observed primarily as encapsulated clus-

ters. High-contrast Back-Scattered Electron (BSE) imaging (*Figure 60*, right panels) further corroborated that the high-atomic-weight metal particles are embedded within the fiber core rather than adsorbed onto the surface. The type of nanoparticle significantly influenced the fiber morphology and diameter distribution. Compared to the pristine Agar/PEO mat (106 ± 25nm), the addition of AuNPs resulted in a slight reduction in average diameter (100 ±13 nm) and a qualitative increase in bead defects (beads-on-string morphology). Dimensional analysis revealed AuNP clusters ranging from 150 to 200 nm; since these aggregates often exceeded the average fiber diameter, this dimensional mismatch likely exacerbated the defects. This suggests that AuNPs likely increased the solution conductivity, leading to higher jet stretching, while simultaneously inducing Rayleigh instabilities. Conversely, the Agar/PEO@AgNPs mat exhibited a marked thickening of the fibers, with an average diameter of 160 ± 24 nm. Although AgNP clusters were of comparable size (100–200 nm), the thicker fibers accommodated these aggregates more effectively, though localized bulging was still observed. This 50% increase in diameter is attributable to the dominance of the viscosity increment caused by AgNPs, which prevented excessive jet thinning during electrospinning.

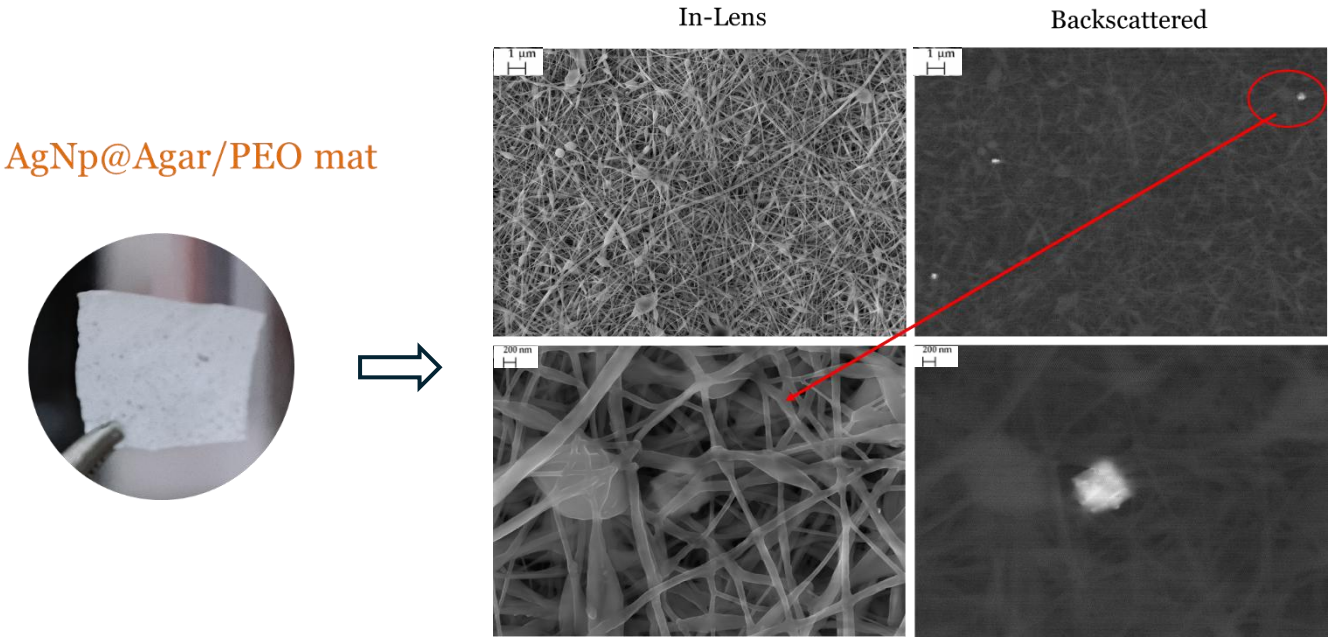

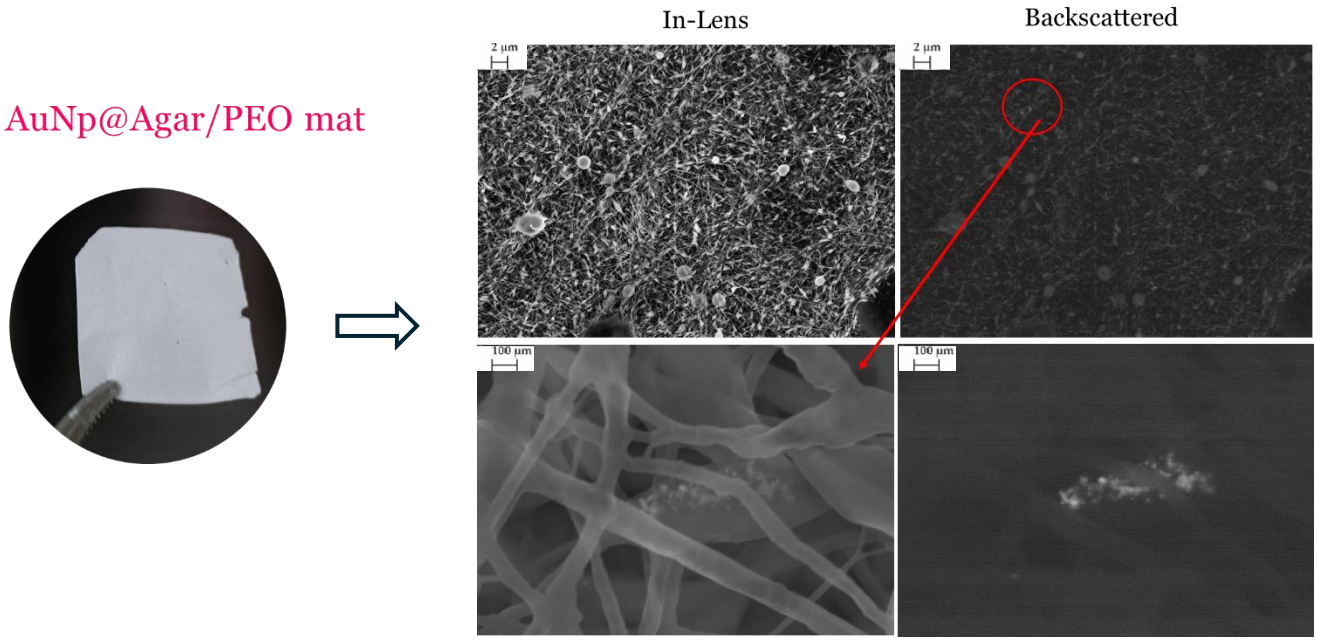

Figure 60- SEM images of Agar/PEO mats with gold and silver nanoparticles. Both InLens and Backscattered modes were presented.

Surface analyses via AFM revealed that the inclusion of nanoparticles preserved the surface topography of the membranes. The Root Mean Square height (Sq) and Arithmetical Mean height (Sa) showed no statistically significant deviation from the pristine mat. The Sa values remained tight between 39 and 45 nm across all samples. This topological stability, combined with the BSE imagery, strongly suggests the effective encapsulation of both AuNPs and AgNPs within the fiber bulk. This observation is reinforced by wettability data; contact angles remained consistent (36°–40°), and Surface Free Energy (SFE) fluctuated negligibly around 53 mN/m. Consequently, the functionalized mats retained the highly hydrophilic nature of the Agar/PEO matrix.

The most striking divergence between the two nanomaterials was observed in their mechanical performance (*Figure 61*). The addition of AgNPs acted as a powerful reinforcement agent, yielding a 5.8-fold increase in Young's Modulus (273±67 MPa) and a 7-fold increase in Tensile Strength (9.8±1.9 MPa) compared to the control. This dramatic enhancement implies the formation of a rigid percolating network or specific interactions between the AgNPs and the Agar/PEO hydroxyl groups, effectively restricting polymer chain mobility.

In contrast, the Agar/PEO@AuNPs mat displayed a different mechanical profile. While the Young's Modulus (35 MPa) and Tensile Strength (1.7 MPa) were statistically comparable to the pristine mat, the AuNPs nearly doubling the Elongation at Break (8.6 %) compared to the control (4.4 %). This suggests that while AgNPs act as rigid fillers, the AuNPs, and potentially the beaded morphology associated with them, may facilitate energy dissipation through polymer chain unfolding or slippage.

Probably, different size of nanoparticles and the different specific interactions between noble metals and polymeric matrix, caused this different behaviour of gold and silver nanoparticles.

Finally, the project has now progressed to evaluating the functional properties of these nanocomposite mats, with antifungal and antibacterial activity assays currently underway.

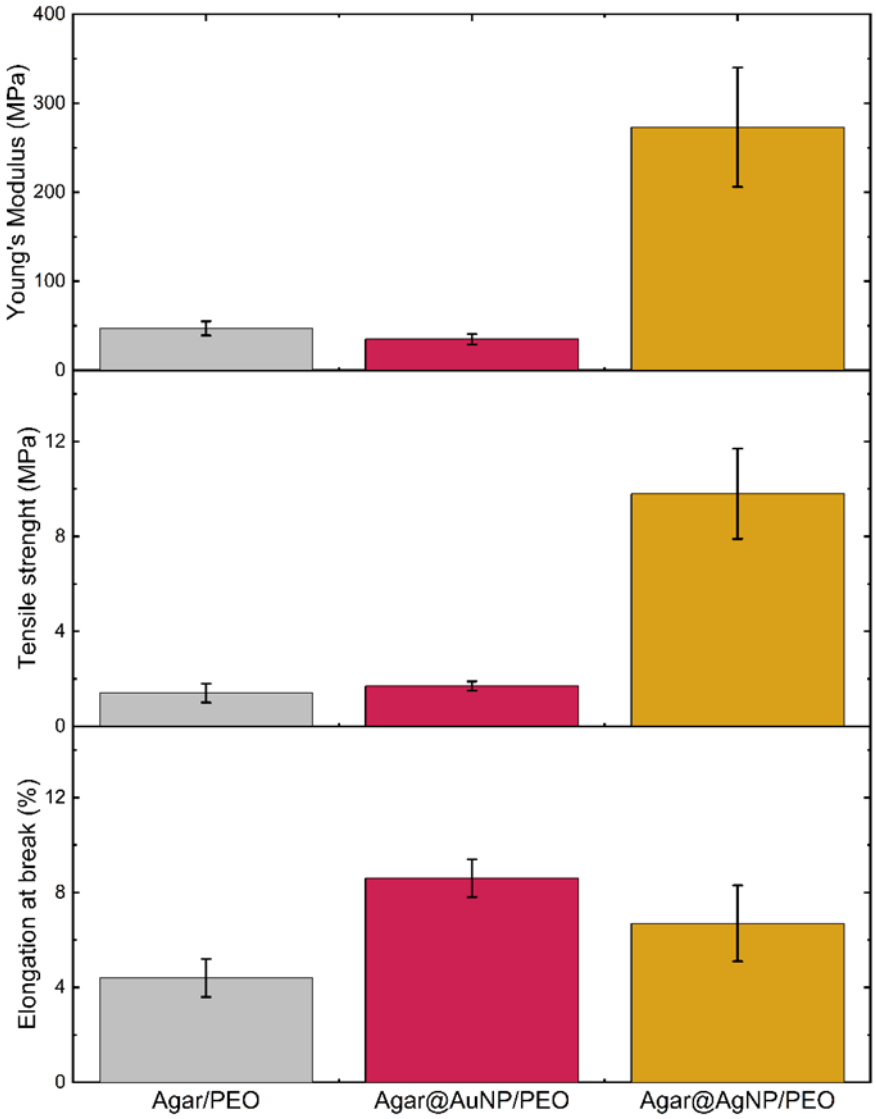

Figure 61- Tensile tests on Agar/PEO, Agar@AuNP/PEO, and Agar@AgNP/PEO mats

Conclusions

This study successfully demonstrated the transition from stable colloidal suspensions to functional solid-state delivery systems via the electrospinning of Agar-based nanocomposites. By blending the previously optimized Agar Sigma formulations with Poly(ethylene oxide) as a co-spinning agent, the research successfully fabricated defect-free nanofibrous mats suitable for cultural heritage conservation. The rheological investigation revealed that while silver nanoparticles acted as active fillers that reinforced the gel network, gold nanoparticles initially induced a viscosity reduction by competitively interacting with the Agar hydroxyl groups. However, the addition of PEO effectively compensated for this disruption in the gold-based systems, likely through the formation of a robust PEO-AuNP entanglement network, thereby ensuring that all formulations met the necessary viscosity thresholds for stable fiber formation.

Morphological and physical assessments confirmed the effective encapsulation of the nanomaterials within the fiber core, with Back-Scattered Electron imaging validating that the particles were not merely adsorbed onto the surface. The type of nanofiller significantly influenced the fiber architecture and mechanical behavior; silver nanoparticles resulted in thicker fibers and a dramatic increase in tensile strength and rigidity, suggesting the formation of a percolating network. Conversely, gold nanoparticles yielded thinner fibers with a "beads-on-string" morphology that enhanced the material's elongation properties. Despite these structural differences, surface characterization via AFM and contact angle measurements confirmed that the functionalized mats retained the essential hydrophilicity and topography of the pristine Agar matrix.

The ultimate validation of these materials lies in their functional capacity to mitigate biological degradation. Consequently, the fabricated mats are currently being evaluated for their biocidal efficacy against common biodeteriogens of cultural heritage, specifically *Aspergillus niger*, *Coniophora puteana*, and *Trametes versicolor*. These antimicrobial assays are currently in progress at the University of Rome La Sapienza. The forthcoming results will be pivotal in defining the practical utility of these nanocomposite textiles as highly targeted, removable disinfection tools, specifically engineered for the non-invasive remediation of mold-infested paper archives, historical textiles, and decaying wooden artifacts

Chapter 11.
Electrospun PCL mats as bacterial supports for sustainable biocleaning in Cultural Heritage Conservation

11.1 Introduction

The conservation of cultural heritage is increasingly turning toward sustainable methodologies that minimize toxicity and environmental impact while maximizing selectivity. Biocleaning represents a significant advancement in this field, utilizing the metabolic versatility of viable microorganisms to remove unwanted inorganic and organic substances from artistic surfaces. Unlike traditional chemicals that pose risks of uncontrolled penetration or substrate damage, biological agents offer high specificity, catalyzing the hydrolysis of specific deposits without affecting the artwork itself. However, the practical application of these biological agents often requires an effective support matrix to overcome the limitations of direct liquid application. Consequently, this chapter focuses on the experimentation regarding the use of Polycaprolactone (PCL) mats as functional bacterial carriers for biocleaning applications.

The selection of Polycaprolactone is grounded in extensive literature highlighting its potential as a material for improving bacterial adhesion. PCL is a biodegradable, hydrophobic polyester that facilitates microbial immobilization through favorable physicochemical surface interactions. Current studies suggest that the hydrophobicity and specific surface roughness of PCL scaffolds significantly enhance bacterial colonization by providing a large surface area and stable micro-environments for cell attachment. For this experimentation, the PCL mats were obtained using the fabrication protocols previously described in Chapter 7. To thoroughly understand the surface properties influencing the bio-interface, the mats were characterized using Atomic Force Microscopy (AFM) to assess nanoscale roughness, contact angle measurements to determine wettability, and Field Emission Scanning Electron Microscopy (FE-SEM) to analyze the microstructural topology.

The biological validation of these carriers was conducted using *Bacillus subtilis* ATCC 6633 and *Pseudomonas stutzeri* ATCC 17588. The initial phase of the study focused on the metabolic characterization of these strains to confirm their specific enzymatic activities reported in the literature, specifically their lipolytic, proteolytic, cellulolytic, and chitinolytic capabilities. These metabolic pathways are critical for restoration purposes, as they can be exploited to remove complex organic layers such as proteinaceous glues and lipid-based grime, as well as for the chitin-targeted removal of fungal infestations. Following the metabolic screening, the research progressed to an in-depth interaction study between the bacteria and the polymer. This included a quantitative assessment of bacterial adhesivity to the PCL mats, followed by a longitudinal study of cell viability over time using different nutrient media and conservation techniques.

11.2 Metabolic characterizations

To define the operational scope of *Bacillus subtilis* and *Pseudomonas stutzeri* in the restoration of cultural heritage, a comparative analysis of their enzymatic outputs was conducted. The study prioritized the identification of extracellular hydrolases, specifically esterases, proteases, cellulases, and chitinases, that target the degradation of organic compounds frequently encountered as contaminants or altered binding media on historical artifacts. The observed metabolic footprints provide the basis for establishing the specific cleaning applications and substrate safety profiles for each strain.

The ability to degrade complex organic mixtures is a fundamental requirement for bio-cleaning agents, as surface deposits often consist of heterogeneous layers of oils, resins, and proteinaceous glues (e.g., "beverone")[57,61].

Analysis of the growth media revealed that both *B. subtilis* and *P. stutzeri* possess a robust, shared capacity for degrading lipids and proteins (*Figure 62-63*). In the lipolytic assays involving Tween 20, metabolic activity was evidenced by the formation of distinct precipitation zones surrounding the bacterial colonies. This turbidity confirms the secretion of esterases capable of hydrolyzing the sorbitan ring and releasing fatty acids, which subsequently form insoluble calcium soaps[177,179]. Similarly, the proteolytic assays on gelatin-supplemented Agar demonstrated clear hydrolysis halos against the Amido Black stained background, indicating the successful cleavage of peptide bonds by extracellular proteases[181].

These observations suggest that both strains are equally suitable for removing hydrophobic layers, such as aged oil varnishes or waxy deposits, as well as for hydrolyzing protein-based binders like casein and animal glues.

While the lipid and protein profiles of the two species were identical, a critical operational divergence was identified regarding cellulose degradation. This distinction dictates the compatibility of each bacterial strain with specific artistic supports.

The assay utilizing Carboxymethyl Cellulose (CMC) visualized via Congo Red staining revealed significant enzymatic activity in *Bacillus subtilis*, characterized by a clarification halo indicative of β-1,4-glucan depolymerization[176]. Conversely, *Pseudomonas stutzeri* exhibited no clarification zones, indicating an absence of extracellular cellulase production under the tested conditions (*Figure 63*).

This metabolic difference identifies B. subtilis as a broad-spectrum agent capable of degrading recalcitrant residues such as starch pastes or vegetable gums, though its application carries an inherent risk when used on cellulosic supports like canvas, paper, or wood. In contrast, the non-cellulolytic nature of *P. stutzeri* positions it as a selective agent, offering a safety margin for the cleaning of fragile paper or textile artifacts where the preservation of the cellulosic structure is paramount.

The investigation into chitin degradation required a comparative methodological approach to overcome substrate physicochemical limitations. The initial protocol utilizing a Chitin Azure overlay proved unsuitable due to the incomplete solubilization of the substrate in the aqueous medium, which prevented the formation of a homogeneous diffusion layer (*Figure 64*).

However, the subsequent biological assay using dehydrated *Velella velella* biomass provided definitive evidence of enzymatic activity. Visual inspection after 48 hours confirmed the partial degradation of the hydrozoan structure by *P. stutzeri* (*Figure 65*). This confirms that this species possesses the metabolic machinery to hydrolyze chitin. While less relevant for standard binding media, this activity suggests a potential utility in biocontrol strategies, specifically for the remediation of surfaces affected by fungal colonization or insect-derived deposits.

The integrated metabolic data delineate two distinct operational niches for the tested strains. Bacillus subtilis presents as a versatile, high-activity strain suitable for robust inorganic substrates, whereas Pseudomonas stutzeri offers a selective enzymatic profile ideal for sensitive organic materials. The comparative enzymatic footprints are summarized in Table 20.

Table 20- Comparative enzymatic characteristics and operational scope

Enzymatic Activity	Bacillus subtills	Pseudomonas stutzeri	Operational Implication
Proteolytic	+	+	Degradation of animal glues and albuminous binders.
Lipolytic	+	+	Hydrolysis of aged oils, waxes, and greasy particulate.
Cellulolytic	+	-	B. subtilis: Potential risk to cellulosic supports.
Chitinolytic	-	+	Removal of fungal mycelia and insect residues.

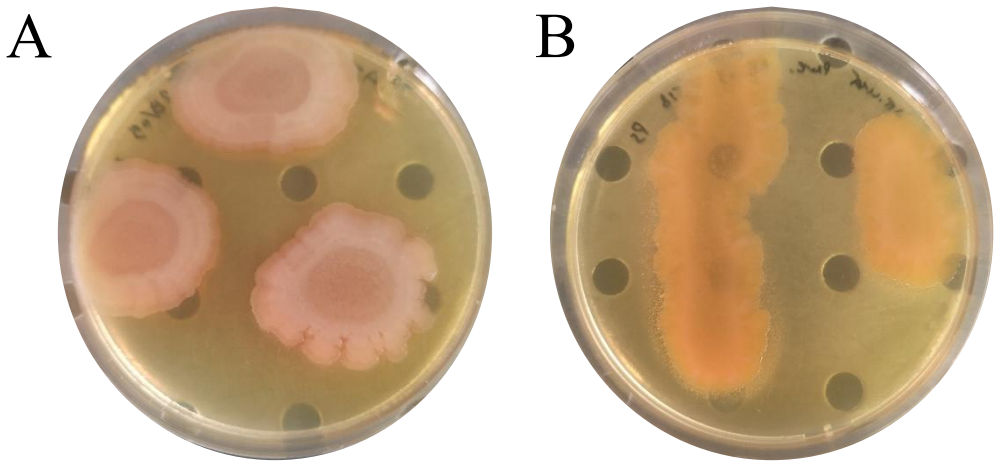

Figure 62- Bacillus subtilis (A) and Pseudomonas stutzeri (B) colonies after growth for seven days on Agar solid medium

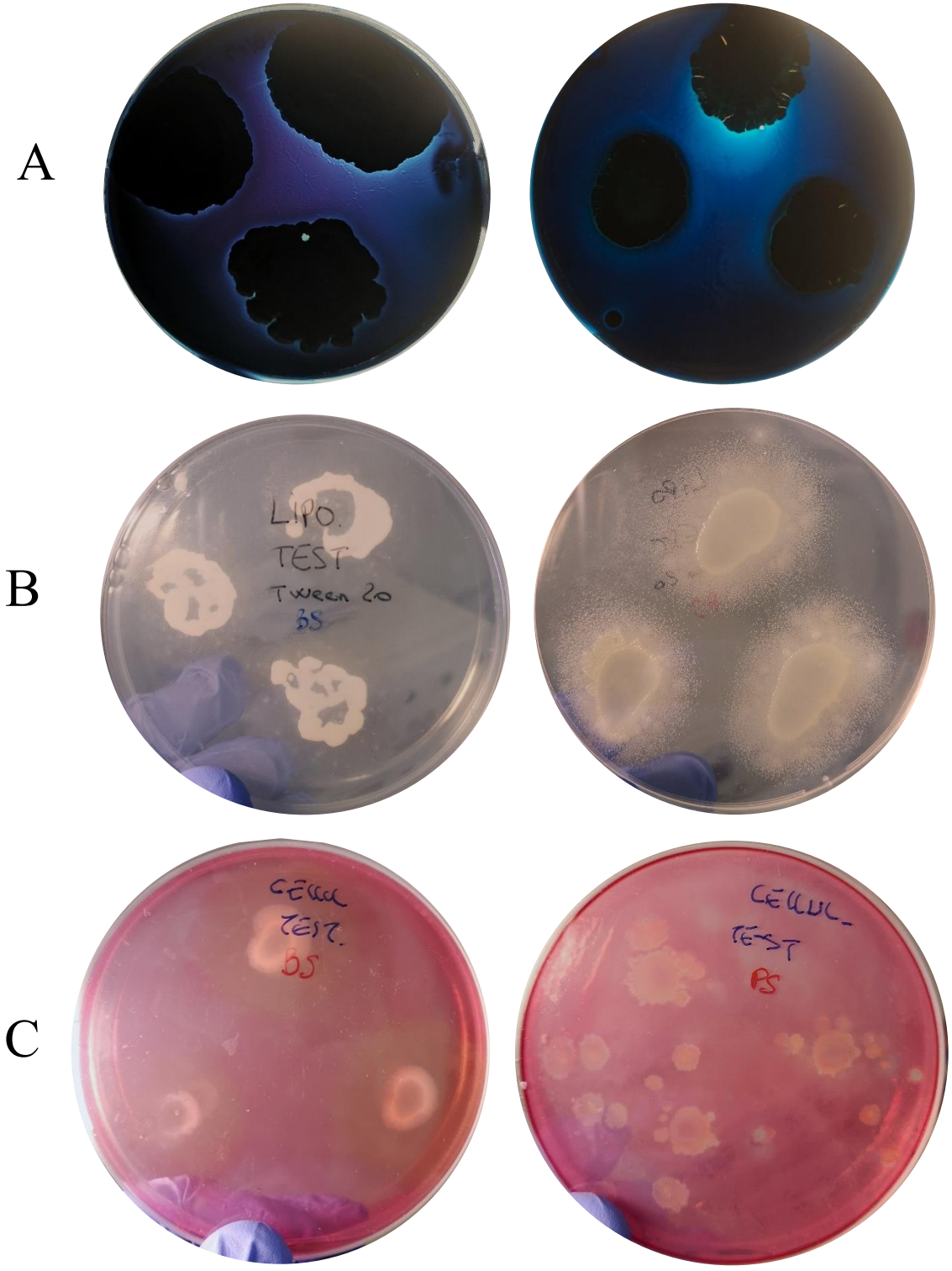

Figure 63- Bacillus subtilis (left column) and *Pseudomonas stutzeri* (right column) colonies after proteolytic (A), lipolytic (B), and cellulolytic (C) metabolic activity test. To see the inhibition and turbid zones.

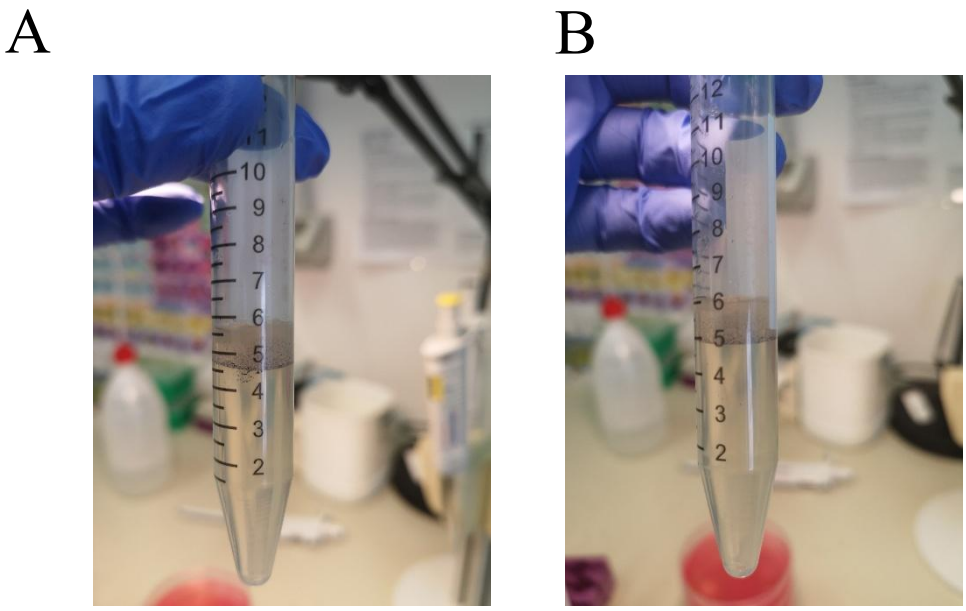

Figure 64- Chitinolytic metabolic test (first method): no diffusion of chitin azure below Agar layer for *Bacillus subitlis* (A) and *Pseudomonas stutzeri* (B).

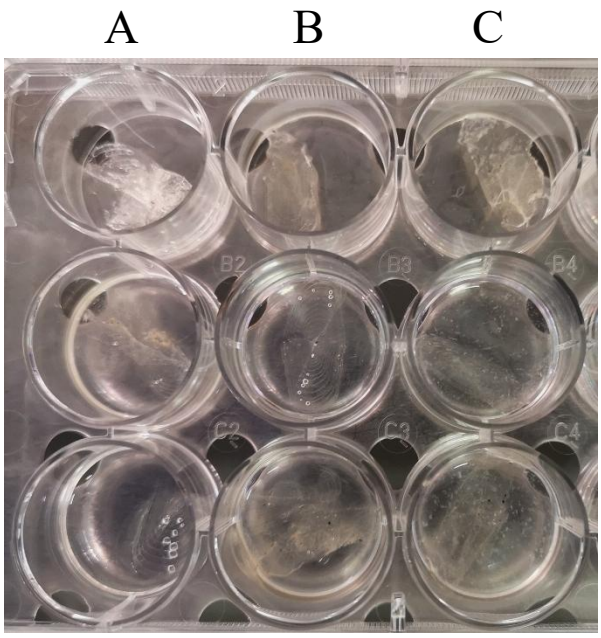

Figure 65- Chitinolytic metabolic test (second method) in triplicate: on the blank (A) and *Bacillus subtilis* (B) wells, there is no degradation of the chitinous body of Vellella vellella. For *Pseudomonas stutzeri* (C), the test was positive with partial degradation.

11.3 PCL mat

A PCL mat was obtained as described in Chapter 7, using an acidic polymer solution composed of PCL (CAPA 6400, Mw = 37 kDa).

11.4 Mats Characterization

The intersection of polymer science and biotechnology has catalyzed the development of advanced fibrous scaffolds designed for specific microbial interactions. Polycaprolactone (PCL), a semi-crystalline aliphatic polyester, has emerged as a foundational material in this domain due to its favorable viscoelastic properties, biocompatibility, and amenability to electrohydrodynamic processing (Chapter 4). While PCL is traditionally valorized for its utility in tissue engineering, specifically for bone and cartilage regeneration due to its long-term structural integrity, its application as a functional carrier for microbial communities represents a burgeoning frontier in industrial biotechnology and bioremediation[168,169,171,196]. The efficacy of such scaffolds is governed by a complex multivariate landscape where morphological parameters, surface thermodynamics, and degradation kinetics converge to dictate biological performance[220].

This chapter presents an exhaustive characterization of a specific electrospun PCL nanofibrous mat, analyzing the interplay between its physicochemical properties and its biological functionality. The subject material exhibits a distinct morphological profile, defined by a consistent fiber diameter of 420 ± 38 nm and sub-micron surface roughness ($Sa = 0.19 \pm 0.02$ μm), properties that are intrinsically linked to its fabrication via electrospinning. Furthermore, the material demonstrates a pronounced hydrophobic character with a water contact angle of 112° and a remarkably low surface free energy of 12.3 mN/m (*Figure 66*). These static physical attributes are contextualized against dynamic biological responses, specifically the immobilization of bacteria and the differential biodegradation profiles observed with *Pseudomonas stutzeri* and *Bacillus subtilis.*

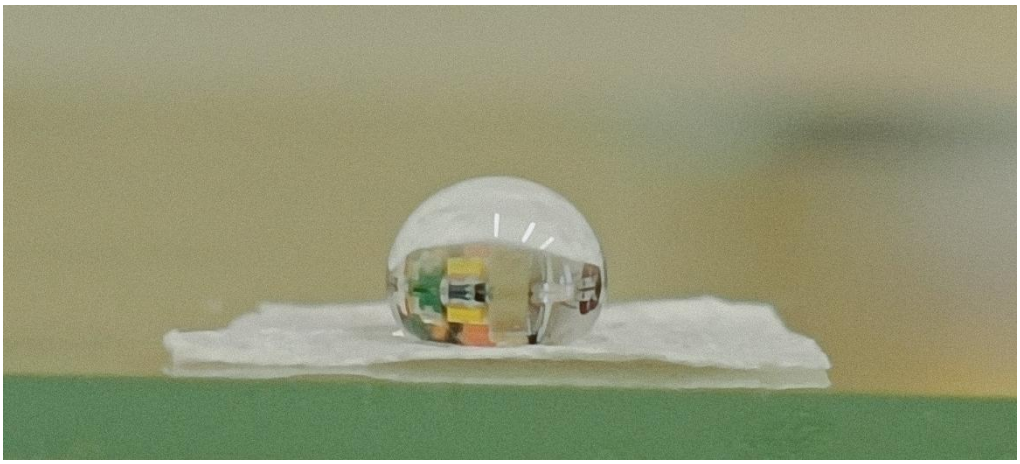

Figure 66- Macroscopical hydrophobic behaviour of PCL electrospun mat

The analysis provided herein synthesizes empirical data with broader scientific literature to elucidate the mechanisms driving bacterial retention and scaffold consumption[220–224]. By examining the thermodynamic drivers of adhesion, the hydrodynamic implications of surface topography, and the enzymatic pathways of degradation, this chapter validates the rational design of the PCL mat. It further explores the implications of these findings for the development of sustainable, bio-integrated materials where the scaffold's end-of-life is as precisely engineered as its functional lifetime.

The structural foundation of the PCL mat is established through electrospinning. The resulting morphology is not merely a passive physical trait but a determinant factor in the material's interaction with biological systems at the micro- and nanoscale.

Field Emission Scanning Electron Microscopy (FE-SEM) analysis confirmed the fabrication of nanofibers with an average diameter of 420 ± 38 nm (*Figure 67*). This dimensional range places the fibers squarely within the sub-micron regime, a scale that is critical for maximizing the surface-area-to-volume ratio relative to conventional microfibers. The uniformity of the fibers, evidenced by the relatively low standard deviation (±38 nm), suggests a stable electrospinning process where critical parameters such as applied voltage, solution viscosity, and solvent evaporation rates were maintained in equilibrium. The consistency observed here indicates an optimized processing window, likely utilizing a solvent system that balances dielectric constant and volatility, such as an acetic acid/acetone mixture, which is known to yield uniform PCL fibers.

The functional implication of the 420 nm diameter is notable when considered in the context of bacterial dimensions. Typical rod-shaped bacteria, including the Pseudomonas and Bacillus species utilized in this study, generally possess diameters between 0.5 and 1.0 µm and lengths ranging from 2 to 5 µm[64,65,69]. Consequently, the PCL fibers are slightly smaller than the width of the bacterial cells they support. This dimensional mismatch prevents the "engulfment" of fibers by individual bacteria. Instead, it promotes a multi-point attachment mechanism where a single bacterium spans across multiple fibers, akin to a body resting on a mesh hammock. This configuration increases the effective contact area and the number of adhesion sites per cell, thereby enhancing the overall binding stability[196,220–222].

Furthermore, fiber diameter has been shown to directly influence bacterial proliferation and biofilm architecture. Research indicates that proliferation rates are often maximized when fiber diameters approximate the size of the bacterial cell, as this provides a topographical guidance cue that aligns with bacterial division axes[225]. Conversely, significantly smaller nanofibers can induce conformational changes in rod-shaped bacteria, potentially limiting colonization or inducing cell death due to membrane stress. The 420 nm diameter supports robust immobilization without inducing bactericidal mechanical stress, a conclusion supported by the successful immobilization verified in the experimental results[123,226].

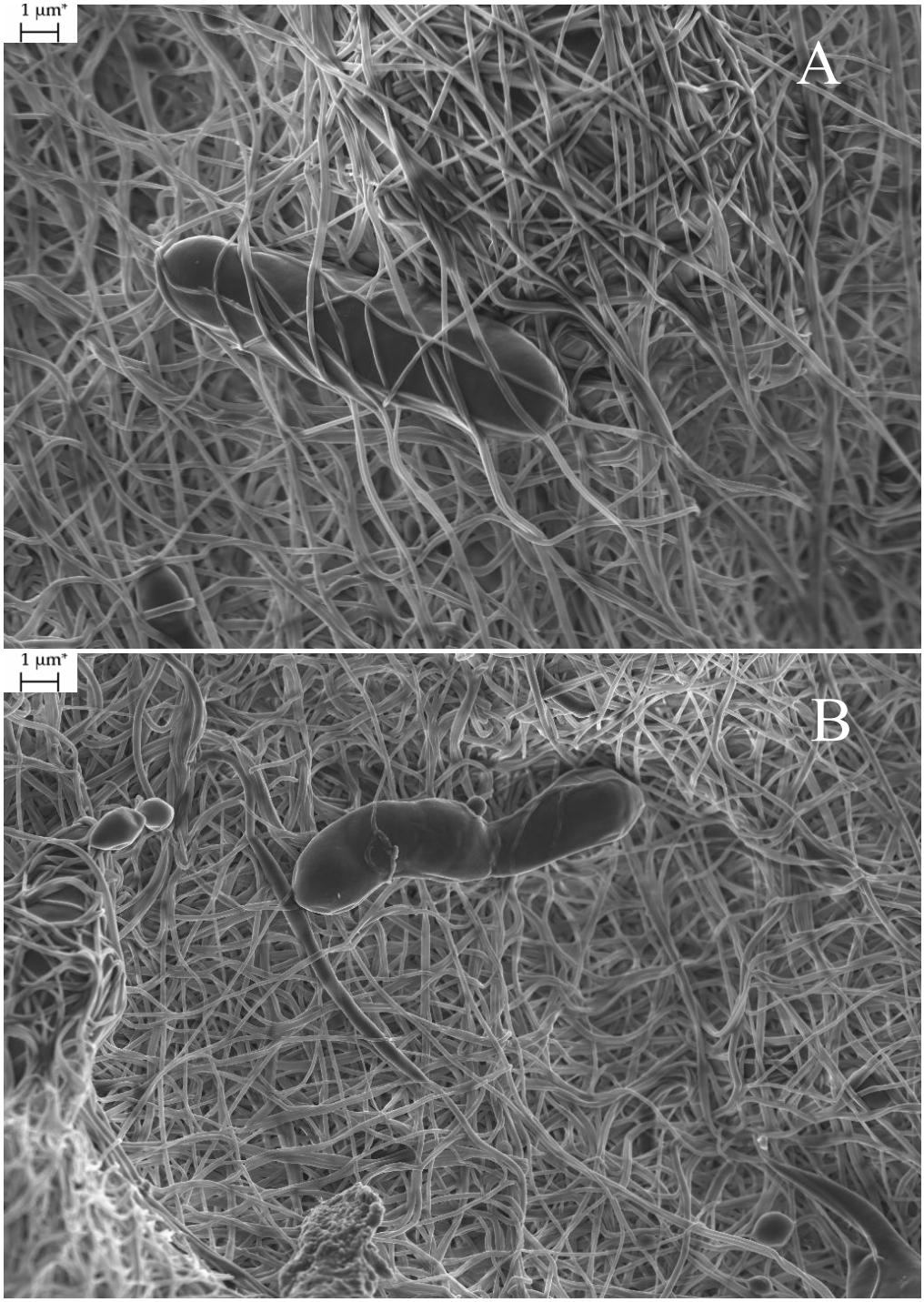

Figure 67- FE-SEM images of PCL mat with *Bacillus subitlis* (A) and *Pseudomonas stutzeri* cells embedded on fibers

The architecture of non-woven electrospun mats is defined not only by the solid fibers but equally by the interstitial voids. The pore size in such mats is inextricably linked to fiber diameter; theoretical and empirical models show that pore size typically scales linearly with fiber diameter[123,226]. For fibers in the 400 nm range, the resulting mean pore size is expected to be in the range of sub-micron to a few microns[123,226].

The results indicate that the matrix facilitates the physical entrapment of bacteria by the fibers (*Figure 67*). This observation confirms that the pore size distribution of the PCL mat overlaps with the dimensions of the bacterial cells. If pores were significantly smaller than the bacteria (e.g., < 200 nm), colonization would be restricted to a superficial layer on the mat, limiting the bacterial carrying capacity to the external surface area. Conversely, if pores were vastly larger, bacteria might pass through the filter unhindered, reducing retention efficiency[123].

The interconnected porous network functions as a depth filter, allowing bacteria to penetrate into the Z-axis of the scaffold. This three-dimensional colonization is advantageous for biotechnological applications for several reasons. First, it significantly increases the biomass loading capacity per unit of surface. Second, bacteria residing within the deep pores are shielded from external mechanical abrasion and desiccation. Third, the porous structure maintains permeability to nutrients and oxygen, which is essential for maintaining the metabolic activity of the immobilized biomass. The structural integrity of these pores is also influenced by the mechanics of the fibers; the high degree of crystallinity typically associated with electrospun PCL (~40-50%) provides the necessary stiffness to prevent pore collapse under the weight of the biomass or hydrostatic pressure.

Beyond the macro-morphology of fibers and pores, the micro-topography of the fiber surfaces plays a decisive role in microbial adhesion. Atomic Force Microscopy (AFM) analysis quantified this roughness, yielding an Sq (Root Mean Square roughness) of 0.25 ± 0.01 µm and an Sa (Arithmetic Mean roughness) of 0.19 ± 0.02 µm. These values provide a quantitative basis for the "topographical refuge" theory posited in the results.

The scale of roughness is paramount. A surface with Sa ~0.2 µm possesses features that are approximately 20-40% of the diameter of a typical bacterium. In the context of bacterial adhesion, this sub-micron regime is widely recognized as promoting attachment. Theoretically, a perfectly smooth surface offers limited contact points for a rigid bacterial cell wall. However, a surface with roughness features matching the scale of the cell allows the bacterium to maximize van der Waals forces and hydrophobic interactions by settling into the "valleys" of the texture.

Comparative literature analysis reinforces this finding. Studies on various polymeric surfaces, including PMMA and modified PCL, consistently show a positive correlation between surface roughness in the sub-micron range and bacterial retention. Specifically, rougher surfaces tend to accumulate higher bacterial loads because the irregularities increase the total available surface area for binding. Furthermore, the specific roughness values observed here (Sa ~0.19 µm) avoid the "superhydrophobic" regime often associated with nano-pillared textures (e.g., cicada wings or lotus leaves), where air entrapment on the nano-scale prevents bacterial contact entirely. Instead, the PCL mat's roughness invites colonization.

One of the most critical insights derived from the topographical analysis is the protection of adhered cells from hydrodynamic shear forces. In biotechnological applications such as bioreactors or filtration systems, fluids are in constant motion, exerting drag forces that seek to detach immobilized cells.

The "topographical refuge" hypothesis suggests that bacteria residing in the microscopic depressions of the rough PCL surface are shielded from the bulk fluid flow. Fluid dynamics dictate that a boundary layer exists at the solid-liquid interface where fluid velocity approaches zero. Surface roughness effectively increases the thickness of this quiescent sub-layer. Bacteria tucked into the rugosities of

the fibers (defined by the Sq of 0.25 μm) or the interstitial spaces between fibers operate below the shear plane.

This protection is vital during the reversible stage of bacterial adhesion. Initial attachment is often mediated by weak physicochemical forces (Lifshitz-van der Waals). If shear forces exceed these weak bonds, the bacteria detach before they can secrete the extracellular polymeric substances (EPS) required for irreversible attachment and biofilm formation. By providing a low-shear microenvironment, the rough PCL fibers allow the bacteria time to deploy adhesins and synthesize the extracellular matrix, thereby securing a permanent foothold. This mechanism explains why the mat is verified as an effective support for bacterial immobilization even in the presence of the hydrodynamic forces implied by biotechnological applications.

PCL mat revealed a Water Contact Angle (WCA) of 112° ± 3° and a Surface Free Energy (SFE) of 12.3 ± 1.2 mN/m.

PCL is intrinsically hydrophobic, with bulk films typically exhibiting WCAs in the range of 60° to 80°. The observation of a WCA of 112° indicates that the electrospun mat is significantly more hydrophobic than those reported in literature. The surface roughness amplifies intrinsic wettability.

Given the porous nature of the mat, this hydrophobicity is best described by the Cassie-Baxter model, which posits that a liquid droplet sits on a composite surface consisting of the solid fibers and the air pockets trapped between them. The high contact angle confirms that water does not easily penetrate the pores spontaneously; rather, the surface exerts a significant capillary pressure barrier. While this might suggest resistance to bacterial suspension, in practice, biological media often contain proteins and surfactants that lower surface tension, eventually allowing wetting. More importantly, this hydrophobicity is a primary driver for the adsorption of hydrophobic solutes and particles—including bacteria.

The reported SFE of 12.3 mN/m is low. For context, typical bulk polymers like polystyrene or PMMA have SFE values around 35-40 mN/m, and even Polytetrafluoroethylene (PTFE/Teflon), the benchmark for low energy, sits around 18-20 mN/m[223,227,228]. Bulk PCL is generally reported to have an SFE between 30 and 50 mN/m[229].

The value of 12.3 mN/m is consistent with superhydrophobic or highly fluorinated surfaces. In the absence of fluorination, this low value must be interpreted as the apparent surface free energy of the porous structure rather than the intrinsic molecular energy of PCL. The measurement technique (likely contact angle goniometry using probe liquids) probes the composite solid-air interface. Since the surface energy of air is effectively zero, the high porosity of the mat dilutes the surface energy contribution of the solid polymer.

The interaction between the bacteria and the PCL mat is governed by the minimization of interfacial free energy explained by Equation 9[227,230–232]:

Equation 9

$$\Delta G_{adh} = \gamma_{BS} - \gamma_{BL} - \gamma_{SL}$$

where γ_{BS}, γ_{BL}, and γ_{SL} are the interfacial tensions between the bacterium, the solid surface, and the liquid medium, respectively.

In an aqueous environment, when a hydrophobic bacterium approaches a hydrophobic surface (like the PCL mat with surface free energy of 12.3 mN/m), the water is displaced. This release of water molecules, making the adhesion process thermodynamically spontaneous and favorable.

The material characterization sets the stage for the biological interactions. The report confirms effective immobilization of Pseudomonas stutzeri and Bacillus subtilis, a result that highlights the interplay between the material's properties and the specific microbiological traits of these organisms.

Pseudomonas stutzeri, a Gram-negative bacterium, is ubiquitous in soil and marine environments and is well-regarded for its metabolic versatility, including denitrification and hydrocarbon degradation. A key characteristic of *P. stutzeri* is its variable cell surface hydrophobicity (CSH)[71]. Literature indicates that P. stutzeri can modulate its CSH depending on the carbon source; strains grown on hydrophobic substrates often exhibit increased surface hydrophobicity to facilitate attachment[70–72].

The hydrophobic PCL mat (12.3 mN/m) acts as a selective substrate for these hydrophobic phenotypes. The bacterium utilizes fimbriae and outer membrane proteins to overcome electrostatic repulsion (if present) and establish contact. Once attached, *Pseudomonas* species are prolific producers of extracellular polymeric substances (EPS), particularly alginate and various polysaccharides, which anchor the cells to the substrate and to each other. The rough, nanofibrous topography provides an ideal scaffold for this EPS matrix to interlock, effectively "gluing" the biofilm to the mat.

Bacillus subtilis, a Gram-positive bacterium, presents a different adhesion profile. It is capable of forming highly structured biofilms characterized by amyloid-like fibers (TasA) and a hydrophobicity-promoting surface protein (BslA) that forms a water-repellent coat over the biofilm[64–67].

Furthermore, *B. subtilis* is a spore former[64,68,233]. Bacterial spores are significantly more hydrophobic than their vegetative counterparts. If the immobilization process involved spores, the thermodynamic drive for adhesion to the hydrophobic PCL would be even stronger than for vegetative cells. Additionally, B. subtilis produces surfactin, a potent cyclic lipopeptide biosurfactant. Surfactin lowers the surface tension of the surrounding liquid, facilitating the wetting of the hydrophobic PCL fibers by the bacterial culture. This surfactant activity likely aids in the penetration of the bacterial cells into the deeper pores of the mat, ensuring that the physical entrapment is not just superficial but volumetric.

The combination of hydrophobic surface proteins, spore hydrophobicity, and surfactant-mediated wetting explains the immobilization observed in the adhesivity test (see next paragraphs). The morphology of the 420 nm fibers supports the rod-shaped B. subtilis cells (typically 0.5-1.0 µm diameter) without causing membrane rupture, allowing them to proliferate and differentiate.

Biodegradation Kinetics[234–236]

The most striking biological finding is the divergence in degradation rates: Pseudomonas stutzeri caused partial degradation over 30 days, while Bacillus subtilis effected complete degradation within 14 days. This disparity elucidates the enzymatic mechanisms at play and defines the operational lifespan of the scaffold.

PCL degradation is primarily an enzymatic process involving the hydrolysis of the ester linkages in the polymer backbone. This reaction yields oligomers and eventually 6-hydroxyhexanoic acid, an intermediate that can be metabolized via the β-oxidation pathway or the TCA cycle. Crucially, because enzymes are macromolecules that cannot diffuse into the crystalline regions of the polymer, enzymatic degradation is a surface erosion process.

The rate of this erosion is proportional to the surface area. The electrospun mat, with its 420 nm fibers, presents a specific surface area order of magnitude higher than a bulk film. This amplifies the degradation rate significantly. However, the rate-limiting step is the availability and specificity of the enzymes produced by the colonizing bacteria.

The rapid degradation (14 days) by B. subtilis is attributed to its aggressive enzymatic arsenal. B. subtilis is a known industrial producer of extracellular lipases (e.g., LipA, LipB) and esterases. PCL, being an aliphatic polyester, is a prime substrate for these lipases.

The degradation mechanism likely follows a "synergistic destruction" pathway:

1. Interfacial Activation: Lipases are interfacially activated enzymes; they require a hydrophobic interface to open their active site "lid." The hydrophobic PCL surface (12.3 mN/m) provides a massive activating interface for the secreted enzymes.
2. Surfactin Enhancement: As noted, B. subtilis produces surfactin. Surfactants are known to enhance the enzymatic degradation of polyesters by improving the contact between the aqueous enzyme and the hydrophobic polymer.
3. Crystallinity Attack: While enzymes attack amorphous regions first, the high concentration of lipases from B. subtilis appears capable of rapid erosion that destabilizes the crystalline domains as well. The "complete degradation" implies that the bacterium successfully mineralized the polymer carbon into CO_2 and biomass.

This result aligns with literature showing B. subtilis causing significant weight loss and surface erosion in PCL within short timeframes, often outpacing other organisms.

In contrast, Pseudomonas stutzeri exhibited a much slower degradation profile. While Pseudomonas species are capable of degrading plastics (especially PHAs) and possess esterases, their specific activity against semi-crystalline PCL appears lower than that of B. subtilis in this specific context.

This "partial degradation" suggests that P. stutzeri may utilize PCL as a secondary or starvation-induced carbon source rather than a primary substrate, or that its specific lipases have lower turnover numbers for the high-molecular-weight PCL used in the mat. For biotechnological applications, this is a feature, not a bug. It implies that a P. stutzeri-loaded PCL mat can function as a stable bioreactor component for weeks (e.g., for denitrification) without catastrophic structural failure.

The convergence of these physical and biological properties validates the use of the PCL mat for specific applications as a high-efficiency bacterial carrier. The high surface area supports high biomass density, the roughness prevents washout in continuous flow systems, and the hydrophobicity enables selective immobilization.

Furthermore, the biodegradation data outline a sustainable lifecycle. The material does not require incineration or landfilling. At the end of its useful life, the PCL mat can be exposed to a B. subtilis-

rich composting environment. The demonstrated 14-day degradation capability ensures rapid mineralization, converting the synthetic polymer into benign biomass and CO_2. This programmable degradation—stable with one organism, fleeting with another—is a cornerstone of next-generation green materials.

11.5 Adhesion of bacterial species and viability over time

The primary objective of this phase was to assess the capacity of electrospun Polycaprolactone (PCL) mats to immobilize bacterial populations and support their viability over a long-term storage period (*Figure 68*). The spectrofluorimetric analysis revealed that the PCL mats acted as highly effective scaffolds for bacterial immobilization. A notable observation from the quantitative data was the significant increment in bacterial density on the mat surface compared to the initial inoculum. While the standardized inoculum was introduced at a concentration of 1 x 10^7 CFU/mL, the final adhered populations consistently ranged between 1 x 10^8 and 1 x 10^9 CFU/mL.

This increase, occurring despite the use of a physiological solution designed to limit proliferation, can be attributed to a physical accumulation effect. The electrospun nanofibers possess an exceptionally high specific surface area-to-volume ratio, which allows the mat to act as a filter, effectively concentrating bacteria from the bulk liquid suspension onto the solid scaffold over the 20-hour incubation period. Furthermore, although the physiological solution creates a nutrient-poor environment, the metabolic versatility of Bacillus subtilis and Pseudomonas stutzeri likely allowed for limited cryptic growth or oligotrophic survival, utilizing trace nutrients or cellular debris to initiate early-stage biofilm formation. This confirms that the adhesion forces between the bacterial cell walls and the hydrophobic PCL fibers are strong enough to capture and retain a biomass density significantly higher than that of the surrounding environment, even after rigorous washing steps.

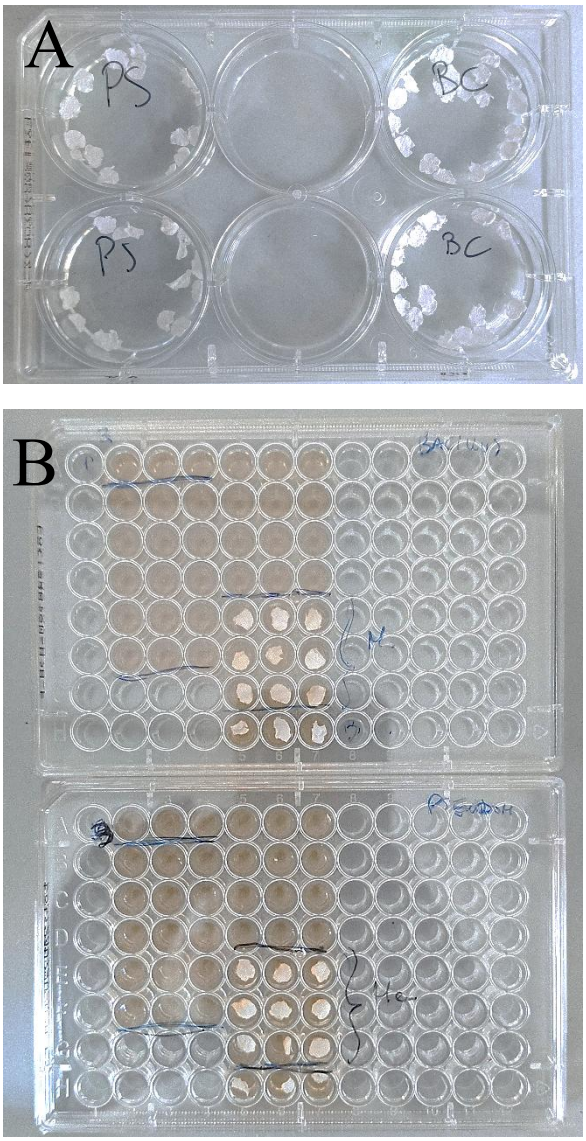

Figure 68- (A) Samples of PCL mat during incubation on bacterial suspension and (B) 96-well plates before the fluorimeter test.

Bacillus subtilis

The first bacterial species exhibited a high degree of biological resilience and a distinct sensitivity to the specific storage conditions applied (*Figure 69*). In the control samples tested immediately after adhesion (Fresh), the viability was recorded at approximately 90%, indicating that the initial interaction with the PCL surface did not induce immediate cytotoxic effects or membrane damage. However, the conservation environment played a critical role in maintaining this viability over the two months. Samples stored in liquid media—specifically Physiological Solution (NaCl) and Phosphate Buffer Solution (PBS)—experienced a significant decline in viability, dropping to approximately 45%. This reduction suggests that while the bacteria remained physically attached to the mats, the prolonged exposure to nutrient-depleted buffer solutions likely induced starvation or osmotic stress, leading to membrane compromise and cell death.

In contrast, the dry conservation methods yielded superior results. The samples stored as dry mats retained a viability of approximately 70%, likely due to the reduction in metabolic activity, which slows down cell death; however, desiccation stress still impacted a portion of the population. The most notable result was observed in the freeze-dried samples, which maintained a viability of approximately 95%, surpassing even the fresh control. This exceptional survival rate validates the efficacy of the modified freeze-drying protocol. The inclusion of a specific cryoprotectant mixture containing skim milk, sucrose, and monosodium glutamate likely formed a stabilizing glass-like matrix around the cells. This matrix protected the bacterial membranes and proteins from mechanical damage caused by ice crystal formation during the freezing process and structural collapse during sublimation.

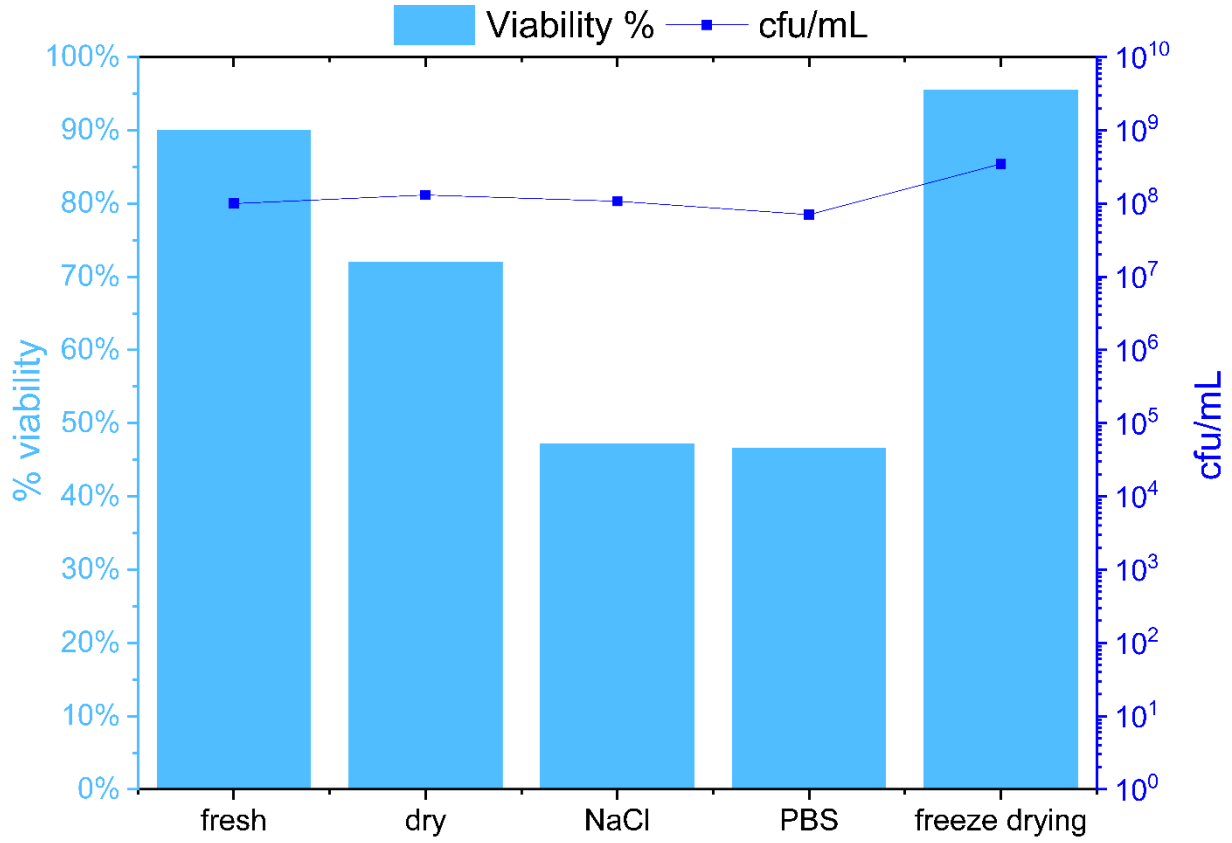

Figure 69- Results of Bacillus subtilis adhesion on PCL mats and viability over time with different conservation methods

Pseudomonas stutzeri

The second bacterial species presented a fundamentally different behavioural profile compared to the first (*Figure 70*). While the physical adhesion to the mats was equally high—benefiting from the same accumulation effect described previously—the biological viability was consistently low across all experimental conditions. The fresh control samples exhibited a viability of only 30% to 35%, suggesting that the primary stress occurred during the initial adhesion phase rather than during storage. This low baseline indicates that this specific species may be particularly sensitive to the

hydrophobic nature of the PCL surface, or that the shear forces exerted during the washing protocol selectively damaged this strain's membranes.

Because the initial population on the "fresh" samples was already largely compromised, the subsequent conservation methods showed little statistical variation. The viability remained relatively flat between 30% and 40% for the dry, physiological solution, PBS solution, and freeze-dried samples. Unlike the first species, the freeze-drying process did not yield a high percentage of live cells because the cryoprotectants were unable to recover cells that were already damaged or dead before the lyophilization process. This highlights that the limiting factor for this species is not the long-term storage method, but the initial biocompatibility at the bacteria-material interface.

Anyway, even though they're less lively, the number of bacteria cells that are still alive and able to do their thing is still high (around 10^8 cfu/mL), thanks there are loads of them stuck to the surface (cfu/mL).

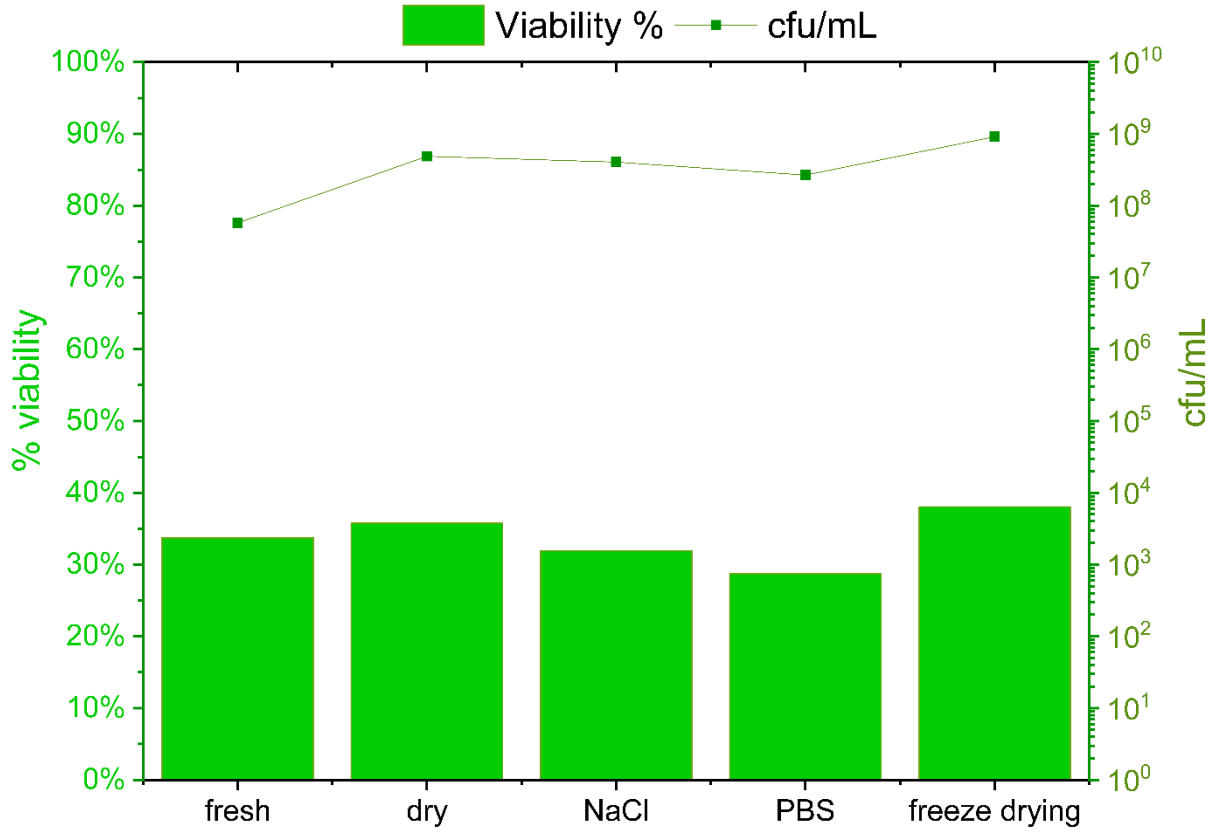

Figure 70- Results of Pseudomonas stutzeri adhesion on PCL mats and viability over time with different conservation methods

Conclusions

In conclusion, the electrospun Polycaprolactone (PCL) mat characterized in this study represents interface between synthetic materials science and microbiology. Morphologically, the high-surface-area mesh effectively supports bacterial suspension and entrapment, while the sub-micron roughness provides topographical shield for the bacteria from shear forces during initial adhesion. The low surface free energy of mat creates a driving force for hydrophobic bacterial attachment, which is complemented biologically by a tunable degradation profile—offering stability for *Pseudomonas stutzeri* for over 30 days, yet a rapidly compostable pathway for *Bacillus subtilis* in under 14 days. These collective findings confirm the material's potential as a versatile, sustainable platform for microbial immobilization, capable of supporting long-term biotechnological processes while ensuring a predetermined, environmentally benign end-of-life pathway.

The comparative analysis of these results demonstrates that electrospun PCL mats are effective as physical carriers, capable of concentrating biomass to densities exceeding that of the initial inoculum for both *Bacillus subtilis* and *Pseudomonas stutzeri*. However, the maintenance of biological activity within this high-density architecture is strictly species dependent. For *Bacillus subtilis*, which demonstrated high physiological resilience, the optimized freeze-drying protocol utilizing a milk-sucrose-glutamate cryoprotectant proved to be the superior conservation strategy. This method produced shelf-stable bioactive materials capable of preserving near-total population viability for at least two months. Conversely, regarding *Pseudomonas stutzeri*, the observed sensitivity suggests that the native hydrophobic interface may be a limiting factor. Therefore, future research should focus on surface modification strategies to obtain a more hydrophilic, physiologically suitable interface. Such investigations are necessary to verify whether tailoring the surface chemistry can improve bacterial adhesion conditions and mitigate the viability loss observed upon contact for sensitive Gram-negative species.

Chapter 12.
Enhancing properties and water resistance of PEO-based electrospun nanofibrous mats by crosslinking

12.1 Introduction

Poly(ethylene oxide) (PEO) has emerged as one of the most widely utilized polymers in electrospinning due to its biocompatibility, low toxicity, and good spinnability in aqueous solutions (see Chapter 4). Its versatility makes it a candidate of choice for diverse applications, including wound dressing, drug delivery systems, and tissue engineering scaffolds. Furthermore, PEO serves a crucial role as a "carrier polymer," facilitating the electrospinning of materials that are otherwise difficult to process, such as polysaccharides like Agarose and Agar.

However, a fundamental limitation restricts the broader applicability of PEO-based nanofibrous mats: their water solubility (Chapter 4). Upon contact with aqueous environments or physiological fluids, pure PEO fibers rapidly dissolve, leading to the immediate loss of the nanofibrous architecture and porosity[237]. This lack of structural endurance in wet conditions poses a significant challenge, particularly for applications requiring sustained mechanical integrity or controlled release profiles. Consequently, developing effective stabilization strategies to render PEO mats water-resistant, while preserving their morphology, is a critical area of research[237].

The primary objective of this chapter is to investigate a method for crosslinking PEO-based electrospun mats to overcome their susceptibility to water dissolution. While PEO serves as an excellent model system, the overarching aim of this project extends beyond the synthetic polymer itself[238,239]. A critical goal is to identify a crosslinking strategy capable of preventing fiber collapse in complex polysaccharide-PEO blends, specifically Agar/PEO and Agarose/PEO systems. Since these polysaccharides rely on the PEO carrier for processability, stabilizing the PEO component is essential to maintain the structural integrity of the composite fibers in wet environments.

To achieve this, we introduce a semi-interpenetrating network approach using an acrylic monomer, Trimethylolpropane trimethacrylate (TMPTMA), initiated by Benzoyl Peroxide (BPO). TMPTMA was selected for its multifunctional nature, which allows for the formation of a rigid, three-dimensional network that can entrap and stabilize the linear polymer chains[240]. The experimental design focuses on optimizing the material composition by evaluating four distinct weight formulations - PEO/TMPTMA ratios of 1:1, 2:1, 3:2, and 4:1 - to determine the minimum concentration of monomer required to achieve effective insolubility without compromising fiber quality.

The study also seeks to compare the efficacy of two distinct reaction initiation methods for the radical polymerization of TMPTMA. The first method utilizes UV radiation within an ad hoc chamber for ten and twenty minutes, while the second employs a thermal crosslinking treatment in an oven at 40 °C, as described in paragraph 6.12. Following these treatments, the fiber morphology is investigated

using Scanning Electron Microscopy (SEM). The efficacy of the crosslinking is validated by immersing the mats in water for five minutes. To accurately visualize the wet-state morphology and ensure that any observed structural integrity is real rather than an artifact of drying, a lyophilization process is applied post-immersion.

12.2 PEO/TMPTMA mats

Solutions preparation

The preparation of the electrospinning precursors was designed to establish a comparative framework between unmodified and chemically crosslinkable matrices. Initially, a solution was established by dissolving Poly(ethylene oxide) (PEO, Mw = 300 kDa) in distilled water to yield a concentration of 10% (w/v); this unmodified solution served as the "blank" control for all subsequent morphological and physicochemical benchmarking. To obtain the crosslinked semi-interpenetrating networks (semi-IPNs), the acrylic monomer Trimethylolpropane trimethacrylate (TMPTMA) was integrated into the aqueous PEO system. To facilitate radical polymerization, Benzoyl Peroxide (BPO) was introduced as the initiator, with its loading strictly maintained at 2% (w/w) relative to the monomer content. The experimental protocol was structured to systematically evaluate the impact of crosslinking on network formation by varying the PEO-to-TMPTMA mass ratio across four distinct formulations: 1:1, 2:1, 3:2, and 4:1 (w/w). Within this experimental matrix, the quantity of PEO was fixed at 1.0 g per 10 mL of solvent for all samples, ensuring that any observed deviations in fiber performance or stability could be attributed only to the variation of the TMPTMA crosslinker concentration.

Solutions characterization

The rheological behavior of the polymer solutions constitutes a critical parameter governing the electrospinning process, as it directly influences jet initiation, stability, and the final morphology of the fibers (Chapter 2). To assess the impact of the acrylic monomer on the viscoelastic properties of the PEO matrix, the steady-shear viscosity of both the neat PEO solution and the PEO/TMPTMA blends was analyzed as a function of shear rate. As illustrated in the viscosity curves (*Figure 71*), all formulations exhibited characteristic non-Newtonian, shear-thinning (pseudoplastic) behavior. At low shear rates, spanning approximately 0.001 to 0.1 s^{-1}, the solutions displayed a distinct Newtonian plateau where viscosity remained independent of the applied shear. This region corresponds to the zero-shear viscosity (η_0), reflecting the equilibrium state of the polymer chains where the rate of entanglement disruption is balanced by the rate of re-entanglement. As the shear rate increased beyond 1 $s^{-1,}$ a marked reduction in viscosity was observed for all samples. This transition occurs because the applied shear forces orient the polymer chains along the flow direction and disentangle the polymer coils faster than they can re-establish equilibrium, a behavior that is generally favourable for electrospinning as it facilitates the flow of the solution through the spinneret capillary.

A closer examination of the low-shear region reveals a systematic dependency of viscosity on the concentration of the crosslinking agent. The pure PEO solution (10% w/v) exhibited the highest zero-shear viscosity, recorded at approximately 13.1 Pa·s. Upon the incorporation of the TMPTMA monomer, a progressive decrease in viscosity was observed as the monomer content increased. The formulations followed a clear trend of $\eta_{PEO} > \eta_{4:1} > \eta_{3:2} > \eta_{2:1} > \eta_{1:1}$ with the 1:1 formulation, containing the highest loading of monomer, displaying the lowest zero-shear viscosity at roughly 10.9 Pa·s. (Table 21).

Table 21- Zero-viscosity of PEO/TMPTMA water solutions

Viscosity	PEO 10% w/v	PEO/TMPTMA 4:1	PEO/TMPTMA 3:2	PEO/TMPTMA 2:1	PEO/TMPTMA 1:1
η_0 [Pa s]	13,1	12,8	12,2	11,1	10,9

This reduction in bulk viscosity can be attributed to two concurrent physical mechanisms resulting from the introduction of the low-molecular-weight monomer into the high-molecular-weight polymer solution[237,240]. First, the addition of liquid TMPTMA increases the total volume of the solution while the mass of PEO remains fixed; this effectively dilutes the polymer concentration per unit volume, thereby reducing the density of chain entanglements responsible for high viscosity. Second, the small TMPTMA molecules likely exert a plasticizing effect on the PEO matrix. By dispersing between the long polymer chains, the monomer increases the free volume within the solution and acts as a lubricant, reducing intermolecular friction and allowing the PEO chains to slide past one another more easily under shear. Despite this reduction, the viscosity values for all PEO/TMPTMA blends remained within the same order of magnitude (10–13 Pa·s). This range is sufficient to maintain a stable polymeric jet during electrospinning, suggesting that the addition of the crosslinker, even at the highest 1:1 ratio, does not compromise the fundamental spinnability of the system.

Beyond the differences in absolute viscosity values, the rheological profiles reveal a subtle but distinct shift in the onset of non-Newtonian behavior, marked by the critical shear rate ($\dot{\gamma}c$)[241]. This parameter defines the transition point where the applied shear rate exceeds the relaxation rate of the polymer chains, forcing them to orient and disentangle rather than recoil into their equilibrium random coil conformation[237,242].

In the pure PEO solution, the transition from the Newtonian plateau to the shear-thinning region occurs earlier (at a lower shear rate) compared to the monomer-loaded blends. As the concentration of TMPTMA increases (moving from the 4:1 to the 1:1 ratio), the Newtonian plateau extends slightly further to the right, indicating a shift of $\dot{\gamma}c$ to higher values. This delayed onset of shear thinning in the presence of higher monomer concentrations corroborates the plasticization mechanism proposed earlier.

By reducing the entanglement density and increasing the free volume, the small TMPTMA molecules enhance the mobility of the PEO chains. This increased mobility allows the polymer chains to relax faster under stress. Consequently, a higher shear rate is required to disrupt the equilibrium entanglement network of the plasticized PEO/TMPTMA blends compared to the more rigid, heavily entangled network of the pure PEO solution. This suggests that the addition of the monomer not only lowers the bulk viscosity but also dynamically stabilizes the random coil conformation against shear forces up to higher deformation rates.

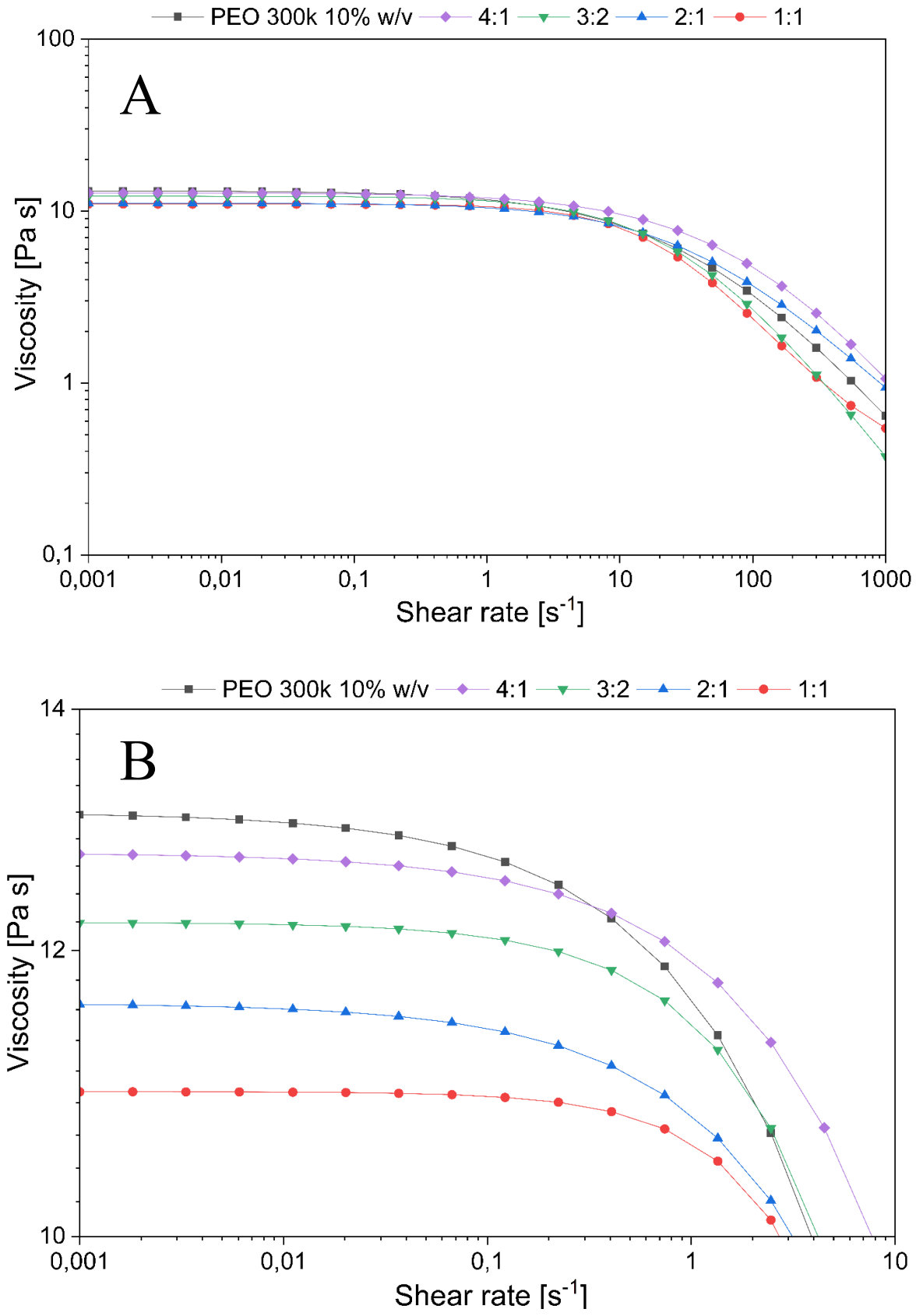

Figure 71- (A) Rheological curves of PEO 10%w/v pure solution and blend solutions with TMPTMA with four different ratios (4:1, 3:2, 2:1, 1:1). (B) Magnification of the curves in the range 0,001-10 s^{-1}.

Electrospinning process

To fabricate the nanofibrous mats, the prepared solutions were processed via electrospinning using a standardized set of operating conditions. This approach was adopted to minimize processing-induced variability and ensure that any observed morphological differences were strictly attributable to solution composition. Each solution was loaded into a syringe fitted with a stainless-steel spinneret having an inner diameter of 0.4 mm. A high-voltage power supply was used to apply a potential of 17 kV to the needle tip, generating an electrostatic field sufficient to overcome the surface tension of the polymer solution. The feed rate was maintained constant at 1.0 mL/h using a syringe pump, and the resultant fibers were deposited onto a grounded collector plate positioned at a fixed working distance of 20 cm. By rigidly controlling the voltage, flow rate, and tip-to-collector distance across all experimental groups (blank and PEO/TMPTMA blends), the influence of processing parameters on fiber diameter and mat architecture was limited.

12.3 Mats characterization

Morphological characterization and water stability assessment

The morphological evolution of the nanofibrous mats, from the as-spun state through the crosslinking process and subsequent water immersion, provides the definitive validation of the stabilization strategy. Scanning Electron Microscopy (SEM) analysis was employed to monitor the structural integrity of the fibers across the four varying PEO/TMPTMA ratios (4:1, 3:2, 2:1, and 1:1).

The PEO electrospun mats (control) exhibited a smooth, cylindrical, and defect-free morphology with a random orientation and high uniformity (*Figure 72*). However, the introduction of the TMPTMA monomer induced noticeable morphological variations in the as-spun (dry) state prior to any crosslinking. While all formulations remained spinnable, a progressive loss of homogeneity was observed as the concentration of the acrylic monomer increased (*Figure 73-74-75-76*). The formulation with the lowest monomer content (4:1) retained a morphology closely resembling the neat PEO reference, displaying smooth and regular fibers. In contrast, as the ratio shifted towards 1:1 (highest monomer content), the mats exhibited reduced homogeneity and an increased presence of defects (Panels A). This suggests that the high loading of the liquid monomer slightly disrupted the stability of the electrospinning jet, leading to irregular fiber diameters and less uniform deposition even before the curing step[103,104].

As reported in paragraph 6.12, following the electrospinning process, the mats were subjected to the designated crosslinking protocols, UV irradiation (10 and 20 minutes), and thermal curing at 40 °C. SEM analysis of the crosslinked samples prior to water immersion (Panels B, C, and D) confirmed that the chosen stabilization methods were non-destructive to the nanofibrous architecture. Across all monomer concentrations, the fibers retained the cylindrical morphology and porosity observed in the as-spun precursor mats. Notably, the thermal treatment at 40 °C was proven to be sufficiently mild to avoid the melting or coalescence of the PEO fibers (typically occurring around 60–65 °C). Similarly, UV exposure did not induce visible degradation or fiber fracture. This structural preservation is a prerequisite for the subsequent functionality of the mats, ensuring that the high surface-area-to-volume ratio is maintained in the dry state before any contact with aqueous media.

The efficacy of the crosslinking network was tested via water immersion followed by lyophilization to preserve the wet-state structure. The results revealed a distinct superiority of the thermal crosslinking method over UV irradiation in preserving the fibrous architecture.

The UV-induced crosslinking displayed a strong time-dependency. Samples treated for only 10 minutes generally failed to maintain structural integrity, resulting in partial dissolution or the formation of fused, film-like structures (Panels B'). This suggests that 10 minutes was insufficient to generate the radical density required for complete network formation. Extending the exposure to 20 minutes significantly improved stability. Within the UV-treated group, the 2:1 and 3:2 ratios proved to be the optimal formulations. In these samples (Panels C'), the fibers successfully resisted dissolution and maintained their individual definition, whereas the 1:1 and 4:1 UV-treated samples exhibited higher degrees of swelling or fusing.

While all thermally treated mats demonstrated water resistance, the 4:1 PEO/TMPTMA ratio was identified as the optimal formulation by the superior morphological homogeneity; as noted in the dry-state analysis, higher monomer concentrations (1:1) introduced defects and irregularities into the fiber structure. The 4:1 formulation contains sufficient TMPTMA to ensure complete insolubility via thermal curing, yet the monomer loading is low enough to preserve the smooth, uniform, and defect-free architecture characteristic of pure PEO.

Regarding the UV crosslinking method specific conclusions can be drawn for its optimization. The UV process exhibited a narrower processing window, proving effective only at intermediate monomer concentrations (3:2 and 2:1) combined with extended exposure times (20 minutes). It failed to effectively stabilize the preferred 4:1 formulation, likely because the lower monomer density combined with the line-of-sight limitations of UV radiation resulted in an insufficient crosslinking degree. Consequently, the 4:1 thermal protocol represents the most robust and scalable strategy for producing stable, high-quality hydrogel nanofibers.

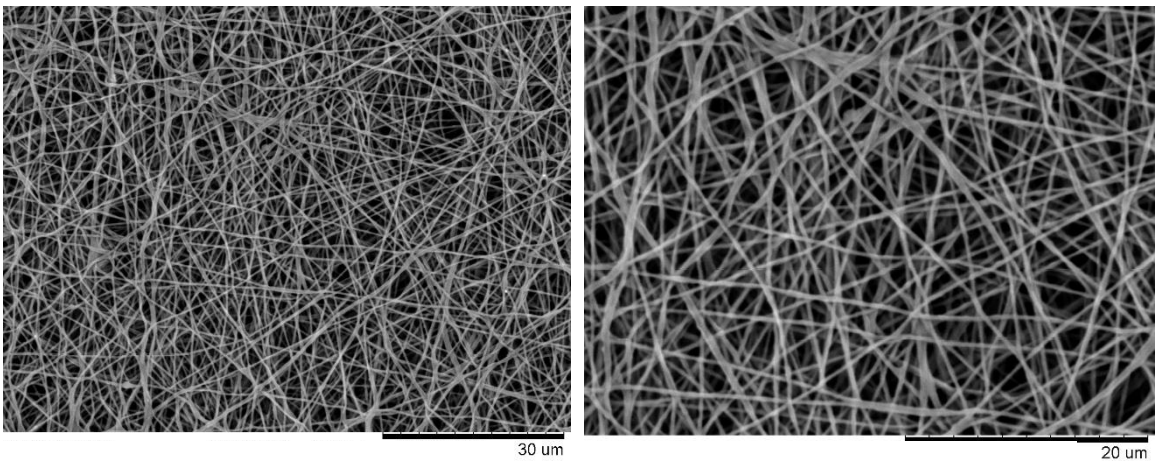

Figure 72- SEM images of PEO 10% w/v mat (blank)

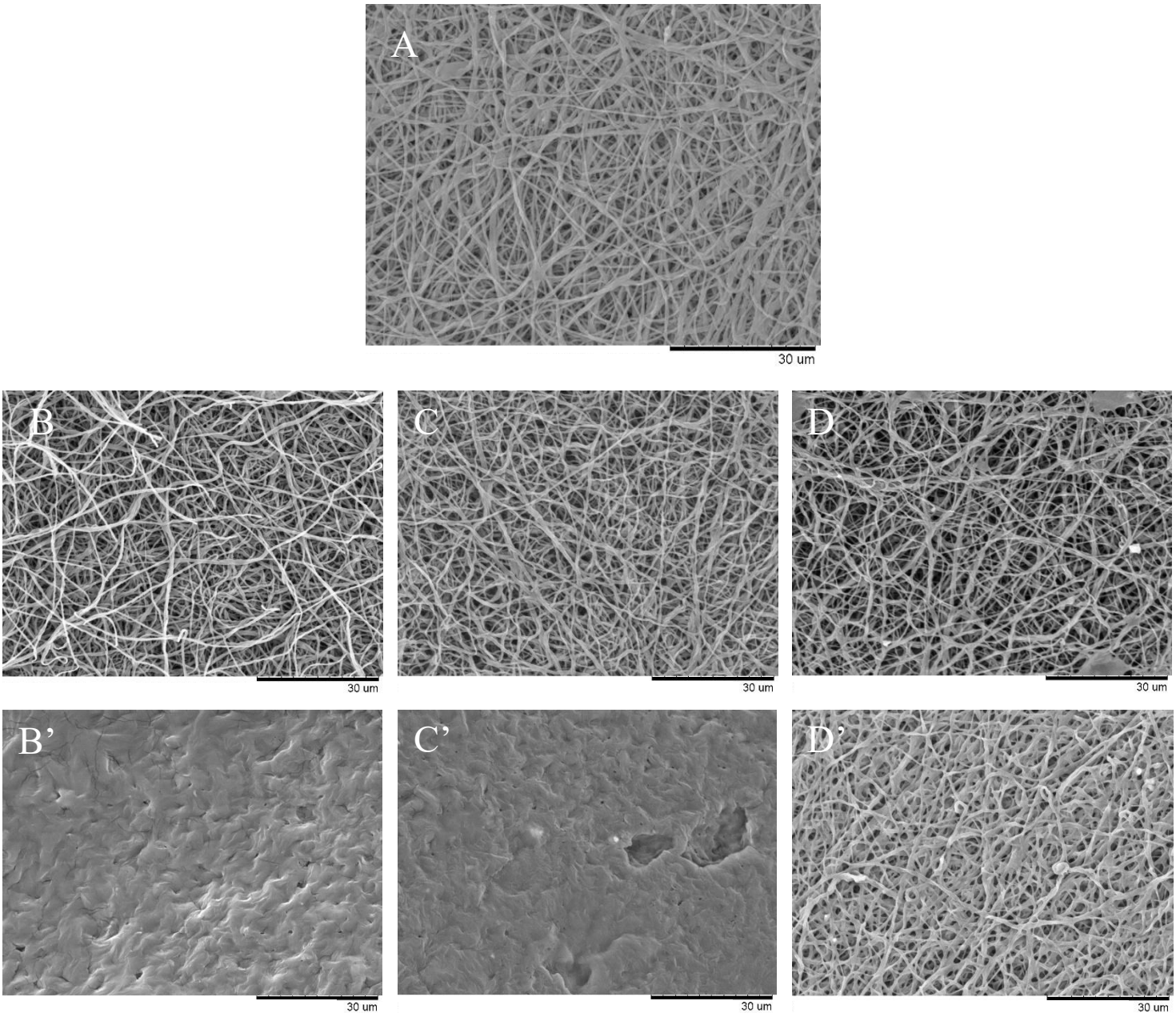

Figure 73- SEM images of PEO/TMPTMA 4:1 mat (A) before crosslinking, (B) after UV-Vis crosslinking (10 minutes), (C) after UV-Vis crosslinking (20 minutes), (D) after thermal crosslinking and after water immersion and lyophilization for each crosslinking method (B', C', D')

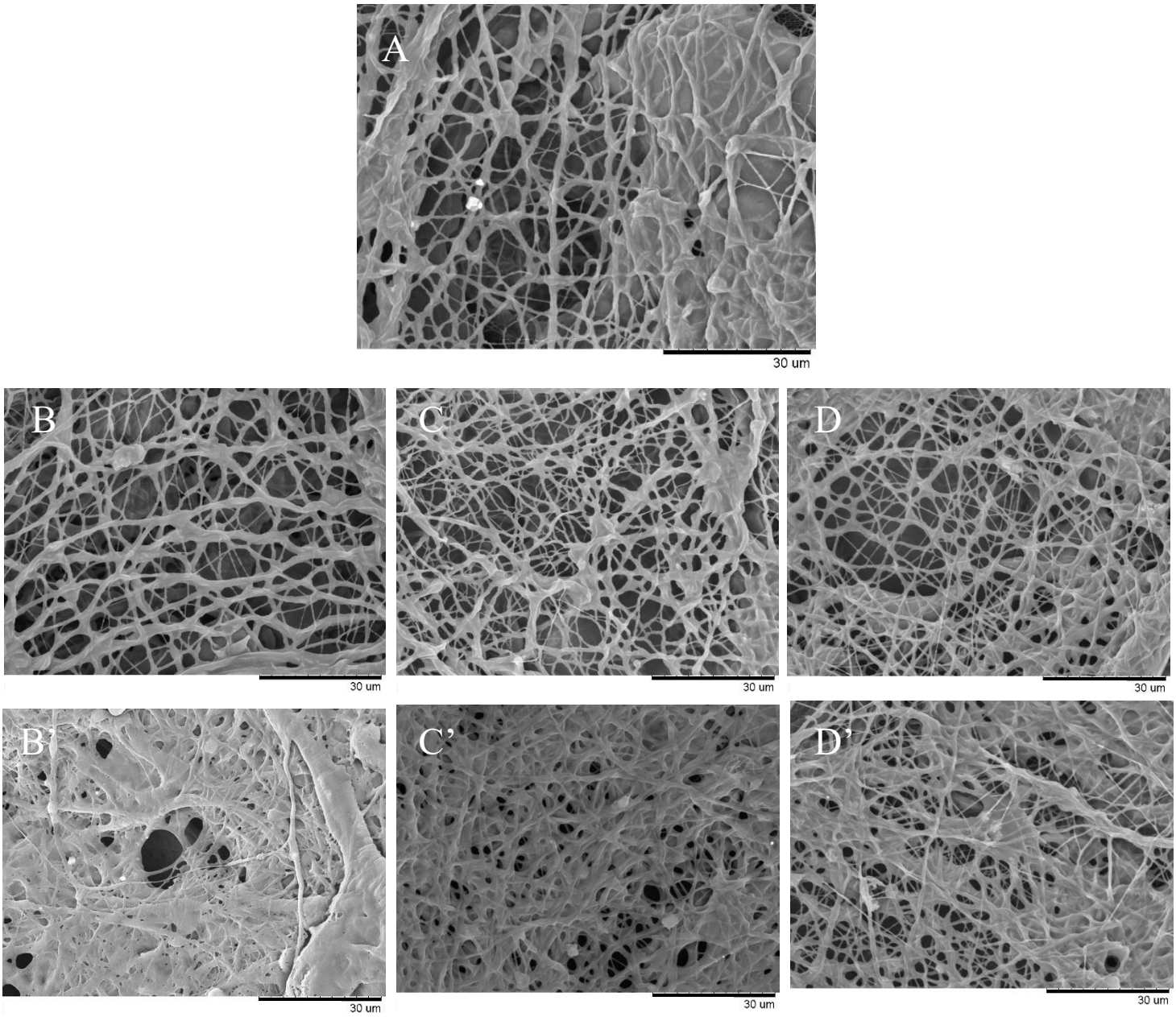

Figure 74- SEM images of PEO/TMPTMA 3:2 mat (A) before crosslinking, (B) after UV-Vis crosslinking (10 minutes), (C) after UV-Vis crosslinking (20 minutes), (D) after thermal crosslinking and after water immersion and lyophilization for each crosslinking method (B', C', D')

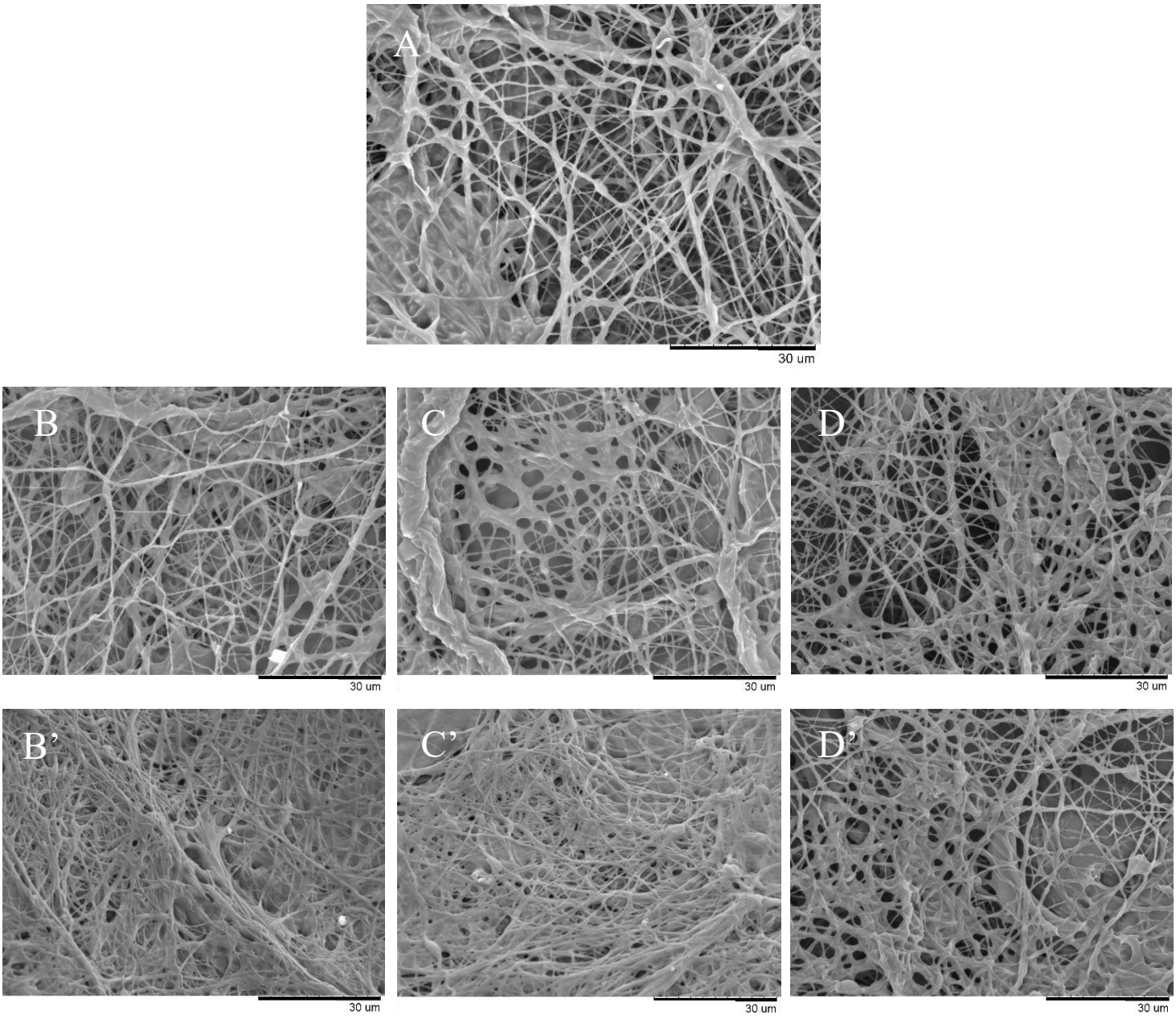

Figure 75- SEM images of PEO/TMPTMA 2:1 mat (A) before crosslinking, (B) after UV-Vis crosslinking (10 minutes), (C) after UV-Vis crosslinking (20 minutes), (D) after thermal crosslinking and after water immersion and lyophilization for each crosslinking method (B', C', D')

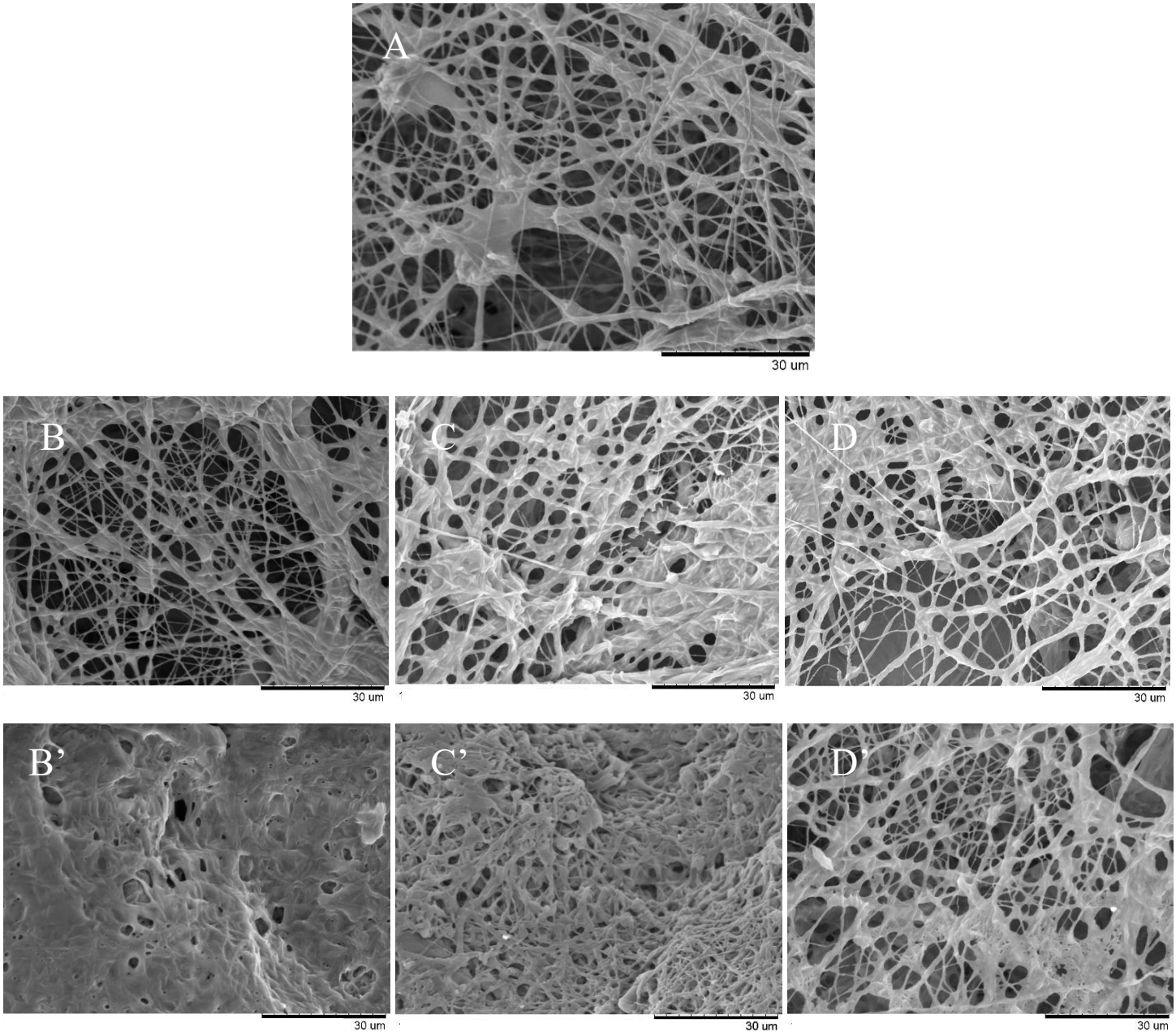

Figure 76- SEM images of PEO/TMPTMA 1:1 mat (A) before crosslinking, (B) after UV-Vis crosslinking (10 minutes), (C) after UV-Vis crosslinking (20 minutes), (D) after thermal crosslinking and after water immersion and lyophilization for each crosslinking method (B', C', D')

Conclusions

This study successfully established a methodology for the stabilization of Poly(ethylene oxide) (PEO) nanofibrous mats, overcoming the water solubility that limits their application in water environments. By implementing a semi-interpenetrating network (semi-IPN) strategy using Trimethylolpropane trimethacrylate (TMPTMA) as the crosslinker and Benzoyl Peroxide (BPO) as the initiator, we were able to transform the water-soluble PEO into a stable hydrogel network while preserving its nanofibrous morphology.

The experimental results highlighted a critical relationship between the crosslinker concentration, the curing method, and the final fiber quality. While UV-induced crosslinking demonstrated feasibility—particularly for the 3:2 and 2:1 ratios after 20 minutes of exposure—it exhibited a narrow processing window and was less effective for lower monomer concentrations. In contrast, thermal crosslinking at 40 °C emerged as the superior activation method, yielding chemically stable mats across all tested formulations (1:1 to 4:1).

Among the thermally treated samples, the 4:1 PEO/TMPTMA formulation was identified as the optimal system. It offered the ideal balance between structural integrity and morphological quality, providing complete water resistance without the loss of fiber homogeneity observed at higher monomer loadings. This protocol effectively preserves the high porosity and specific surface area of the electrospun mats after water immersion, validating the semi-IPN approach as a viable route for producing water-stable PEO-based hydrogel nanofibers.

Building upon the stabilization protocols defined in this work, several ways for further investigation are currently being pursued to deepen the understanding of the crosslinking mechanism and expand its applicability.

Furthermore, the primary motivation for developing this crosslinking strategy was to establish a foundational method for stabilizing complex biopolymer blends. Consequently, the immediate next phase of this research involves turning the optimized protocols to Polysaccharide-PEO composite mats, specifically Agar/PEO and Agarose/PEO systems. Future experiments will test the efficacy of the thermal crosslinking method on these blends, utilizing the varying PEO/TMPTMA ratios established in this study (4:1, 3:2, etc.) to determine the minimum crosslinker concentration required to prevent the collapse of the polysaccharide fibers in wet environments.

Conclusions

This doctoral thesis has demonstrated the efficacy of the electrospinning technique in generating advanced nanostructured materials tailored for the conservation of Cultural Heritage. The primary aim was to address the limitations of traditional restoration methods by exploiting sustainable, nanofibrous mats capable of performing specific cleaning, disinfection, and biocleaning tasks. In the context of surface cleaning, the research successfully fabricated biopolymer-based mats acting as retentive sponges for the controlled release of organic solvents. Specifically, Agar and Agarose were successfully electrospun when blended with high molecular weight Poly(ethylene oxide), with a 50/50 ratio proving optimal for fiber uniformity. These mats demonstrated chemical stability in non-polar organic solvents and a biphasic release mechanism, ensuring a rapid initial transfer of solvent followed by a slow, controlled release that protects sensitive surfaces. The practical application on a 16th-century wood painting validated these findings, where both Poly(vinyl alcohol) and Agarose/PEO mats effectively removed aged varnish and repainting layers using benzyl alcohol. While PVA mats exhibited superior contaminant capture, Agarose-based mats provided better physical conformability to the artwork's texture.

To address the need for sustainable disinfection, the research utilized polysaccharides as both reducing and stabilizing agents for the green synthesis of gold and silver nanoparticles. The chemical composition of the matrix was identified as a decisive factor; impurity-rich matrices acted as reducing agents, yielding high concentrations of anisotropic particles, whereas purified Agarose served as a passive stabilizer, yielding uniform spherical particles. These colloidal suspensions were successfully processed into solid-state nanocomposite mats via electrospinning. The integration of silver nanoparticles notably reinforced the mechanical structure, increasing the Young's modulus significantly, while gold nanoparticles enhanced elasticity. These functionalized textiles represent a promising, removable solution for treating biological colonization on artworks.

In the realm of biocleaning, the study established electrospun Polycaprolactone (PCL) mats as effective carriers for viable bacterial strains. The hydrophobicity and sub-micron roughness of the PCL fibers promoted strong bacterial adhesion, concentrating the biomass significantly beyond the initial inoculum levels. A critical achievement was the stabilization of *Bacillus subtilis* on these mats through a freeze-drying protocol using a specific cryoprotectant mixture, which maintained high viability for at least two months. Furthermore, the research highlighted distinct biodegradation profiles: *Bacillus subtilis* rapidly degraded the PCL scaffold, suggesting a disposable, compostable application, whereas *Pseudomonas stutzeri* left the mat structurally stable, suitable for longer treatment durations.

To overcome the inherent water solubility of PEO-based mats and expand their utility to aqueous treatments, a chemical stabilization strategy was developed. A semi-interpenetrating network was established using the monomer TMPTMA, activated by thermal curing at 40°C. An optimized formulation rendered the nanofibers completely insoluble in water while preserving their morphology and porosity, thereby laying the groundwork for stabilizing complex biopolymer blends in wet environments. Building upon these foundational results, the experimentation will continue with the specific antimicrobial evaluation of the nanocomposite membranes to quantify their biocidal efficacy

against heritage biodeteriogens. Furthermore, the fabrication protocols will be expanded to the electrospinning of Gellan gum solutions, aiming to translate the properties of this widely used conservation biopolymer into a functional nanofibrous format.

In conclusion, this work illustrates that combining natural biopolymers with synthetic reinforcing agents allows for the engineering of textiles that offer the selectivity of biological agents and the precision of controlled release systems, providing restorers with versatile, shelf-stable, and removable conservation tools.

List of Figures and Tables

List of Figures

List of Tables

Appendix A: List of Publications

Published

1) **Pannico, M.; Musto, P.; Ligresti, A.; Allarà, M.; Castellano, M.; Pettineo, S.; Vicini, S.; Alloisio, M.**
   Polydiacetylene-coated gold colloids: A multifunctional nanostructure for theranostic applications. In Applied Surface Science, 2025; Vol. 690, 162586.
2) **Tahir, M.; Vicini, S.; Pettineo, S.; Madhyastha, H.; Sionkowska, A.**
   Polymer and biopolymer blends in wound healing and bone repair - a review. In Engineering of Biomaterials, 2024 Vol. 172, 12.
3) **Moussa, M.; Mirata, S.; Moni, L.; Asnaghi, V.; Alloisio, M.; Pettineo, S.; Castellano, M.; Vicini, S.; Chiantore, M.; Scarfi, S.** *Structural Characterization and Anti-inflammatory Properties of an Alginate Extracted from the Brown Seaweed Ericaria amentacea.* In Marine Drugs (MDPI).
4) **Bouhidel, Z.; Elkolli, M.; Bouanane, Z.; Cavallo, D.; Pettineo, S.; Baouch, Z.; Vicini, S.; Castellano, M.** *Impact of Oxidation Method on the Properties of Carboxymethylcellulose Hydrogels: Enzymatic versus Chemical TEMPO/Periodate Systems.* In the International Journal of Biological Macromolecules.

Being published

1) **Thorat, A.S.; Bardelli, A.; Pettineo, S.; Castellano, M.; Alloisio, M.; Vicini, S.**
   Fabrication and Characterization of Cellulose Derivatives Electrospun Nonwoven Mats. In Cellulose.
2) **Tahir, M.; Pettineo, S.; Vicini, S.; Castellano, M.; Alloisio, M.; Popat, K.; Madhyastha, H.; Sionkowska, A.**
   S*odium Alginate for Wound Healing Applications – A Review*. In Polymers in Medicine.

Appendix B: Conference contributions

Oral Communications

1) **Pannico, M.; Musto, P.; Ligresti, A.; Allarà, M.; Castellano, M.; Pettineo, S.; Vicini, S.; Alloisio, M.**
Polydiacetylene-coated gold colloids: A multifunctional nanostructure for theranostic applications
Giornate Scientifiche di Dipartimento Area della Ricerca CNR di Bologna, 21 – 23 October 2025, Bologna (Italy)

2) **Pettineo, S.; Mairani, A.; Tonini; V.; Vassallo, S.; Parodi, P., Alloisio, M.; Castellano, M.; Vicini, S.**
Electrospun mats for the cleaning of paints in Cultural Heritage
XXI Congresso Nazionale della Divisione di Chimica dell'Ambiente e dei Beni Culturali, 10-13 September 2025, Cremona (Italy)

3) **Sidane I.; Pettineo, S.; Castellano, M.; Peddis, D.; Alberti, S.; Slimani**
PDMS-based magnetic Nanocomposite: effect of magnetic nanoparticles on viscosity and wettability
26th Annual Conference on Material Science, 1-5 September 2025, Herceg Novi (Montenegro)

4) **Moussa, M.; Mirata, S.; Moni, L.; Asnaghi, V.; Alloisio, M.; Pettineo, S.; Castellano, M.; Vicini, S.; Chiantore, M.; Scarfi, S**.
Structural Characterization and Anti-inflammatory Properties of an Alginate Extracted from the Brown Seaweed Ericaria amentacea
13th International Marine Biotechnology Congress, 7-11 July 2025, Brest (France)

5) **Pettineo, S.; Vicini, S.; Castellano, M.; Alloisio, M.**
Electrospun Agar-Based Nanocomposite Mats for Artworks Disinfection
16th International Conference on Surfaces, Coatings and Nanostructured Materials (Nanosmat), 6-10 July 2025, Naples (Italy)

6) **Pettineo, S.; Scarfi, S.; Pozzolini, M.; Tahir, M.; Sionkowska, A.; Alloisio, M.; Castellano, M.; Vicini, S.**
Electrospun pcl mats as bacterial carriers for biocleaning applications in cultural heritage conservation
Macrogiovani 2025 (AIM), 28-30 May 2025, Pisa (Italy)

7) **Vicini, S.; Pettineo, S.; Alloisio, M.; Castellano, M.**
Biopolymeric Membranes and Gels for Advanced Applications

Membrane Materials - Modification and Separation (M3-S) 3rd conference, 27-30 May 2025, Torun (Poland)

8) **Pettineo, S.; Castellano, M.; Alloisio, M.; Vicini, S.**
Nanostructured agar mats for application in the cleaning and disinfection of sensitive surfaces
VI Symposium Biomaterials in Medicine and Cosmetology, 21 February 2025, Torun (Poland)

9) **Vicini, S.; Pettineo, S.**
Biopolymers and electrospinning techniques for the development of advanced applications
International Conference on Polymers for Sustainable Development, 7 February 2025 - Bengaluru (India, Online mode)

10) **Pettineo, S.; Castellano, M.; Alloisio, M.; Vicini, S.**
Agar electrospun nanofibers for an innovative application in the cleaning and disinfection of Cultural Heritage
TechnoHeritage 2024, 25-27 September 2024, Santiago de Compostela (Spain)

11) **Vicini, S.; Pettineo, S.; Alloisio, M.; Castellano, C.**
Multilayer Agar-Polycaprolactone Electrospun mats for an innovative application on cleaning of sensitive surfaces
XXV Convegno Nazionale Associazione Italiana di Scienza e Tecnologie delle Macromolecole (AIM), 8-11 September 2024, Naples (Italy)

Poster Communications

1) **Pettineo, S.; Scarfi, S.; Pozzolini, M.; Alloisio, M.; Castellano, M.; Vicini, S.**
Electrospun PCL mats as bacterial supports for sustainable biocleaning in Cultural Heritage conservation
XXI Congresso Nazionale della Divisione di Chimica dell'Ambiente e dei Beni Culturali, 10-13 September 2025, Cremona (Italy)

2) **Giovine, M.; Pettineo, S.; Vicini, S.; Castellano, M.; Bagnato, A.; Pozzolini, M.**
Collagen beads from Chondrosia reniformis as antioxidant-retaining biomaterials for wound environments
World Sponge Conference 12th, 9-13 September 2025, Vila Do Conde (Portugal)

3) **Pettineo, S.; Tahir, M.; Vicini, S.; Sionkowska, A.**
Polymeric blend of Alginate/PVA/L-arginine for wound healing applications
VI Symposium Biomaterials in Medicine and Cosmetology, 21 February 2025, Torun (Poland)

4) **Tahir, M.; Pettineo, S.; Vicini, S.; Sionkowska, A.**
Composite based on Polyvinyl alcohol, Chitosan, caffeine, and Polydopamine for wound healing
VI Symposium Biomaterials in Medicine and Cosmetology, 21 February 2025, Torun (Poland)

5) **Pettineo, S.; Alloisio, M.; Vicini, S.; Castellano, M.**
Agarose low gelling temperature: correlation between rheological proprieties and spinnability
XVIII Italian Society of Rheology Conference, 12-14 September 2024, Capri (Italy)

6) **Pettineo, S.; Geido, A.; Alloisio, V.; Vicini, S.; Castellano, M.**
Electrosprayed chitosan sub-microbeads for controlled drug release
XXV Convegno Nazionale Associazione Italiana di Scienza e Tecnologie delle Macromolecole (AIM), 8-11 September 2024, Naples (Italy)

7) **Bouhidel, Z.; Pettineo, S.; Merbah Elkolli, M.**
Grafted carboxymethyl cellulose as functional matrixes for mucoadhesive properties
7th International Conference on Sustainable Science and Technology (ICSuSaT-2024), 12-14 July 2024, Istanbul (Turkey)

References

(1) Lamarque, P. Reflections on the Ethics and Aesthetics of Restoration and Conservation. *British Journal of Aesthetics*. Oxford University Press July 1, 2016, pp 281–299. https://doi.org/10.1093/aesthj/ayw041.

(2) Cinquepalmi, F.; Tiburcio, V. A. Sustainable Restoration of Cultural Heritage in the Digital Era. *Vitruvio 2023*, 8 (2), 76–87. https://doi.org/10.4995/vitruvio-ijats.2023.20545.

(3) Gueidão, M.; Vieira, E.; Bordalo, R.; Moreira, P. Available Green Conservation Methodologies for the Cleaning of Cultural Heritage: An Overview. *ECR Estudos de Conservação e Restauro* 2020, 12*,* 2098. https://doi.org/10.34632/ecr.2020.10679.

(4) Sansonetti, A.; Riminesi, C.; Mironiouk, S.; Proietti, N.; Di Tullio, V.; Nisticò, R.; Sacchi, B.; Canevali, C. Gel Cleaning in Heritage: Comparison of the Water Release among Gels and Traditional Pads. *Gels 2024*, 10 (11). https://doi.org/10.3390/gels10110708.

(5) Giraud, T.; Gomez, A.; Lemoine, S.; Pelé-Meziani, C.; Raimon, A.; Guilminot, E. Use of Gels for the Cleaning of Archaeological Metals. Case Study of Silver-Plated Copper Alloy Coins. *J. Cult. Herit.* 2021, 52, 73–83. https://doi.org/10.1016/j.culher.2021.08.014.

(6) Khaksar-Baghan, N.; Koochakzaei, A.; Hamzavi, Y. An Overview of Gel-Based Cleaning Approaches for Art Conservation. *Heritage Science.* Springer Science and Business Media Deutschland GmbH December 1, 2024. https://doi.org/10.1186/s40494-024-01369-0.

(7) Alisi, C.; Magrini, D.; Vettori, S.; Salvadori, B.; Vincenti, M.; Manna, D.; Bietti, M.; Sprocati, A. R. Sustainable Restoration Guided by Scientific and Archival Investigations: The Bio-Cleaning of Lorenzo Duke of Urbino's Sarcophagus, a Michelangelo's Masterpiece in the Medici Chapels. *Heritage 2022*, 5 (4), 3359–3373. https://doi.org/10.3390/heritage5040172.

(8) Viñas, S. M. Contemporary Theory of Conservation; *Taylor and Francis*, 2012. https://doi.org/10.4324/9780080476834.

(9) Zhang, Y.; Dong, W. Determining Minimum Intervention in the Preservation of Heritage Buildings. *International Journal of Architectural Heritage* 2021, 15(5), 698–712. https://doi.org/10.1080/15583058.2019.1645237.

(10) Fonti, R. Heritage for a sustainable future. The Theoretical Principle of Reversibility and Its Reflections on Architecture. Agathon - *International Journal of Architecture, Art and Design* 2024, 16, 144–155. https://doi.org/10.19229/2464-9309/16122024.

(11) Gravagnuolo, A.; Angrisano, M.; Bosone, M.; Buglione, F.; De Toro, P.; Fusco Girard, L. Participatory Evaluation of Cultural Heritage Adaptive Reuse Interventions in the Circular Economy Perspective: A Case Study of Historic Buildings in Salerno (Italy). *Journal of Urban Management* 2024, 13 (1), 107–139. https://doi.org/10.1016/j.jum.2023.12.002.

(12) Ormsby, B.; Bartoletti, A.; van den Berg, K. J.; Stavroudis, C. Cleaning and Conservation: Recent Successes and Challenges. *Heritage Science*. Springer Science and Business Media Deutschland GmbH December 1, 2024. https://doi.org/10.1186/s40494-023-01113-0.

(13) Avdanina, D. A.; Zhgun, A. A. Rainbow Code of Biodeterioration to Cultural Heritage Objects. *Heritage Science*. Springer Science and Business Media Deutschland GmbH December 1, 2024. https://doi.org/10.1186/s40494-024-01298-y.

(14) Di Turo, F. The Chemistry behind Paper Restoration: Diagnostic Techniques and Cutting-Edge Innovation. *ChemTexts* 2025, 11 (3). https://doi.org/10.1007/s40828-025-00203-9.

(15) Ormsby, B.; Bartoletti, A.; van den Berg, K. J.; Stavroudis, C. Cleaning and Conservation: Recent Successes and Challenges. *Heritage Science*. Springer Science and Business Media Deutschland GmbH December 1, 2024. https://doi.org/10.1186/s40494-023-01113-0.

(16) Cirone, M.; Figoli, A.; Galiano, F.; La Russa, M. F.; Macchia, A.; Mancuso, R.; Ricca, M.; Rovella, N.; Taverniti, M.; Ruffolo, S. A. Innovative Methodologies for the Conservation of Cultural Heritage against Biodeterioration: A Review. *Coatings (MDPI)*, 2023. https://doi.org/10.3390/coatings13121986.

(17) Weththimuni, M. L.; Licchelli, M. Heritage Conservation and Restoration: Surface Characterization, Cleaning and Treatments. *Coatings. MDPI*, 2023. https://doi.org/10.3390/coatings13020457.

(18) El Ouahabi, M.; Cools, C.; Rousseau, V.; Gautier, J. Different Cleaning Techniques for Archeological Ceramics: A Review. *Heritage.* (MDPI), 2025. https://doi.org/10.3390/heritage8100434.

(19) Rode, A. V.; Baldwin, K. G. H.; Wain, A.; Madsen, N. R.; Freeman, D.; Delaporte, P.; Luther-Davies, B. Ultrafast Laser Ablation for Restoration of Heritage Objects. *Appl. Surf. Sci*. 2008, 254 (10), 3137–3146. https://doi.org/10.1016/j.apsusc.2007.10.106.

(20) Zanini, A.; Trafeli, V.; Bartoli, L. The Laser as a Tool for the Cleaning of Cultural Heritage. In IOP Conference Series: *Materials Science and Engineering*; Institute of Physics Publishing, 2018; Vol. 364. https://doi.org/10.1088/1757-899X/364/1/012078.

(21) Zhou, Z.; Sun, W.; Wu, J.; Chen, H.; Zhang, F.; Wang, S. The Fundamental Mechanisms of Laser Cleaning Technology and Its Typical Applications in Industry. *Processes. (MDPI)* May 1, 2023. https://doi.org/10.3390/pr11051445.

(22) Palomar, T.; Cano, E. Comparative Assessment of Mechanical, Chemical and Electrochemical Procedures for Conservation of Historical Lead. *J. Cult. Herit*. 2018, 30, 34–44. https://doi.org/10.1016/j.culher.2017.10.010.

(23) Pinna, D. Physical and Mechanical Methods for the Removal of Lithobionts - A Review. *Coatings. (MDPI)* March 1, 2024. https://doi.org/10.3390/coatings14030272.

(24) Turner-Walker, G. The Nature of Cleaning: Physical and Chemical Aspects of Removing Dirt, Stains and Corrosion.

(25) Melchiorre, C.; Melchiorre, M.; Marra, M.; Rizzo, E.; Fatigati, G.; Rossi, P.; Cerruti, P.; Improta, I.; Amoresano, A.; Marino, G.; Ruffo, F.; Carpentieri, A. Green Solvents and Restoration: Application of Biomass-Derived Solvents in Cleaning Procedures. *J. Cult. Herit.* 2023, 62, 3–12. https://doi.org/10.1016/j.culher.2023.05.013.

(26) Teixeira, S.; Vilarigues, M.; Lima, A.; Branquinho, R.; Dias, L.; Coutinho, M. L. Testing the Harmfulness of Chemical Cleaning Methods for the Removal of Incrustations from a Glazed Stoneware Public Artwork. *J. Cult. Herit.* 2022, 55, 48–57. https://doi.org/10.1016/j.culher.2022.02.007.

(27) Biribicchi, C.; Giuliani, L.; Macchia, A.; Favero, G. Organogels for Low-Polar Organic Solvents: Potential Applications on Cultural Heritage Materials. *Sustainability* 2023, 15 (23). https://doi.org/10.3390/su152316305.

(28) Ormsby, B.; Bartoletti, A.; van den Berg, K. J.; Stavroudis, C. Cleaning and Conservation: Recent Successes and Challenges. *Heritage Science*. Springer Science and Business Media Deutschland GmbH December 1, 2024. https://doi.org/10.1186/s40494-023-01113-0.

(29) Weththimuni, M. L.; Licchelli, M. Heritage Conservation and Restoration: Surface Characterization, Cleaning and Treatments. *Coatings. MDPI*, 2023. https://doi.org/10.3390/coatings13020457.

(30) Samorì, C.; Basaglia, M.; Casella, S.; Favaro, L.; Galletti, P.; Giorgini, L.; Marchi, D.; Mazzocchetti, L.; Torri, C.; Tagliavini, E. Dimethyl Carbonate and Switchable Anionic Surfactants: Two Effective Tools for the Extraction of Polyhydroxyalkanoates from Microbial Biomass. *Green Chemistry* 2015, 17 (2), 1047–1056. https://doi.org/10.1039/c4gc01821d.

(31) Chelazzi, D.; Baglioni, P. From Nanoparticles to Gels: A Breakthrough in Art Conservation Science. *Langmuir. American Chemical Society*, 2023, pp 10744–10755. https://doi.org/10.1021/acs.langmuir.3c01324.

(32) Baglioni, P.; Dei, L.; Carretti, E.; Giorgi, R. Gels for the Conservation of Cultural Heritage. *Langmuir* 2009, 25 (15), 8375–8377. https://doi.org/10.1021/la900961k.

(33) Jia, D.; Muthukumar, M. Theory of Charged Gels: Swelling, Elasticity, and Dynamics. *Gels. MDPI.* https://doi.org/10.3390/gels7020049.

(34) Horkay, F.; Douglas, J. F. Polymer Gels: Basics, Challenges, and Perspectives. In *ACS Symposium Series*; American Chemical Society, 2018; Vol. 1296, pp 1–13. https://doi.org/10.1021/bk-2018-1296.ch001.

(35) Shibayama, M.; Li, X.; Sakai, T. Gels: From Soft Matter to BioMatter. *Industrial and Engineering Chemistry Research*. American Chemical Society January 31, 2018, pp 1121–1128. https://doi.org/10.1021/acs.iecr.7b04614.

(36) Banerjee, S.; Bhattacharya, S. Food Gels: Gelling Process and New Applications. *Crit. Rev. Food Sci. Nutr*. 2012, 52 (4), 334–346. https://doi.org/10.1080/10408398.2010.500234.

(37) Paun, V. P.; Paun, M. A. Gels: Synthesis, Characterization and Applications in High Performance Chemistry (2nd Edition). *Gels. (MDPI)*, 2025. https://doi.org/10.3390/gels11050351.

(38) Fan, L.; Cai, Z.; Zhao, J.; Mahmoudi, N.; Wang, Y.; Cheeseman, S.; Aguilar, L. C.; Reis, R. L.; Kundu, S. C.; Kaplan, D. L.; Nisbet, D. R.; Li, J. L. Gelation Dynamics, Formation Mechanism, Functionalization, and 3D Bioprinting of Silk Fibroin Hydrogel Materials for

Biomedical Applications. *ACS Nano*. American Chemical Society, 2025, pp 17979–18002. https://doi.org/10.1021/acsnano.4c18568.

(39) Samorì, C.; Galletti, P.; Giorgini, L.; Mazzeo, R.; Mazzocchetti, L.; Prati, S.; Sciutto, G.; Volpi, F.; Tagliavini, E. The Green Attitude in Art Conservation: Polyhydroxybutyrate–Based Gels for the Cleaning of Oil Paintings. *ChemistrySelect* 2016, 1 (15), 4502–4508. https://doi.org/10.1002/slct.201601180.

(40) Prati, S.; Volpi, F.; Fontana, R.; Galletti, P.; Giorgini, L.; Mazzeo, R.; Mazzocchetti, L.; Samorì, C.; Sciutto, G.; Tagliavini, E. Sustainability in Art Conservation: A Novel Bio-Based Organogel for the Cleaning of Water Sensitive Works of Art. *In Pure and Applied Chemistry*; Walter de Gruyter GmbH, 2018; Vol. 90, pp 239–251. https://doi.org/10.1515/pac-2017-0507.

(41) Yiming, J.; Sciutto, G.; Prati, S.; Catelli, E.; Galeotti, M.; Porcinai, S.; Mazzocchetti, L.; Samorì, C.; Galletti, P.; Giorgini, L.; Tagliavini, E.; Mazzeo, R. A New Bio-Based Organogel for the Removal of Wax Coating from Indoor Bronze Surfaces. *Herit. Sci*. 2019, 7 (1). https://doi.org/10.1186/s40494-019-0276-8.

(42) Prati, S.; Sciutto, G.; Volpi, F.; Rehorn, C.; Vurro, R.; Blümich, B.; Mazzocchetti, L.; Giorgini, L.; Samorì, C.; Galletti, P.; Tagliavini, E.; Mazzeo, R. Cleaning Oil Paintings: NMR Relaxometry and SPME to Evaluate the Effects of Green Solvents and Innovative Green Gels. *New Journal of Chemistry* 2019, 43 (21), 8229–8238. https://doi.org/10.1039/c9nj00186g.

(43) Vilgis, T. A. Gels: Model Systems for Soft Matter Food Physics. *Current Opinion in Food Science*. Elsevier Ltd June 1, 2015, pp 71–84. https://doi.org/10.1016/j.cofs.2015.05.009.

(44) Karoyo, A. H.; Wilson, L. D. Physicochemical Properties and the Gelation Process of Supramolecular Hydrogels: A Review. *Gels. MDPI* AG March 1, 2017. https://doi.org/10.3390/gels3010001.

(45) Pianorsi, M. D.; Raudino, M.; Bonelli, N.; Chelazzi, D.; Giorgi, R.; Fratini, E.; Baglioni, P. Organogels for the Cleaning of Artifacts. In *Pure and Applied Chemistry*; Walter de Gruyter GmbH, 2017; Vol. 89, pp 3–17. https://doi.org/10.1515/pac-2016-0908.

(46) Mazzuca, C.; Micheli, L.; Cervelli, E.; Basoli, F.; Cencetti, C.; Coviello, T.; Iannuccelli, S.; Sotgiu, S.; Palleschi, A. Cleaning of Paper Artworks: Development of an Efficient Gel-Based Material Able to Remove Starch Paste. *ACS Appl. Mater. Interfaces* 2014, 6 (19), 16519–16528. https://doi.org/10.1021/am504295n.

(47) Mazzuca, C.; Micheli, L.; Cervelli, E.; Basoli, F.; Cencetti, C.; Coviello, T.; Iannuccelli, S.; Sotgiu, S.; Palleschi, A. Cleaning of Paper Artworks: Development of an Efficient Gel-Based Material Able to Remove Starch Paste.

(48) Guilminot, E. The Use of Hydrogels in the Treatment of Metal Cultural Heritage Objects. *Gels* 2023, 9 (3). https://doi.org/10.3390/gels9030191.

(49) Sansonetti, A.; Bertasa, M.; Canevali, C.; Rabbolini, A.; Anzani, M.; Scalarone, D. A Review in Using Agar Gels for Cleaning Art Surfaces. *Journal of Cultural Heritage*. Elsevier Masson SAS July 1, 2020, pp 285–296. https://doi.org/10.1016/j.culher.2020.01.008.

(50) Chen, Y.; Li, J.; Lu, J.; Ding, M.; Chen, Y. Synthesis and Properties of Poly(Vinyl Alcohol) Hydrogels with High Strength and Toughness. *Polym. Test.* 2022, 108. https://doi.org/10.1016/j.polymertesting.2022.107516.

(51) Wang, M.; Bai, J.; Shao, K.; Tang, W.; Zhao, X.; Lin, D.; Huang, S.; Chen, C.; Ding, Z.; Ye, J. Poly(Vinyl Alcohol) Hydrogels: The Old and New Functional Materials. *International Journal of Polymer Science*. Hindawi Limited 2021. https://doi.org/10.1155/2021/2225426.

(52) Roca-Arroyo, A. F.; Gutierrez-Rivera, J. A.; Morton, L. D.; Castilla-Casadiego, D. A. Hydrogel Network Architecture Design Space: Impact on Mechanical and Viscoelastic Properties. *Gels. (MDPI)*, 2025. https://doi.org/10.3390/gels11080588.

(53) Richard, F.; Hermans, J. J.; Angelova, L. Rigid Solvent-Gels in Paper Conservation: A New Approach to Sticky Problems. *Journal of Paper Conservation* 2024, 25 (2), 86–106. https://doi.org/10.1080/18680860.2024.2343671.

(54) Wang, M.; Bai, J.; Shao, K.; Tang, W.; Zhao, X.; Lin, D.; Huang, S.; Chen, C.; Ding, Z.; Ye, J. Poly(Vinyl Alcohol) Hydrogels: The Old and New Functional Materials. *International Journal of Polymer Science*. Hindawi Limited 2021. https://doi.org/10.1155/2021/2225426.

(55) Tamagawa, H.; Popovic, S.; Taya, M. Pores and Diffusion Characteristics of Porous Gels.

(56) Franco, S.; Severini, L.; Buratti, E.; Tavagnacco, L.; Sennato, S.; Missori, M.; Ruzicka, B.; Mazzuca, C.; Zaccarelli, E.; Angelini, R. Gellan-Based Hydrogels and Microgels for Cultural Heritage: A Rheological Perspective.

(57) Bosch-Roig, P.; Ranalli, G. The Safety of Biocleaning Technologies for Cultural Heritage. Front. Microbiol. 2014, 5 (APR). https://doi.org/10.3389/fmicb.2014.00155.

(58) Bosch-Roig, P.; Lustrato, G.; Zanardini, E.; Ranalli, G. Biocleaning of Cultural Heritage Stone Surfaces and Frescoes: Which Delivery System Can Be the Most Appropriate? *Annals of Microbiology*. Springer Verlag, 2015, pp 1227–1241. https://doi.org/10.1007/s13213-014-0938-4.

(59) Ranalli, G.; Bosch-Roig, P.; Crudele, S.; Rampazzi, L.; Corti, C.; Zanardini, E. Dry Biocleaning of Artwork: An Innovative Methodology for Cultural Heritage Recovery? *Microbial Cell* 2021, 8 (6), 91–105. https://doi.org/10.15698/MIC2021.05.748.

(60) Singh, M. R.; Ghosh, B. Microbial Biotechnology for Sustainable Preservation of Cultural Heritage: Bio-Cleaning and Self-Healing Preservation Materials. *European Journal of Sustainable Development Research* 2025, 9 (4). https://doi.org/10.29333/ejosdr/16580.

(61) Sanmartín, P.; Bosch-Roig, P. Biocleaning to Remove Graffiti: A Real Possibility? Advances towards a Complete Protocol of Action. *Coatings* 2019, 9 (2). https://doi.org/10.3390/coatings9020104.

(62) Cattò, C.; Sanmartín, P.; Gulotta, D.; Troiano, F.; Cappitelli, F. Bioremoval of Graffiti Using Novel Commercial Strains of Bacteria. *Science of the Total Environment* 2021, 756. https://doi.org/10.1016/j.scitotenv.2020.144075.

(63) Romano, I.; Abbate, M.; Poli, A.; D'Orazio, L. Bio-Cleaning of Nitrate Salt Efflorescence on Stone Samples Using Extremophilic Bacteria. *Sci. Rep.* 2019, 9 (1). https://doi.org/10.1038/s41598-018-38187-x.

(64) Heinzmann, S.; Entian, K. D.; Stein, T. Engineering Bacillus Subtilis ATCC 6633 for Improved Production of the Lantibiotic Subtilin. Appl. *Microbiol. Biotechnol*. 2006, 69 (5), 532–536. https://doi.org/10.1007/s00253-005-0023-9.

(65) Maksimova, Y.; Eliseeva, A.; Maksimov, A. Metabolic and Morphological Aspects of Adaptation of Alkaliphilic Bacillus Aequororis 5-DB and Alkali-Tolerant Bacillus Subtilis ATCC 6633 to Changes in PH and Mineralization. *Int. J. Microbiol*. 2024, 2024. https://doi.org/10.1155/2024/3087296.

(66) Werb, M.; García, C. F.; Bach, N. C.; Grumbein, S.; Sieber, S. A.; Opitz, M.; Lieleg, O. Surface Topology Affects Wetting Behavior of Bacillus Subtilis Biofilms. *NPJ Biofilms Microbiomes* 2017, 3 (1). https://doi.org/10.1038/s41522-017-0018-1.

(67) Errington, J.; van der Aa, L. T. Microbe Profile: Bacillus Subtilis: Model Organism for Cellular Development, and Industrial Workhorse. *Microbiology* 2020, 166 (5), 425–427. https://doi.org/10.1099/mic.0.000922.

(68) Petronikolou, N.; Ortega, M. A.; Borisova, S. A.; Nair, S. K.; Metcalf, W. W. Molecular Basis of Bacillus Subtilis ATCC 6633 Self-Resistance to the Phosphono-Oligopeptide Antibiotic Rhizocticin. *ACS Chem. Biol.* 2019, 14 (4), 742–750. https://doi.org/10.1021/acschembio.9b00030.

(69) Lalucat, J.; Bennasar, A.; Bosch, R.; García-Valdés, E.; Palleroni, N. J. Biology of Pseudomonas Stutzeri . *Microbiology and Molecular Biology Reviews* 2006, 70 (2), 510–547. https://doi.org/10.1128/mmbr.00047-05.

(70) Vidaković, A. M.; Šovljanski, O. L.; Ranitović, A. S.; Cvetković, D. D.; Markov, S. L. Determination of Culture Medium Composition for Maximizing the Biomass Production of Pseudomonas Stutzeri. *Acta Periodica Technologica* 2017, 48, 295–305. https://doi.org/10.2298/APT1748295V.

(71) Kaczorek, E.; Jesionowski, T.; Giec, A.; Olszanowski, A. Cell Surface Properties of Pseudomonas Stutzeri in the Process of Diesel Oil Biodegradation. *Biotechnol. Lett.* 2012, 34 (5), 857–862. https://doi.org/10.1007/s10529-011-0835-x.

(72) Vidaković, A.; Šovljanski, O.; Vučurović, D.; Racić, G.; Đilas, M.; Ćurčić, N.; Markov, S. *Novel denitrifying bacteria Pseudomonas stutzeri strain d1-from isolation to the biomass production*.

(73) Vilas Boas, D.; Lima, C. M. G.; Margalho, L. P.; Amorim-Neto, D. P.; Canales, H. D. S.; Lemos Junior, W. J. F.; Ramos, A. C.; Saraiva, G.; Sant'Ana, A. S. Impact of Hydrophobic and Hydrophilic Surface Properties on Pseudomonas Aeruginosa Adhesion in Materials Used in Mineral Water Wells. *Biofouling* 2024, 40 (10), 735–742. https://doi.org/10.1080/08927014.2024.2410771.

(74) Cremonesi, P.; Casoli, A. Enzymes as Tools for Conservation of Works of Art. *Journal of Cultural Heritage.* Elsevier, 2021, pp 73–87. https://doi.org/10.1016/j.culher.2021.06.005.

(75) Practical Applications of Protease Enzymes in Paper Conservation. http://aic.stanford.edu/bpg/annual/.

(76) Ranalli, G.; Alfano, G.; Belli, C.; Lustrato, G.; Colombini, M. P.; Bonaduce, I.; Zanardini, E.; Abbruscato, P.; Cappitelli, F.; Sorlini, C. Biotechnology Applied to Cultural Heritage: Biorestoration of Frescoes Using Viable Bacterial Cells and Enzymes. *J. Appl. Microbiol.* 2005, 98 (1), 73–83. https://doi.org/10.1111/j.1365-2672.2004.02429.x.

(77) Hong, A.; Turner, S.; Glazer, R.; Weishampel, Z. A.; Vispute, A.; Huang, A.; Holmes, Z. A.; Schleupner, B.; Dunphy-Daly, M. M.; Eward, W. C.; Somarelli, J. A. A Sequence- and Structure-Based Characterization of Microbial Enzymes Identifies P. Stutzeri as a Plastic-Degrading Species, 2024. https://doi.org/10.1101/2024.04.12.589142.

(78) Morlotti, M.; Forlani, F.; Saccani, I.; Sansonetti, A. Evaluation of Enzyme Agarose Gels for Cleaning Complex Substrates in Cultural Heritage. *Gels 2024*, 10 (1). https://doi.org/10.3390/gels10010014.

(79) Hamed, S. A. E. K. M. A Preliminary Study on Using Enzymes in Cleaning Archaeological Wood. J. *Archaeol. Sci.* 2012, 39 (7), 2515–2520. https://doi.org/10.1016/j.jas.2012.02.026.

(80) Matthias Schöller, S.; Prozell, S. *Biological Control of Cultural Heritage Pests-a Review*.

(81) He, D.; Wu, F.; Ma, W.; Gu, J. D.; Xu, R.; Hu, J.; Yue, Y.; Ma, Q.; Wang, W.; Li, S. W. Assessment of Cleaning Techniques and Its Effectiveness for Controlling Biodeterioration Fungi on Wall Paintings of Maijishan Grottoes. *Int. Biodeterior. Biodegradation* 2022, 171. https://doi.org/10.1016/j.ibiod.2022.105406.

(82) Romani, M.; Warscheid, T.; Nicole, L.; Marcon, L.; Di Martino, P.; Suzuki, M. T.; Lebaron, P.; Lami, R. Current and Future Chemical Treatments to Fight Biodeterioration of Outdoor Building Materials and Associated Biofilms: Moving Away from Ecotoxic and towards Efficient, Sustainable Solutions. *Science of the Total Environment*. Elsevier B.V., 2022. https://doi.org/10.1016/j.scitotenv.2021.149846.

(83) Sakr, A. A.; Ghaly, M. F.; Ali, M. F. The use of gamma irradiation in the sterilization of Streptomyces colonizing the tempera paintings in ancient Egyptian tombs; International *Journal of Conservation Science*, Vol. 4. www.ijcs.uaic.ro.

(84) Harrell, C. R.; Djonov, V.; Fellabaum, C.; Volarevic, V. Risks of Using Sterilization by Gamma Radiation: The Other Side of the Coin. *Int. J. Med. Sci*. 2018, 15 (3), 274–279. https://doi.org/10.7150/ijms.22644.

(85) Vujcic, I.; Masic, S.; Medic, M.; Putic, S.; Dramicanin, M. D. "Ecological truth" Gamma irradiation of Leather gloves in terms of Cultural Heritage preservation, *ECO-IST'17*.

(86) Palla, F.; Bruno, M.; Mercurio, F.; Tantillo, A.; Rotolo, V. Essential Oils as Natural Biocides in *Conservation of Cultural Heritage*. Molecules 2020, 25 (3). https://doi.org/10.3390/molecules25030730.

(87) Albasil, M. D.; Mahgoub, G.; El Hagrassy, A.; Reyad, A. M. Evaluating the antimicrobial activity of essential oils in the conservation of mural paintings, *Conservation Science in Cultural Heritage* 2021, 21, 125–148. https://doi.org/10.48255/1973-9494.JCSCH.21.2021.05.

(88) Russo, R.; Palla, F. Plant Essential Oils as Biocides in Sustainable Strategies for the Conservation of Cultural Heritage. *Sustainability MDPI*, 2023. https://doi.org/10.3390/su15118522.

(89) Mateus, D.; Costa, F.; de Jesus, V.; Malaquias, L. Biocides Based on Essential Oils for Sustainable Conservation and Restoration of Mural Paintings in Built Cultural Heritage. *Sustainability* 2024, 16 (24). https://doi.org/10.3390/su162411223.

(90) Gibała, A.; Żeliszewska, P.; Gosiewski, T.; Krawczyk, A.; Duraczyńska, D.; Szaleniec, J.; Szaleniec, M.; Oćwieja, M. Antibacterial and Antifungal Properties of Silver Nanoparticles - Effect of a Surface-Stabilizing Agent. *Biomolecules* 2021, 11 (10). https://doi.org/10.3390/biom11101481.

(91) Altammar, K. A. A Review on Nanoparticles: Characteristics, Synthesis, Applications, and Challenges. *Frontiers in Microbiology.* Frontiers Media S.A. 2023. https://doi.org/10.3389/fmicb.2023.1155622.

(92) Umamaheswari, K.; Abirami, M. Assessment of Antifungal Action Mechanism of Green Synthesized Gold Nanoparticles (AuNPs) Using Allium Sativum on Candida Species. *Mater. Lett.* 2023, 333. https://doi.org/10.1016/j.matlet.2022.133616.

(93) Shukla, M. K.; Singh, R. P.; Reddy, C. R. K.; Jha, B. Synthesis and Characterization of Agar-Based Silver Nanoparticles and Nanocomposite Film with Antibacterial Applications. *Bioresour. Technol.* 2012, 107, 295–300. https://doi.org/10.1016/j.biortech.2011.11.092.

(94) Aguilar-Garay, R.; Lara-Ortiz, L. F.; Campos-López, M.; Gonzalez-Rodriguez, D. E.; Gamboa-Lugo, M. M.; Mendoza-Pérez, J. A.; Anzueto-Ríos, Á.; Nicolás-Álvarez, D. E. A Comprehensive Review of Silver and Gold Nanoparticles as Effective Antibacterial Agents. *Pharmaceuticals. (MDPI)*, 2024. https://doi.org/10.3390/ph17091134.

(95) Skłodowski, K.; Chmielewska-Deptuła, S. J.; Piktel, E.; Wolak, P.; Wollny, T.; Bucki, R. Metallic Nanosystems in the Development of Antimicrobial Strategies with High Antimicrobial Activity and High Biocompatibility. *International Journal of Molecular Sciences. MDPI* February 1, 2023. https://doi.org/10.3390/ijms24032104.

(96) Duman, H.; Eker, F.; Akdaşçi, E.; Witkowska, A. M.; Bechelany, M.; Karav, S. Silver Nanoparticles: A Comprehensive Review of Synthesis Methods and Chemical and Physical Properties. *Nanomaterials. (MDPI)*, 2024. https://doi.org/10.3390/nano14181527.

(97) Tharwat, N. A.; Al-Bedak, O. A.; Hamouda, R. E.; Shreif, R. H. El; Mounir, R. M.; Sami, A. M. Antifungal effect of gold nanoparticles on fungi isolated from onychomycosis patients; 2019; Vol. 60.

(98) Mussin, J.; Giusiano, G. Biogenic Silver Nanoparticles as Antifungal Agents. *Frontiers in Chemistry.* Frontiers Media S.A. October 6, 2022. https://doi.org/10.3389/fchem.2022.1023542.

(99) Rhim, J. W.; Kanmani, P. Synthesis and Characterization of Biopolymer Agar Mediated Gold Nanoparticles. *Mater. Lett*. 2015, 141, 114–117. https://doi.org/10.1016/j.matlet.2014.11.069.

(100) Timoszyk, A.; Grochowalska, R. Mechanism and Antibacterial Activity of Gold Nanoparticles (AuNPs) Functionalized with Natural Compounds from Plants. *Pharmaceutics. MDPI*, 2022. https://doi.org/10.3390/pharmaceutics14122599.

(101) Khatoon, U. T.; Rao, G. V. S. N.; Mohan, M. K.; Ramanaviciene, A.; Ramanavicius, A. Comparative Study of Antifungal Activity of Silver and Gold Nanoparticles Synthesized by Facile Chemical Approach. *J. Environ. Chem. Eng*. 2018, 6 (5), 5837–5844. https://doi.org/10.1016/j.jece.2018.08.009.

(102) Shireesha, Y.; Nandipati, G. *State of Art Review on Natural Fibers*; 2019; Vol. 18. www.sciencedirect.comwww.materialstoday.com/proceedings

(103) Shin, Y. M.; Hohman, M. M.; Brenner, M. P.; Rutledge, G. C. *Experimental Characterization of Electrospinning: The Electrically Forced Jet and Instabilities*. www.elsevier.com/locate/polymer.

(104) Feng, K.; Huangfu, L.; Liu, C.; Bonfili, L.; Xiang, Q.; Wu, H.; Bai, Y. Electrospinning and Electrospraying: Emerging Techniques for Probiotic Stabilization and Application. *Polymers. MDPI*, 2023. https://doi.org/10.3390/polym15102402.

(105) Xue, J.; Wu, T.; Dai, Y.; Xia, Y. Electrospinning and Electrospun Nanofibers: Methods, Materials, and Applications. *Chemical Reviews. American Chemical Society*, 2019, pp 5298–5415. https://doi.org/10.1021/acs.chemrev.8b00593.

(106) Keirouz, A.; Wang, Z.; Reddy, V. S.; Nagy, Z. K.; Vass, P.; Buzgo, M.; Ramakrishna, S.; Radacsi, N. The History of Electrospinning: Past, Present, and Future Developments. *Advanced Materials Technologies*. John Wiley and Sons Inc June 9, 2023. https://doi.org/10.1002/admt.202201723.

(107) Kumar Sharma, G.; Rachel James, N. Electrospinning: The Technique and Applications. In Recent Developments in Nanofibers Research; *IntechOpen,* 2023. https://doi.org/10.5772/intechopen.105804.

(108) Tucker, N.; Stanger, J. J.; Staiger, M. P.; Razzaq, H.; Hofman, K. *The History of the Science and Technology of Electrospinning from 1600 to 1995*; 2012; Vol. 63. http://www.jeffjournal.org.

(109) Ahmadi Bonakdar, M.; Rodrigue, D. Electrospinning: Processes, Structures, and Materials. *Macromol. (MDPI)* 2024, pp 58–103. https://doi.org/10.3390/macromol4010004.

(110) Reneker, D. H.; Yarin, A. L. Electrospinning Jets and Polymer Nanofibers. *Polymer. Elsevier* BV May 13, 2008, pp 2387–2425. https://doi.org/10.1016/j.polymer.2008.02.002.

(111) Baji, A.; Mai, Y. W.; Wong, S. C.; Abtahi, M.; Chen, P. Electrospinning of Polymer Nanofibers: Effects on Oriented Morphology, Structures and Tensile Properties. *Composites Science and Technology.* Elsevier Ltd 2010, pp 703–718. https://doi.org/10.1016/j.compscitech.2010.01.010.

(112) Zahra, F. T.; Zhang, Y.; Ajayi, A. O.; Quick, Q.; Mu, R. Optimization of Electrospinning Parameters for Lower Molecular Weight Polymers: A Case Study on Polyvinylpyrrolidone. *Polymers (Basel).* 2024, 16 (9). https://doi.org/10.3390/polym16091217.

(113) Song, J.; Lin, X.; Ee, L. Y.; Li, S. F. Y.; Huang, M. A Review on Electrospinning as Versatile Supports for Diverse Nanofibers and Their Applications in Environmental Sensing. *Advanced Fiber Materials.* Springer, 2023, pp 429–460. https://doi.org/10.1007/s42765-022-00237-5.

(114) Cho, Y.; Beak, J. W.; Sagong, M.; Ahn, S.; Nam, J. S.; Kim, I. D. Electrospinning and Nanofiber Technology: Fundamentals, Innovations, and Applications. *Advanced Materials*. John Wiley and Sons Inc July 17, 2025. https://doi.org/10.1002/adma.202500162.

(115) Liu, J.; Dong, Z.; Huan, K.; He, Z.; Zhang, Q.; Deng, D.; Luo, L. Application of the Electrospinning Technique in Electrochemical Biosensors: An Overview. Molecules. (MDPI) June 1, 2024. https://doi.org/10.3390/molecules29122769.

(116) Waqas Munir, M.; Ali, U. *Classification of Electrospinning Methods*. www.intechopen.com.

(117) Palwai, S. Physics of Electrospinning. In Electrospinning - Theory, Applications, and Update Challenges; *IntechOpen*, 2024. https://doi.org/10.5772/intechopen.113010.

(118) Klapstova, A.; Honzikova, P.; Dasek, M.; Ackermann, M.; Gergelitsova, K.; Erben, J.; Samkova, A.; Jirkovec, R.; Chvojka, J.; Horakova, J. Effective Needleless Electrospinning for the Production of Tubular Scaffolds. *ACS Applied Engineering Materials* 2024, 2 (2), 492–500. https://doi.org/10.1021/acsaenm.3c00780.

(119) Raja, V.; Mahalakshmi, L.; Leena, M. M.; Moses, J. A.; Anandharamakrishnan, C. Needleless Electrospinning: Concepts and Applications in the Food Industry. *Food Engineering Reviews*. Springer, 2024, pp 252–269. https://doi.org/10.1007/s12393-023-09362-2.

(120) Niu, H.; Wang, X.; Lin, T. *Needleless Electrospinning: Developments and Performances*.

(121) Junghare, S. L.; Bhosale, V. B.; Shewale, S. K. Effect of Processing Parameters on Morphology of Electrospun Fibers. *International Journal of Pharmaceutical Research and Applications* 6, 1033. https://doi.org/10.35629/7781-060310331038.

(122) Gaydhane, M. K.; Sharma, C. S.; Majumdar, S. Electrospun Nanofibres in Drug Delivery: Advances in Controlled Release Strategies. *RSC Advances*. Royal Society of Chemistry March 6, 2023, pp 7312–7328. https://doi.org/10.1039/d2ra06023j.

(123) Abrigo, M.; Kingshott, P.; McArthur, S. L. Electrospun Polystyrene Fiber Diameter Influencing Bacterial Attachment, Proliferation, and Growth. *ACS Appl. Mater. Interfaces* 2015, 7 (14), 7644–7652. https://doi.org/10.1021/acsami.5b00453.

(124) Khaleel, S.I. General polymers, structures, properties, and applications: A review, MINAR *International Journal of Applied Sciences and Technology* 2025, 07 (01). https://doi.org/10.47832/2717-8234.22.15.

(125) Baolin, G.; Ma, P. X. Synthetic Biodegradable Functional Polymers for Tissue Engineering: A Brief Review.

(126) Satchanska, G.; Davidova, S.; Petrov, P. D. Natural and Synthetic Polymers for Biomedical and Environmental Applications. *Polymers. (MDPI)*, 2024. https://doi.org/10.3390/polym16081159.

(127) Baranwal, J.; Barse, B.; Fais, A.; Delogu, G. L.; Kumar, A. Biopolymer: A Sustainable Material for Food and Medical Applications. *Polymers. MDPI* March 1, 2022. https://doi.org/10.3390/polym14050983.

(128) Khan, I.; Khan, I.; Saeed, K.; Ali, N.; Zada, N.; Khan, A.; Ali, F.; Bilal, M.; Akhter, M. S. Polymer Nanocomposites: An Overview. In *Smart Polymer Nanocomposites: Design, Synthesis, Functionalization, Properties, and Applications*; Elsevier, 2022; pp 167–184. https://doi.org/10.1016/B978-0-323-91611-0.00017-7.

(129) Yang, M., Guo, M., Xu, E. *et al.* Polymer nanocomposite dielectrics for capacitive energy storage. *Nat. Nanotechnol.* 19, 588–603 (2024). https://doi.org/10.1038/s41565-023-01541-w

(130) Jamil, H.; Faizan, M.; Adeel, M.; Jesionowski, T.; Boczkaj, G.; Balčiūnaitė, A. Recent Advances in Polymer Nanocomposites: Unveiling the Frontier of Shape Memory and Self-Healing Properties - A Comprehensive Review. *Molecules* 2024, *29*, 1267. https://doi.org/10.3390/molecules29061267

(131) Han, W. H.; Wang, Q. Y.; Kang, Y. Y.; Zhou, X.; Hao, C. C. Electrospun Polymer Nanocomposites for Thermal Management: A Review. *Nanoscale. Royal Society of Chemistry*, 2023, pp 2003–2017. https://doi.org/10.1039/d2nr06360c.

(132) Zhang, W.; Li, J.; Chen, M.; Jin, X.; He, C.; Li, W. Mass Production of Polymer-Derived Ceramic Nanofibers through Solution Blow Spinning: Implications for Flexible Thermal Insulation and Protection. *ACS Appl. Nano Mater*. 2023, 6 (22), 21048–21057. https://doi.org/10.1021/acsanm.3c04048.

(133) Zhang, J.; Zhang, X.; Wang, L.; Zhang, J.; Liu, R.; Sun, Q.; Ye, X.; Ma, X. Fabrication and Applications of Ceramic-Based Nanofiber Materials Service in High-Temperature Harsh Conditions - A Review. *Gels. MDPI*, 2023. https://doi.org/10.3390/gels9030208.

(134) Xue, J.; Xie, J.; Liu, W.; Xia, Y. Electrospun Nanofibers: New Concepts, Materials, and Applications. *Acc. Chem. Res*. 2017, 50 (8), 1976–1987. https://doi.org/10.1021/acs.accounts.7b00218.

(135) Ding, L.; Li, R.; Gao, Y.; Yan, B.; Zhang, C.; Zhang, G.; Yu, P.; Long, Y. Z.; Zhang, J. Electrospun Nanofibers for Fragile Artifact Conservation. *Composites Communications* 2024, 46. https://doi.org/10.1016/j.coco.2024.101824.

(136) Menichetti, A.; Ramacciotti, F.; Sciutto, G.; Focarete, M. L.; Montalti, M.; Prati, S.; Gualandi, C. Nanofibrous Photothermal Materials from Natural Resources: A Green Approach for

Artwork Restoration. *ACS Appl. Mater. Interfaces* 2024, 16 (50), 69829–69838. https://doi.org/10.1021/acsami.4c14532.

(137) Ramacciotti, F.; Sciutto, G.; Cazals, L.; Biagini, D.; Reale, S.; Degano, I.; Focarete, M. L.; Mazzeo, R.; Thoury, M.; Bertrand, L.; Gualandi, C.; Prati, S. Microporous Electrospun Nonwovens Combined with Green Solvents for the Selective Peel-off of Thin Coatings from Painting Surfaces. *J. Colloid Interface Sci.* 2024, 663, 869–879. https://doi.org/10.1016/j.jcis.2024.03.006.

(138) Benalaya, I.; Alves, G.; Lopes, J.; Silva, L. R. A Review of Natural Polysaccharides: Sources, Characteristics, Properties, Food, and Pharmaceutical Applications. *International Journal of Molecular Sciences. (MDPI)* January 1, 2024. https://doi.org/10.3390/ijms25021322.

(139) Mohammed, A. S. A.; Naveed, M.; Jost, N. Polysaccharides; Classification, Chemical Properties, and Future Perspective Applications in Fields of Pharmacology and Biological Medicine (A Review of Current Applications and Upcoming Potentialities). *Journal of Polymers and the Environment.* Springer August 1, 2021, pp 2359–2371. https://doi.org/10.1007/s10924-021-02052-2.

(140) Keung, W. S.; Zhang, W. H.; Luo, H. Y.; Chan, K. C.; Chan, Y. M.; Xu, J. Correlation between the Structures of Natural Polysaccharides and Their Properties in Regulating Gut Microbiota: Current Understanding and Beyond. *Carbohydrate Polymers*. Elsevier Ltd March 15, 2025. https://doi.org/10.1016/j.carbpol.2024.123209.

(141) Guo, M. Q.; Hu, X.; Wang, C.; Ai, L. Polysaccharides: Structure and Solubility. In *Solubility of Polysaccharides*; InTech, 2017. https://doi.org/10.5772/intechopen.71570.

(142) Xu, B. wen; Li, S. sai; Ding, W. li; Zhang, C.; Rehman, M. U.; Tareen, M. F.; Wang, L.; Huang, S. cheng. From Structure to Function: A Comprehensive Overview of Polysaccharide Roles and Applications. *Food Front.* 2025, 6 (1), 15–39. https://doi.org/10.1002/fft2.490.

(143) Hao, Z. Q.; Chen, Z. J.; Chang, M. C.; Meng, J. L.; Liu, J. Y.; Feng, C. P. Rheological Properties and Gel Characteristics of Polysaccharides from Fruit-Bodies of Sparassis Crispa. *Int. J. Food Prop*. 2018, 21 (1), 2283–2295. https://doi.org/10.1080/10942912.2018.1510838.

(144) Sansonetti, A.; Bertasa, M.; Canevali, C.; Rabbolini, A.; Anzani, M.; Scalarone, D. A Review in Using Agar Gels for Cleaning Art Surfaces. *Journal of Cultural Heritage*. Elsevier Masson SAS July 1, 2020, pp 285–296. https://doi.org/10.1016/j.culher.2020.01.008.

(145) Bertasa, M.; Dodero, A.; Alloisio, M.; Vicini, S.; Riedo, C.; Sansonetti, A.; Scalarone, D.; Castellano, M. Agar Gel Strength: A Correlation Study between Chemical Composition and Rheological Properties. *Eur. Polym. J.* 2020, 123. https://doi.org/10.1016/j.eurpolymj.2019.109442.

(146) Bertasa, M.; Botteon, A.; Brambilla, L.; Riedo, C.; Chiantore, O.; Poli, T.; Sansonetti, A.; Scalarone, D. Cleaning Materials: A Compositional Multi-Analytical Characterization of Commercial Agar Powders. *J. Anal. Appl. Pyrolysis* 2017, 125, 310–317. https://doi.org/10.1016/j.jaap.2017.03.011.

(147) Meena, R.; Siddhanta, A. K.; Prasad, K.; Ramavat, B. K.; Eswaran, K.; Thiruppathi, S.; Ganesan, M.; Mantri, V. A.; Rao, P. V. S. Preparation, Characterization and Benchmarking of Agarose from Gracilaria Dura of Indian Waters. *Carbohydr. Polym*. 2007, 69 (1), 179–188. https://doi.org/10.1016/j.carbpol.2006.09.020.

(148) Jiang, F.; Xu, X. W.; Chen, F. Q.; Weng, H. F.; Chen, J.; Ru, Y.; Xiao, Q.; Xiao, A. F. Extraction, Modification and Biomedical Application of Agarose Hydrogels: A Review. *Marine Drugs. MDPI* , 2023. https://doi.org/10.3390/md21050299.

(149) Ghebremedhin, M.; Seiffert, S.; Vilgis, T. A. Physics of Agarose Fluid Gels: Rheological Properties and Microstructure. *Curr. Res. Food Sci.* 2021, 4, 436–448. https://doi.org/10.1016/j.crfs.2021.06.003.

(150) Lee, P. Y.; Costumbrado, J.; Hsu, C. Y.; Kim, Y. H. Agarose Gel Electrophoresis for the Separation of DNA Fragments. *Journal of Visualized Experiments* 2012, No. 62. https://doi.org/10.3791/3923.

(151) Renn, D. W. *Agar and Agarose: Indispensable Partners in Biotechnology*; 1984; Vol. 23. https://pubs.acs.org/sharingguidelines.

(152) Park, S. H.; Lee, C. R.; Hong, S. K. Implications of Agar and Agarase in Industrial Applications of Sustainable Marine Biomass. *Applied Microbiology and Biotechnology*. Springer April 1, 2020, pp 2815–2832. https://doi.org/10.1007/s00253-020-10412-6.

(153) Padmesh, S.; Singh, A. *Agars: Properties and Applications*; 2021.

(154) Zamrud Adnan, A.; Asra, R. *Isolation of Agarose and Its Application as Medium of Gel Electrophoresis Method for HPV (Human Papillomavirus) DNA Identification*.

(155) Morris, E. R.; Nishinari, K.; Rinaudo, M. Gelation of Gellan - A Review. *Food Hydrocolloids*. Elsevier B.V. 2012, pp 373–411. https://doi.org/10.1016/j.foodhyd.2012.01.004.

(156) Henniges, U.; Brückle, I.; Khaliliyan, H.; Böhmdorfer, S. Gellan Residues on Paper: Quantification and Implication for Paper Conservation. *Herit. Sci.* 2024, 12 (1). https://doi.org/10.1186/s40494-024-01160-1.

(157) Mazzuca, C.; Micheli, L.; Carbone, M.; Basoli, F.; Cervelli, E.; Iannuccelli, S.; Sotgiu, S.; Palleschi, A. Gellan Hydrogel as a Powerful Tool in Paper Cleaning Process: A Detailed Study. *J. Colloid Interface Sci.* 2014, 416, 205–211. https://doi.org/10.1016/j.jcis.2013.10.062.

(158) Severini, L.; Franco, S.; Celi, E.; Sennato, S.; Paialunga, E.; Tavagnacco, L.; Micheli, L.; Angelini, R.; Zaccarelli, E.; Mazzuca, C. Methacrylated Gellan Gum Microgels: A Further Step in the Gel-Based Cleaning System. *J. Cult. Herit.* 2025, 71, 97–105. https://doi.org/10.1016/j.culher.2024.11.008.

(159) Abdl Aali, R. A. K.; Al-Sahlany, S. T. G. Gellan Gum as a Unique Microbial Polysaccharide: Its Characteristics, Synthesis, and Current Application Trends. *Gels. (MDPI)* March 1, 2024. https://doi.org/10.3390/gels10030183.

(160) Gomes, D.; Batista-Silva, J. P.; Sousa, A.; Passarinha, L. A. Progress and Opportunities in Gellan Gum-Based Materials: A Review of Preparation, Characterization and Emerging

Applications. *Carbohydrate Polymers.* Elsevier Ltd, 2023. https://doi.org/10.1016/j.carbpol.2023.120782.

(161) Petrella, G.; Mazzuca, C.; Micheli, L.; Cervelli, E.; De Fazio, D.; Iannuccelli, S.; Sotgiu, S.; Palleschi, G.; Palleschi, A. A new sustainable and innovative work for paper artworks cleaning process: gellan hydrogel combined with hydrolytic enzymes; *International Journal of Conservation Science,* 2016; Vol. 7. www.ijcs.uaic.ro.

(162) Herzberger, J.; Niederer, K.; Pohlit, H.; Seiwert, J.; Worm, M.; Wurm, F. R.; Frey, H. Polymerization of Ethylene Oxide, Propylene Oxide, and Other Alkylene Oxides: Synthesis, Novel Polymer Architectures, and Bioconjugation. *Chemical Reviews.* American Chemical Society December 29, 2016, pp 2170–2243. https://doi.org/10.1021/acs.chemrev.5b00441.

(163) Bary, E. M. A.; Fekri, A.; Soliman, Y. A.; Harmal, A. N. Characterization and Swelling–Deswelling Properties of Porous Superabsorbent Hydrogel Membranes Made of PVA and Ziziphus Spina-Christi Fibers Reinforced with Nanosilica Manufactured by Compression Moulding Process. *Polymer Bulletin* 2018, 75 (11), 4977–4997. https://doi.org/10.1007/s00289-018-2315-0.

(164) Türkoğlu, G. C.; Khomarloo, N.; Mohsenzadeh, E.; Gospodinova, D. N.; Neznakomova, M.; Salaün, F. PVA-Based Electrospun Materials—A Promising Route to Designing Nanofiber Mats with Desired Morphological Shape—A Review. *International Journal of Molecular Sciences. (MDPI)*, 2024. https://doi.org/10.3390/ijms25031668.

(165) Ma, L.; Deng, L.; Chen, J. Applications of Poly(Ethylene Oxide) in Controlled Release Tablet Systems: A Review. *Drug Development and Industrial Pharmacy*. Informa Healthcare 2014, pp 845–851. https://doi.org/10.3109/03639045.2013.831438.

(166) Malikmammadov, E.; Tanir, T. E.; Kiziltay, A.; Hasirci, V.; Hasirci, N. PCL and PCL-Based Materials in Biomedical Applications. *J. Biomater. Sci. Polym*. Ed. 2018, 29 (7–9), 863–893. https://doi.org/10.1080/09205063.2017.1394711.

(167) Salaris, V.; López, D.; Kenny, J. M.; Peponi, L. Hydrolytic Degradation and Bioactivity of Electrospun PCL-Mg-NPs Fibrous Mats. *Molecules* 2023, 28 (3). https://doi.org/10.3390/molecules28031001.

(168) Amirul A Halim, M. N.; H-Y Hashim, Y. Z.; Samsudin, N.; Salleh, H. M. Development of Porous PCL-Based Microcarrier. 2018, 8, 4–6.

(169) Rodrigues, A. L.; Machado, A. V.; Nóbrega, J. M.; Albuquerque, A.; Brito, A. G.; Nogueira, R. A Poly-ε-Caprolactone Based Biofilm Carrier for Nitrate Removal from Water. *International Journal of Environmental Science and Technology* 2014, 11 (2), 263–268. https://doi.org/10.1007/s13762-013-0250-z.

(170) Atanasova, N.; Paunova-Krasteva, T.; Stoitsova, S.; Radchenkova, N.; Boyadzhieva, I.; Petrov, K.; Kambourova, M. Degradation of Poly(ε-Caprolactone) by A Thermophilic Community and Brevibacillus Thermoruber Strain 7 Isolated from Bulgarian Hot Spring. *Biomolecules* 2021, 11 (10). https://doi.org/10.3390/biom11101488.

(171) Ntrivala, M. A.; Pitsavas, A. C.; Lazaridou, K.; Baziakou, Z.; Karavasili, D.; Papadimitriou, M.; Ntagkopoulou, C.; Balla, E.; Bikiaris, D. N. Polycaprolactone (PCL): The Biodegradable Polyester Shaping the Future of Materials – a Review on Synthesis, Properties, Biodegradation, Applications and Future Perspectives. *European Polymer Journal.* Elsevier Ltd, June 23, 2025. https://doi.org/10.1016/j.eurpolymj.2025.114033.

(172) Altenbach, H. Rheological Modeling - Historical Remarks and Actual Trends in Solid Mechanics. In *Advanced Structured Materials*; Springer Science and Business Media Deutschland GmbH, 2023; Vol. 188, pp 1–16. https://doi.org/10.1007/978-3-031-22401-0_1.

(173) Santesarti, G.; Marino, M.; Viola, F.; Verzicco, R.; Vairo, G. An Insight into Parameter Identifiability Issues in the Carreau–Yasuda Model: A More Consistent Rheological Formulation for Shear-Thinning Non-Newtonian Inelastic Fluids. *J. Nonnewtonian. Fluid Mech*. 2025, 342. https://doi.org/10.1016/j.jnnfm.2025.105438.

(174) Stanciu, I.; Ouerfelli, N. An Extended Casson Equation for Rheological Properties of Soybean Oil at Different Temperatures and Atmospheric Pressure. *J Biochem Tech* 2020, 11 (3), 52–57.

(175) Vicini, S.; Castellano, M.; Mauri, M.; Marsano, E. Gelling Process for Sodium Alginate: New Technical Approach by Using Calcium Rich Micro-Spheres. *Carbohydr. Polym*. 2015, 134, 767–774. https://doi.org/10.1016/j.carbpol.2015.08.064.

(176) Solid Media Containing Carboxymethylcellulose to Detect C, *Cellulase Activity of Micro-Organisms;* 1977; Vol. 98.

(177) Sakai, Y.; Hayatsu, M.; Hayano, K. Use of Tween 20 as a Substrate for Assay of Lipase Activity in Soils. *Soil Sci. Plant Nutr.* 2002, 48 (5), 729–734. https://doi.org/10.1080/00380768.2002.10409263.

(178) Sirisena, D. M.; Manamendra, T. P. *Isolation and characterization of cellulolytic bacteria from decomposing rice straw;* 1995; Vol. 23.

(179) Plou, F. J.; Ferrer, M.; Nuero, O. M.; Calvo, M. V; Alcalde, M.; Reyes, F.; Ballesteros, A. *Analysis of Tween 80 as an Esterase/ Lipase Substrate for Lipolytic Activity Assay*; 1998.

(180) Smith, R. E. *Rapid Tube Test for Detecting Fungal Cellulase Production*; 1977. https://journals.asm.org/journal/aem.

(181) Vermelho, A. B.; Nazareth, M.; Meirelles, L.; Lopes, A.; Dias, S.; Petinate, G.; Chaia, A. A.; Branquinha, M. H. *Detection of Extracellular Proteases from Microorganisms on Agar Plates*; Vol. 91.

(182) Cruz, M. G. da; Silva, A. M. S. da; Prada-Mejia, K. D.; Koolen, H. H. F.; Tavares, G. C.; Valladão, G. M. R. Skim Milk as a Multifunctional Cryoprotectant for Fish Probiotic Enterococcus Spp.: Impact on Viability During Lyophilization and Long-Term Storage. *Microorganisms* 2025, 13 (11), 2486. https://doi.org/10.3390/microorganisms13112486.

(183) Ge, S.; Han, J.; Sun, Q.; Ye, Z.; Zhou, Q.; Li, P.; Gu, Q. Optimization of Cryoprotectants for Improving the Freeze-Dried Survival Rate of Potential Probiotic Lactococcus Lactis ZFM559 and Evaluation of Its Storage Stability. *LWT* 2024, 198. https://doi.org/10.1016/j.lwt.2024.116052.

(184) Tutrina, A.; Zhurilov, P. Efficacy Assessment of Different Cryoprotectants for Preserving the Viability of Enterobacterales Strains at − 20 °C. *Sci. Rep.* 2024, 14 (1). https://doi.org/10.1038/s41598-024-71529-6.

(185) Bodzen, A.; Jossier, A.; Dupont, S.; Mousset, P. Y.; Beney, L.; Lafay, S.; Gervais, P. Design of a New Lyoprotectant Increasing Freeze-Dried Lactobacillus Strain Survival to Long-Term Storage. *BMC Biotechnol*. 2021, 21 (1). https://doi.org/10.1186/s12896-021-00726-2.

(186) Sardar, D.; Morol, I.; Bari, J.; Sarkar, A.; Habib, A. Optimization of Cryoprotectants and Storage Temperatures for Preserving Viability and Probiotic Properties of Lyophilized Bacterial Strains from Chicken Gut. *PLoS One* 2025, 20 (7 July). https://doi.org/10.1371/journal.pone.0328216.

(187) Nuamcharoen, P.; Kobayashi, T.; Potiyaraj, P. Influence of Volatile Solvents and Mixing Ratios of Binary Solvent Systems on Morphology and Performance of Electrospun Poly(Vinylidene Fluoride) Nanofibers. *Polym. Int.* 2021, 70 (10), 1465–1477. https://doi.org/10.1002/pi.6218.

(188) Luque-Agudo, V.; Gallardo-Moreno, A. M.; González-Martín, M. L. Influence of Solvent and Substrate on Hydrophobicity of Pla Films. *Polymers (Basel).* 2021, 13 (24). https://doi.org/10.3390/polym13244289.

(189) Sousa, A. M. M.; Souza, H. K. S.; Uknalis, J.; Liu, S. C.; Gonçalves, M. P.; Liu, L. Electrospinning of Agar/PVA Aqueous Solutions and Its Relation with Rheological Properties. *Carbohydr. Polym.* 2015, 115, 348–355. https://doi.org/10.1016/j.carbpol.2014.08.074.

(190) Jakić, M.; Santro, A.; Zečić, E.; Jozić, S. P. Thermal Analysis of the Biodegradable Polymer PVA/PEO Blends. *Tehnicki Glasnik* 2024, 18 (2), 224–228. https://doi.org/10.31803/tg-20231008184941.

(191) Higashi, S.; Hirai, T.; Matsubara, M.; Yoshida, H.; Beniya, A. Dynamic Viscosity Recovery of Electrospinning Solution for Stabilizing Elongated Ultrafine Polymer Nanofiber by TEMPO-CNF. *Sci. Rep.* 2020, 10 (1). https://doi.org/10.1038/s41598-020-69136-2.

(192) He, H.; Kara, Y.; Molnar, K. *Effect of Needle Characteristic on Fibrous PEO Produced by Electrospinning. Resolution and Discovery* 2019, 4 (1), 7–11. https://doi.org/10.1556/2051.2018.00063.

(193) Elbadawi, M. Rheological and Mechanical Investigation into the Effect of Different Molecular Weight Poly(Ethylene Glycol)s on Polycaprolactone-Ciprofloxacin Filaments. *ACS Omega* 2019, 4 (3), 5412–5423. https://doi.org/10.1021/acsomega.8b03057.

(194) Chae, D. W.; Nam, Y.; An, S. G.; Cho, C. G.; Lee, E. J.; Kim, B. C. Effects of Molecular Architecture on the Rheological and Physical Properties of Polycaprolactone. *Korea Australia Rheology Journal* 2017, 29 (2), 129–135. https://doi.org/10.1007/s13367-017-0014-2.

(195) Dodero, A.; Alloisio, M.; Castellano, M.; Vicini, S. Multilayer Alginate-Polycaprolactone Electrospun Membranes as Skin Wound Patches with Drug Delivery Abilities. *ACS Appl. Mater. Interfaces* 2020, 12 (28), 31162–31171. https://doi.org/10.1021/acsami.0c07352.

(196) Pompa-Monroy, D. A.; Figueroa-Marchant, P. G.; Dastager, S. G.; Thorat, M. N.; Iglesias, A. L.; Miranda-Soto, V.; Pérez-González, G. L.; Villarreal-Gómez, L. J. Bacterial Biofilm

Formation Using Pcl/Curcumin Electrospun Fibers and Its Potential Use for Biotechnological Applications. *Materials* 2020, 13 (23), 1–22. https://doi.org/10.3390/ma13235556.

(197) Kasaai, M. R. Calculation of Mark-Houwink-Sakurada (MHS) Equation Viscometric Constants for Chitosan in Any Solvent-Temperature System Using Experimental Reported Viscometric Constants Data. *Carbohydr. Polym*. 2007, 68 (3), 477–488. https://doi.org/10.1016/j.carbpol.2006.11.006.

(198) Sousa, A. M. M.; Souza, H. K. S.; Uknalis, J.; Liu, S. C.; Gonçalves, M. P.; Liu, L. Electrospinning of Agar/PVA Aqueous Solutions and Its Relation with Rheological Properties. *Carbohydr. Polym*. 2015, 115, 348–355. https://doi.org/10.1016/j.carbpol.2014.08.074.

(199) Cahyani, A.; Kurniasari, J.; Nafingah, R.; Rahayoe, S.; Harmayani, E.; Saputro, A. D. Determining Casson Yield Value, Casson Viscosity and Thixotropy of Molten Chocolate Using Viscometer. In *IOP Conference Series: Earth and Environmental Science*; Institute of Physics Publishing, 2019; Vol. 355. https://doi.org/10.1088/1755-1315/355/1/012041.

(200) Kim, H. seok; Seo, Y. S.; Kim, K.; Han, J. W.; Park, Y.; Cho, S. Concentration Effect of Reducing Agents on Green Synthesis of Gold Nanoparticles: Size, Morphology, and Growth Mechanism. *Nanoscale Res. Lett*. 2016, 11 (1). https://doi.org/10.1186/s11671-016-1393-x.

(201) Ponnuchamy, K.; Jacob, J. A. Metal Nanoparticles from Marine Seaweeds - A Review. *Nanotechnology Reviews.* Walter de Gruyter GmbH, 2016, pp 589–600. https://doi.org/10.1515/ntrev-2016-0010.

(202) Faoucher, E.; Nativo, P.; Black, K.; Claridge, J. B.; Gass, M.; Romani, S.; Bleloch, A. L.; Brust, M. In Situ Preparation of Network Forming Gold Nanoparticles in *Agarose Hydrogels. Chemical Communications* 2009, No. 43, 6661–6663. https://doi.org/10.1039/b915787e.

(203) De Matos, R. A.; Da Silva Cordeiro, T.; Samad, R. E.; Vieira, N. D.; Courrol, L. C. Green Synthesis of Gold Nanoparticles of Different Sizes and Shapes Using Agar-Agar Water Solution and Femtosecond Pulse Laser Irradiation. *Appl. Phys. A Mater. Sci. Process*. 2012, 109 (3), 737–741. https://doi.org/10.1007/s00339-012-7108-y.

(204) Farkas, S.; Holló, G.; Schuszter, G.; Deák, Á.; Janovák, L.; Hornok, V.; Itatani, M.; Nabika, H.; Horváth, D.; Tóth, Á.; Lagzi, I. *Supporting Information Reaction-Diffusion Assisted Synthesis of Gold Nanoparticles: Route from the Spherical Nano-Sized Particles to Micron-Sized Plates.*

(205) Komatani, S.; Aoyama, T.; Nakazawa, T.; Tsuji, K. Comparison of SEM-EDS, Micro-XRF and Confocal Micro-XRF for Electric Device Analysis. *e-Journal of Surface Science and Nanotechnology* 2013, 11, 133–137. https://doi.org/10.1380/ejssnt.2013.133.

(206) Latahir, A. Z.; Wai, C. K.; Yaacob, S. F. F. S.; Rahim, R. A. Exploring the Elemental Detection on Portable XRF vs SEM-EDX in Household Alloy Materials Analysis. *Microchemical Journal* 2025, 213. https://doi.org/10.1016/j.microc.2025.113667.

(207) Garg, S.; Rong, H.; Miller, C. J.; Waite, T. D. Oxidative Dissolution of Silver Nanoparticles by Chlorine: Implications to Silver Nanoparticle Fate and Toxicity. *Environ. Sci. Technol*. 2016, 50 (7), 3890–3896. https://doi.org/10.1021/acs.est.6b00037.

(208) Koczorowski, T.; Glowacka-Sobotta, A.; Michalak, M.; Mlynarczyk, D. T.; Güzel, E.; Goslinski, T.; Sobotta, L. Connections between Metallic Nanoparticles and Chlorin E6—An Overview of Physicochemical and Biological Properties and Prospective Medical Applications. *Applied Sciences MDPI* March 1, 2023. https://doi.org/10.3390/app13063933.

(209) Yang, F.; Armentrout, P. B. Hydration Energies of Calcium Hydroxide Cation, CaOH+(H2O)x (x = 1–6), Studied Using Guided Ion Beam Tandem Mass Spectrometry. *Int. J. Mass Spectrom*. 2024, 503. https://doi.org/10.1016/j.ijms.2024.117284.

(210) Góral, D.; Góral-kowalczyk, M. Application of Metal Nanoparticles for Production of Self-Sterilizing Coatings. *Coatings. MDPI*, 2022. https://doi.org/10.3390/coatings12040480.

(211) Scarabelli, L.; Coronado-Puchau, M.; Giner-Casares, J. J.; Langer, J.; Liz-Marzán, L. M. Monodisperse Gold Nanotriangles: Size Control, Large-Scale Self-Assembly, and Performance in Surface-Enhanced Raman Scattering. *ACS Nano* 2014, 8 (6), 5833–5842. https://doi.org/10.1021/nn500727w.

(212) Scarabelli, L.; Sánchez-Iglesias, A.; Pérez-Juste, J.; Liz-Marzán, L. M. A "Tips and Tricks" Practical Guide to the Synthesis of Gold Nanorods. *Journal of Physical Chemistry Letters* 2015, 6 (21), 4270–4279. https://doi.org/10.1021/acs.jpclett.5b02123.

(213) He, M.; Chen, M.; Dou, Y.; Ding, J.; Yue, H.; Yin, G.; Chen, X.; Cui, Y. Electrospun Silver Nanoparticles-Embedded Feather Keratin/Poly(Vinyl Alcohol)/Poly(Ethylene Oxide) Antibacterial Composite Nanofibers. *Polymers (Basel)*. 2020, 12 (2). https://doi.org/10.3390/polym12020305.

(214) Castellano, M.; Alloisio, M.; Darawish, R.; Dodero, A.; Vicini, S. Electrospun Composite Mats of Alginate with Embedded Silver Nanoparticles: Synthesis and Characterization. *J. Therm. Anal. Calorim*. 2019, 137 (3), 767–778. https://doi.org/10.1007/s10973-018-7979-z.

(215) Sindram, J.; Karg, M. Polymer Ligand Binding to Surface-Immobilized Gold Nanoparticles: A Fluorescence-Based Study on the Adsorption Kinetics. *Soft Matter* 2021, 17 (32), 7487–7497. https://doi.org/10.1039/d1sm00892g.

(216) Zhang, R. C.; Sun, D.; Zhang, R.; Lin, W. F.; Macias-Montero, M.; Patel, J.; Askari, S.; McDonald, C.; Mariotti, D.; Maguire, P. Gold Nanoparticle-Polymer Nanocomposites Synthesized by Room Temperature Atmospheric Pressure Plasma and Their Potential for Fuel Cell Electrocatalytic Application. *Sci. Rep*. 2017, 7. https://doi.org/10.1038/srep46682.

(217) Kaboudin, B.; Khanmohammadi, H.; Kazemi, F. Polymer Supported Gold Nanoparticles: Synthesis and Characterization of Functionalized Polystyrene-Supported Gold Nanoparticles and Their Application in Catalytic Oxidation of Alcohols in Water. *Appl. Surf. Sci*. 2017, 425, 400–406. https://doi.org/10.1016/j.apsusc.2017.07.033.

(218) Ouyang, R.; Liu, J. X.; Li, W. X. Atomistic Theory of Ostwald Ripening and Disintegration of Supported Metal Particles under Reaction Conditions. *J. Am. Chem. Soc*. 2013, 135 (5), 1760–1771. https://doi.org/10.1021/ja3087054.

(219) Voorhees, P. W. *The Theory of Ostwald Ripening*; 1985; Vol. 38.

(220) Yuan, Y.; Hays, M. P.; Hardwidge, P. R.; Kim, J. Surface Characteristics Influencing Bacterial Adhesion to Polymeric Substrates. *RSC Adv.* 2017, 7 (23), 14254–14261. https://doi.org/10.1039/c7ra01571b.

(221) Oliveira, R.; Azeredo, J.; Teixeira, P.; Fonseca, A. P. The role of hydrophobivity in bacterial adhesion; *Hydrophobicity and adhesion BioLine*, 2001.

(222) Bruinsma, G. M.; Van Der Mei, H. C.; Busscher, H. J. *Bacterial Adhesion to Surface Hydrophilic and Hydrophobic Contact Lenses*; 2001; Vol. 22.

(223) Boks, N. P.; Norde, W.; van der Mei, H. C.; Busscher, H. J. Forces Involved in Bacterial Adhesion to Hydrophilic and Hydrophobic Surfaces. *Microbiology (N Y).* 2008, 154 (10), 3122–3133. https://doi.org/10.1099/mic.0.2008/018622-0.

(224) Salerno, M. B.; Logan, B. E.; Velegol, D. Importance of Molecular Details in Predicting Bacterial Adhesion to Hydrophobic Surfaces. *Langmuir* 2004, 20 (24), 10625–10629. https://doi.org/10.1021/la048372z.

(225) Dantas, L. C. D. M.; Silva-Neto, J. P. Da; Dantas, T. S.; Naves, L. Z.; Das Neves, F. D.; Da Mota, A. S. Bacterial Adhesion and Surface Roughness for Different Clinical Techniques for Acrylic Polymethyl Methacrylate. *Int. J. Dent*. 2016, 2016. https://doi.org/10.1155/2016/8685796.

(226) Lencova, S.; Stindlova, M.; Havlickova, K.; Jencova, V.; Peroutka, V.; Navratilova, K.; Zdenkova, K.; Stiborova, H.; Hauzerova, S.; Kostakova, E. K.; Jankovsky, O.; Kejzlar, P.; Lukas, D.; Demnerova, K. Influence of Fiber Diameter of Polycaprolactone Nanofibrous Materials on Biofilm Formation and Retention of Bacterial Cells. *ACS Appl. Mater. Interfaces* 2024, 16 (20), 25813–25824. https://doi.org/10.1021/acsami.4c03642.

(227) Pereni, C. I.; Zhao, Q.; Liu, Y.; Abel, E. Surface Free Energy Effect on Bacterial Retention. *Colloids Surf. B Biointerfaces* 2006, 48 (2), 143–147. https://doi.org/10.1016/j.colsurfb.2006.02.004.

(228) Zheng, S.; Bawazir, M.; Dhall, A.; Kim, H. E.; He, L.; Heo, J.; Hwang, G. Implication of Surface Properties, Bacterial Motility, and Hydrodynamic Conditions on Bacterial Surface Sensing and Their Initial Adhesion. *Frontiers in Bioengineering and Biotechnology*. Frontiers Media S.A. February 12, 2021. https://doi.org/10.3389/fbioe.2021.643722.

(229) Fan, L.; Dong, W.; Lu, J.; Peng, Y.; Xie, B.; Wei, P.; Jiang, M.; Chen, S. Robust Controlled Degradation of Enzyme Loaded PCL-Based Fibrous Scaffolds Toward Scarless Skin Tissue Regeneration. *Advanced Science* 2025, 12 (25). https://doi.org/10.1002/advs.202501053.

(230) Tamayo-Ramos, J. A.; Rumbo, C.; Caso, F.; Rinaldi, A.; Garroni, S.; Notargiacomo, A.; Romero-Santacreu, L.; Cuesta-López, S. Analysis of Polycaprolactone Microfibers as Biofilm Carriers for Biotechnologically Relevant Bacteria. *ACS Appl. Mater. Interfaces* 2018, 10 (38), 32773–32781. https://doi.org/10.1021/acsami.8b07245.

(231) Dwivedi, R.; Kumar, S.; Pandey, R.; Mahajan, A.; Nandana, D.; Katti, D. S.; Mehrotra, D. Polycaprolactone as Biomaterial for Bone Scaffolds: Review of Literature. *Journal of Oral*

Biology and Craniofacial Research. Elsevier B.V. January 1, 2020, pp 381–388. https://doi.org/10.1016/j.jobcr.2019.10.003.

(232) Oh, J. K.; Yegin, Y.; Yang, F.; Zhang, M.; Li, J.; Huang, S.; Verkhoturov, S. V.; Schweikert, E. A.; Perez-Lewis, K.; Scholar, E. A.; Taylor, T. M.; Castillo, A.; Cisneros-Zevallos, L.; Min, Y.; Akbulut, M. The Influence of Surface Chemistry on the Kinetics and Thermodynamics of Bacterial Adhesion. *Sci. Rep.* 2018, 8 (1). https://doi.org/10.1038/s41598-018-35343-1.

(233) Markelova, N.; Chumak, A. Antimicrobial Activity of Bacillus Cyclic Lipopeptides and Their Role in the Host Adaptive Response to Changes in Environmental Conditions. *International Journal of Molecular Sciences. (MDPI)*, 2025. https://doi.org/10.3390/ijms26010336.

(234) Paloyan, A.; Tadevosyan, M.; Ghevondyan, D.; Khoyetsyan, L.; Karapetyan, M.; Margaryan, A.; Antranikian, G.; Panosyan, H. Biodegradation of Polyhydroxyalkanoates: Current State and Future Prospects. *Frontiers in Microbiology*. Frontiers Media SA 2025. https://doi.org/10.3389/fmicb.2025.1542468.

(235) Krumov, N.; Atanasova, N.; Boyadzhieva, I.; Petrov, K.; Petrova, P. Biodegradation of Poly(ε-Caprolactone): Microorganisms, Enzymes, and Mechanisms. *International Journal of Molecular Sciences. (MDPI)*, 2025. https://doi.org/10.3390/ijms26125826.

(236) Hermanová, S.; Bálková, R.; Voběrková, S.; Chamradová, I.; Omelková, J.; Richtera, L.; Mravcová, L.; Jančár, J. Biodegradation Study on Poly(ε-Caprolactone) with Bimodal Molecular Weight Distribution. *J. Appl. Polym. Sci.* 2013, 127 (6), 4726–4735. https://doi.org/10.1002/app.38078.

(237) Kianfar, P.; Vitale, A.; Dalle Vacche, S.; Bongiovanni, R. Enhancing Properties and Water Resistance of PEO-Based Electrospun Nanofibrous Membranes by Photo-Crosslinking. *J. Mater. Sci.* 2021, 56 (2), 1879–1896. https://doi.org/10.1007/s10853-020-05346-3.

(238) Papagiannopoulos, A.; Vlassi, E.; Pispas, S.; Tsitsilianis, C.; Radulescu, A. Polyethylene Oxide Hydrogels Crosslinked by Peroxide for the Controlled Release of Proteins. *Macromol* 2021, 1 (1), 37–48. https://doi.org/10.3390/macromol1010004.

(239) Maccaferri, E.; Canciani, A.; Mazzocchetti, L.; Benelli, T.; Giorgini, L.; Albonetti, S. Water-Resistant Photo-Crosslinked PEO/PEGDA Electrospun Nanofibers for Application in Catalysis. *Membranes (Basel).* 2023, 13 (2). https://doi.org/10.3390/membranes13020212.

(240) Ghasaban, S.; Atai, M.; Imani, M.; Zandi, M.; Shokrgozar, M. A. Photo-Crosslinkable Cyanoacrylate Bioadhesive: Shrinkage Kinetics, Dynamic Mechanical Properties, and Biocompatibility of Adhesives Containing TMPTMA and POSS Nanostructures as Crosslinking Agents. *J. Biomed. Mater. Res.* A 2011, 99 A (2), 240–248. https://doi.org/10.1002/jbm.a.33181.

(241) Panwar, P.; Michael, P.; Devlin, M.; Martini, A. Critical Shear Rate of Polymer-Enhanced Hydraulic Fluids. *Lubricants* 2020, 8 (12), 1–15. https://doi.org/10.3390/lubricants8120102.

(242) Weßling, B. *Critical Shear Rate-the Instability Reason for the Creation of Dissipative Structures in Polymers;* 1995.